University of Southampton

Faculty of Physical Sciences and Engineering

Electronics and Computer Science

Optimal Cost versus Efficiency Configuration of a Grid-Connected Photovoltaic System Exploiting the Weighted-Sum Method with Focus on Kuwaiti National Grid

by

Faisal Q. Kh. S. AL-Enezi

A thesis submitted for the degree of Doctor of Philosophy

January 2015

ABSTRACT

by Faisal Q. Kh. S. Al-Enezi

An overview of the production and consumption of Kuwait electrical energy, installed capacity and peak loads is presented in this research. The results show that Kuwait has a serious problem because of insufficient electrical energy installed and load peaking, which is considered unacceptable. The research also identifies and analyses the geographical and temporal variability of solar energy inside Kuwait. The fundamental solar models are modified to estimate and identify daily and hourly global (direct-beam) and total solar radiation (SR) on horizontal surfaces on the basis of the more readily available meteorological data such as latitude angle, longitude angle, clearness index, solar time and corresponding hour angle. The presented results demonstrate that Kuwait has an abundance of solar energy capability in terms of almost cloudless atmosphere for nine months and twelve hours solar time a day throughout the year. The daily global and monthly averaged solar intensity have been computed. This research shows that the knowledge of SR data is essential for design and sizing of the photovoltaic (PV) systems. A specific type of PV module has been modelled and its characteristics such as *I-V* and *P-V* curves for each month of the year have been calculated and analysed using MATLAB/Simulink to determine the amount of DC current, voltage and power. These results form the basis of the grid-connected PV system (GCPV) design from array construction to the reliability of electrical supply. A technical sizing procedure based on sizing algorithm using iterative manual approach (*SAIMA*) for meeting specific amount of GWh output required by a potential PV system sponsor in Kuwait is presented. *SAIMA* has been implemented to determine the configuration of the PV array, inverter-to-PV array sizing factor and efficiency of the system according to previous PV module and inverter database.

A novel methodology for approximating Pareto front multi-criteria cost-efficiency optimization problem for a proposed GCPV system has been constructed using system planning constraints. The proposed algorithm is based on bi-objective weighted-sum (*BoWS*) method to maximize the system efficiency and minimize the system cost. A main objective function of both GCPV system cost and efficiency has been stated as function of PV output power and inverter rated power. The proposed function is performed with the Sequential Quadratic Programing (SQP).

The results presented in this research have been acquired through simulation of the proposed GCPV to a specific section of Alsabyia generation station part of Kuwait national grid with efficient maximum power point tracking (MPPT) algorithm incorporated into a DC-DC boost converter. The simulations were performed using Power Simulation Software (PSIM). The analytical model of the PV module has been combined with a ‘perturb and observe’ (P&O) method so that MPP is achieved with the external temperature and SR also considered. An inverter is used to track the output voltage of the converter and interface the PV array with the grid. The results show that the model not only achieves the MPP function but also improves the output of the inverter by reducing the ripples in the sine waveforms. Moreover, this research involved using the software package ERACS to analyze the impact of penetrating approximately 100 MW of the proposed PV generation to a part of the generation unit at Alsybia electrical station in Kuwait. The one-line diagram of the network was modeled in ERACS and it’s used to conduct power flow and fault studies. Four network locations were chosen as potential sites to connect the PV system. Power flow studies were conducted on the network for every hour that the PV array contributed power to the network and for 35 different network configurations for each daylight hour. Computer programs were created to conduct all of these power flow studies and to help analyze the data. Fault studies were then carried out on the network, with the PV array connected at all of the potential locations. There were a few faults that caused a fault level greater than 40 kA to flow through the 13.8 kV busbars.

Key Words

Solar Radiation (SR), Extra-terrestrial Solar Insolation (ET), Photovoltaic (PV), Silicon Mono-Crystalline Photovoltaic (SMC-PV), Standard Test Conditions (STC), Grid-Connected Photovoltaic (GCPV), Bi-objective weighted-sum (*BoWS*) Maximum Power Point Tracking (MPPT), Perturb and Observe (P&O), Sizing Algorithm Iterative Approach (*SAIMA*)

Contents

List of Figures

List of Tables

Nomenclature

δ	Declination angle of the sun
n	Day number
t	Solar time
β	Solar altitude angle
L	Latitude angle of the site
γ	Longitude angle of the site
H	Solar hour angle
H_{SR}	Sunrise hour angle
K_t	Clearness index
S_{ET}	Extra-terrestrial solar insolation
$S_{ET}\ (ave)$	Average daily extra-terrestrial solar isolation on a horizontal surface
S_G	Global (direct-beam) solar radiation on horizontal surfaces
D_f	Sky diffuse factor
S_D	Diffuse insolation on a horizontal surface
S_H	Total solar radiation on horizontal surfaces
I_{sc}	Short-circuit current per module
V_{oc}	Open-circuit voltage per module
I_{ph}	Photo-generated current
I_o	Reverse saturation current of diode
q	Electron charge
B	Boltzmann's constant
T	Junction (cell) temperature
S_s	Standard solar radiation at cell or module level
P_m	Output Power of the PV module
E_{oc}	Open-circuit voltage of the proposed module
I_{sc}	Short-circuit current of the proposed module
E_{sys}	Maximum system voltage
$E_{stc}(\max)$	Voltage at maximum power
$(P_{PV})_{\max p}$	Maximum power
T_{Eoc}	Temperature coefficient for open-circuit voltage
T_{Emax}	Temperature coefficient for maximum power voltage
$E_{inv}(\max)$	Maximum input voltage
$E_{inv}(\min)$	Minimum input voltage
$I_{inv}(\max)$	Maximum input current

P_{inv}	Inverter nominal power output
$\eta_{conv.}$	Conversion efficiency
$\eta_{inv.}$	Nominal efficiency
n_s	Number of series PV modules
n_p	Number of parallel string in the proposed PV array
$(P_{PV})_{act}$	Actual capacity of the PV array
$(energy)_{exp}$	Expected annual energy output
Sf	Inverter-to-PV array sizing factor
Ef	Excess factor
A_{panel}	Area of one panel
α	GCPV economical factor
$\eta_{conv.}$	Conversion factor
G	Government subsidization rate
C_{tariff}	Feed in tariff
d	Nominal annual discount rate
C_{PV}	Module price
C_{inv}^{i}	*i*th inverter price
$C_{ins.}$	PV module's mounting structure, required land, DC and AC cables costs
P_{sys}^{i}	Nominal power of PV array connected to *i*th inverter
sf_i	Sizing factor of *i*th inverter
f	Annual inflation rate
C_{mPV}	Annual maintenance cost of PV array
C_{minv}^{i}	Annual maintenance cost of *i*th inverter
C_{rinv}^{i}	*i*th inverter repair cost
P_{PV}	Output power of PV array
AE_{GCPV}	Net present profit of sold production energy
$C_{\{c,m\}}$	Capital cost and net present cost of maintenance, operation and repair
C_{sys}	Total cost of the GCPV
η_{sys}	GCPV system efficiency
D	Duty cycle of the switching transistor
t_{on}, t_{off}	On/Off duty cycle time of the switching transistor
T	Commutation period of the boost converter

DECLARATION OF AUTHORSHIP

I, Faisal Q. Kh. S. Alenezi, declare that the thesis entitled:

Optimal Cost versus Efficiency Configuration of a Grid-Connected Photovoltaic System Exploiting the Weighted-Sum Method with Focus on Kuwaiti National Grid

and the work presented in the thesis are both my own, and have been generated by me as the result of my own original research. I confirm that:

1) this work was done wholly or mainly while in candidature for a research degree at this University;
2) where any part of this thesis has previously been submitted for a degree or any other qualification at this University or any other institution, this has been clearly stated;
3) where I have consulted the published work of others, this is always clearly attributed;
4) where I have quoted from the work of others, the source is always given. With the exception of such quotations, this thesis is entirely my own work;
5) I have acknowledged all main sources of help;
6) where the thesis is based on work done by myself jointly with others, I have made clear exactly what was done by others and what I have contributed myself;
7) parts of this work have been published as:

- F. Q. Al-Enezi, J. K. Sykulski, and N. A. Ahmed (2011), *Visibility and Potential of Solar Energy on Horizontal Surface at Kuwait Area.* In Proceedings of the IEEE International Conference on Smart Grid and Clean Energy Technologies (IEEE- ICSGCE), 27-30 September 2011, Chengdu, China

- F. Q. Al-Enezi and J. K. Sykulski (2012), *Modelling of a Photovoltaic Module Considering the Solar Energy Available from Horizontal Surfaces over Kuwait Area.* Journal of Electronic Science and Technology, 10 (2), Summer Issue, pp. 173-180, ISSN 1674-862X

- F. Q. Al-Enezi, J. K. Sykulski and M. Rotaru (2014), *Grid-connected photovoltaic module and array sizing based on an iterative approach.* SGCE International Journal of Smart Grid and Clean Energy, 3 (2), Spring Issue, pp. 247-254

- F. Q. Al-Enezi, J. K. Sykulski and M. Rotaru (2014), *Modelling and Simulation of a Grid-Connected PV System based on Efficient Maximum Power Point Tracking Algorithm.* Engineering Research and Applications, Vol. 4 – Issue 11 (part III), 1-9, ISSN: 2248-9622

Signed: Faisal Alenezi

Date: January 2015

Acknowledgements

The thesis on optimal cost versus efficiency configuration of a grid-connected photovoltaic system exploiting the weighted-sum method with focus on Kuwaiti national grid has been completed through the researching and troubleshooting, which have led to the findings obtained throughout the four years of study at Southampton, which were both very personal but also shared experiences.

Firstly, I would like to express my deepest gratitude and thanks to my research supervisor, Professor Jan K. Sykulski for his valuable advice and guidance and also his patience, encouragement and counselling offered throughout this research.

I would also like to express my sincere appreciation to Dr. Mihai Rotaru for the kind assistance that he has given me during the research.

Finally, it is my duty to express my deeply felt thanks to my wife, Laila.

Chapter 1
Introduction

1.1 Research Background

For hundreds of years, electricity has been a challenge to scientists. Even if they knew about its existence, they found it difficult to explain what electricity actually was. In the late nineteenth century, engineers were able to put electricity to residential and industrial areas for usage. The rapid expansion of the electrical technology within this period brought the advances of electricity as a source of energy that remain the backbone of our modern industry and economy. For the foreseeable future, the electrical power is expected to grow as electricity is adapted to a huge and growing number of uses in domestic applications and also due to the industrial expansion. Consequently, there is no doubt that electricity is the mainstay of all plans for economic and social development including industrial projects, commercial, agricultural and urban expansion.

Discovering oil in Kuwait, which is considered the basic source of national wealth, had enormous influence at beginning of civilization advancement in Kuwait. This progress has included the different aspects of live, such as social, constructional, educational and economic. Electricity has contributed to this progress and to satisfy the different needs of the country when abilities of vital services have been significantly developed in line with production development of electrical power in Kuwait. Recognizing the importance of the electric utility and its fundamental role and influence in the modern society, Kuwait tries to provide support for development to stay in line with the growing demand for its services, especially in light of the natural growth of population and expansion of development projects at all levels.

Energy demand is rapidly increasing in Kuwait; during the past half century the electrical demand has in fact quintupled. Thus inevitably there is high cost incurred by the state budget to keep providing this service to all consumers without interruption, especially in the light of the dependence on oil and its derivatives in the operation of electric power stations. Due to the increasing global demand for oil, and because it represents the main income for Kuwait, it is becoming paramount to stop the wasteful consumption of electricity as well as reduce the amount of fuel used for generation. In response to the foregoing, the state of Kuwait – during the past years and through government foundations and academic centres – initiated campaigns and practical solutions to reduce waste and excessive consumption of electricity, which currently has

one of the highest rates in the world [1], in the hope of the consumers to apply more rational and moderate way of life, especially that this moderation refers to the extravagance of the extent of urbanization and is applied in the context of the society's awareness of environmental issues.

The contribution of this research is to find solutions to the rationing of energy use with the aim to preserve Kuwait's oil wealth and to prioritise future needs during the gradual shift towards the use of alternative and renewable energy in power generation, with emphasis on solar energy and photovoltaic (PV) generation. Solar energy as a renewable energy resource will play a major role in Kuwait's future energy supply. The direct photovoltaic conversion of sunlight into electricity is one of the promising technologies. Photovoltaic cells can indeed supply energy to systems with power levels varying from milli-watt to megawatt level. They are also reliable, static and maintenance-free [2].

Nowadays the world production of solar PV has reached more than 136 GW peak in 2013, reflecting an annual growth rate in the range of 15% to 50% for the past few years as shown in Fig. 1.1. The distribution of the systems into which the PV modules and arrays were incorporated has changed considerably; while a few years ago most of them were installed in rather small stand-alone systems, the majority of today´s arrays are used in grid-connected systems. This growth is mostly due to ambitious subsidy programs in five countries: Germany, China, USA, Japan and Italy, where more than 41.8 GW were installed in 2012 and 2013. Several other countries are implementing or close to implementing similar programs to promote grid-connected systems; amongst them are Australia, Spain, Netherlands, Denmark and UK. In 2012, an estimated 29.1 GW of solar PV power capacity was installed world-wide (76.4% in the countries that report to International Energy Agency-Photovoltaic Power System, IEA-PVPS). An impressive addition of 36.7% of new solar PV power capacity in 2013 is observed in Fig.1.1. In UAE, out of a total renewable energy generation capacity of 150 MW, solar PV generation capacity accounts for 120 MW [3]. The world's largest solar PV power plant with an installed capacity of 290 MW was completed and started commercial operation in Arizona (USA), in April 2013 [4].

Grid-connected PV systems (GCPV) provide a quiet, low maintenance, pollution-free, safe, reliable and independent alternative to conventional generation sources. Major breakthroughs in solar cell manufacturing technologies have enabled it to compete with conventional generation technologies in the large-scale (over 50 kWp) as well. Hence, an expected global shift toward GCPV power world-wide is observed (Fig. 1.2);

according to IEA, 98.6% of the total solar PV capacity added during 2012 was grid-connected. The European PV Technology Platform Group ambitiously forecasts solar PV to reach grid parity in most of Europe by 2019. At the beginning of 2013, the total large-scale or MW-scale PV system installed capacity reported by the IEA had reached about 11.7 GW. A report submitted by IEA-PVPS Task 12 participants predicts that during the first quarter of the 21st century PV systems of even greater installed capacity ranging in GW could be realized. Thus large-scale PV systems are a promising option to meet future global electricity demand. Prior to investigating the potential and feasibility of solar energy in Kuwait, I will present overview data and information about the production and consumption of Kuwait electrical energy.

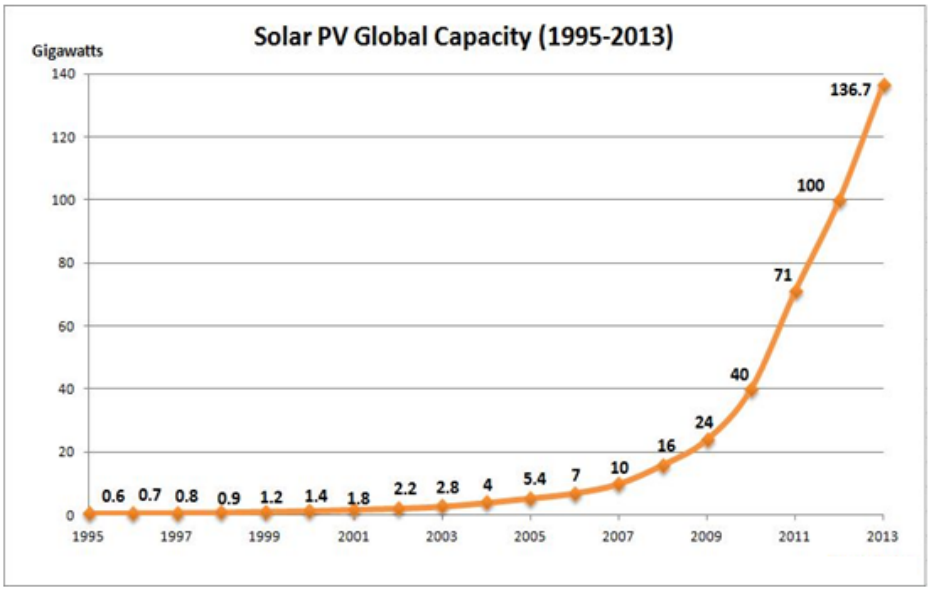

Figure 1.1: World production of photovoltaics electrical power (1995-2013)
(Source: Department of Energy and Climate Change - UK, May, 2014)

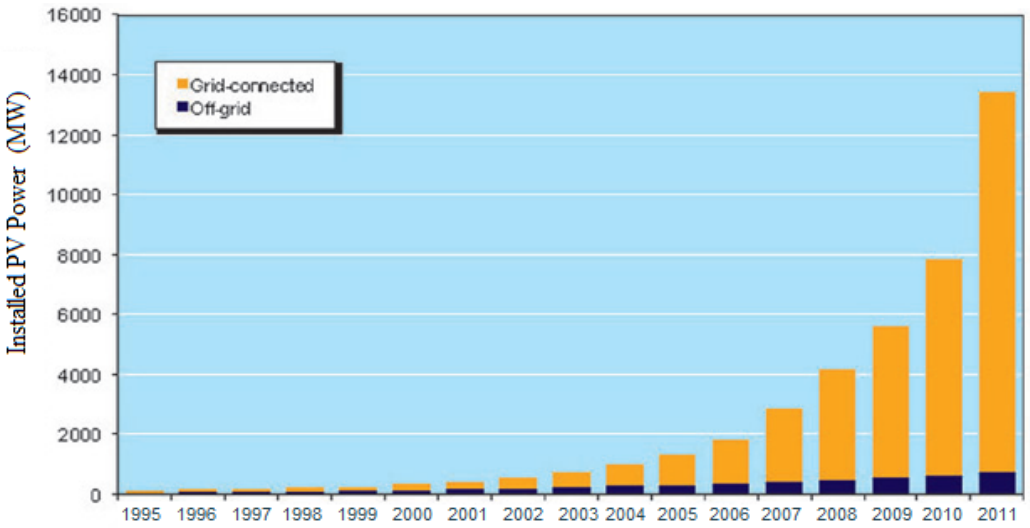

Figure 1.2: Cumulative installed grid-connected and off-grid PV power in the reporting countries (source: IEA-PVPS Task 12)

1.2 Production and Consumption of Kuwait Electrical Energy

The primary source of electrical energy consumed in Kuwait is the chemical energy contained in the fossil fuel which consists of natural gas and liquid oil products. The process of transforming the primary energy of the fuel into electrical energy passes through several stages inside the power stations which comprise special complicated equipment and plants requiring huge financial investments. These include very large boilers which burn tremendous quantities of fuels and transform the chemical energy into thermal energy that produces large quantities of high pressure super-heated steam. This steam drives the steam turbines which transform the thermal energy into mechanical energy which rotates the electrical generators that transform the mechanical energy into electrical energy which is exported to the networks for their transmission and distribution.

1.2.1 Statistical Data and Information (Overview)

i) Kuwait power generation utility consists of six power stations:
   1. Az-Zour South Power Station.
   2. Al-Shuaiba Power Station.
   3. Doha West Power Station.
   4. Doha East Power Station.
   5. Alsabiya Power Station.
   6. Shuwaikh Power Station (subjected to severe destruction by the brutal Iraqi invasion).

ii) The electrical utility in Kuwait mainly employs thermal steam turbines for the generation of power needed to satisfy demand. However, thermal gas turbines (GT) are also used, which make up around 26.3% of total installed capacity. The GT is usually used in emergencies and during the time of peak load [5] in the spite of their high operational costs and low thermal efficiency.

iii) Power generating plants use different types of fossil fuel available in Kuwait, such as natural gas, heavy fuel oil, crude oil and gas – depending on boiler design – with priority given to natural gas within the limits of the available quantities. Older plants can burn natural gas and gas oil in case of emergency, while the newer ones are capable of burning the four types of fuel.

iv) Electrical load for selected years [5] is shown in Table 1.1:

Table 1.1: Electrical Load for Selected Years

Year	Peak load (MW)	Installed capacity (MW)	Mean annual rate of peak load growth over 10 year periods (%)
1979	1950	2578	-
1989	4150	7411	7.9
1999	7160	8289	5.6
2009	11960	12579	8.4

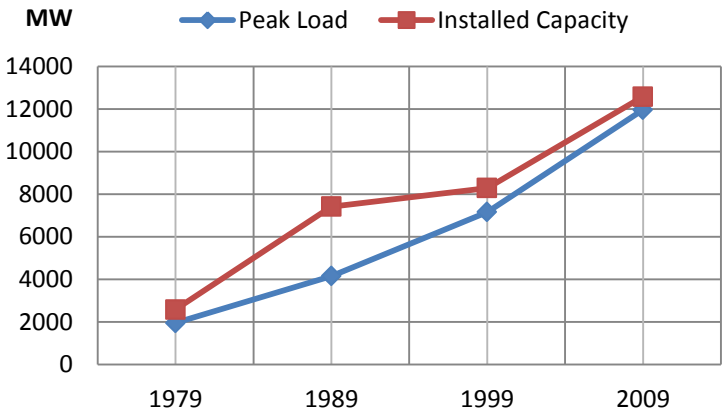

Figure 1.3: Kuwait installed capacity and peak load for selected years

To meet the ever growing load demand in Kuwait, a new electrical power generation plant is installed almost every year in Kuwait. As shown in Fig. 1.3, the total installed power generation capacity in Kuwait has increased rapidly from 2578 MW in 1979 to 12579 MW in 2009.

The consumption of electrical energy in Kuwait indicates that almost one half of the generated energy in Kuwait is consumed for domestic purposes as a result of the government and the citizens establishing more and more residential areas every year [6]. At the same time, most of the load in residential, industrial and commercial areas is due to air conditioning (A/C) systems [7]. To clarify the picture in another manner, the comparative figures of per capita consumption of electrical energy for the same years [5] outlined in Table 1.2:

Table 1.2: Per Capita Consumption of Electrical Energy for the Same Selected Years

Year	Population	Per capita consumption (kWh/person)	Mean annual rate of growth during 10 year periods %
1979	1332611	5656	-
1989	2097570	8606	4.4
1999	2148032	12552	3.9
2009	3483881	14372	2.2

1.2.2 Generating Stations in Kuwait during 2013

The power generating units are [8]:

1) Steam Turbine Units:
    a. These units comprise the large capacity units (134 – 300) MW in all power stations.
    b. Total installed capacity of these units is 11602 MW.
    c. The above units are operated according to the system power demand.
    d. Maximum capacity in summer (loads α temp.) and minimum in winter (annual maintenance season).
2) Gas Turbine Units:
    a. These are smaller capacity units (18 – 165) MW.
    b. Total installed capacity of these units is 3609 MW.
    c. Operate at peak load time and emergency.

Therefore, the total generation capacity of the whole Kuwait power stations in 2013 is 15211 MW. Table 1.3 and Fig. 1.4 give us a clear picture about the total power generation capacity in MW in Kuwait during the period 2009 – 2013 [8]. The installed power generation capacity with the peak load as a percentage of installed capacity during 2009 – 2013 [8] is shown in Table 1.4.

Table 1.3: Total Power Generation Capacity in MW in Kuwait (2009 – 2013)

Period	Installed power (MW)
2009	12579
2010	12869
2011	13062
2012	14650
2013	15211

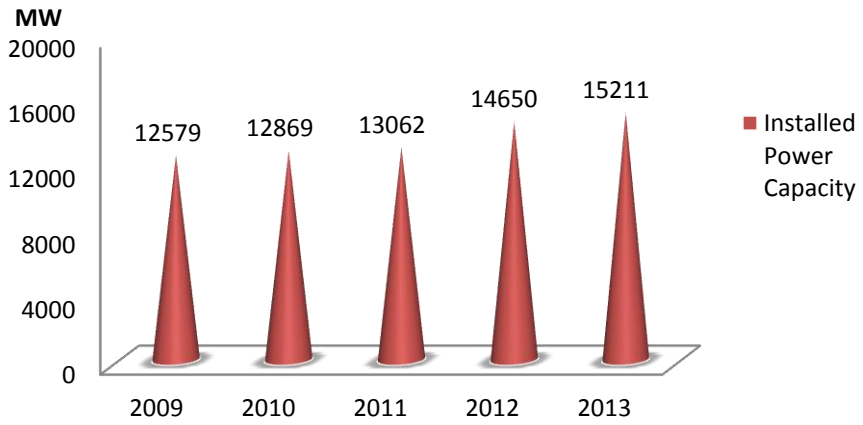

Figure 1.4: Kuwait installed power capacity (2009-2013)

Table 1.4: Peak Load as Percentage of Installed Power (2009-2013)

Year	Installed power capacity (MW)	Peak load (MW)	Peak load as percentage of installed power (%)
2009	12579	11960	95.1
2010	12869	12100	94.0
2011	13062	12655	96.9
2012	14650	12980	88.6
2013	15211	13810	90.8

From the data shown in Table 1.4 and Fig. 1.5, it is obvious that the installed power capacity is stabilized at around 5% to 12% above peak load demand; therefore this situation is unacceptable and it can be dangerous. However, according to the Energy Ministerial Council of the Gulf Cooperation Council (GCC) of the Arab States in the Gulf, a safety margin of 15% or more is required by GCC which is fulfilled always because of the Project of Interconnection of Electrical Systems in GCC Countries in 2001 (from GCC website). Therefore, there are no possibilities that the peak load will reach 100% of the installed capacity.

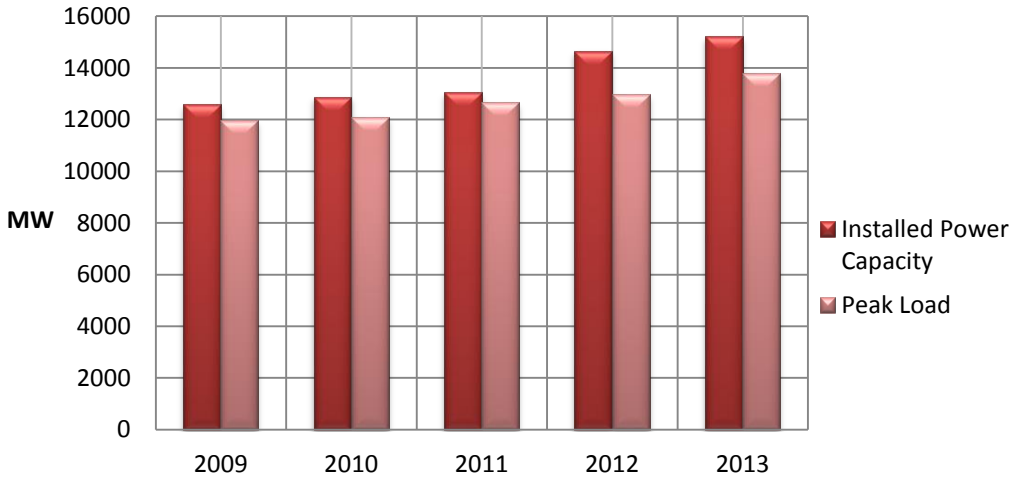

Figure 1.5: Installed power generation capacity and peak load during (2009-2013)

The peak load, average peak load, minimum load and average minimum load during year 2010 [8] are illustrated in Table 1.5.

Table 1.5: Peak Load, Average Peak Load, Minimum Load and Average Minimum Load during Year 2010

Month	Peak load (MW)	Av. peak load (MW)	Min. load (MW)	Av. min. load (MW)
January	5180	4810	3280	3540
February	4500	4345	3140	3230
March	5020	4650	3190	3485
April	6960	6960	3350	4190
May	9180	7800	5120	6030
June	11850	11460	7550	7905
July	12100	11850	7980	8045
August	12060	11600	7540	7650
September	10260	9595	5670	5845
October	7500	7055	4900	5465
November	7060	5440	3390	4305
December	4850	4695	3410	3490

According to the maximum and minimum load distributions shown in Fig. 1.6 for the year 2010, Kuwait's electrical load is characterized by high load in summer and low load in winter, depending on the increases and decreases in the values of temperature and relative humidity.

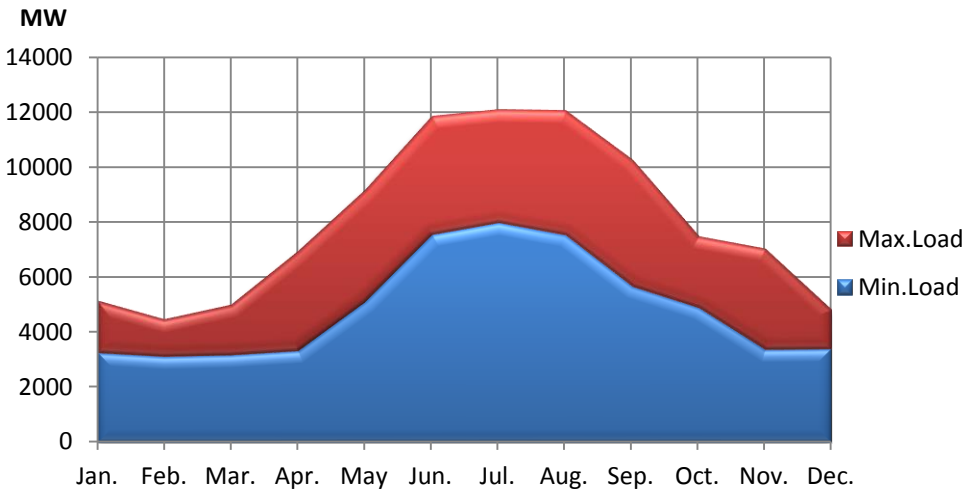

Figure 1.6: Maximum and minimum loads during 2010

1.3 Research Aims and Objectives

When I decided to undertake my PhD studies in 2011, I committed myself to conduct my research for the benefit of my country Kuwait. By early 2006, Kuwait was already facing a serious problem with electric power production which could not meet the electric power demand of the country. In summer 2006 to 2013, a scheduled electric power-cut programme was implemented to prevent electric power over-loading. It was also the requirement of my sponsors that I pursue studies which were likely to assist the electricity industry in Kuwait. The scope of this work was developed under these special circumstances.

The main objective of this research is to develop efficient/low cost utility integrated large-scale GCPV generation system that can be installed in generation or distribution areas, such as homes, parks, etc., or centralized large-scale GCPV system in certain region in the state of Kuwait. In order to achieve this goal, the research provides a design of GCPV system for a specific electrical network in Kuwait (mainly part of the power generation unit at Alsybia electrical network) including suggested load profiles, sizing of the PV system for supplying this electrical load using algorithm based on iterative approach and optimal configuration and operating plan for the GCPV system using Pareto front optimization. Both sizing processes contain a number of energy components and evaluate suitable lists of PV modules and DC-AC inverters. Analysis with both approaches requires information on economic constraints and power limitations. It also requires input on component types, their numbers, costs, efficiencies, lifetimes, etc. Sensitivity analysis could be done with variables having a range of values instead of a specific number. This allows one to ascertain the effects of change in a certain parameter on the overall system.

This research will cover the PV generation systems topologies, modelling, simulation, and electrical requirements on the DC side of the installation (modules, wiring, DC junction voltage) as well as requirements for the inverter (sizing factor, power quality) up to the interface to the public grid. It is also intended to study the impact of power penetration of the GCPV into distribution network in Kuwait.

According to the above, the following plan of research had been agreed:

1) Investigate the visibility and potential of solar energy over Kuwait area, by identifying and analyzing the geographical and temporal variability of PV energy sources inside Kuwait.

2) Develop an analytical model for PV module based on the extracted physical parameters of solar cells to simplify mathematical modeling for different PV configuration of modules and panels.
3) Derive a mathematical model and design equations to obtain theoretical predictions.
4) Model the selected topology of the GCPV generation system.
5) Describe an optimal planning model using manual algorithm approach to determine the size and configuration of the PV panel and array.
6) Develop and implement a novel design strategy aiming to find the optimal configuration for a GCPV system using Pareto frontier taking into account that the bi-objective design criteria are the system cost and efficiency.
7) Undertake computer simulation on the selected topologies using PSIM software and present the PSIM implementation of the boost converter and PWM DC-AC inverter with and without LC filter to satisfy the interfacing to Kuwait national grid.
8) Attempt to achieve higher efficiency by introducing proposed MPPT control.
9) Penetrate the proposed GCPV system with its optimal parameters into Alsybia electrical network in Kuwait.

1.4 Outline of the Thesis

This thesis concentrates on the grid integration of an efficient/low cost PV energy generation system and the impact of its penetration on distribution networks in Kuwait. It will be organized as follows:

Chapter 1 provides the background reading of the importance of the provision of electricity in Kuwait. Some data and information about Kuwait electrical grid, current problems due to the lack of sufficient production of electrical energy and load peaking are demonstrated, therefore allowing a better understanding of the results that will be obtained in the following chapters.

Chapter 2 introduces and emphasises the importance of the solar radiation (SR) as a renewable energy source. It presents a brief description of different models and techniques of solar energy. A simple trigonometric model for both global (direct-beam) and total solar radiation on horizontal surfaces over Kuwait area is developed. Diffuse

sunlight has been taken into consideration. Data and results for solar energy over Kuwait area are also presented showing the availability and visibility of solar energy in Kuwait.

Chapter 3 presents the history and development of the PV cells. It discusses the physics of the PV cells and some of their basics, such as equivalent circuit, characteristics with their ranges, and their electrical wirings. Moreover, this chapter focuses on a MATLAB/Simulink model of a PV cell and module. This model is based on mathematical equations and is described through an ideal PV equivalent circuit. The developed model allows the prediction of PV module behaviour under different physical and environmental parameters such as temperature and SR. The *I-V* characteristic and output power of the module at each month are obtained as a result of this modelling. Thereafter, the sizing process of the proposed GCPV system was fulfilled using manual iterative algorithm approach called *SAIMA* and consequently the size of the PV array has been estimated based on a combination of PV module and DC-AC inverter.

In Chapter 4, a novel algorithm for bi-objective weighted-sum (*BoWS*) Pareto front optimization has been constructed to find optimal cost-efficiency curve for sizing GCPV system. The objectives were formulated based on the aim to minimize the system cost and maximize the system efficiency using one main objective function with two variables. Apart from that, the optimization problem has been performed with the Sequential Quadratic Programing (SQP).

A complete simulation model of the proposed grid-connected photovoltaic system (GCPV) using PSIM presents in Chapter 5. The simulation results are carried out in order to confirm that the modelling and sizing approaches taken are robust and lead to a system with acceptable performance. The simulation model is using an adequate maximum power point tracking (MPPT) algorithm with adjusted Perturb-and-Observe (P&O) method and depends on the environmental factors, such as temperature and SR. The MPP is achieved using a DC-DC boost (step-up) converter. The results of the simulation process have been evaluated after a Pulse-Width Modulation (PWM) DC-AC inverter has been implemented.

Chapter 6 investigates the possibilities of integration the proposed GCPV system to one of main Kuwait electrical grid. A power flow analysis is being conducted on a part of generation unit at Alsybia electrical network within Kuwait electrical grid to assess the effect of increasing the capacity when the proposed PV panels are connected. A model of the network will be created using ERACS, a power system analysis software package.

This model is presently being interrogated to determine its accuracy. Once an accurate model is produced, ERACS will be used to examine the effect of connecting a proposed future PV array to a part of the power generation unit at Alsybia electrical network in Kuwait. This examination would include looking at how the network would have to be upgraded to cope with the increased capacity. Also, any changes in fault levels will be investigated and measures will be taken to restrict the fault currents to acceptable levels.

In chapter 7, the conclusions from the research thesis are summarized and topics for further research are outlined.

Chapter 2
Visibility and Potential of Solar Energy on Horizontal Surfaces over Kuwait Area

2.1 Introduction

The development of economy and the improvement of people's living standards throughout the world lead to the continuing growth in demand for electric power. Conventional methods of generating electricity (e.g. burning coal and other fossil fuels) can produce pollutants such as carbon dioxide which is the main gas responsible for global warming. Furthermore, the reserves of fossil fuel and uranium are declining. So, it has been universally acknowledged that there is a necessity to exploit the solar energy as renewable energy and corresponding generation technologies [9].

Solar energy is the emitted light and heat from the sun that the human has spent for him since ancient times using a range of technology that is constantly evolving. Solar energy techniques include the use of solar thermal energy for generating electricity via PV phenomena using PV arrays and panels or in the process of converting mechanical to electrical energy or movement or it can use for heating, in addition to architectural designs which are dependent on the exploitation of solar energy. These techniques can contribute significantly to solving some of the world's most pressing problems today. Most renewable energy sources available on the surface of the earth to solar radiation (SR) in addition to secondary energy sources such as wind and wave power, hydroelectricity and biomass. It is important here to mention that only a small part of the available solar energy is used in our lives. Solar energy is clean, quiet and abundant. It produces no pollution to the environment [10]. Therefore, solar energy as a renewable energy source occupies one of the most prominent places among various alternative energy sources and is increasingly adopted in many applications [11].

Accurate knowledge of solar radiation (SR) availability at a particular geographical location is of vital importance for the development of solar energy systems and for the estimation of their efficiencies and outputs [12]. The knowledge of SR data is a prerequisite for the modelling and design of all PV systems [13, 14]. Familiarity with SR data is valuable to architects, agriculturalists, air conditioning engineers and energy designers as an aid to proper design and operation of engineering projects. The information about SR is also useful for the atmospheric energy-balance, climatology and pollution studies.

2.2 Different Models and Techniques Relevant to Solar Radiation (SR)

Solar technology is not new. Its history spans from the 7th century B.C. to today [2]. They started out concentrating the sun's heat with glass and mirror to light fires. Today, we have everything from solar-powered buildings to solar-powered vehicles [15]. There are hundreds of models with different techniques available which correlate the global SR to other climatic parameters such as sunshine hours (solar time), maximum temperature and relative humidity. In this section, only the most widely used SR models will be reviewed.

The basic and fundamental empirical model was proposed by Angstrom in 1924 [16]. Many authors have modified this model for estimating SR data at their places of interest; for example some researchers have proposed trigonometric models, others suggested linear logarithmic models or quadratic models. In 1958, R. C. Jordan and Threlkeld [17] established a new model by which they correlated the SR with the climatic parameters and applied this model for moderately dusty atmosphere with atmospheric water vapour content. In 1960, B. Liu and R. Jordan [18] successfully developed new model for SR after they computed the geometrical dimensions and angles of the earth (solar geometry) and they made interrelationship between direct, diffuse and total SR. Also included is a solar constant, S_o, that will be introduced later in this chapter. This model was widely used for measurements of SR until 1970 when the National Oceanic and Atmospheric Administration (NOAA) in United States, and later by the National Renewable Energy Laboratory (NREL), established the first SR data base for 239 sites in the United States [19]. In 1973, during the oil crisis, many countries that were importing oil and had limited fossil fuel resources initiated research into SR to guarantee their national energy security. M. Collares-Pereira and A. Rable [19] built their own model in 1979 based on the attenuation of the incoming radiation as a function of the distance that the beam has to travel through the atmosphere as well as factors such as dust, air pollution, atmospheric water vapour and clouds. A commonly used model treats attenuation as an exponential decay function. Moreover, this model correlates the diffuse insolation with hemispherical. As they were working on solar engineering of thermal processes, J. Duffie and W. Beckman [19] found in 1991 a new approach to SR based on the extra-terrestrial solar radiation in clear sky, solar geometry and solar time. They estimated the direct (beam) and diffuse solar radiations. From this time onwards, the researches and developments in SR were carried out with numerous models that have been developed based on the previous models in order to estimate the SR around the world.

2.3 A simple Model for Global SR on Horizontal Surfaces at the Earth's Surface

Solar radiation (SR) is considered to be the most important parameter for the design and development of various solar energy systems. Knowledge of SR incoming on horizontal surfaces is often necessary in order to study the surface energy balance, the local and large-scale climate, or to design technological applications such as renewable energy conversion systems, either in urban or in rural zones [20]. Realistically, at many national meteorological stations in the Sunbelt countries, global irradiance has been measured only on horizontal surfaces and rarely on inclined ones [20] due to higher solar altitude angles with the horizon. Practically, the solar altitude angle over Kuwait area is ranging between 88° and 74° with the horizon for nine months of the year [21]. The prime objective of the present study is to propose a simple approach and derive a formula for both daily and hourly global (direct-beam) and total SR intensity on horizontal surfaces at the earth's surface. This approach will be modified and applied to Kuwait area taking into consideration the country's geographical parameters and climate conditions.

2.3.1 Declination Angle of the Sun at Solar Noon

The earth revolves around the sun in an elliptical orbit, making one revolution every 365.25 days. We know that the sun rises in the east and sets in the west and reaches its highest point sometime in the middle of the day. But, we need to predict exactly where in the sky the sun will be at any location on any day of the year. On June 21 (the summer solstice), the sun reaches its highest point and makes an angle of 23.45° with the earth's equator. On that day, the sun is directly over the Tropic of Cancer. On December 21 (the winter solstice), the sun is 23.45° below the equator and it's directly over the Tropic of Capricorn.

As shown in Fig. 2.1, the angle formed between the plane of the equator and a line drawn from the centre of the sun to the centre of the earth is called the solar declination angle, δ. It varies between the extremes of ± 23.45° [22]. A simple sinusoidal relationship that assumes 365 days a year and which puts the autumn equinox on day 284 provides a very good approximation and it is called Cooper equation. Table 2.1 lists the typical day number for the first day of each month. The declination angle of the sun can be approximated using Cooper's equation 2.1 as

$$\delta = 23.45 \times \sin\left(\frac{360 \cdot (n + 284)}{365}\right) \tag{2.1}$$

where

δ = declination angle of the sun in degrees.

n = day number (from 1 to 365) from Table 2.1.

Although n is not repeated counter and it will not take values bigger than 365 [22], the term (n+284) is implemented arbitrary as the autumn equinox on day 284.

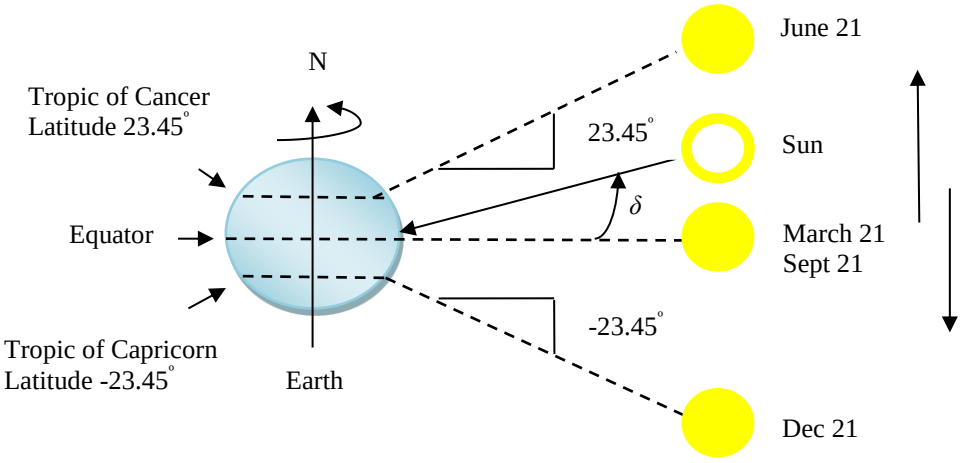

Figure 2.1: The declination angle of the sun

Table 2.1: Day Number for the First Day of Each Month

Month	*n*
January	1
February	32
March	60
April	91
May	121
June	152
July	182
August	213
September	244
October	274
November	305
December	335

2.3.2 Position of the Sun at any Time of Day

The time of day, t, is the most important factor in calculating the location of the sun at any time of day. Different time systems are in use in many SR models and techniques. Local mean time (LMT), often called clock time, differs from local apparent time (LAT), often called solar time or sunshine hours, and the difference depends on the longitude of the site (longitude = 47.5° for Kuwait area). The solar time, which is the most commonly used parameter for estimating global SR [23], is determined from the movements of the sun. The moment when the sun has its highest elevation in the sky is

defined as solar noon. The solar noon at any place defines the instant the sun crosses from east to west meridian (line of longitude). The solar time is converted to its angular form, the solar hour angle, for trigonometric calculations of the solar path. The solar hour angle, *H*, is referenced to solar noon. Considering the earth to rotate 15°/h, for trigonometric calculations that follow, the solar time, *t*, is expressed as an hour angle, *H*, where

$$H = 15^{\circ}\left(t - 12\right) \tag{2.2}$$

where

H = solar hour angle in degrees.

t = solar time in hours (i.e. LAT).

The standard convention used is that *H* is taken as positive after and negative before the solar noon. Now the location of the sun at any time of day can be described in terms of its altitude angle, β, as shown in Fig. 2.2.

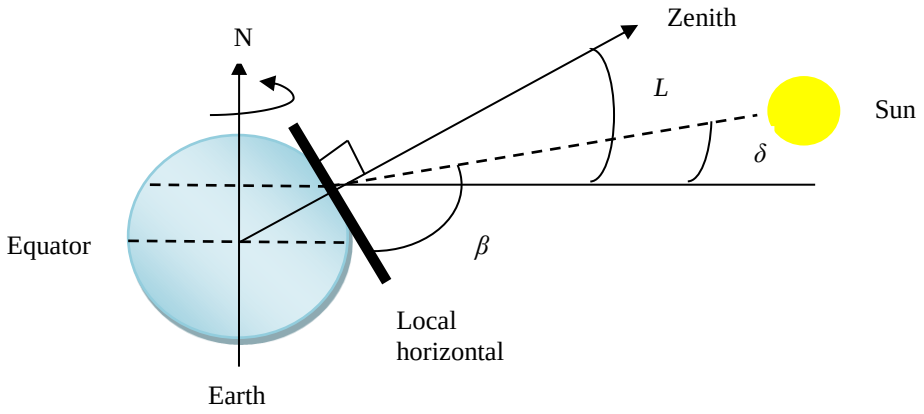

Figure 2.2: The altitude angle of the sun at solar noon

Hence the solar altitude angle may be expressed as equation 2.3 below and depends on the latitude angle of the site, day number and, most importantly, the time of day [24]:

$$\sin\beta = \cos L \cos\delta \cos H + \sin L \sin\delta \tag{2.3}$$

where

β = solar altitude angle in degrees.

L = latitude angle of the site (*L* = 29.33° for Kuwait area).

A straightforward calculation of sunrise time and sunset time may be based on a simple manipulation of eqn. 2.3. At sunrise and sunset, the solar altitude angle β is zero. It follows that the sunrise hour angle, H_{SR}, or sunset hour angle is given by

$$H_{SR} = \cos^{-1}\left(-\tan L \times \tan \delta\right) \tag{2.4}$$

where

H_{SR} = sunrise hour angle.

2.3.3 The Estimation of Daily Global SR on Horizontal Surfaces

The goal of this section is to be able to derive a simple model for daily global SR intensity on horizontal surfaces at the earth's surface. This model should incorporate improvements in methodology as well as the algorithm to calculate the SR based on the model by Duffie and Beckman [25], which in turn relies on two approaches to estimate the daily SR. The first approach is based on that the solar flux striking any surface will be a combination of *direct-beam* radiation that passes in a straight line through the atmosphere to the surface, *diffuse* radiation that has been scattered by clouds and molecules in the atmosphere, and *reflected* radiation that has bounced off the ground or other surface in front of the collector. The second approach is based on the estimation of the extra-terrestrial (ET) solar insolation, S_{ET}, which passes perpendicular through an imaginary surface just outside the earth's atmosphere. The ET insolation depends on the distance between the earth and the sun, which varies with the time of year. It also depends on the intensity of the sun, which rises and falls according to a fairly predictable cycle. I considered the second approach to estimate the daily global SR on horizontal surfaces because the ET insolation really consists of the three components of SR (beam, diffuse and reflect) in a clear sky and Kuwait's climate for almost nine months (from 1st of March to 30th of November) means cloudless atmosphere. Moreover, the second approach is suitable for dry and temperate areas typical for Kuwait.

The starting point for a clear sky daily global SR calculation is with an estimate of the ET insolation, S_{ET}. One expression that is used to describe the day-to-day variation in ET solar insolation is

$$S_{ET} = S_o \times \left[1 + 0.034 \cos\left(\frac{360 \times n}{365}\right)\right] \tag{2.5}$$

where

S_{ET} = extra-terrestrial (ET) solar insolation in W/m^2.

S_o = solar constant in W/m^2.

The solar constant, S_o, is an estimate of the average annual ET insolation [26] and the accepted value of S_o is 1377 W/m^2. Now, the average daily ET solar insolation on a horizontal surface, $S_{ET}\,(ave)$, can be calculated by averaging (numerical integration over time) the product of eqn. 2.5 and the sine of the solar altitude angle β in eqn. 2.3 from sunrise to sunset, resulting in

$$S_{ET}(ave) = \left(\frac{24}{\pi}\right) S_o \times \left[1 + 0.034\cos\left(\frac{360n}{365}\right)\right] \times \left[\cos L\cos\delta\sin H_{SR} + \left(\frac{\pi}{180}\cdot H_{SR}\right)\sin L\sin\delta\right] \tag{2.6}$$

The sunrise hour angle, H_{SR}, is in radians. Substitute the value of S_o into eqn. 2.6, we obtain

$$S_{ET}(ave) = \left(\frac{33048}{\pi}\right) \times \left[1 + 0.034\cos\left(\frac{360n}{365}\right)\right] \times \left[\cos L\cos\delta\sin H_{SR} + \left(\frac{\pi}{180}\cdot H_{SR}\right)\sin L\sin\delta\right] \tag{2.7}$$

where, $S_{ET}\,(ave)$ = average daily ET isolation on a horizontal surface in Wh/m^2 – day.

In clear sky atmosphere calculations, we have to define the clearness index, K_t, which is the ratio of the horizontal insolation at the site S_G to the ET insolation on a horizontal surface above the site and just outside the atmosphere $S_{ET}\,(ave)$.
Hence,

$$K_t = \frac{S_G}{S_{ET}(ave)} \tag{2.8}$$

where

K_t = clearness index (varies from 0 to 1.0).

A high clearness index (K_t > 0.5) corresponds to clear skies, where most of the SR will be direct beam, while a low one (K_t < 0.5) indicates overcast conditions having diffused SR. A monthly averaged clearness index for the site of Kuwait can be obtained from National Aeronautics and Space Administration (NASA) website for Kuwait area over 22 years (1983 – 2005), as given in Table 2.2.

Table 2.2: Monthly Averaged Clearness Index K_t for Kuwait Area

Latitude 29.33° Longitude 47.5°	**22-Year average K_t**	**Latitude 29.33° Longitude 47.5°**	**22-Year average K_t**
January	0.52	July	0.68
February	0.57	August	0.67
March	0.56	September	0.65
April	0.56	October	0.60
May	0.62	November	0.50
June	0.69	December	0.47
Annual average		**0.59**	

From the best curve fitting (interpolation) for the values of K_t in Table 2.2, we need to use the standard form of a quadratic equation which is $K_t = an^2 + bn + c$. We plug in the n and K_t values for each month, and get three equations. Solve the three equations and three unknowns using the elimination of variables method. The clearness index can be expressed to a good accuracy as a function of the day number n as

$$K_t = -3.807 \times 10^{-6} n^2 + 0.001124n + 0.6139 \tag{2.9}$$

Finally, according to eqn. 2.8, the daily global SR on horizontal surfaces, S_G, can be found from

$$S_G = K_t \cdot S_{ET}(ave) \tag{2.10}$$

where

S_G = global SR on horizontal surfaces in Wh/m^2.

2.3.4 The Estimation of Hourly Global SR on Horizontal Surfaces

The hour by hour SR data is essential if the radiation on the horizontal surfaces is to be estimated. We can follow the same procedure as for the daily radiation, except for expressing the hour angle in terms of solar time in hours (i.e. LAT), t, as in eqn. 2.2 and letting the solar time t vary between sunrise time to sunset time according to the longitude of site. For the Kuwait area with a longitude of 47.5°, the standard sunrise and sunset times are 6:00 am and 18:00 pm, respectively, and may be obtained from Kuwait Metrological Centre (also see [26]).

Replace the new values of the hour angles H in degrees into eqn. 2.2 and multiply it with the average ET insolation S_{ET} *(ave)* in eqn. 2.7 without averaging the sine of the solar altitude angle β, we get

$$S_{ET}(ave) = \left(\frac{33048}{\pi}\right) \times \left[1 + 0.034 \cos\left(\frac{360n}{365}\right)\right]$$
$$\times \left(\cos L \cos\delta \cos H + \sin L \sin\delta\right) \quad (2.11)$$

From eqn. 2.11, substitute S_{ET} *(ave)* into eqn. 2.10 to readily estimate the hourly global SR on horizontal surfaces.

2.4 Diffuse Sunlight

The sunlight rays (insolation) from the sun travel relatively parallel creating a highly directional beam of light (extra-terrestrial radiation, ET). When the ET enters the clouds, the light rays pass through the cloud molecules scattering the light in various directions. Even under a cloudless sky, the ET have been scattered by atmospheric constituents (e.g. gas molecules, particulates, aerosols, moisture). The percentage of the SR that is diffuse is much greater in higher latitudes (L > 40.1° N) and cloudier places than in lower latitudes and sunnier places (as Kuwait region) [22]. Also, the percentage of the diffuse insolation, S_D, to the global SR, S_G, tends to be higher in the winter than the summer in these higher latitudes, cloudier places. The sunniest places, by contrast, tend to have less seasonal variation in the ratio between diffuse and total SR. As an example, compare London, UK (51° North; wet and mild climate) to Kuwait City, Kuwait (29.33° North; dry and hot climate). In London's sunniest month (June), the average daily SR is about 5.5 kWh/m^2 and about 50% of that is diffused. In December, the irradiation is less than 1 kWh/m^2 and by far the majority of that radiation is scattered. The consequences of atmospheric scattering are evident by comparing the global or total SR and diffuse radiation reference spectra. The global SR reference spectrum has significantly more power in the visible because of the wavelength dependence of scattering. As scattering increases, for example because of intermittent or thin cloud layers, a greater proportion of SR in the visible becomes diffuse, and a concentrator's output power diminishes. This variability in direct and diffuse radiation is a reason why flat plate solar products are so widely used.

For numerous applications, particularly those involving horizontal surfaces, it is necessary to know both the total SR, S_H, and diffuse components of the incident solar intensity. Because constant care is needed to measure these components, considerable information is available about the total SR on a horizontal surface (see Section 2.3). This information can then be used to estimate the relative amounts of SR and diffuse insolation in a statistically significant manner by utilizing a procedure developed by

Duffie and Beckman [25]. The empirical procedure of Duffie and Beckman involves a one-parameter correlation between the diffuse to global SR ratio (often referred to as the sky diffuse fraction, D_f) and the clearness index, K_t. Formally, this quantity is obtained from a detailed statistical analysis, Duffie and Beckman discovered that a firm relationship existed between K_t and D_f. A monthly averaged sky diffuse factor, D_f, for the site of Kuwait can be calculated from American Society of Heating, Refrigerating and Air-Conditioning Engineers (ASHRAE) website for Kuwait area over 25 years (1985-2010) ranging from January to December (The solar constant used in all calculations was 1370 W/m^2), as given in Table 2.3. Linear regression fits are sufficient for the monthly correlations. Higher order fits are statistically indistinguishable from the linear fits but more accurate. The model developed by Duffie and Beckman, which is used in the ASHRAE Clear-Day Solar Flux Model (1995), suggests that diffuse insolation on a horizontal surface, S_D, is proportional to the global (direct-beam) radiation S_G no matter where in the sky the sun happens to be

$$D_f = \frac{S_D}{S_G} \tag{2.12}$$

where D_f is a sky diffuse factor.

It's interesting to note that the solar parameter given in Table 2.3 is for the 21st day of each month averaged for 25 years. In the present investigation, the ASHRAE cloudless model is run for every day in the year. Therefore, the values of the diffuse factor D_f for days other than the 21st day in each month are obtained by best curve fitting and a convenient approximation using trigonometric equation as a function of n is as follows

$$D_f = 0.0948 + 0.041\sin\left(\frac{360}{365}\cdot[n-100]\right) \tag{2.13}$$

Table 2.3: Averaged Sky Diffuse Factor D_f for the 21st Day of Each Month for Kuwait

Latitude 29.33^o Longitude 47.5^o	**25-Year average D_f**
January	0.056
February	0.059
March	0.068
April	0.096
May	0.118
June	0.133
July	0.134
August	0.120
September	0.092
October	0.062
November	0.061
December	0.055
Annual average	**0.088**

By substituting eqn. 2.13 into eqn. 2.12, we can conclude that the diffuse insolation, S_D, is given by

$$S_D = D_f \cdot S_G \tag{2.14}$$

Hence, the daily SR on horizontal surfaces, S_H , can be found from

$$S_H = S_G - S_D \tag{2.15}$$

where

S_H = Total SR on horizontal surfaces in Wh/m^2.

2.5 Availability of SR in Kuwait

Recognizing all the reasons mentioned in Chapter 1, Kuwait is in a dangerous position due to insufficient electrical energy supply and load peaking, making the situation unacceptable. On the other hand, Kuwait has an abundance of solar energy. Unfortunately, SR measurements for Kuwait are not easily available because of the country not being able to afford the necessary measuring equipment and techniques involved. Instead the developed model is designed in sections 2.3.1 to 2.3.4 and section 2.4 to estimate and identify the SR on horizontal surfaces on the basis of the more readily available meteorological data. Section 2.3 presented some meteorological data for Kuwait area, such as latitude angle (L = 29.33º), longitude angle (γ = 47.5°), clearness index K_t (almost cloudless atmosphere for nine months), solar time t (varying from 6:00-18:00) and the corresponding hour angle H.

These meteorological data for Kuwait area has been used in the model and the intensity of daily and hourly global SR on horizontal surfaces S_H over Kuwait area has been obtained as a function of both day number n (with a day number increment of one day) and time t (with a time increment of one hour) using eqns. from 2.1 to 2.15. These results can be obtained for any day of the year and for any hour of the LAT in Kuwait. Consequently, the total solar energy received by Kuwait area during each hour or day or month can be calculated using the developed model. A computer program using MATLAB is developed and employed to solve these equations for any day number n and any solar time t in hours (see appendix A). Moreover, we can use a modelling software package called *HOMER* to obtain the SR calculations.

2.5.1 Results of Daily Global SR on Horizontal Surfaces at Kuwait Area

The simulation results using the model developed of the daily SR on horizontal surfaces over Kuwait area will now be graphically presented. As shown in Fig. 2.3, it is observed

that the daily SR is a conditional function with boundary condition is as follows,

$$n = \begin{cases} 1 \le n \le 365 & S_G \; as \; in \; eqn. 2.10 \\ n > 365 & S_G \; does \; not \; exist \end{cases}$$

Moreover, both K_t and D_f are obtained from monthly averaged values over 22-years and both are differing from month to month, therefore SR function doesn't repeat itself and has a unique curve shape. Although the function (2.10) is defined and has a limit at the point where n=365, but the limit and the value of the function do not agree with each other causing discontinuity and this is due to the stochastic nature of the term (n+284) in the declination angle equation. The daily SR on horizontal surface in Kuwait increases rapidly from 3786.5 Wh/m^2 on 15th of January to 7984.9 Wh/m^2 on 15th of June, and then decreases very rapidly to 3691.6 Wh/m^2 on 15th of November. It reaches its peak during months from April to August (for n between 91 and 244) and the maximum daily SR occurs in June, as shown in Fig. 2.4. These results indicate very good agreement between the calculated data and the climatic conditions, because during hot months in Kuwait (April – August) the solar altitude angle β reaches its highest values from 64.69° on 1st of April to 83.85° on 30th of June and again down to 68.77° on 31st of August (see Fig. 2.5), this explains the high temperatures in Kuwait during these months. This is in conformity with the clear sky (cloudless) atmospheres and high clearness index K_t values for these months with the average K_t varying between 0.56 in April to 0.67 in August (see Table 2.2). Even for the remaining months of the year (September – March), Kuwait has high values for daily or averaged monthly SR on horizontal surfaces with a minimum value of not less than 2902 Wh/m^2 occurring in December, which is still very high if we compare it to the daily or monthly SR in some cities in Europe; for example London has monthly averaged SR on horizontal surfaces of not more than 2800 Wh/m^2 in June.

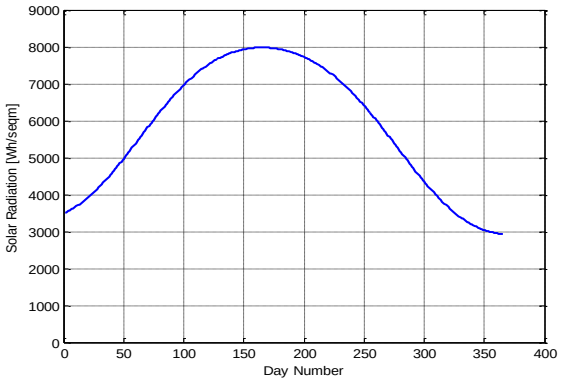

Figure 2.3: Daily global SR intensity on horizontal surfaces in Kuwait area (Wh/m^2 –day)

In general, for the daily SR on horizontal surfaces, the maximum value (on the summer solstice of 21 June) is 7959 Wh/m^2, the minimum value (on the winter solstice of 21 December) is 2902 Wh/m^2, while for the equinoxes (21 March and September) it is 6210 Wh/m^2-day and 5909 Wh/m^2, respectively. The monthly averaged global SR intensity on a horizontal surface in Kuwait area is plotted in Fig. 2.4. Table 2.4 shows the results for monthly averaged SR intensity on a horizontal surface at Kuwait area as a 22-year average obtained from NASA website. The closeness of the obtained results and these from NASA is evident, which validates the developed mathematical model.

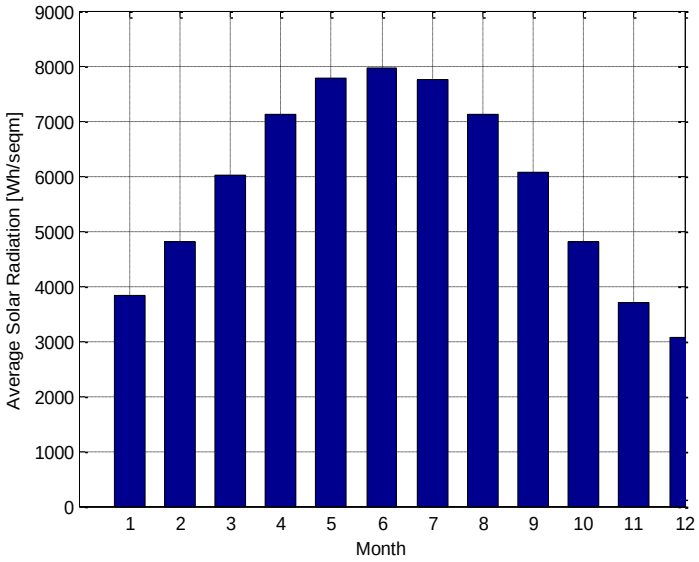

Figure 2.4: Monthly averaged global SR intensity on horizontal surfaces (Wh/m^2 –day)

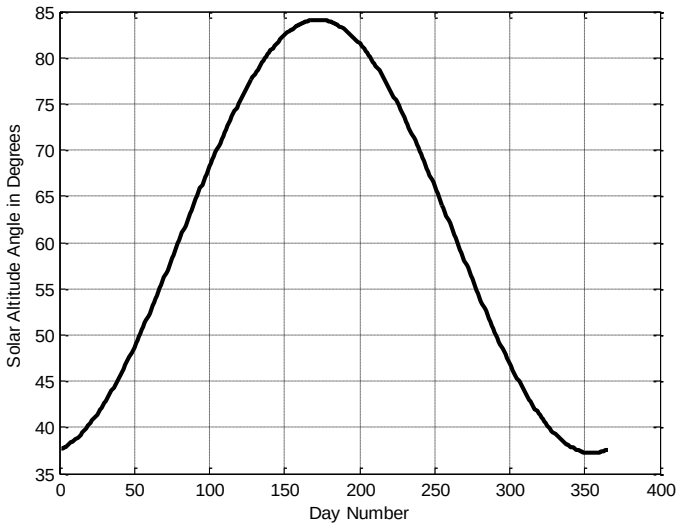

Figure 2.5: Daily solar altitude angle in degrees at solar noon over Kuwait area.

Fig. 2.6 focuses on the influence of diffuse radiation on the total SR over Kuwait area and shows both the global SR and the total SR after subtracting the diffuse insolation for each day. The resulting curves typically predict that about 3% to 12% of the total

horizontal SR on a clear day will be diffused. It's obvious that the hotter and sunnier months in Kuwait region (April – September) the average daily SR is about 8 kWh/m^2 and less than 5% of the radiation is scattered. Whereas, in December and January the SR is around 5.25 kWh/m^2 and about 12% is diffused into sky. Moreover, Table 2.5 estimated the total SR that will be used later in the proposed PV model.

Table 2.4: Monthly Averaged Global Insolation Incident on Horizontal Surface at Kuwait Area (kWh/m^2/day)

Latitude 29.33^o Longitude 47.5^o	**22-Year Average S_G**
January	3.89
February	4.96
March	6.09
April	6.91
May	7.80
June	8.16
July	7.76
August	7.29
September	6.28
October	5.05
November	3.82
December	3.26
Annual Average	**5.94**

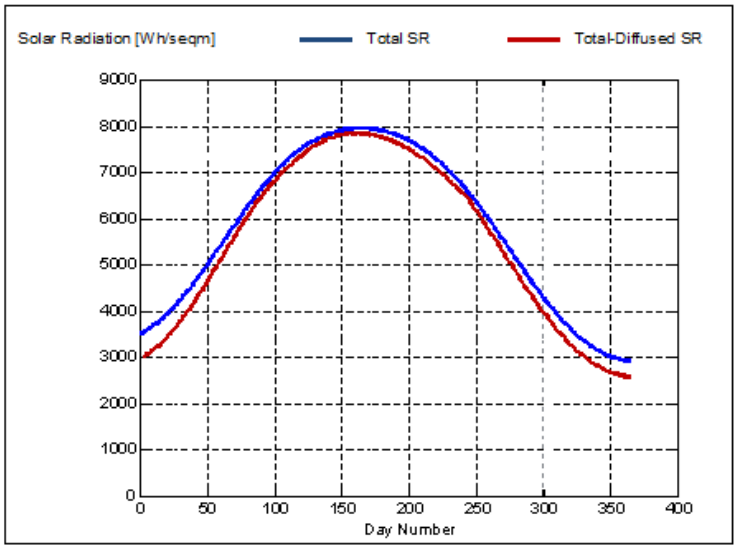

Figure 2.6: Daily global and total SR on horizontal surfaces over Kuwait area (Wh/m^2)

Table 2.5: Monthly Averaged Total SR over Kuwait Area (kWh/m^2/day)

Latitude 29.33^o Longitude 47.5^o	**25-Year Average S_H**
January	3.19
February	4.39
March	5.77
April	6.81
May	7.68
June	7.94
July	7.58
August	7.11
September	6.09
October	4.84
November	3.46
December	2.82
Annual Average	**5.64**

2.5.2 Results of Hourly Global SR on Horizontal Surfaces at Kuwait Area

The results obtained for the hourly SR on horizontal surfaces is graphically shown in Figs. 2.7 to 2.9 for selected days in a specific months of the year. The hourly SR is calculated every hour with a range according to the solar time *t* in hours (i.e. LAT) from sunrise to sunset. It is clear that the hourly SR is increased from the sunrise hour *H* and reaches its peak at solar noon and then decreases until the sunset hour. It can be easily noticed that the peak hourly SR always occurs at solar noon (according to the longitude where γ equals 47.5º for Kuwait area) where the sun at its highest altitude in sky during its daily path.

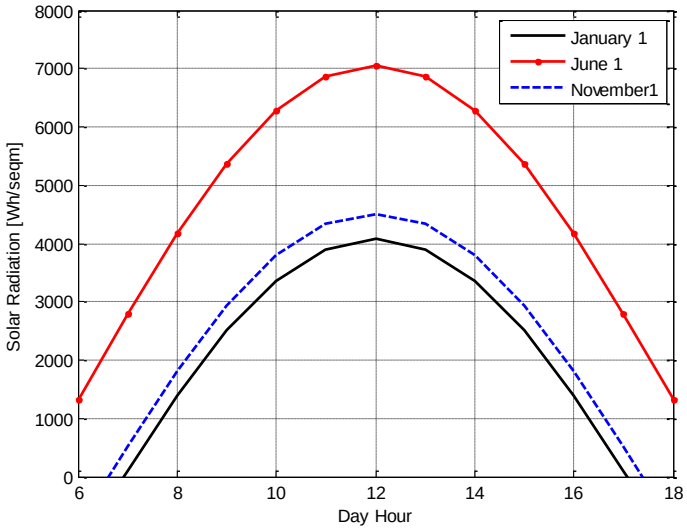

Figure 2.7: Hourly global SR intensity on horizontal surfaces over Kuwait area on 1st of Jan., June and Nov.

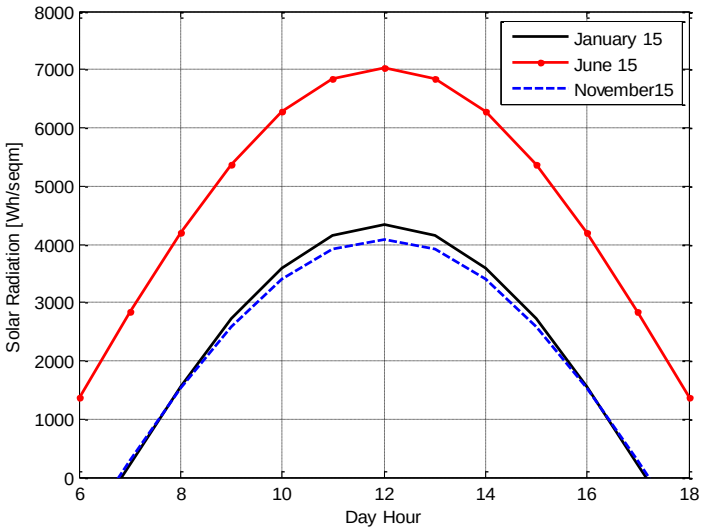

Figure 2.8: Hourly global SR intensity on horizontal surfaces over Kuwait area on 15th of Jan., June and Nov.

2.6 Average Monthly Power From Clear-Sky Insolation Over Kuwait Area

Kuwait atmosphere is almost cloudless during nine months and sometimes more. Therefore, the SR over Kuwait area with its related energy has been manipulated based

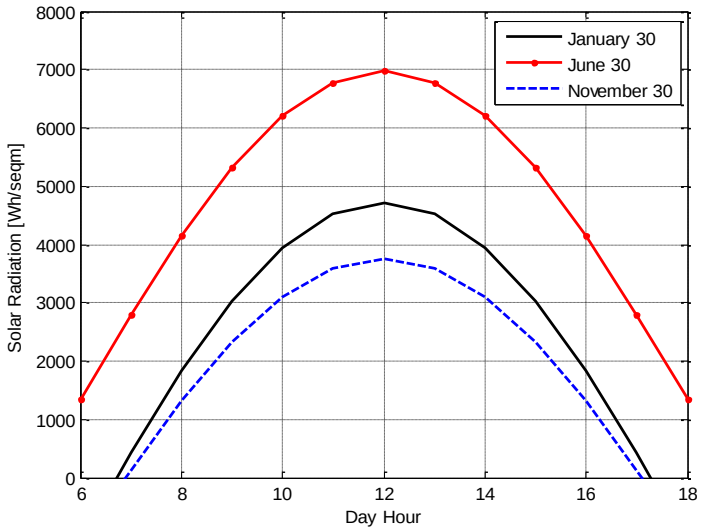

Figure 2.9: Hourly global SR intensity on horizontal surfaces over Kuwait area on 30th of Jan., June and Nov.

on a clear-sky condition. In addition to that, the average monthly electrical power has been calculated using the same condition. The average monthly power generated from the insolation which is expected to strike horizontal surfaces at Kuwait area is obtained from dividing eq. 2.10 by solar time during sun rise or sun set and the results are shown in Fig. 2.10 and Table 2.6.

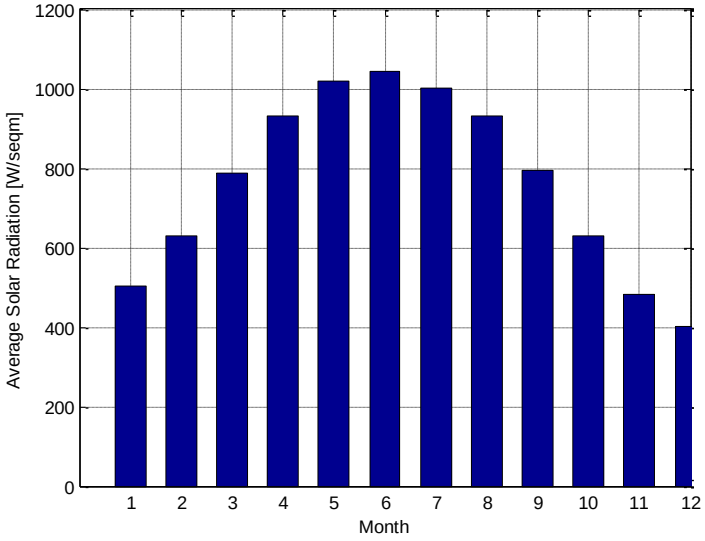

Figure 2.10: Monthly averaged clear sky global SR incident on horizontal surfaces over Kuwait area in (W/m^2)

In the same manner, the average monthly power generated from the total SR without the scattered radiation is calculated from dividing eq. 2.15 by solar time during sun rise or sun set. It yields the solar power received per unit area at horizontal surfaces in W/m^2 that can be delivered to the photovoltaic cells at cloudless weather as shown Table 2.7. The resulting data in Table 2.5, Fig. 2.4 and Fig. 2.6 will be used later for the proposed GCPV system.

Table 2.6: Monthly Averaged Global SR Incident on Horizontal Surfaces at Kuwait Area (W/m^2/day)

Month	S_G **(W/m^2)**
January	501.90
February	628.17
March	787.80
April	931.71
May	1017.63
June	1042.70
July	1000.61
August	930.86
September	794.48
October	628.84
November	483.63
December	401.02

Table 2.7: Monthly Averaged Total SR Incident on Horizontal Surfaces at Kuwait Area ($W/m^2/day$)

Month	S_H (W/m^2)		Month	S_H (W/m^2)
January	478.12		July	981.23
February	591.44		August	897.41
March	743.70		September	752.95
April	908.16		October	587.28
May	989.89		November	452.97
June	1009.33		December	377.86

2.7 Conclusions

The potential of using solar energy in Kuwait has been identified and analysed in this chapter. The fundamental solar models have been modified for estimating solar data in Kuwait for any day of the year and for any hour of the day. The obtained results demonstrate that Kuwait has an abundance of solar energy capability due to almost cloudless atmosphere for nine months and twelve hours solar time a day over the year. Also, Figs. 1.4, 2.4 and 2.9 show that the peak load matches the maximum incident SR and its relative averaged electrical power and these results are very promising in terms of the capabilities for Kuwait to use solar energy in electrical power generation. The daily global and monthly averaged solar intensity on horizontal surface at Kuwait is ranging from 3 kWh/m^2 in winter to 8 kWh/m^2 in summer. Diffuse insolation data is extracted analytically and analysed from previous measured data on a horizontal surface. In the worst cases, the difference between global SR and total SR without the scattered radiation over Kuwait area is not exceed 450 kWh/m^2 during the year. Monthly averaged clear sky global solar radiation on horizontal surfaces at Kuwait area is ranging from 500 $W/m^2/day$ to 1042 $W/m^2/day$.

Using the solar energy as an alternative energy source in Kuwait is expected to contribute to the development and improvement of Kuwait grid by eliminating power system quality problems, reducing environmental impacts, reducing electricity prices, savings in reduction of joule losses by decentralized production of electricity, improving the quality of service in peak hours, improving the continuity of service by shaving of consumption peaks, savings in investments for additional distribution equipment and saving in investments for additional power production. This will be the subject of future work.

Chapter 3
Modelling and Sizing of the Photovoltaic Module and Array

3.1 The Necessity for Photovoltaic (PV) Energy Conversion

A solar photovoltaic (PV) cell is a technology that converts SR into a DC electric current. Solar PV panels convert daylight, rather than direct sunlight, into electricity – so even in dusty conditions (typical for Kuwait) they can still be relied upon to produce energy. The electricity produced by PV cells can be used to deliver power to distributed areas, such as residential and commercial areas or it may be exported to support national utility grid needs.

Solar PV power is clean, silent and renewable energy source with no harmful emissions and totally environmentally friendly. Solar PV panels may also bring other advantages to buildings, such as insulation and security [27].

There are four reasons that can be put forward for the general interest and research in PV. First, its long-term energy potential is tremendous [28]; almost everywhere on earth the PV cells seize enough solar energy to supply the electrical load provided that enough storage is installed. Secondly, the increasing demand for electrical energy will be accompanied by a geographical shift [29], and one of the largest growth rates is situated in Gulf countries in the Middle East. Thirdly, PV electricity is a very attractive approach as it makes stand-alone or large- scale systems which are fuel free and highly reliable. Moreover, the decentralised electricity generation is necessary for almost all of the developing countries. Such decentralised power generation capability is an excellent companion to solar energy [30]. Finally, solar PV cells costs are decreasing rapidly in price nowadays making PV electric power affordable and competitive especially in the Sunbelt areas of the world [31].

3.2 History and Development of PVs

The history of PVs began in 1839 [32], when Becquerel published his work on photoelectric experimentation with acidic electrolyte solutions and he was able to cause a voltage. Almost 40 years later, Adams and Day were the first to work on PV effects in solid-state [33]. They built cells made of selenium and they studied its energy conversion efficiency (1% to 2% efficient). The close match of the spectral (colour) sensitivity of selenium (copper oxide) cells that they made it with that of the human eye made these cells desirable for a wide range of photometric applications [34], in fact, they are still used for that purpose today. Albert Einstein published a theoretical

explanation of the PV effect in 1904 as a part of his development of quantum theory [35].

Intensive research conducted on selenium and many other semiconductor compounds or metal oxide type barrier devices during 1920s and 1930s provided the foundations for the theoretical understanding of PV potential barrier solar cells and their mathematical modelling. After considerable theoretical and experimental work, which started in 1930s and carried on with great vigour during 1940s, the Bell Telephone Laboratories produced the first practical solar cell in 1954 [36]. This cell was of the planer junction single crystal silicon type. At the same time, a significant technological progress in modern electronics in general and PVs in particular, was due Czochralski, a Polish scientist, who began to develop a method to grow perfect crystals of silicon [37] by forming p-n junctions using high-temperature vapour diffusion. During the late 1940s and early 1950s, the Czochralski's process was used to make the first generation of single-crystal silicon PV and that technique continues to dominate the PV industry today.

In 1950s there were several attempts to commercialize PVs, but their cost was prohibitive [38]. PVs, as a practical energy source arrived in 1958 when they were first used in space for the Vanguard I satellite, because the weight and the reliability were more important than the cost for space vehicles. From that time PVs cells have played pivotal role in supplying electrical power for satellite and other space vehicles. During the energy crisis in 1970s, the development works on PV cells, which were supported by the space programme, began to pay back on the ground. Therefore, the first step in PV cells efficiency improvement was announced in 1972 [39]. Efficiency increased for the PV cells applications in space by almost 30%, and this improvement was achieved by revising the existing theories, increasing the cell response, decreasing the internal resistance of the PV cell to about 0.05 Ω and improving the charge carrier collection process within the cell [40]. Furthermore, in 1972 another new development was announced. It was the Vertical Multi- Junction (VMJ) PV cell device [41]. The VMJ device is an experimental array that has been assembled from the silicon cells and tested. It constructed from many alternate layers of n-type and p-type silicon and they form a multilayer stack.

Higher efficiencies (Fig. 3.1) and lower cost brought PV cells and modules closer and closer to reality by the end of 1980s [42], their applications included calculators, highway lights, signs, traffic lights and small home systems.

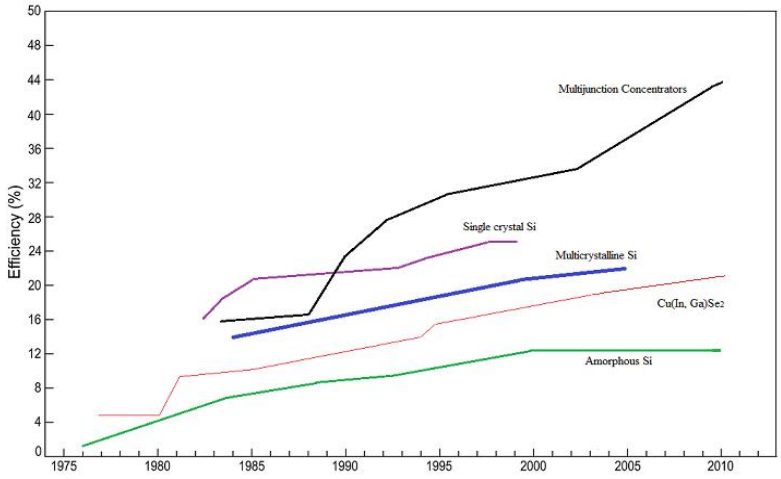

Figure 3.1: Best laboratories PV cell efficiencies for various technologies. (From National Centre for Photovoltaics, www.nrel.gov/ncpv 2010)

In 1990s and 2000s the cost of the PV module dropped dramatically (Fig. 3.2) while the efficiency was increasing. From year 2000 to 2010, the developing countries (with China, Brazil and India) production of PVs had increased from 600 MWp up to 11300 MWp with annual growth rate of around 50% as shown in Fig. 3.3.

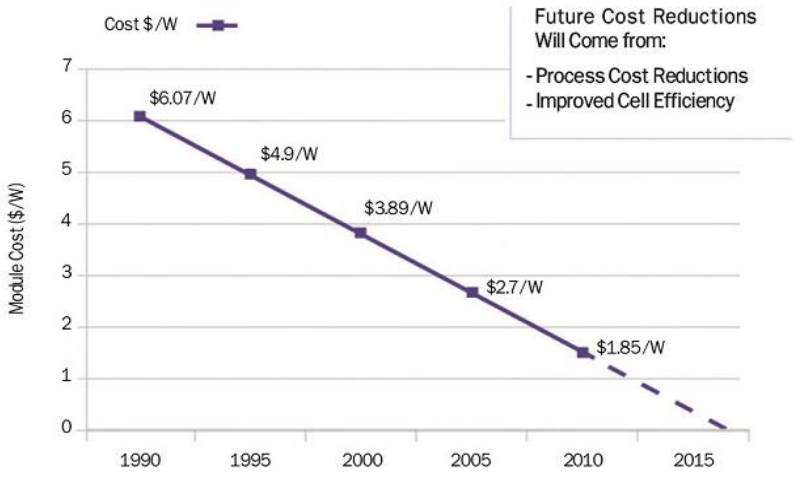

Figure 3.2: PV module manufacturing cost per watt (Source: SEMI PV Group)

3.3 Some Basics about PV Cells

SR is composed of photons with appropriate energy, and any material or device that is capable of converting this energy into an electrical current is called photovoltaic (PV). When SR interacts with a PV cell, a reflection of some power at the cell surface occurs and a useful absorption begins. This absorption results in the generation of electron-hole pairs and a parasitic absorption heat [43]. A photo-generated current is produced and

collected towards the external contacts. This generated current is a DC current and it has a specific value depending on the amount of SR that falls on the PV cell surface, the type of the PV cell circuit and the number of PV cells.

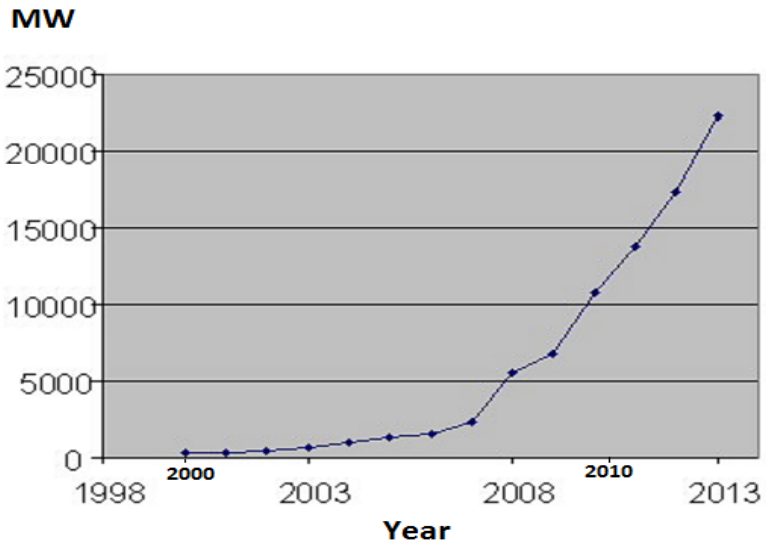

Figure 3.3: Growth of the PV industry in developing countries (source: EPIA PV Group)

3.3.1 The Equivalent Circuit for a PV Cell

All basic circuits for the PV cells stem from one simple equivalent circuit model. It consists of a real diode in parallel with an ideal current source as shown in Fig. 3.4 [43]. The ideal current source is driven by SR to which it is exposed and it delivers a dc current in proportion to SR.

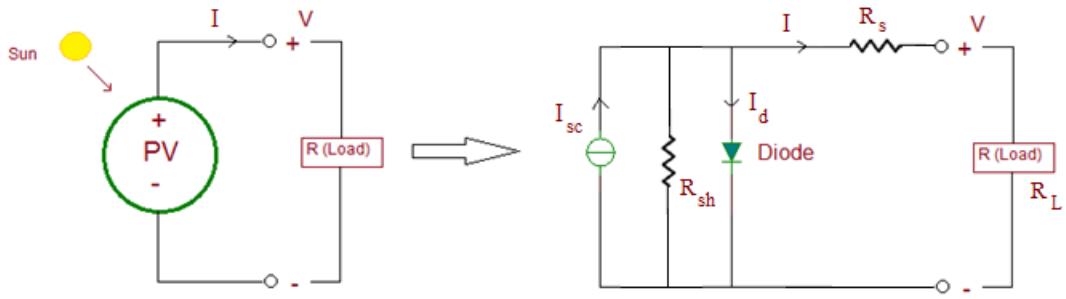

Figure 3.4: Equivalent circuit of PV cell

For the equivalent circuit of PVs, there are two important factors that we have to consider. First, the short-circuit current I_{sc} (when the cell terminal voltage is zero), as shown in Fig. 3.5a, and secondly, the open-circuit voltage V_{oc} (when the cell terminal current is zero) as shown in Fig. 3.5b.

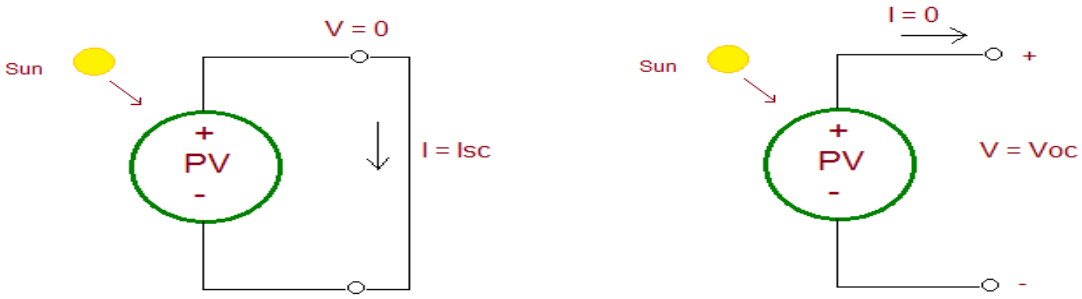

(a) Short-circuit current (b) Open-circuit voltage

Figure 3.5: PV cells have two important factors (a) I_{sc} (short-circuit current) (b) V_{oc} (open-circuit voltage)

3.3.2 Characteristics of PV Cells and their Ranges

The fundamental electrical characteristics of the PV cells and their ranges in commercially available cells are the very prominent parameters in the modelling of PV cells [44]. A number of variables influences these typical characteristics and depend upon make model and geometry of the cell and upon the composition of the photosensitive material. Therefore, the purpose of the listing below is only to show the obtainable values for each characteristic but these values are not necessarily to be loaded as inputs to the PV cells all at the same time [45]. The characteristics of the PV cells and their ranges are listed below:

- Output current, I_{sc}, varies with incident SR, active area of the PV cell and load resistance. The typical values of the PV cell current range from 5 mA to 2.1 A.
- Output voltage, V_{oc}, directly proportional to active area and incident SR. The typical values of the PV cell voltage range from 0.3 V to .85 V.
- Output power varies with incident SR, active area and load resistance. Maximum power occurs when the load resistance is equal to the internal resistance of the PV cell. The typical values of the PV cell output power vary between 15 mW and 2W.

3.3.3 PV Cells Wiring

An individual cell is characterised by an open-circuit voltage of 0.55 V to 0.6 V. Since the *I-V* curve of the PV cell will vary according to temperature, we can notice that the PV cell voltage range differs within the typical values and according to its sensitivity to temperature. When a PV cell is exposed to higher temperature (excess of SR), the V_{oc} decreases more significantly and vice versa. But no PV system consists of only one cell. Therefore, a module is the cornerstone for PV applications. A module is a weather-

resistant package consisting of a number of PV cells pre-wired in series. The series connection of 34 to 36 cells therefore results in a module open-circuit voltage of 12 V, even though it is capable of delivering much higher voltages than that [44]. A common large module available commercially consists of 72 cells [46]. Some of these 72-cell modules act as 24-V modules if all 72 cells are wired in series or as 12-V modules with two parallel strings having 36 series cells in each. A combination of modules is called an array as shown in Fig. 3.6.

The way of wiring the modules inside an array is an important parameter in PV system design because it is determining the output power [47]. In order to increase the output current of the PV array, modules can be connected in parallel and to increase the voltage of the array, modules can be wired in series. To increase the output power, arrays are built as a combination of series and parallel modules.

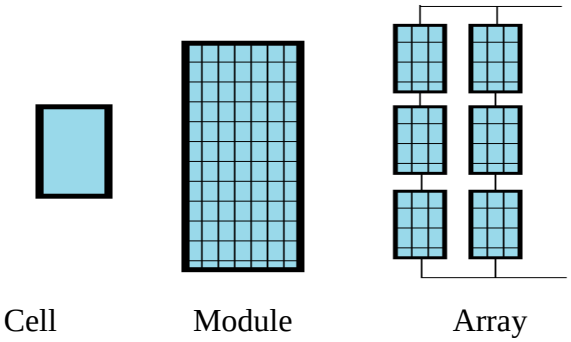

Figure 3.6: PV cell, module and array

The *I-V* characteristics of series-wired modules may be found by adding, for each current, the different voltages of the individual module as shown in Fig. 3.7a. On the other hand, for parallel-wired modules the currents of the individual module must be added at each voltage in order to find the overall *I-V* curve as shown in Fig. 3.7b.

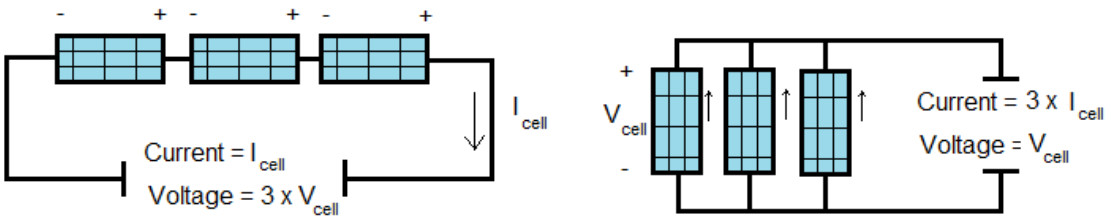

(a) Series connection (b) Parallel connection

Figure 3.7: PV modules wiring (a) Series connection of modules (b) Parallel connection of modules

A combination of series and parallel connections between modules inside an array gives a high power output and we can argue that there are only two ways of wiring the modules [48]:

[1] The parallel modules can be wired together first and then combined in series as shown in Fig. 3.8a.

[2] The series modules can be wired as strings and the strings wired in parallel as shown in Fig. 3.8b.

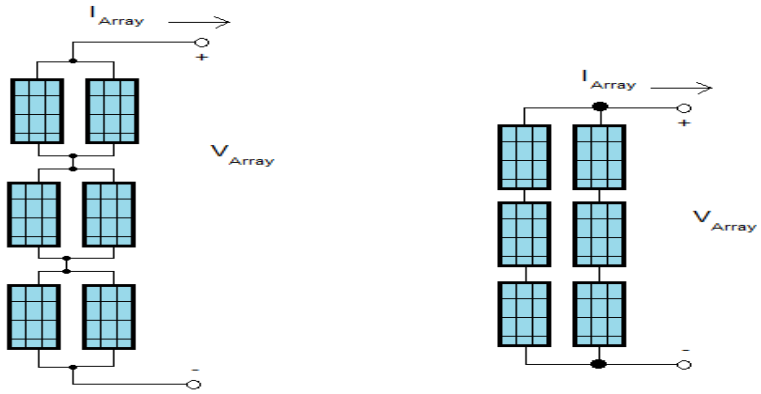

(a) Two parallel modules then combined in series with others

(b) Two parallel strings of three series modules each

Figure 3.8: Two ways of wiring the PV modules in an array

The total *I-V* characteristic of the array is a sum of the individual module *I-V* characteristics, and both ways give the same resultant *I-V* curve. The second way of wiring (Fig.3.8b) is preferred as it has the advantage to deliver power to the system at a prescribed voltage even when one of the series circuits is faulted, whereas the first connection (Fig. 3.8a) does not have this useful characteristic.

3.4 Modelling of the PV Modules and Arrays

The individual PV cells must be connected to provide an appropriate electrical DC current, voltage, and power. The design of a PV module depends on the application for which it is to be used and the expansion of the PV applications in recent years has led to a range of alternative module designs and sizes and their suitability in different scenarios. The PV array consists of a number of modules connected in series and in parallel to provide the necessary electrical outputs.

3.4.1 Type of the Selected PV Module

There are many types of such modules on the international markets, the best of which is the silicon mono-crystalline (SMC) PV type. This PV type is the world's single most

powerful PV module with rated power ranges between 120 W to 320 W and efficiency of not less than 23% and it has the following specifications [44]:

- The module delivers maximum power in large systems that require higher voltages and currents.
- It resists the environmental effects, such as dust, humidity, and hot areas. All these effects are typical for Kuwait region.
- Every module is tested utilizing a calibrated solar simulator to ensure that the electrical ratings are within the specified tolerance for power, voltage, and current.
- The electrical data for this module is listed below:
  - [1] Short-circuit current, I_{sc}, is 6.5 A per module.
  - [2] Open-circuit voltage, V_{oc}, is 63.2 V per module.
  - [3] Maximum output power, P_{max}, is 300 W per module.
- This type of PV module is independently certified to meet the IEEE, IEC, and UL standards.

Therefore, this type of PV module has been chosen for this research work.

The electrical data of this module applies to the standard test conditions (STC) of SR at the cell level which are 1000 W/m^2 (S_s = 1000 W/m^2) with the spectrum air mass ratio of 1.5 (AM = 1.5) and a cell temperature of 25°C. Manufacturers always provide performance and electrical data of the PV cells under these operating conditions. This module is then used in an electrical circuit with other similar modules to form a PV array. The SMC type of a PV module is a 63-V module that has 216 field-wired cells connected in three parallel strings having 72 series cells in each as shown in Fig. 3.9.

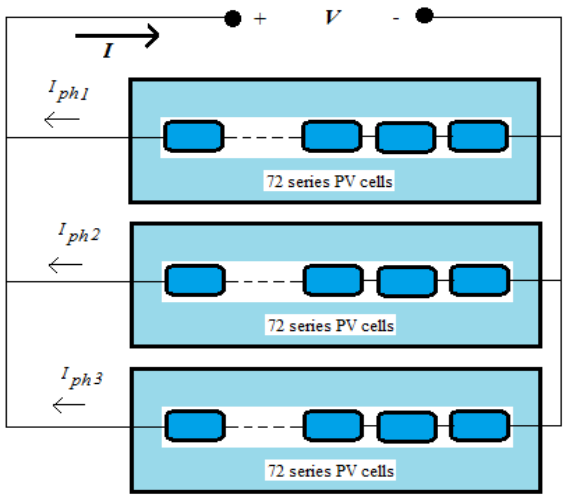

Figure 3.9: Wiring of one silicon mono-crystalline (SMC) PV module

3.4.2 The Selected Module *I-V* Characteristics

The most meaningful test of a PV cell and module is the measurement of an *I-V* curve [49]. This curve shows the behaviour of the PV system under all load conditions from open circuit to short circuit. *I-V* curves can be taken for any portion of an array provided there is electrical access. Irregular shapes in the curve are indications of problems such as electrical faults. The *I-V* curve of the entire module will also give the peak power rating of the module and it's simply a plot of a cell, or a module, or an array current versus voltage and it can be used to measure the maximum power of the system by plotting the *P-V* curve. Based on the equivalent circuit of PV cell in Fig. 3.4, the corresponding *I-V* characteristic may be described as below,

$$I = I_{ph} - I_d - I_{R_{sh}} \tag{3.1}$$

a well-known Shockley equation gives the ideal diode equation as,

$$I_d = I_o \cdot \left(e^{\frac{qV_d}{BT}} - 1 \right) \tag{3.2}$$

Substitute eqn. 3.2 and $I_{R_{sh}} = \left(\frac{V + IR_s}{R_{sh}} \right)$ into eqn. 3.1, we get

$$I = I_{ph} - I_o \cdot \left(e^{\frac{q(V+IR_s)}{aBT}} - 1 \right) - \left(\frac{V + IR_s}{R_{sh}} \right) \tag{3.3}$$

but the PV cell's reverse saturation current is given by,

$$I_o = I_{or} \left[\frac{T}{T_r} \right]^3 \exp[\frac{qE_B}{Bb}(\frac{1}{T_r} - \frac{1}{T})] \tag{3.4}$$

and the photon current (photo-generated current) is equal to,

$$I_{ph} = \left[I_{SCT} + K_I (T - 298) \right] \times \left(\frac{S_H}{1000} \right) \tag{3.5}$$

where

I = cell output current (A).

V = cell output voltage (V).

I_{ph} = photon current or photo-generated current which equals to the short circuit current, I_{sc}, A (V=0).

I_o = PV cell's reverse saturation current (dark current) = 0.424 *10^{-6} A (for SMC-PV).

R_{sh} = PV cell intrinsic parallel resistance (Ω).

R_s = PV cell intrinsic series resistance (Ω).

q = electron charge = 1.602 * 10^{-19} C.

B = Boltzmann's constant = 1.381 * 10^{-23} J/°K.

T = junction (cell) temperature or PV cell operating temperature = 25°C = 298 °K (for SMC-PV).

K_l = temperature coefficient of the short-circuit current (A/°K).

I_{STC} = short-circuit current at STC (A).

E_B = band-gap energy of the semiconductor (J).

b = ideality constant, between 1 and 2.

T_r = PV cell absolute temperature at STC = 301.18 °K.

I_{or} = PV cell's reverse saturation current at temperature T_r (A).

In equation (3.5), the photo-generated current, I_{ph}, is directly proportional to SR on the PV cell surface, S_H. Thus the value of the photo-generated current, I_{ph}, at any other insolation, S_H is given by

$$\left(\frac{I_{ph}(S_H)}{I_{ph}(S_S)}\right)=\left(\frac{S_H}{S_S}\right) \tag{3.6}$$

or,

$$I_{ph}(S_H)=\left(\frac{S_H}{S_S}\right)\times I_{ph}(S_S) \tag{3.7}$$

where, S_H is the monthly averaged SR incident on the modules surfaces and it has already been estimated in Chapter 2 for the Kuwait area. Substituting $I_{ph}\ (S_s)$ as 6.5 A, which is the short-circuit current of the module, and S_s of 1000 W/m^2, which is the standard SR at the cell or module level, into (3.7) yields

$$I_{ph}(S_H)=(6.5\times10^{-3}S_H) \tag{3.8}$$

It's obvious that in the PV cell model, I_{ph}, I_o, R_{sh}, and R_s are related to cells temperature and SR, and are not easy to be determined. This makes the engineering application very difficult. Manufacturers of PV arrays provide only a few experimental technical parameters such as open-circuit voltage V_{oc}, short-circuit current I_{sc}, the maximum power point voltage V_m, the maximum power point current I_m, and the maximum power point power P_m. Normally, R_{sh} is between 100 Ω and 10000 Ω, so the current $I_{R_{sh}}$ can be ignored compared with photon current I_{ph}. R_s is less than 1 Ω, so $I_{ph} = I_{sc}$. This will simplify the PV model to match with the parameters provided by industry.

Under open-circuit state, $I = 0$, $V = V_{oc}$

$$I = I_{sc}\left[1 - a_1\left(e^{(\frac{V}{a_2 \cdot V_{oc}})} - 1\right)\right] \tag{3.9}$$

where, a_1 and a_2 are the PV cell's constants at maximum power point. At maximum power point, when $V = V_m$, $I = I_m$

$$I_m = I_{sc}\left[1 - a_1\left(e^{(\frac{V_m}{a_2 \cdot V_{oc}})} - 1\right)\right] \tag{3.10}$$

under normal temperature,

$$e^{(\frac{V_m}{a_2 \cdot V_{oc}})} >> 1 \quad \text{and} \quad a_1 = \left(1 - \frac{I_m}{I_{sc}}\right) \times e^{(\frac{-V_m}{a_2 \cdot V_{oc}})} \tag{3.11}$$

Therefore, under open-circuit state

$$0 = I_{sc} \cdot \left[1 - \left(1 - \frac{I_m}{I_{sc}}\right) \cdot e^{(\frac{-V_m}{a_2 \cdot V_{oc}})} \times (e^{(\frac{1}{a_2})} - 1)\right] \tag{3.12}$$

under normal temperature,

$$e^{(\frac{1}{a_2})} >> 1 \quad \text{and} \quad a_2 = \frac{\left(\frac{V_m}{V_{oc}} - 1\right)}{\ln\left(1 - \frac{I_m}{I_{sc}}\right)} \tag{3.13}$$

Being seen, with common parameters like V_{oc}, I_{sc}, V_m, I_m, a_1 and a_2 can be calculated and the PV cell or module model can be created. Moreover, we can calculate V_m and I_m produced by the PV cell at different operating conditions. The output power of the module, P_m, is expressed by

$$P_m = V_m I_m \tag{3.14}$$

3.5 Results and Conclusions for the Modelling of the PV Module

The electrical data of the selected SMC-PV module and the results obtained from the proposed SR model in the previous chapter are used as input data to solve the governing equations for the PV module. Eqns. 3.1 to 3.14 are solved to predict the performance of a typical SMC-PV cell or module model. Results are shown in Figs. 3.10, 3.11, 3.12,

and 3.13 as the *I-V* characteristics of the selected module at different monthly averaged SR intensity over Kuwait area. It is easy to notice that the open-circuit voltage of the module ranges between 56 V and 61 V (actual value is 63.2 V at STC) and these differences are related to the differences in SR for each month. Moreover, the value of the short-circuit current of the PV module ranges from 2.8 A to 6.8 A (actual value is 6.5 A at STC). The dotted points in these curves show the maximum power point which is the operating point of the module at each month, and this signifies the importance of the *I-V* curve of the PV module.

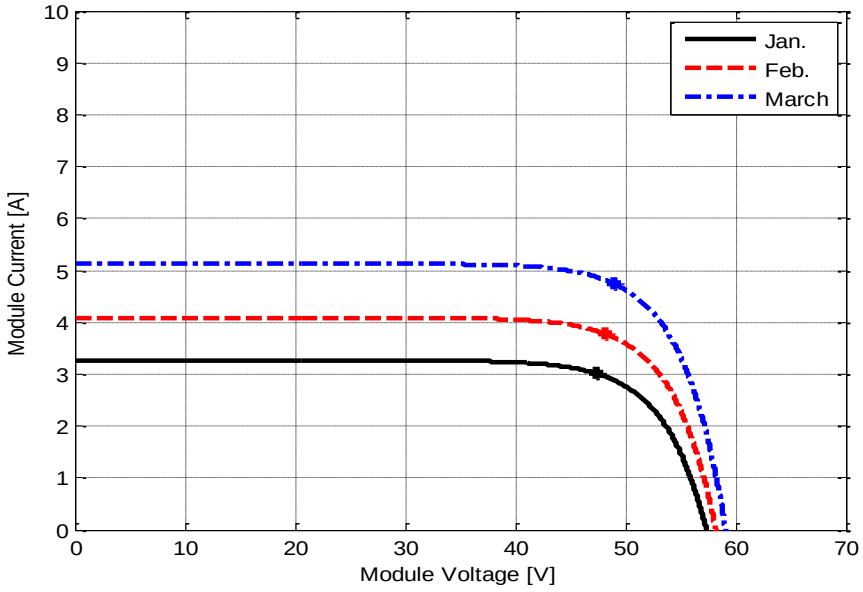

Figure 3.10: *I-V* characteristics of a typical SMC-PV module at different SR intensity from January to March

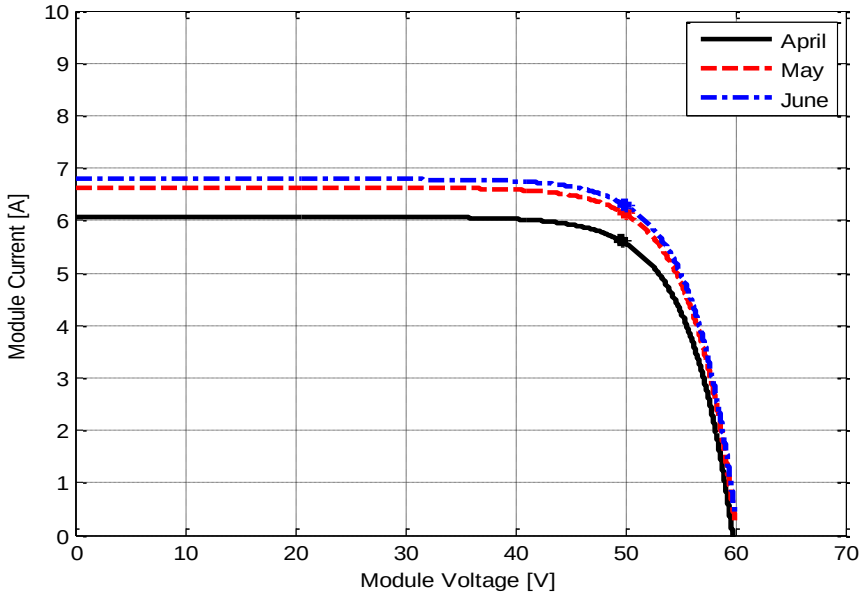

Figure 3.11: *I-V* characteristics of a typical SMC-PV module at different SR intensity from April to June

The *I-V* curve of the entire module or array will give the peak power rating of the PV systems. Substituting the values of *I* (module current) for each month into eqn. 3.7 and letting *V* (module voltage) vary between 0 and 70 V yields the DC output power rating of the module for different months (see appendix A), as illustrated in Fig. 3.14 to 3.17. It is obvious that the rated power of the module is directly proportional to the SR intensity. Therefore, the rated power of the module in June has the highest value (320 W) due to the peak SR intensity occurs in June.

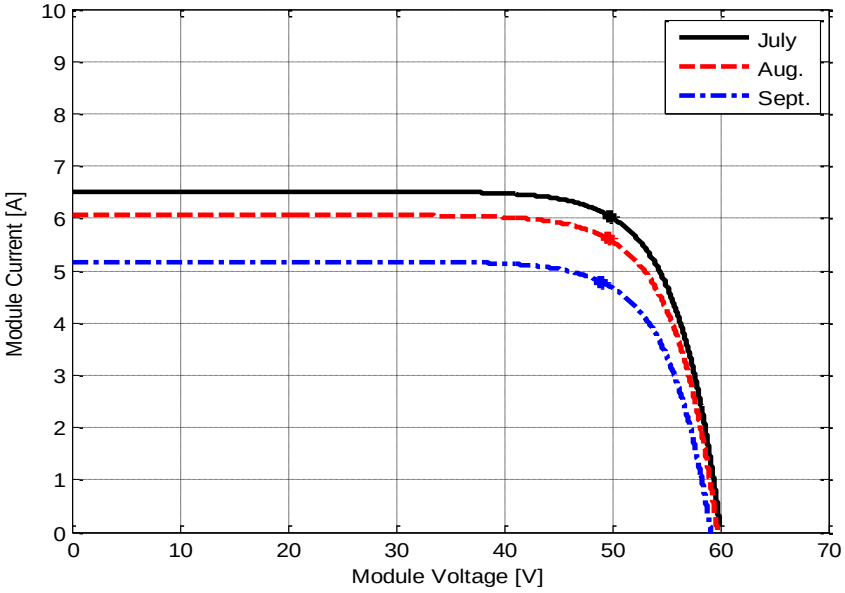

Figure 3.12: *I-V* characteristics of a typical SMC-PV module at different SR intensity from July to September

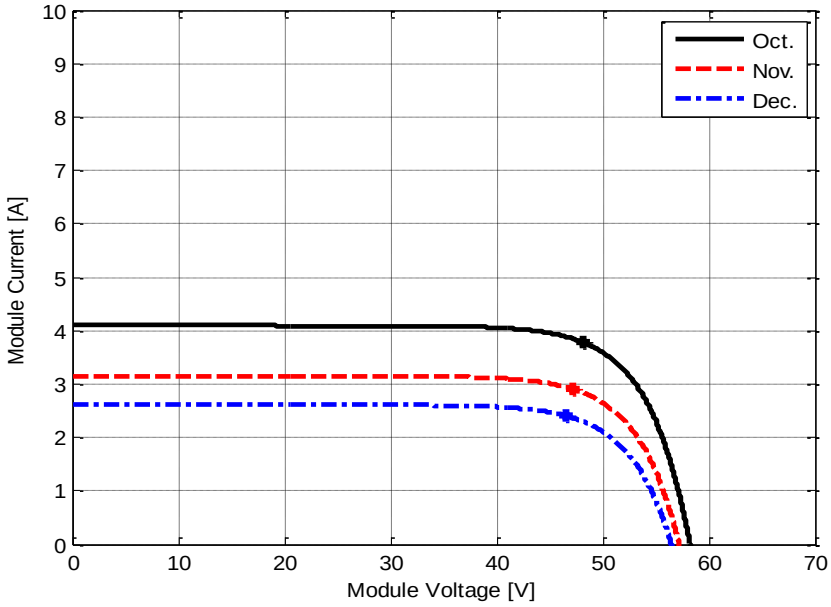

Figure 3.13: *I-V* characteristics of a typical SMC-PV module at different SR intensity from October to December

Moreover, the maximum output power of the module is ranges from 120 W in December to 320 W in June. These maximum values of the DC output power of the PV module are of significance in the future works of the research.

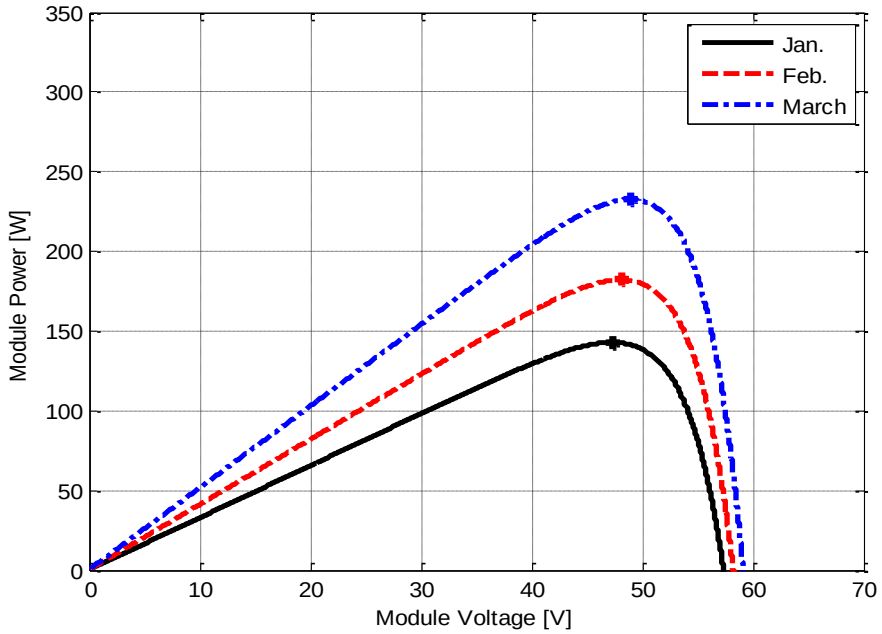

Figure 3.14: The output power of a typical SMC-PV module at different SR intensity from January to March

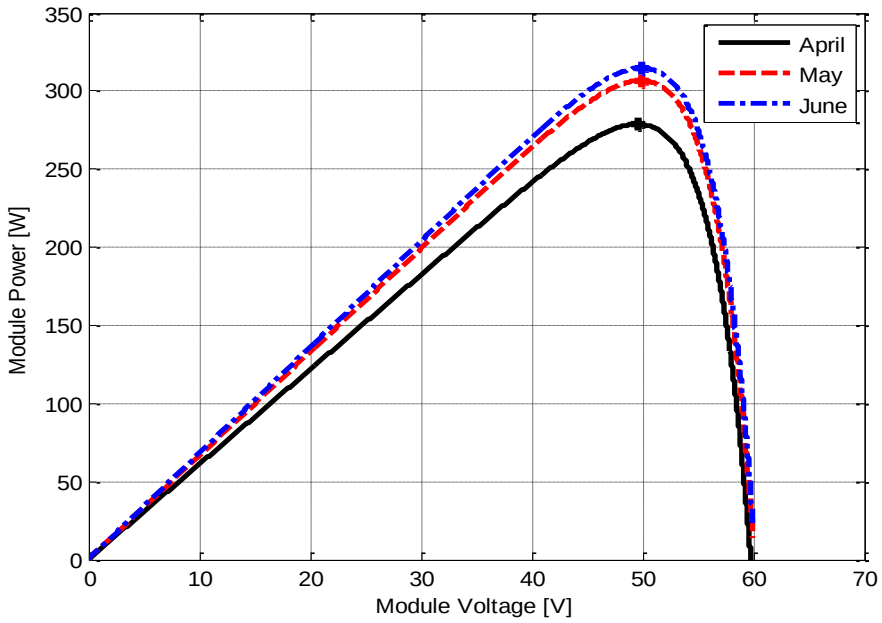

Figure 3.15: The output power of a typical SMC-PV module at different SR intensity from April to June

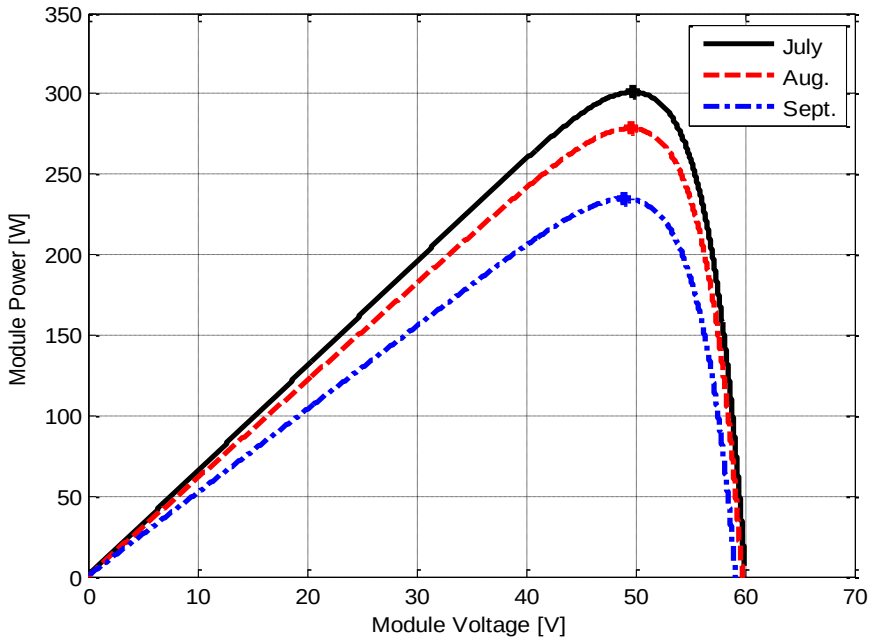

Figure 3.16: The output power of a typical SMC-PV module at different SR intensity from July to September

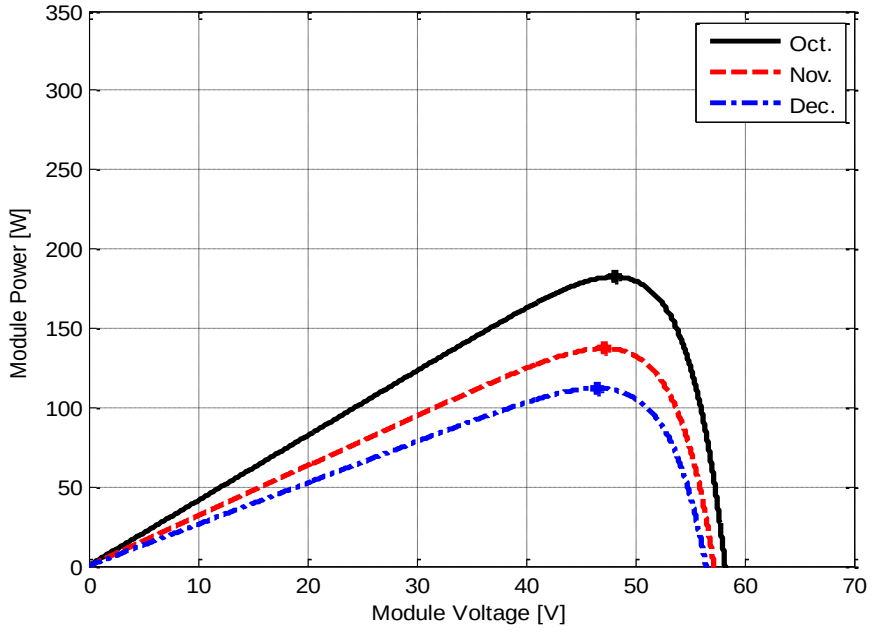

Figure 3.17: The output power of a typical SMC-PV module at different SR intensity from October to December

3.6 Types of PV Systems

The PV system consists of a number of interconnected components including PV cells or modules, electrical connections, mechanical mounting and a power conditioning unit (PCU) to convert the electrical output. This design is to accomplish a specific task which maybe to power a small calculator, to pump water from a well, to feed electricity

into the main distribution grid or one of many more possible uses of solar-generated electricity [50]. Accordingly, three commonly configurations of PV systems are encountered: systems in which load is directly connected to the PVs as in the case for most PV–powered water pumping systems, stand-alone systems that charge batteries perhaps with generator back-up and systems that feed power directly into the utility grid (grid-connected) or utility interactive (UI) systems in which PVs are supplying power to residential and commercial buildings.

Each PV system has its own attributes and all of these attributes contribute to the cost effectiveness of those systems. As shown in Fig. 3.18, the first system type has PVs directly coupled to their loads (PV-powered water pumping) without any power conditioning unit or batteries. These systems are the ultimate in simplicity and reliability and the least costly as well [51].

Stand-alone PV system (off-grid system) contains battery storage and a generator for back-up power as shown in Fig. 3.19. An inverter is needed to convert battery DC voltage into AC for conventional household electricity, but in case of low voltage is needed, everything run on DC and no inverter maybe necessary. The back-up generator is to top-up the batteries when SR is insufficient. Stand-alone PV systems have the following attributes:

- They can be very cost effective in remote locations where the only alternative maybe noisy and high-maintenance generators burning relatively expensive fuel.
- Extending the existing utility grid to the stand-alone system site (emergency cases) can cost hundreds of thousands of dollars per kilometre.
- The system suffers from the battery power losses and the well-off operation of the PVs most efficient operating point (reducing the system's efficiency) [52].

As shown in Fig. 3.20, grid-connected PV systems can be subdivided into central and decentralized grid-connected and both systems have a number of desirable characteristics:

- High reliability due to their relative simplicity.
- Offer the opportunity to generate significant quantities of large-scale energy near the consumption point, avoiding transmission and distribution losses.
- Assuring high PV efficiency according to their maximum power tracking unit.

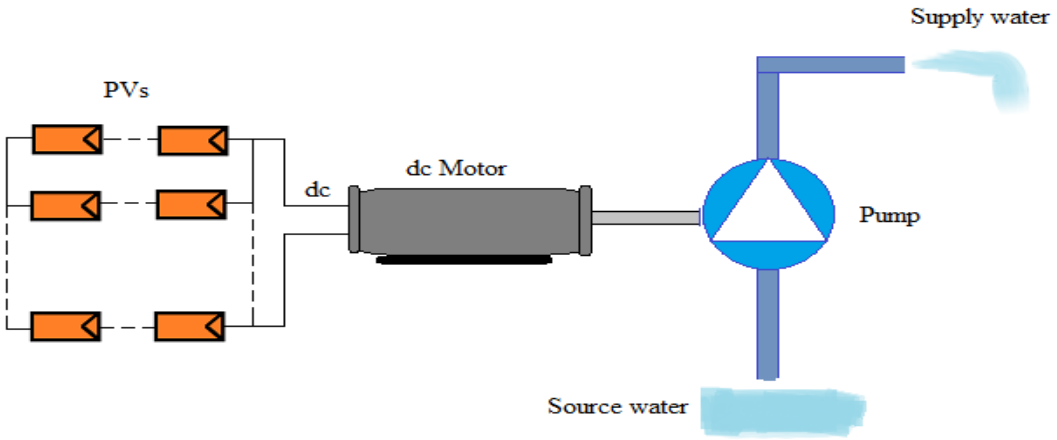

Figure 3.18: PV-powered water pumping system (conceptual diagram)

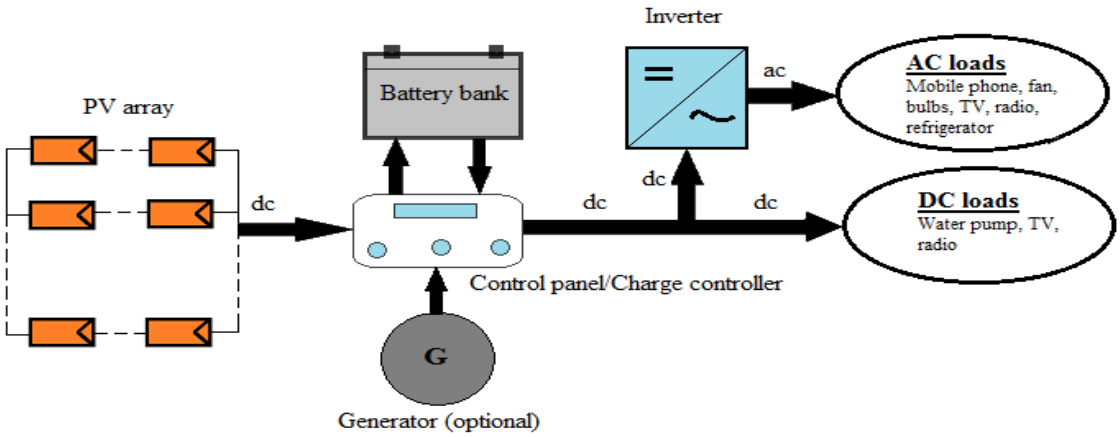

Figure 3.19: Stand-alone PV system with optional generator

- The economic value of their kilowatt-hour increases during the peak load times because of their ability to deliver a specified electrical power during the peaks (peak shaving).
- Their potential to be integrated into the structure of the building means that there are no additional costs for land [53].

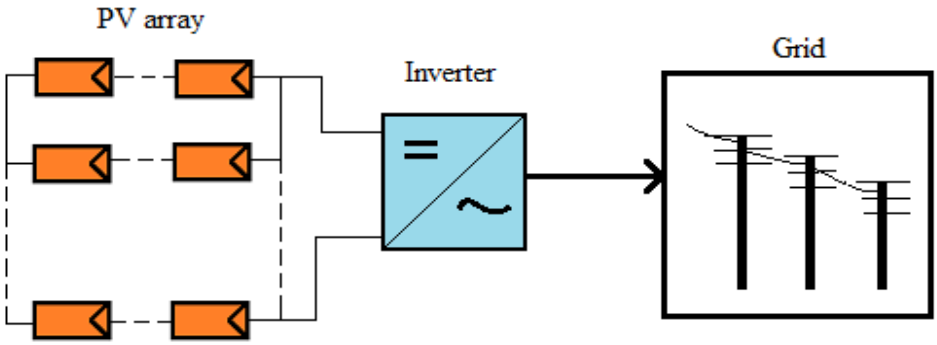

(a) Central grid-connected PV system

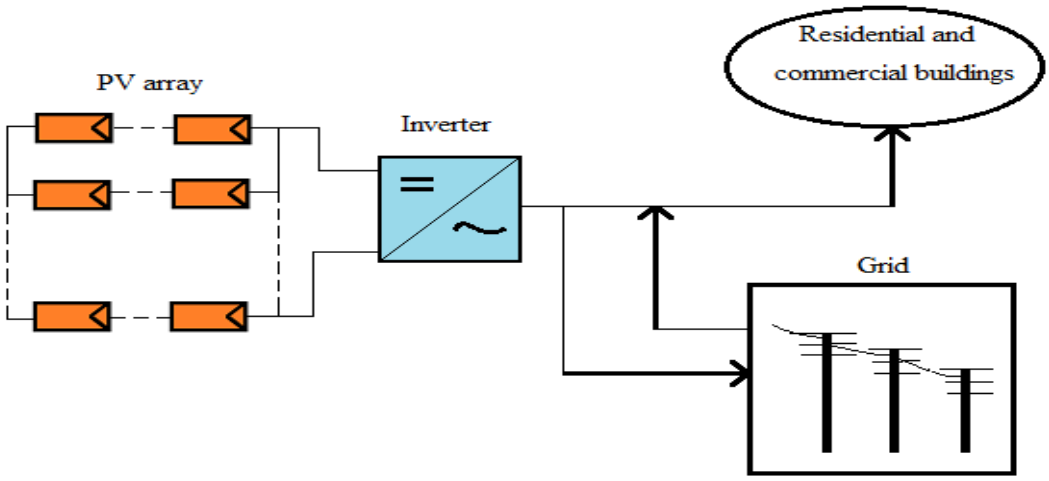

(b) Decentralized grid-connected PV system

Figure 3.20: Grid-connected PV systems

Grid-connected PV system with its desirable attributes gives promising power capabilities to be added to Kuwait energy network. Therefore, this chapter is focusing on the designing and sizing of the grid-connected PV system.

3.7 Grid-Connected PV System

The PVs in a grid-connected system operate in parallel with the conventional electricity distribution system. It can be used to feed electricity into the grid distribution network or to power loads which can also be fed from the grid. However, the PVs in this system deliver DC electrical power to a power conditioning unit (PCU) that converts DC into AC and sends power to the distribution area. Fig. 3.21 shows a simple diagram of a grid-connected or UI system at which PVs are supplying power to a distribution area such as residential and commercial loads or it can feed power into the power station itself.

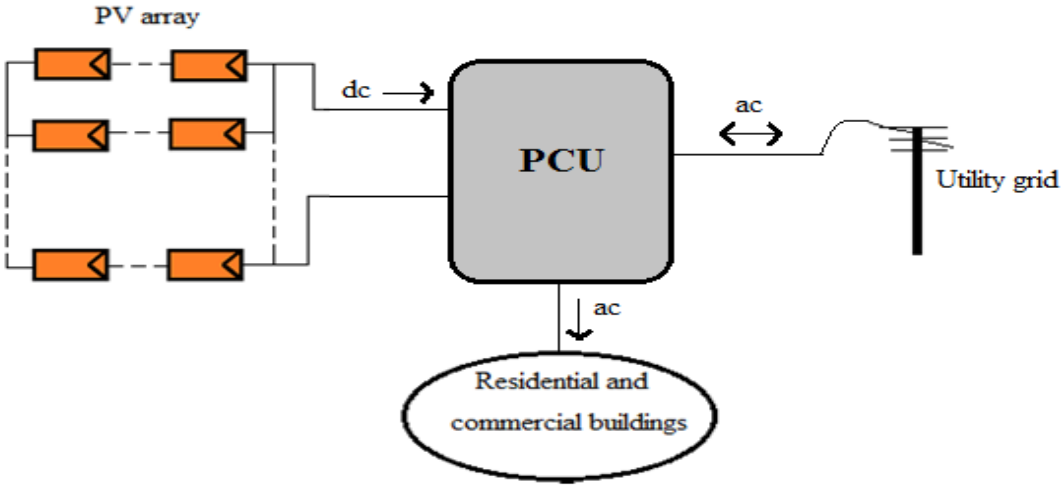

Figure 3.21: Simplified grid-connected PV system

The design of the GCPV system depends on the task it must perform and the location and other site conditions under which it must operate.

3.7.1 System Components

The principal components in a GCPV system are the PV arrays (which consist of PV modules with their wiring) and PCU with its control equipment. In Section 3.4, the SMC-PV type module has been selected to deliver maximum performance in large systems that require higher voltages. The specifications and the electrical data of this module had been illustrated. Moreover, the wiring of the cells inside the SMC-PV module had been demonstrated. It is often advantageous to include a PCU to insure that the PV system operates under optimum conditions. A DC-DC converter, inverter, protection devices (fuses, switches and circuit breakers) and maximum power point tracker (MPPT) are usually integrated into a single PCU as shown in Fig. 3.22.

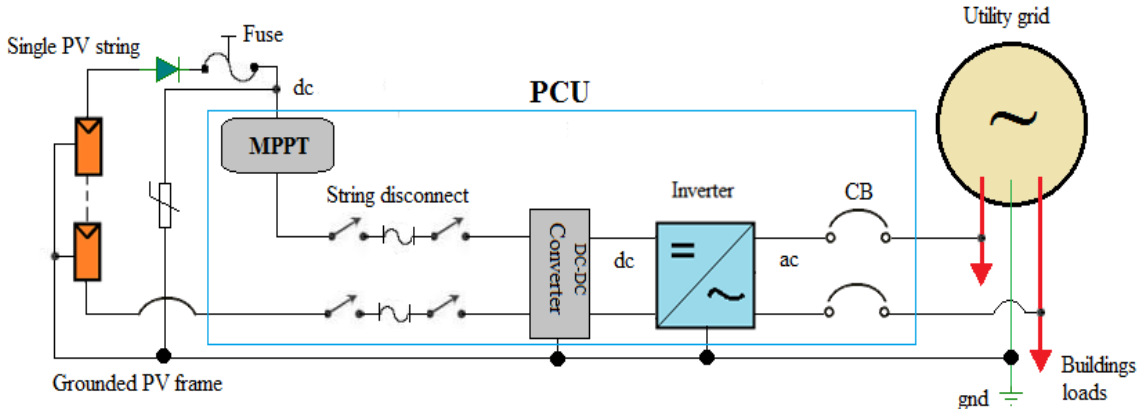

Figure 3.22: Principal components of a single power conditioning unit (PCU) in a GCPV system using a single series string of PVs

3.8 Sizing of the Grid-Connected PV System

One of the primary concerns in designing any PV system is the determination of the correct size of the PV array or panel to supply a required unit of energy at a specified reliability [54-56]. It is adequate to use monthly and annually averaged SR to determine array capacity because the dynamic behaviour of the PV system and the stochastic nature of SR also significantly influence the required array capacity. Therefore, the design should be done on meteorological data, SR and on the exact load profile of consumers over long periods. It is very important to be able to predict as accurately as possible the annual energy delivered by the system in order to decide whether it makes economic sense (see Chapter 4). Certain components will dictate some of the details, but what has already been developed on monthly and annually averaged SR provides a good

start to GCPV system sizing. It is nonetheless, system sizing is straightforward. The sizing process is to meet a desired amount of output energy in kWh required from the GCPV system and its objective is to minimize the difference between the electrical energy generated by the GCPV system and the required energy.

Sizing process is based on manual approach. This approach is based on iterative algorithm and is called sizing algorithm using iterative manual approach (*SAIMA*). Using this approach, a system designer is required to select a PV module and inverter from a list of PV modules and inverters before trying to match the PV module and inverter characteristics. Then, compute the PV panel or array size with its configuration as well as the electrical data of the prospective system. If the PV panel or array matches the inverter characteristics, the sizing procedure is reached its optimal case. Otherwise, repeat the same procedure after selecting another combination of PV module and inverter. A MATLAB program is used to develop and employ *SAIMA* equations. Fig. 3.23 shows the main stages that can be deal with in order to satisfy the conditions of *SAIMA*. The most frequently asked questions in sizing process are:

- How many kWh/yr are required?
- How many peak watts of dc PV power are needed to provide that amount?
- How much area will that system require?

The realities of design, however, revolve around real components, which are available only in certain sizes and which have their own design constraints.

3.8.1 Calculation of PV Outputs

The electrical energy produced by a PV array is estimated using data from the monthly averaged SR on the horizontal plane, ambient temperature and the electrical data sheet of the PV module given by the manufacturer. These ratings are also used as inputs to the sizing process. The first step in *SAIMA* is to estimate the rated power, $(P_{PV})_{dc,}$ of the proposed PV array taking into consideration the following constraints:

- All the PV system is designed under STC.
- Select a PV module and an inverter from a respective list for the proposed GCPV system (see Table 3.1).

Since, the electrical energy required, $(energy)_r$ in (GWh/yr)

and, $(energy)_r = 200$ GWh/yr (sponsor requirement)

By using the peak hour approach we can write

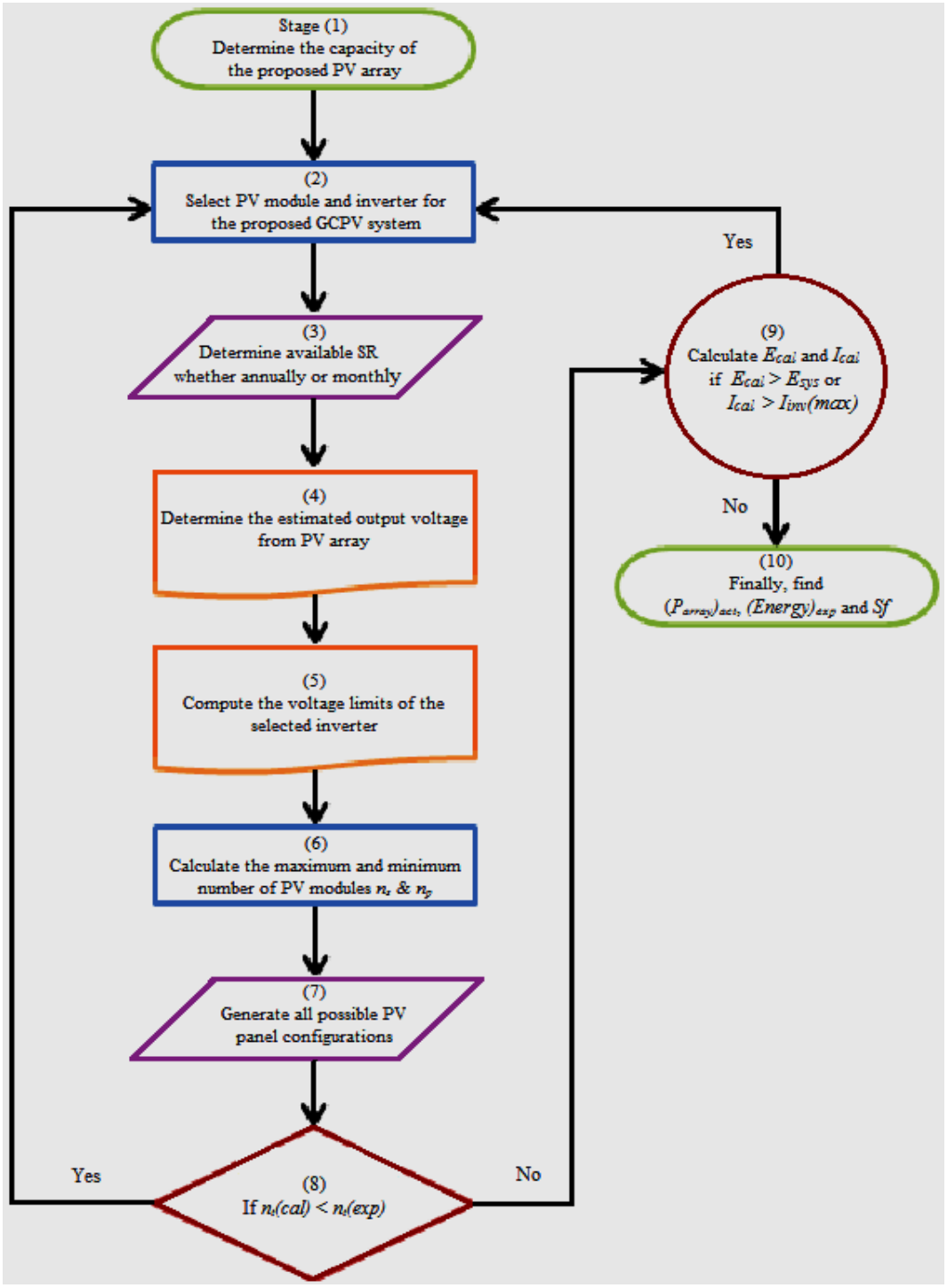

Figure 3.23: Flowchart of *SAIMA* for sizing the proposed GCPV system

$$(energy)_r = (P_r)_{ac} \times \left[\frac{S_H(kWh/m^2/yr)}{S_S(kW/m^2)}\right] \times 365\left(\frac{days}{yr}\right) \tag{3.15}$$

and

$$(P_r)_{ac} = \eta_{conv.} \times (P_{PV})_{dc} \tag{3.16}$$

Hence,

$$(energy)_r = (P_{PV})_{dc} \cdot \eta_{conv.} \times 365\left(\frac{S_H}{S_S}\right) \tag{3.17}$$

or,

$$(P_{PV})_{dc} = \left[\frac{(energy)_r \times S_S}{365 \times S_H \times \eta_{conv.}} \right] \quad (3.18)$$

where

$(P_{PV})_{dc}$ = DC output power of the proposed PV array in Watts.

$(P_r)_{ac}$ = AC output power of the inverter in Watts.

$\eta_{conv.}$ = conversion efficiency from DC to AC according to inverter efficiency, DC cabling, temperature impact and module mismatch (select $\eta_{conv.}$ = 97%).

Table 3.1: Required PV Ratings for Sizing Algorithm

Required ratings for the PV combination	
Module	Inverter
Open-circuit voltage, E_{oc} in volts	Maximum input voltage, $E_{inv}(max)$ in volts
Short-circuit current, I_{sc} in amps	Minimum input voltage, $E_{inv}(min)$ in volts
Maximum system voltage, E_{sys} in volts	Maximum input current, $I_{inv}(max)$ in amps
Voltage at maximum power, $E_{stc}(max)$ in volts	Nominal power output, P_{inv} in W
Maximum power, $(P_{PV})_{maxp}$ in Wp	Conversion efficiency, $\eta_{conv.}$ in %
Temperature coefficient for open-circuit voltage, T_{Eoc} in % per ºC	Nominal efficiency, $\eta_{inv.}$ in %
Temperature coefficient for maximum power voltage, T_{Emax} in % per ºC	

If we take S_H equals 5.64 kWh/m^2/day and S_s equals 1 kW/m^2 we will end up with the estimated rated power, $(P_{PV})_{dc}$ to be equal to 100 MW approximately.

The second step is to determine the expected output voltages from the PV array such as the maximum value of the PV module open-circuit voltage, $E_{oc}(max)$, the minimum voltage at maximum power of the PV module, $E_{PV}(min)$, and the maximum voltage at maximum power of the PV module, $E_{PV}(max)$. Therefore, the maximum voltage at maximum power of the PV module,

$$E_{PV}(max) = E_{stc}(max) \text{ x } [\, 1 - (\, T_{Emax} \text{ x } (t_{cmin} - t_{STC}))] \quad \text{in volts} \qquad (3.19)$$

where

$E_{stc}(max)$ = voltage at maximum power of the PV module at STC in volts.

T_{Emax} = temperature coefficient for maximum power voltage in % per °C.

t_{cmin} = recorded minimum effective cell temperature of the PV panel at site in °C (set t_{cmin} = 21 °C).

t_{STC} = module temperature at STC in °C.

The minimum voltage at maximum power of the PV module,

$$E_{PV}(min) = E_{stc}(max) \text{ x } [\, 1 - (T_{Emax} \text{ x } (t_{cmax} - t_{STC}))] \quad \text{in volts} \qquad (3.20)$$

where

t_{cmax} = recorded maximum effective cell temperature of the PV panel at site in °C (set t_{cmax} = 78 °C).

On the other hand, the maximum PV module open-circuit voltage,

$$E_{oc}(max) = E_{oc} \text{ x } [\, 1 - (T_{Eoc} \text{ x } (t_{cmin} - t_{STC}))] \quad \text{in volts} \qquad (3.21)$$

where

E_{oc} = open-circuit voltage of the module at STC.

T_{Eoc} = temperature coefficient for open-circuit voltage in % per °C.

The maximum percentage allowable of voltage drop across the DC cables as specified in the GCC standard is equal to 7.5%. Applying this percentage, we can recalculate eqn. 3.20 using

$$E_{PV}(min)_f = 0.925 \text{ x } E_{PV}(min) \quad \text{in volts} \qquad (3.22)$$

where, $E_{PV}(min)_f$ is the final minimum voltage at maximum power of the PV module.

3.8.2 Inverter Sizing using *SAIMA*

There are three criteria that can be based on to decide the type and number of the inverters [57]: maximum admissible input voltage, $E_{inv}(max)_{ad}$, minimum admissible input voltage, $E_{inv}(min)_{ad}$ and the current compatibility. The design of inverter will impose how to wire the PV modules together. If the maximum input voltage of the

inverter, $E_{inv}(max)_{ad}$, is less than the PV output voltage, $E_{PV}(max)$, the inverter will be damaged. Moreover, as the PV voltages in series are added, the value of $E_{inv}(max)_{ad}$ will therefore determine the maximum number of modules in series. As currents are added when strings are in parallel, the value of the input current of the inverter, I_{inv}, will determine the maximum number of parallel strings. In order to determine the number of panels connected within the whole array, the value of the maximum output power of the PV array, $(P_{PV})_{dc}$, should not exceed the maximum allowable power of the connected inverters. *SAIMA* of a GCPV system will be implemented as explained in section 3.8 and the three criteria can be satisfied.

Calculate the admissible input voltage (limits) of the inverter, $E_{inv}(max)_{ad}$ and $E_{inv}(min)_{ad}$, respectively. The maximum admissible input voltage of the inverter, $E_{inv}(max)_{ad}$, can be computed using

$$E_{inv}(max)_{ad} = \eta_{inv.} \times E_{inv}(max) \quad \text{in volts} \tag{3.23}$$

where

$E_{inv}(max)$ = maximum input voltage of the inverter in volts.

$\eta_{inv.}$ = nominal efficiency of the inverter (select $\eta_{inv.}$ = 94 %).

Whereas, the minimum admissible input voltage of the inverter, $E_{inv}(min)_{ad}$, can be calculated using

$$E_{inv}(min)_{ad} = (\eta_{inv.} - \eta_{Edrop}) \times E_{inv}(min) \quad \text{in volts} \tag{3.24}$$

where

$E_{inv}(min)$ = minimum input voltage of the inverter in volts.

η_{Edrop} = maximum percentage allowable of voltage drop across the terminals of the inverter (select η_{Edrop} = 14 %).

3.8.3 Panel or Array Sizing using *SAIMA*

A GCPV system works using a number of panels (an array), which is normally mounted on a horizontal surfaces. A small increase or decrease in the size of the solar PV system can result in substantial differences in the outputs and return on investment of the system. Once we know the size of the solar PV array we can use any leading enterprise resource planning software to calculate the output of the array and the whole system in kWh (kilowatt hours). These calculations take into consideration the number of series and parallel PV modules, output voltages and currents, size of the inverter and some

other factors such as the orientation of the collectors and over shading to produce a conservative figure. Again *SAIMA* can be implemented to compute the maximum number of parallel strings, n_p, as well as the maximum, $n_s(max)$, and minimum, $n_s(min)$, number of PV modules per string that satisfy the inverter voltage and current limits. These limits are subjected to the following criteria:

a. $n_s(mp)$ and $n_s(oc)$ are rounded down to the nearest integer.
b. $n_s(\min)$ is rounded up to the nearest integer.
c. $E_{PV}(\max) < E_{inv}(\max)_{ad}$ for both maximum power and open circuit conditions.
d. $E_{PV}(\max) > E_{inv}(\min)_{ad}$ for both maximum power and open circuit conditions.
e. $n_s(\max)$ are the smaller value between $n_s(mp)$ and $n_s(oc)$.
f. f_o = oversized factor of PV module current (set f_o = 20 %)

   where

   $n_s(mp)$ = maximum number of PV modules per string based on voltage at maximum power of the PV module.

   $n_s(oc)$ = maximum number of PV modules per string based on open circuit voltage of the PV module.

Therefore, the maximum number of parallel string in the proposed PV array, n_p, will be computed as follows

$$n_p = \left(\frac{I_{inv}(\max)}{(1+ f_o) \times I_{sc}} \right) \tag{3.25}$$

where

$I_{inv}(\max)$ = maximum input current of the inverter in amps.

I_{sc} = short-circuit current of the module at STC in amps.

A part from that, $n_s(mp)$ can be calculated using

$$n_s(mp) = \left(\frac{E_{inv}(\max)_{ad}}{E_{PV}(\max)} \right) \tag{3.26}$$

and $n_s(oc)$ can be determined using

$$n_s(oc) = \left(\frac{E_{inv}(\max)_{ad}}{E_{oc}(\max)} \right) \tag{3.27}$$

Besides that, $n_s(\min)$ is calculated as follows

$$n_s(\min) = \left(\frac{E_{inv}(\min)_{ad}}{E_{PV}(\min)_f} \right) \tag{3.28}$$

Now, the total number of calculated PV modules for the proposed PV array, $n_t(cal)$, can be determined as follows

$$n_t(cal) = n_p \text{ x } n_s \tag{3.29}$$

where

n_s = number of series PV modules.

Also, maximum calculated voltage of the array, E_{cal}, is determined by

$$E_{cal} = n_s \text{ x } E_{oc}(max) \qquad \text{in volts} \tag{3.30}$$

and maximum calculated current of the array, I_{cal}, is computed by

$$I_{cal} = n_p \text{ x } I_{sc} \qquad \text{in amps} \tag{3.31}$$

The PV array can take many configurations because n_s may take two possibilities due to $n_s(\min)$ and $n_s(\max)$. Any PV array configuration will be discarded if it is not agreed with the following condition:

1) $n_t(cal) > n_t(\exp)$
2) $I_{cal} < I_{inv}(\max)$
3) $E_{cal} < E_{sys}$

where $n_t(\exp)$ is the total number of expected PV modules for the proposed system and it is calculated by

$$n_t(\exp) = \left(\frac{(P_{PV})_{dc}}{(P_{PV})_{\max p}} \right) \tag{3.32}$$

3.8.4 Calculation of some Important Parameters using *SAIMA*

Some important parameters have to be calculated in order to finalize the sizing of the GCPV system such as the actual capacity of the PV array, $(P_{PV})_{act}$, expected annual energy output, $(energy)_{exp}$, inverter-to-PV array sizing factor, Sf ($Sf_{min} < Sf < Sf_{max}$, for the GCC countries, Sf_{max} is 0.85 and Sf_{min} is 0.65) and the excess factor, Ef. These data have to be calculated for all the possible array configurations that remain after applying

all the criteria in Section (3.8.3). Using the following equations we will end up with these data.

$$(P_{PV})_{act} = n_t(cal) \text{ x } (P_{PV})_{\text{maxp}} \qquad (\text{MW}_\text{P}) \tag{3.33}$$

$$Sf = \frac{P_{inv}}{(P_{PV})_{act}} \tag{3.34}$$

where P_{inv} is the nominal power output of the inverter.

and $$(energy)_{\text{exp}} = (P_{PV})_{act} \cdot \eta_{conv.} \times 365\left(\frac{S_H}{S_S}\right) \qquad (\text{GWh/yr}) \tag{3.35}$$

After determining all these data, then the array configuration which yields the highest *Sf* will be selected as the final design solution. Thereafter, the area of one panel, A_{panel}, can be estimated using

$$A_{panel} = n_t(cal) \text{ x } A_m \qquad (\text{in m}^2) \tag{3.36}$$

where A_m is the area of one PV module in m^2.

3.9 *SAIMA* Results and Conclusions

The interactions between modules, inverters and the PV array have been determined and the sizing results of *SAIMA* have been investigated using different PV modules and inverters and how those impact the layout of the PV panel or array as shown in Table 3.2. According to the input of *SAIMA* (see appendix B), it is clear that combination of Type 3 (Sharp SKK-300 mono-crystal SMC- PV module and Sunny Boy SB2500 inverter) has been chosen for the proposed GCPV system due to the highest value of *Sf* which is approximately 0.8131 with 43 PV modules in series in one string, 42 PV modules in parallel in one panel and 132 PV panels in the whole array. This suggests using an array with the above configuration to achieve a maximum electrical energy of about 198.927 GWh/yr, an actual rated power output with 97.268 MW and array area of 0.5786814 km^2.

It is important that the proposed algorithm (*SAIMA*) estimated the maximum open-circuit voltage of the panel to be sure that it doesn't violate the highest DC voltage that the inverter can accept, which in this case is 3000 V. With 43 modules in series in one string, each having E_{oc} at STC of 58.1 V, the string voltage could reach 43 x 63.2 =

2717.6 V. This is well below the 3000-V limit. As shown in Fig. 3.24 and Fig. 3.25, the inverter-PV array sizing factor has been performed for each type of the combination selected with respect to the percentage of the inverter rated power. However, all types of combinations had produced higher sizing factor of not less than 62% but type (3) combination had obtained the highest sizing factor of the system with more than 90%.

Table 3.2: Sizing Results using *SAIMA*

Results	PV module and inverter combination			
	Type 1	Type 2	Type 3	Type 4
PV modules in series, n_s	178	154	43	49
PV modules in parallel, n_p	93	48	42	51
Panel configuration (n_s x n_p)	178 x 93	154 x 48	43 x 42	49 x 51
Number of total panels	47	83	132	67
P_{PV} in MWp	78.213	81.103	97.268	88.292
Sf	0.6218	0.7116	0.9131	0.7745
E_{system} (GWh)	133.024	146.546	198.927	171.469
A_{panel} in m^2	15601.81	9440.32	4383.95	8619.34

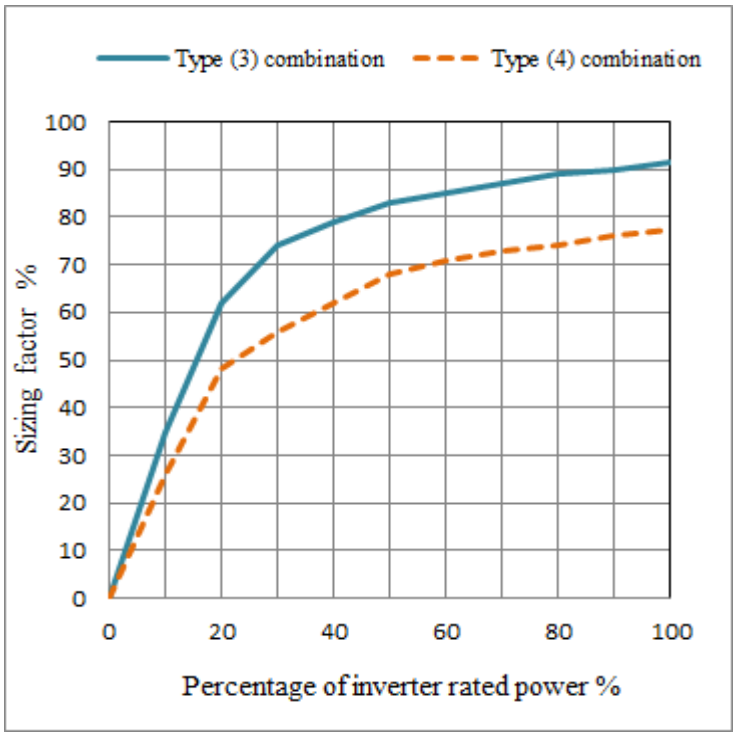

Figure 3.24: Sizing factor of the GCPV system for both Type (1) and (2) combinations

SAIMA was ran out using the annual average SR, S_H, which is equal to 5.64 kWh/m^2, but if average monthly SR is used for type 3 combination (for example) we will obtain the total power output of the proposed PV array as shown in Fig. 3.26. The output power, $(P_{PV})_{act}$, is floating between 40 MW in January and almost 98 MW in June with the maximum output power in June.

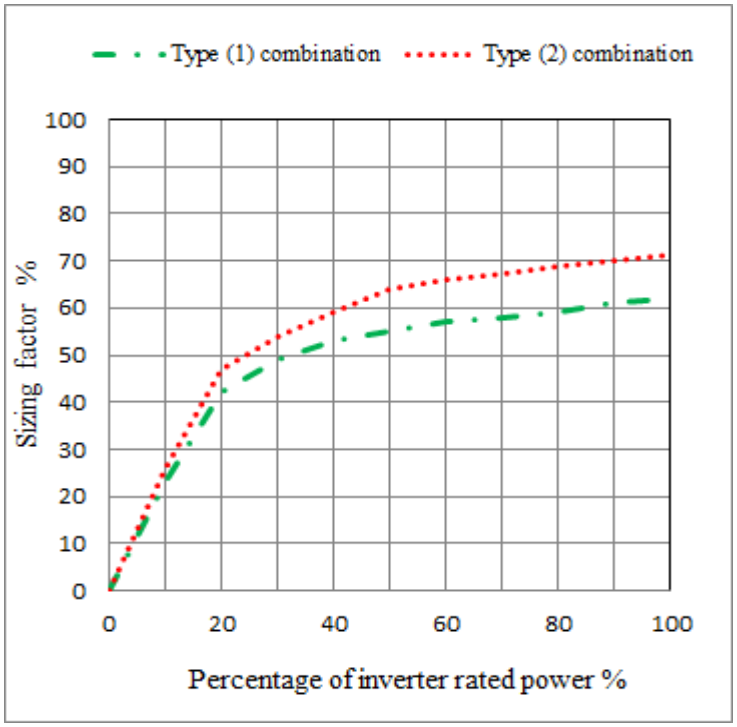

Figure 3.25: Sizing factor of the GCPV system for both Type (3) and (4) combinations

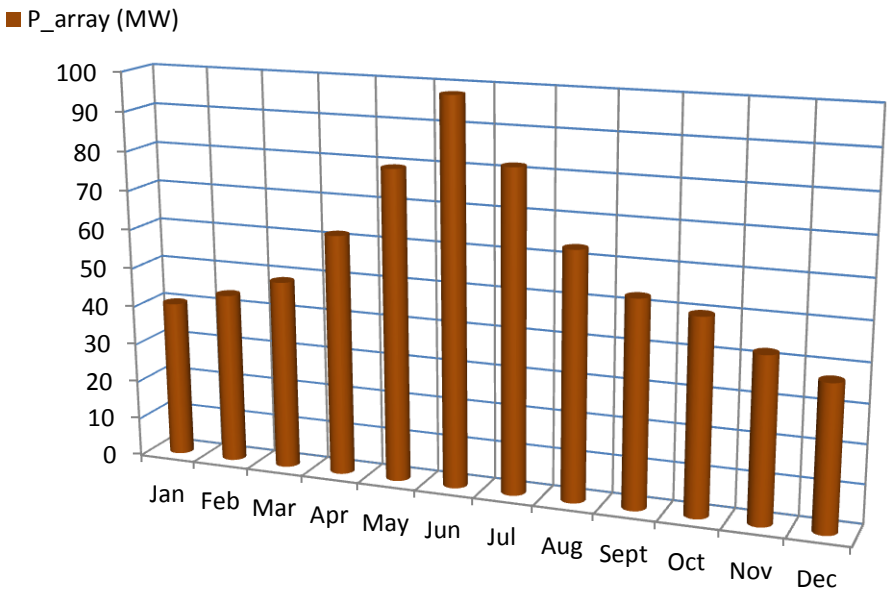

Figure 3.26: Total power output of the proposed PV array at monthly averaged SR

An iterative manual approach to the GCPV system sizing has been developed which gives a multi–combination of array size and inverter capacity to meet the reliability requirement and the possibility to integrate the proposed GCPV system to Kuwait national grid. The conclusions of the study are summarized as follows:

(i) Monthly and yearly averaged SR profile influence the size of the PV panel

or array as well as the inventor size significantly.

(ii) *SAIMA* curves indicate the importance of the relationship between modules and inverters in the GCPV system. Different PV modules and inverters combinations on *SAMIA* curve have different array configuration (n_p x n_s).

(iii) The proposed GCPV system using *SAIMA* exhibits minimum system ratio of the generated energy by the system to the required energy.

(iv) Technical sizing outputs such as the number of PV modules, PV panel configuration and inverter-to-PV panel sizing factor are the most important outputs of the proposed algorithm for the integration process to the grid.

Chapter 4
GCPV System Cost-Efficiency Optimization Problem

4.1 Multi-Objective Management

Many problems in the design of GCPV systems are formulated as optimization problems, where design choices are encoded as valuations of decision variables and the relative merits of each choice are expressed via a utility-cost function over the decision variables. For multiple-objective problems, the objectives are generally conflicting, preventing simultaneous optimization of each objective. Many, or even most, real engineering problems actually do have multiple objectives, i.e., minimize cost, maximize performance, maximize reliability, etc. These are difficult but realistic problems. In most real-life optimization situations, however, the cost function is multidimensional. For example, a PV array that we want to develop or purchase can be evaluated according to its cost, size, electrical characteristics levels (i.e. power, voltage and current), efficiency and performance. Consequently, there is no unique optimal solution but rather a set of efficient solutions, also known as Pareto Frontier solutions, characterized by the fact that their cost cannot be improved in one dimension without being worsened in another [58]. The set of all Pareto solutions, the Pareto front, represents the problem trade-offs, and being able to sample this set in a representative manner is a very useful aid in decision making. Multiple-criteria or multi-objective optimization problems (Pareto optimization) is an area of multiple criteria decision making, that is concerned with mathematical optimization problems involving more than one objective function to be optimized simultaneously [59-61]. Multi-objective optimization has been applied where optimal decisions need to be taken in the presence of trade-offs between two or more conflicting objectives. Minimizing cost and maximizing efficiency while designing and modeling a PV system is an example of multi-objective optimization problems involving two objectives (bi-objective), respectively. It is clear that a model that considers simultaneously two or more such objectives could produce solutions with a higher level of equity [62]. In practical problems, there can be more than two objectives.

There are two general approaches to multiple-objective optimization [63, 64]. One is to combine the individual objective functions into a single composite function or move all but one objective to the constraint set. In the former case, determination of a single objective is possible with methods such as utility theory, weighted sum method, etc., but the problem lies in the proper selection of the weights or utility functions to characterize

the decision maker's preferences [64]. In practice, it can be very difficult to precisely and accurately select these weights, even for someone familiar with the problem domain. Compounding this drawback is that scaling amongst objectives is needed and small perturbations in the weights can sometimes lead to quite different solutions [66]. In the latter case, the problem is that to move objectives to the constraint set, a constraining value must be established for each of these former objectives [66]. This can be rather arbitrary. In both cases, an optimization method would return a single solution rather than a set of solutions that can be examined for trade-offs. For this reason, decision-makers often prefer a set of good solutions considering the multiple objectives [65]. The second general approach is to determine an entire Pareto optimal solution set or a representative subset [69]. A Pareto optimal set is a set of solutions that are non-dominated with respect to each other. While moving from one Pareto solution to another, there is always a certain amount of sacrifice in one objective(s) to achieve a certain amount of gain in the other(s). Pareto optimal solution sets are often preferred to single solutions because they can be practical when considering real-life problems

In this work I explore an alternative approach to find the optimal solution of the cost-efficiency curve problem of the GCPV system using a weighted-sum of one main objective function (bi-objective) and to solve the problem based on constraint solvers that can answer whether there is an assignment of values to the decision variables which satisfies a set of constraints on the Pareto front line. This method scalarizes the set of objectives into a single bi-objective by multiplying each objective with a user supplied weight. It transforms multiple objectives into an aggregated objective function by multiplying each objective function by a weighting factor and summing up all weighted objective functions. Each single objective optimization determines one particular optimal solution point on the Pareto front. The weighted sum method then changes weights systemically, and each different single objective optimization determines a different optimal solution. The solutions obtained approximate the Pareto front. The value of the weights depends on the relative importance of each objective. In the following subsections, the problem formulation is presented.

It is well known, in the single-criterion case, that such solvers can be used for optimization by searching the space of feasible costs and asking queries of the form: is there a solution which satisfies the problem constraints and its cost is not larger than some constant? Asking such questions with different constants we obtain both positive and negative answers (satisfied and unsatisfied answers). Taking the minimal cost x

among the positive points and the maximal cost y among the negative points we obtain both an approximate solution x and an upper bound x-y on its distance from the optimum, that is, on the quality of the approximation. In this research I extend the idea to our multi-criteria optimization problem which is the cost-efficiency of the GCPV system. Our goal is to use the positive points as an approximation of the Pareto front of the problem, use the negative points to guarantee computable bounds on the distance between these points and the actual Pareto front and to direct the search toward parts of the cost-efficiency space so as to reduce this distance. A prototype implementation of our algorithm demonstrates the quality and efficiency of our approach on numerous Pareto fronts.

4.2 Design Objectives

The objective of this thesis is to develop and implement a design strategy aiming to find the optimal configuration and operating plan for a GCPV that can supply the energy demand of a grid-connected power distribution system, taking into account that the two design criteria are the system total cost and efficiency. Moreover, the design taking into accounts the following considerations:

- The stochastic nature of solar energy sources shall be taken into account.
- The solution obtained shall not violate the technical and operational constraints of the system, and shall achieve a certain level of supply reliability.
- The optimization model shall be applicable and tractable, while giving fairly accurate results.

4.2.1 Efficiency Maximization

One of the GCPV design objectives was maximizing system efficiency which is defined as the ratio of the rated power of inverter to a PV array rated power. Therefore, it is a function of conversion devices efficiency and the amount of dumped energy. The peak energy, $energy_{(pv,peak)}$, received from the PV array is a function of SR and is equal to

$$energy_{(pv,peak)} = 365 \times S_H \times P_{dc}\left(peak\right) \tag{4.1}$$

The calculation of costs and efficiencies is based on the energy balance throughout the year. The value of loss efficiency will be very high when most of the excess PV energy cannot be used due to the shaded panels or limited storage capacity or unmatched inverter. When all the PV energy either is directly converted to the inverter or is stored in storage devices, the value of the used efficiency is equal to that of the system

efficiency, namely the value of the loss efficiency is equal to zero. In general, the overall GCPV system efficiency, η_{sys}, from PV to AC grid, also called "DC to AC sizing factor", is given by

$$\eta_{sys} = \frac{P_{inv}(Rated)}{P_{PV}(Rated)} \tag{4.2}$$

and the efficiency factor in this case is including:

- Derating of PV nominal peak power (e.g. due to tolerances, temperature, or aging).
- Module mismatches.
- Dirt.
- Shading.
- Losses due to wiring, blocking diodes and connectors.
- MPP tracking performance of the PV system.

The rated power of a PV array must be optimally matched with the inverter rated power in order to achieve maximum PV array output power [68]. The optimal inverter sizing depends on the local SR, ambient temperature, and inverter performance [68]. For instance, under low SR levels, a PV array generates power at only part of its rated power and consequently the inverter operates under part load conditions with lower system efficiency. The PV array efficiency is also adversely affected when an inverter rated capacity is much lower than the rated PV capacity. On the other hand, under overloading condition, excess PV output power which is greater than the inverter rated capacity is lost [68]. Overloading does not adversely affect PV Powered inverters. If the power available from the array exceeds the nameplate rating of the inverter, the inverter will limit the power and current coming from the array to the inverter's maximum nameplate power and current rating. The inverter does this by reducing the DC input current, which causes the DC operating voltage to rise above the maximum power point of the array, thereby 'clipping' the array output and this will reduce the array efficiency and much of the PV output power will be lost. This effectively limits the output of the array without stressing the inverter. It is important to note that this statement does not hold true for all inverter manufacturers. Some non-PV Powered inverters will not self-limit. They will convert all the power available from the array and may be damaged by overloading. This to say that optimal sizing of PV inverter plays a significant role in increasing PV system efficiency and feasibility. Regardless of inverter topology, its output power is highly dependent on its input power. For determining the optimal inverter size neglecting the dependency of inverter efficiency to its input voltage, the inverter

efficiency curve which is described by a power function (η_{inv} - $P_{PV,pu}$) is given as follows,

$$\eta_{inv} = \begin{cases} e_1 P_{PV,pu} + \frac{e_2}{P_{PV,pu}} + e_3 & \frac{P_{inv}}{P_{PV}} > 0 \\ 0 & \frac{P_{inv}}{P_{PV}} = 0 \end{cases} \quad (4.3)$$

where P_{pv} and P_{inv} are PV module output power and inverter rated power, respectively, while e_1, e_2 and $e3$ are the model coefficients and should be determined [70]. By solving a system of three linear equations with three unknowns, the three parameters e_1, e_2 and e_3 can be easily determined. The three linear equations can be extracted from the efficiency curve data in nominal rated voltage level after neglecting the relationship between η_{inv} and the input voltage. The efficiency curve of any inverter which presented in its technical datasheet provided by the manufacture is usually presented in three different voltage levels including lowest, nominal and highest. According to reference [70], good choices for $P_{PV,pu}$ are 0.1, 0.2 and 1 p.u. which correspond to the rising front, peak region and tail region of the efficiency curve, respectively.

The optimization problem is formulated such that the objective function is to maximize the annual average system efficiency and is given by

$$\text{Maximize:} \quad \eta_{sys}(p) = \frac{\sum_n \eta_{daily}}{365} = \frac{\sum_n (\frac{P_{inv}}{P_{PV}})}{365} \quad (4.4)$$

The system efficiency is in terms of the daily averages of SR (S_H), ambient temperature (t_{amb}), and inverter rated power (P_{inv}). In general, the system efficiency is a function of the power flow in the GCPV system and this power is required for the grid.

4.2.2 Cost Minimization

Cost minimization has been always the chief objective sought when a GCPV system is designed. GCPV system is more expensive than other conventional electricity resources. This fact results in the careful selection of every individual portion of this system to guarantee the economic performance. So for a PV array with specific nominal power, the optimal inverter sizing is an important issue. Therefore, sizing factor, *Sf*, is defined as the ratio of the nominal output power of inverter to nominal DC power of PV array. In the case of inverter selection with higher size, the capital cost of GCPV system increases. Therefore, in inverter sizing selection there is a trade off in energy

maximization and cost minimization [67]. In this research, the optimum sizing factor is determined based on solving an optimization problem.

Total cost of GCPV system consists of both capital cost (one-time cost such as installation, support structures, acquisition, and commissioning) and operating cost (recurring cost such as operation, maintenance, replacement, etc.), occurring at different points of time [67]. Total cost of the GCPV, C_{sys}, includes the net present value of the purchased energy, the capital cost and net present cost of maintenance and repair. The objective function of the optimization problem that describes the total cost of a GCPV system in terms of PV array cost, inverter cost, and others will be a function of the power required for the grid, total energy produced per day and hours of average SR. We will ignore adding in the cost of the charge controller, since this is only a few thousand dollars whereas the whole system cost will be in the millions of dollars. Eventually, the objective function of the total cost is defined as the net present profit of GCPV system minus its net present cost, as follows:

$$\text{Minimize:} \quad C_{sys}(p) = AE_{GCPV}(p) + C_{\{c,m\}}(p) \tag{4.5}$$

where

AE_{GCPV} = net present value of the purchased energy.

$C_{\{c,m\}}$ = capital cost and net present cost of maintenance, operation and repair.

Profit of GCPV system is due to the sold produced energy in its operating lifetime. Therefore, for a GCPV system with predetermined array size, annual produced energy of GCPV system should be determined. In any arbitrary SR and cell temperature, the output power of PV array (which is proportionally dependent on SR) with specific nominal power at STC can be determined as follows:

$$P_{PV} = P_{PV(STC)} \times (\frac{S_H}{S_{STC}})[1 - T_{MPP}(t_{cell} - t_{STC})] \tag{4.6}$$

where

P_{PV} = output power of PV array.

$P_{PV(STC)}$ = nominal PV power at STC.

S_{STC} = SR at STC.

T_{MPP} = temperature coefficient of maximum power point (MPP) in % per °C.

t_{cell} = effective PV module temperature at site in °C.

When current flows through the PV cell, its average temperature rises 30 °C above the average ambient temperature. Therefore, cell temperature (t_{cell}) should be estimated from the ambient temperature (t_{amb}) as follows:

$$t_{cell} = 30 + t_{amb} \tag{4.7}$$

In some researches, the average cell temperature is supposed to be 25 °C or 35 °C more than the average ambient temperature [70]. So, in the proposed method, eqns. 4.6 and 4.7 are applied to compute the output power of PV array. The PV array output power connected to *i*th inverter in different weather conditions can be determined through using eqns. 4.3, 4.6 and 4.8. The simulation sampling interval is considered as $\Delta t = 1/60$ hour and the annual produced energy of PV array connected to *i*th inverter can be determined as follows:

$$energy^{i}_{ann.} = \sum_{n}\sum_{w} \Delta t \times \frac{(P_{PV} \times \eta_{inv})_i}{sf_i} \times \frac{1}{1000/kWh} \tag{4.8}$$

where

w = sample time number in each day.

Finally, annual energy production can be computed by adding the all above calculated energies for a GCPV system with r different inverters.

$$energy_{ann.} = \sum_{i=1}^{r} energy^{i}_{ann.} \tag{4.9}$$

Under the assumption that annual produced energy of GCPV system in all years of system operating lifetime is supposed to be constant, the net present value of the purchased energy for q years as the operating lifetime of system can be determined by the following equation:

$$AE_{GCPV}(p) = \alpha \times \eta_{conv.} \times energy_{ann.} \tag{4.10}$$

where $\eta_{conv.}$ shows the effect of DC and AC cables losses in the output energy. As an example, in a GCPV system that cable losses are equal to 2 % of output power, $\eta_{conv.}$ Will be 98 %. The GCPV economical factor, α, is given by

$$\alpha = \frac{1-(\frac{1}{1+d})^{q}}{d} \times C_{tariff} \tag{4.11}$$

where C_{tariff} and d are feed in tariff and nominal annual discount rate, respectively. Note that in most literature, the operating lifetime of a PV panel is taken as 25 years, and that is the value used in our case.

Capital cost (initial) and the maintenance and repair cost, $C_{\{c,\ m\}}$, as in eqn. 4.5 are consisting the net present cost of GCPV system. Therefore, if G (in %) shows the government subsidization rate, the capital (initial), maintenance and repair costs (in $) can be determined by the following equation:

$$C_{\{c,m\}}(p) = (1-\frac{G}{100}) \times ((P_{sys} \cdot C_{PV}) + C_{ins.}) + (\sum_{i=1}^{r} \frac{P_{sys}^{i} \cdot C_{inv}^{i}}{sf_i}) + [C_{mPV} + C_{minv}^{i} + (C_{rinv}^{i})^{q_m}](\frac{1+f}{1+d})^{q} \quad (4.12)$$

where

C_{PV} = module price in $/W.

C_{inv}^{i} = ith inverter price in $/W (in this study, cost of string inverter is supposed to be 2-3.5 $/W).

$C_{ins.}$ = PV module's mounting structure, required land, DC and AC cables costs in $/module.

P_{sys}^{i} = nominal power of PV array connected to ith inverter in kW.

sf_i = sizing factor of ith inverter.

f = annual inflation rate in %.

C_{mPV} = annual maintenance cost of PV array in $/kW.

C_{minv}^{i} = annual maintenance cost of ith inverter in $/W.

C_{rinv}^{i} = the ith inverter repair cost in $/W.

q_m = the year number in which inverter fails and needs to be repaired.

In some cases, the GCPV designer might have multiple design objectives to be realized simultaneously. Some objectives such as minimizing operations cost and maximizing system efficiency are inherently conflicting. If more AC power output is delivered to the site, more PV generation units and inverters are needed to supply power. In such cases, the aim is usually to find the best attainable trade-offs between the contradicting objectives.

4.3 Problem Description

Unlike previous studies which focused on the sizing of GCPV system based on a single objective optimization problem, the sizing of GCPV system in this research was initially

converted into a bi-objective optimization problem. The objectives were formulated based on the aim to maximize the expected technical and economic performance indicators for the system design. At the outset of the GCPV design process, the designer often needs a simple and quick tool giving rough estimates of the design parameters and ensuring the feasibility of the problem, before proceeding with more sophisticated and accurate design techniques. In this research, a developed optimization model is used for this purpose, the problem entails finding the cost of the system and the gross energy PV generation and AC power output of the inverters that needs to be installed in the GCPV system in order to satisfy the load demand. In the proposed model, the network technical characteristics and constraints are taken into consideration.

In this novel approach for tackling this problem, the GCPV design and operation problem is formulated as a system of equations linking the design variables and then solved using a standard solver to optimality. A weighted-sum method for bi-objective optimization using Pareto front approximation was proposed to find the optimal PV generation units with DC-AC inverters capable of satisfying the annual energy demand (maximizing efficiency) at the minimum cost. This method is probably the most widely used method in multi-criteria optimization [71-75].

4.3.1 Nomenclature

(a) Subscripts and indices

$p \in \{P_{PV}, P_{inv}\}$

$n = \{1,2,3,\ldots\ldots,365\}$

$i \in \{\text{no. of inv.}\}$ a set of system component: DC-AC inverter(s).

$r \in \{\text{type of inv.}\}$

$q = \{1,2,\ldots\ldots,25\}$ operating lifetime of GCPV system in years.

q_m = the year number in which inverter fails and needs to be repaired.

(b) Scalars and parameters

α = GCPV economical factor.

$\eta_{conv.}$ = conversion factor.

G = government subsidization rate in %.

C_{tariff} = feed in tariff in $.

d = nominal annual discount rate in %.

$C_{ins.}$ = PV module's mounting structure, required land, DC and AC cables costs in $.

P_{sys}^{i} = nominal power of PV array connected to ith inverter in kW.

sf_i = sizing factor of *i*th inverter.

C_{mPV} = annual maintenance cost of PV array in \$/W.

C^i_{minv} = annual maintenance cost of *i*th inverter in \$/W.

C^i_{rinv} = the *i*th inverter repair cost in \$/W.

(c) Decision variables

P_{PV} = output power of PV array in W.

P_{inv} = inverter rated power in W.

AE_{GCPV} = net present value of the purchased energy in \$.

$C_{\{c,m\}}$ = capital cost and net present cost of maintenance, operation and repair in \$.

C_{sys} = total cost of the GCPV in \$.

η_{sys} = corresponding GCPV system efficiency in %.

Note that, most of the subscripts, indices, scalars, parameters and decision variables are illustrated in previous subsections.

4.3.2 Main Objective Function

The main objective function is the weighted-sum of the objective functions of both cost and system efficiency of the GCPV system, as follows:

Main Objective Function: $$obj(p) = k_\eta \eta_{sys}(p) + k_C C_{sys}(p) \quad (4.13)$$

where

k_η = user supplied weight of efficiency.

k_c = user supplied weight of cost.

If we let,

k_η = 1- k_c

Hence, $k_c \in [0, 1]$ is the weight of the cost objective function. It is usual to choose weights such that its sum is equal to one. Substitute eqns. 4.4 and 4.5 into eqn. 4.13, we obtain

$$obj(p) = k_\eta [\frac{\sum_n (\frac{P_{inv}}{P_{PV}})}{365}] + k_C [AE_{GCPV}(p) + C_{\{c,m\}}(p)] \quad (4.14)$$

Substituting AE_{GCPV} and $C_{\{c,m\}}$ in eqn. 4.14, we get

$$obj(p) = k_{\eta}[\frac{\sum_{n}(\frac{P_{inv}}{P_{PV}})}{365}] + k_C\Big([\alpha \times \eta_{conv.} \times \sum_{i=1}^{r}\sum_{n}\sum_{w}\Delta t \times \frac{(P_{PV} \times \eta_{inv})_i}{sf_i} \times \frac{1}{1000/kWh}] +$$

$$[(1-\frac{G}{100}) \times ((P_{sys} \cdot C_{PV}) + C_{ins.}) + (\sum_{i=1}^{r}\frac{P_{sys}^{i} \cdot C_{inv}^{i}}{sf_i}) + [C_{mPV} + C_{minv}^{i} + (C_{rinv}^{i})^{q_m}](\frac{1+f}{1+d})^{q}]\Big) \quad (4.15)$$

The first term denotes the annual average efficiency of the GCPV system associates with the PV power generated and inverter output power. The second and the third terms represent the net present value of the purchased energy, capital cost and net present cost of maintenance, operation and repair, respectively.

4.3.3 Constraints

For a solution to be feasible, it must be subjected to the following set of constraints:

i. For *i*th inverter of system: Sum of the PV parallel string currents, $I_{PV,string}$, must be greater than or equal to MPPT current range of inverter, $I_{inv,MPPT}$, to guarantee a high system efficiency.

$$I_{PV,string} \geq I_{inv,MPPT} \quad (4.16)$$

ii. For *i*th inverter of system: Sum of the PV parallel string currents, $I_{PV,string}$, must not exceed inverter maximum input current, $I_{inv,max}$, to avoid damaging of inverter due to overcurrent.

$$I_{PV,string} \leq I_{inv,max} \quad (4.17)$$

That is meant that the number of parallel PV modules must satisfy both inequalities (i) and (ii).

iii. For *i*th inverter of system: Sum of the PV string voltages, $E_{PV,string}$, must be greater than or equal to MPPT voltage range of inverter, $E_{inv,MPPT}$, to guarantee a high system efficiency.

$$E_{PV,string} \geq E_{inv,MPPT} \quad (4.18)$$

iv. For *i*th inverter of system: Sum of the PV string voltages, $E_{PV,string}$, must not exceed inverter maximum input voltage, $E_{inv,max}$, to avoid damaging of inverter due to overvoltage.

$$E_{PV,string} \leq E_{inv,max} \tag{4.19}$$

That is meant that the number of series PV modules must satisfy both inequalities (iii) and (iv).

v. Inverter rating: the PV system is connected to the main grid with an electrical inverter having a certain rating that must not be exceeded.

$$0 \leq P_{PV} \leq P_{inv} \tag{4.20}$$

vi. Non-negativity constraints: all variables cannot take a negative value.

4.3.4 Bi- objective Weighted Sum Method (*BoWS*) Procedures

In this research, I'm simultaneously trying to maximize GCPV efficiency while minimizing the cost and that this is clearly impossible as shown by the utopia point in Fig. 4.1(a). In other words, one objective cannot be reduced without increasing the other (conflicting objectives). Therefore, Pareto front not needed to make decisions but to focus on Limiting Behavior (Utopia Point) and try to get close to it. The proposed method (*BoWS*) is scalable to multiple objectives. The idea of the weighted sum method is to adaptively refine the Pareto front [72-75]. It can effectively solve bi-objective optimization problem whose Pareto front has convex regions with non-uniform curvature at which most of the solutions obtained with this method are concentrated in this region (relatively non-uniform).

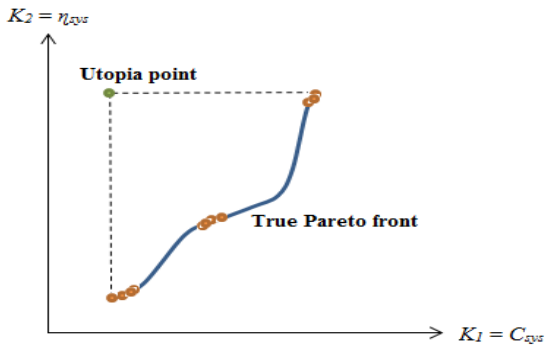

Figure 4.1(a): Original *BoWS*

As shown in Figs. 4.1(a) and 4.1(b), the first step is to estimate the length of each Pareto line segment of cost-efficiency (two-dimensional) problem after determining a rough profile of the Pareto front using this method. Because the segments lengths between (P_1, P_2), (P_2, P_3) and (P_3, P_4) are larger than others, a feasible region for further refinement in the objective space is established in these segments, using the weighted-sum method.

In the subsequent step, an optimization is then conducted only within this region as feasible domain for sub-optimization by subjecting additional constraints. The usual weighted sum method is then performed as sub-optimization in these feasible domains obtaining more Pareto optimal solutions. These steps are repeated and Pareto line segment estimation is again performed to determine the regions for further refinement until a termination criterion is met. This makes the distribution of solutions more uniform.

The main flow chart of *BoWS* is shown in Fig. 4.2 (a). The dashed box in Fig. 4.2(a) is detailed in Fig. 4.2(b) and it stated as follows:

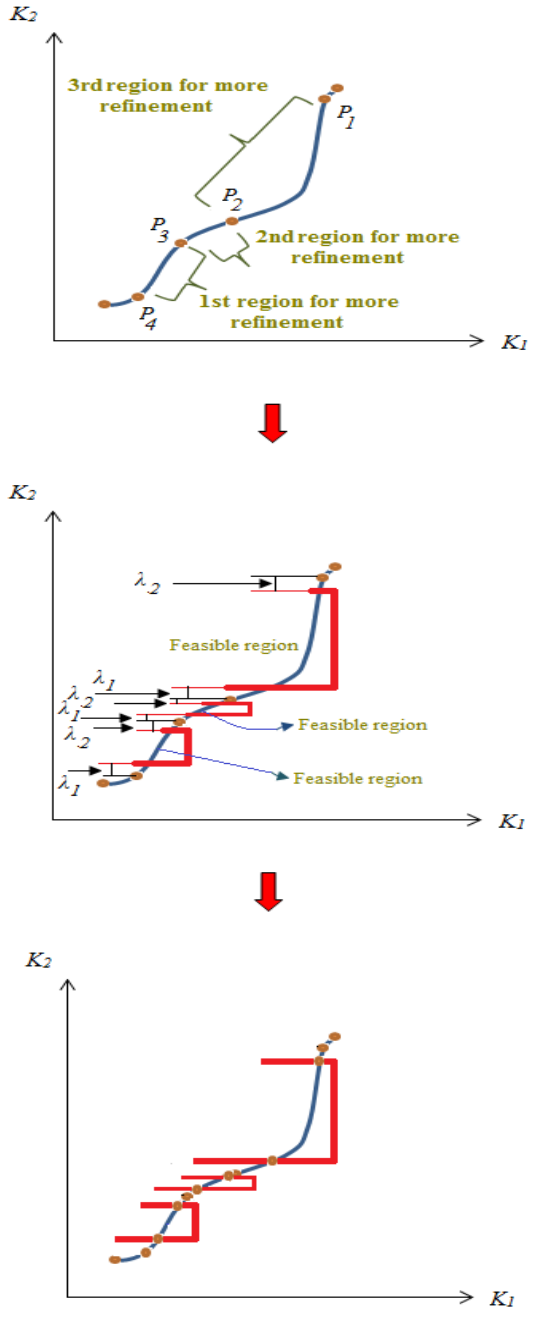

Figure 4.1(b): Proposed procedure of *BoWS*

Let *obj(p)* in eqn. 4.15 be an objective function vector ***K(z, a)*** with ***z*** as a variable vector and ***a*** as a vector of fixed parameter.

$$obj(p) = \min \boldsymbol{K(z, a)} \quad , \quad p = \boldsymbol{z} \tag{4.21}$$

subjected to all constraints mentioned in the previous section.

But

$$\boldsymbol{K(z)} = [K_1(z) \;\; K_2(z)] \tag{4.22}$$

where $K_1(z) = C_{sys}(p)$ as appears in eqn. 4.5 and $K_2(z) = \eta_{sys}(p)$ as appears in eqn. 4.4.

and

$$\boldsymbol{z} = [z_1 \; z_2], \quad z_1 = p_1 \text{ and } z_2 = p_2, \quad p \in \{P_{PV}, P_{inv}\} \tag{4.23}$$

Now, let

$$K_c = \gamma_1 \text{ and } k_\eta = \gamma_2 \tag{4.24}$$

where γ_1 and γ_2 are the weighting factors for first and second objective functions (cost, efficiency), respectively. Let γ_i (i = {1, 2}) is a weighting factor for the ith objective function.

Hence, from eqn. 4.13 and according to the above assumptions, the main objective function will be in the form of:

$$K_{\text{weighted-sum}} = \gamma_1 K_1 + \gamma_2 K_2 \tag{4.25}$$

As shown in Fig. 4.2(b), these assumptions make eqn. 4.15 to be applicable for *BoWS*. The detailed procedure for implementing the bi-objective adaptive weighted-sum method is described in the following:

a. Normalize the objective functions in the objective space. When $\boldsymbol{z}^{i*}$ is the optimal solution vector for the single-objective optimization of the ith objective function K_i, the utopia point, $\boldsymbol{K}^{utopia}$, is defined as

$$\boldsymbol{K}^{utopia} = [K_1(\boldsymbol{z}^{1*}) \;\; K_2(\boldsymbol{z}^{2*})] \tag{4.26}$$

since, each component of the pseudo nadir point, K_i^{nadir}, expressed as

$$K_i^{nadir} = \max [K_i(\boldsymbol{z}^{1*}) \;\; K_i(\boldsymbol{z}^{2*})] \tag{4.27}$$

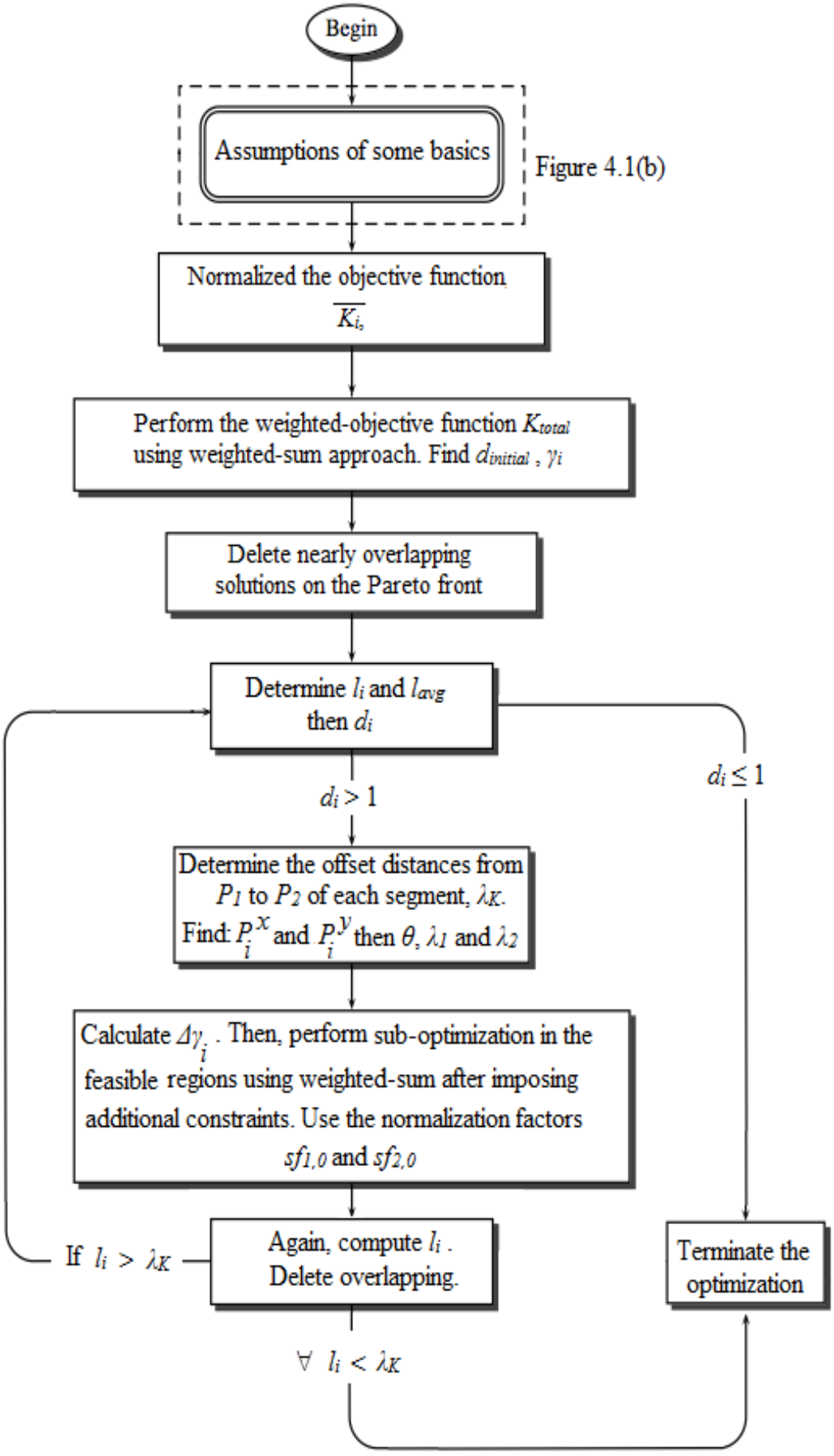

Figure 4.2(a): Main flow chart of *BoWS*

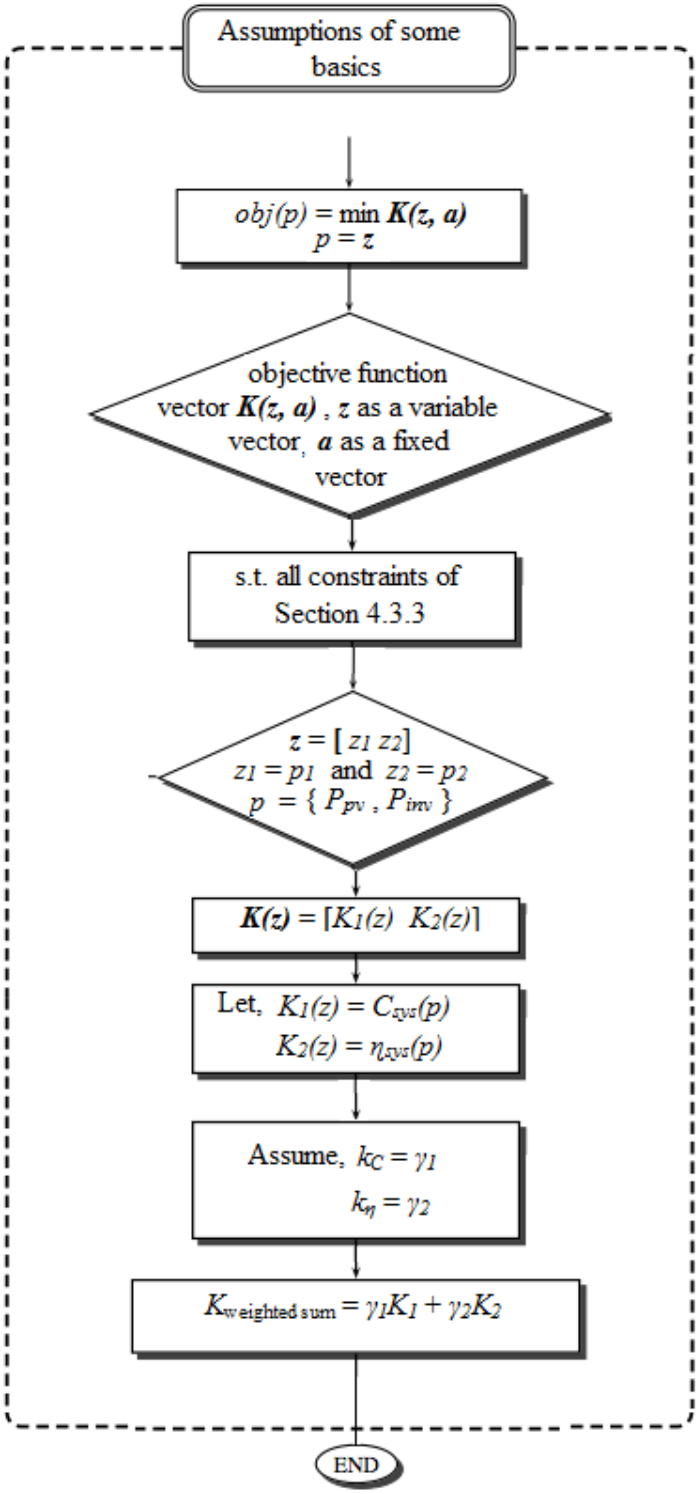

Figure 4.2(b): Detailed dashed box of Fig. 4.2(a)

where, the pseudo nadir point, $\boldsymbol{K}^{nadir}$, is defined as

$$\boldsymbol{K}^{nadir} = [\, K_1^{nadir} \;\; K_2^{nadir} \,] \tag{4.28}$$

then, the normalized objective function, $\overline{K_i}$, is obtained from

$$\overline{K_i} = \frac{K_i - K_i^{utopia}}{K_i^{nadir} - K_i^{utopia}} \tag{4.29}$$

b. Perform bi-objective optimization using the usual weighted-sum approach with a small number of divisions, $d_{initial}$. The uniform step size of the ith weighting factor γ_i is determined by the number of initial divisions along the ith objective dimension:

$$\Delta\gamma_i = \frac{1}{d_{initial,i}} \tag{4.30}$$

The weighting factor reveals the relative importance between K_1 and K_2. By using a large step size of the weighting factor, $\Delta\gamma$, a small number of solutions is obtained. For bi-objective functions, the weighted single objective function, K_{total}, is obtained as

$$K_{total} = \gamma_1\gamma_2 K_1 + (1-\gamma_1)\gamma_2 K_2 \quad , \qquad \gamma_i \in [0, 1] \tag{4.31}$$

In this work, we use the same step size for all weighting factors.

c. Compute the lengths of the line segments between all the neighboring solutions. Delete nearly overlapping solutions. It occurs often that several nearly identical solutions are obtained when the weighted-sum method is used. The Euclidian distances between these solutions are nearly zero, and among these, only one solution is needed to represent the Pareto front. In the computer implementation, if the distance among solutions is less than a predetermined distance (ε), then all solutions except one are deleted.

d. Determine the number of further refinements in each of the regions. The longer the segment is, relative to the average length of all segments, the more it needs to be refined. The refinement is determined based on the relative length of the segment:

$$d_i = [c\frac{l_i}{l_{ave.}}] \quad , d_i \text{ is rounded off to the nearest integer.} \tag{4.32}$$

where

d_i = the number of further refinements for the ith segment.

l_i = length of the ith segment.

$l_{avg.}$ = average length of all the segments.

c = constant of the algorithm.

If

$d_i \leq 1$, no further refinement is conducted in the line segment.

$d_i > 1$, go to Step (e).

e. Determine the offset distances from the two end points of each segment. First, a piecewise linearized secant line is made by connecting the end points, P_1 and P_2. Then, the user selects the offset distance along the piecewise linearized Pareto front, λ_K. The distance λ_K determines the final density of the Pareto solution distribution, because it becomes the maximum segment length during the last phase of the algorithm. In order to find the offset distances parallel to the objective axes, the angle θ is calculated as

$$\tan\theta = \left[\frac{P_2^y - P_1^y}{P_1^x - P_2^x} \right] \tag{4.33}$$

where P_i^x and P_i^y are the x (K_1) and y (K_2) positions of the end points P_1 and P_2, respectively. Then, λ_1 and λ_2 are determined with λ_K and θ as follows,

$$\lambda_1 = \lambda_K \cos\theta \quad \text{and} \quad \lambda_2 = \lambda_K \sin\theta \tag{4.34}$$

f. Impose additional inequality constraints and conduct sub-optimization with the weighted-sum method in each of the feasible regions. The feasible region is offset from P_1 and P_2 by the distance of λ_1 and λ_2 in the direction of K_1 and K_2. Performing sub-optimization in this region, the problem is stated as

$$\min \quad \gamma \left[\frac{K_1(x)}{sf_{1,0}(x)} \right] + (1-\gamma) \left[\frac{K_2(x)}{sf_{2,0}(x)} \right] \tag{4.35}$$

subjected to

$$K_1(x) \le P_1^x - \lambda_1$$

$$K_2(x) \le P_2^y - \lambda_2$$

where λ_1 and λ_2 are the offset distances obtained in Step (e), P_i^x and P_i^y are the x and y position of the end points, and $sf_{1,0}$ and $sf_{2,0}$ are normalization factors. The uniform step size of the weighting factor γ_i for each feasible region is determined by the number of refinements, d_i, obtained in Step (d):

$$\Delta\gamma_i = \frac{1}{d_i} \tag{4.36}$$

Eventually, we reduce the non-linear bi-objective problem into a scalar problem of the form illustrated in Step (f). The segments in which no converged optimum solutions are obtained are removed from the segment set for further refinement, because in this case these regions are non-convex and do not contain Pareto optimal solutions.

g. Compute the length of the segments between all the neighboring solutions.

Delete nearly overlapping solutions. If all the segment lengths are less than a prescribed maximum length, λ_K, terminate the optimization procedure. If there are segments whose lengths are greater than the maximum length, go to Step (d) and iterate.

4.4 Case Study

4.4.1 Supply and Demand Data

The *BoWS* approach is implemented to find the optimal configuration (cost and efficiency) of a GCPV system to be installed on the generation section I (GSI) of Alsabyia generation station part of Kuwait national grid [5,7,8]. This section has a peak active power of 196.12 MW. The generation profiles in the problem are assumed identical to the generation pattern of Kuwait, with the generation profiles in each season averaged to get a single representative profile. Likewise, the supply power profiles of the PV panels for each season are illustrated in Fig. 4.3 (using Ch.1, Ch.2, Ch3 and MATLAB). The PV solar power data used in this case study was extracted from the data calculated in Chapter 2. As mentioned in Chapter 3, the SMC-PV module type having a rated capacity of 300 W_P, participated in this approach. Regarding Table 3.2, the data collected for one panel of the SMC-PV modules was used to obtain an average supply profile for each season.

The daily electrical demand pattern of the system is assumed constant for each season, so there are four demand patterns representing the entire year. There patterns are assumed similar to those of Kuwait. Demand data for January and August 2013 published by Kuwait Water and Electricity Ministry (KWEM) [8] was used to extract the demand patterns for the rest of the months through linear interpolation. Then the demand patterns for the three months of each season (Winter: December, January, and February, Spring: March, April, and May, Summer: June, July, and August, and Autumn: September, October, and November) are averaged to get the demand pattern for the corresponding season. Fig. 4.4 shows the average daily demand patterns of the four seasons used in the model.

4.4.2 Model Parameters

a) Cost of system components

Current cost for a typical commercial scale SMC-PV module is 4 $/W, in line with current market prices for PV panels, depending on the number of PV modules in each

series and parallel strings (Table 3.2) and including installation and salvage costs, which are estimated as 30 % above this figure.

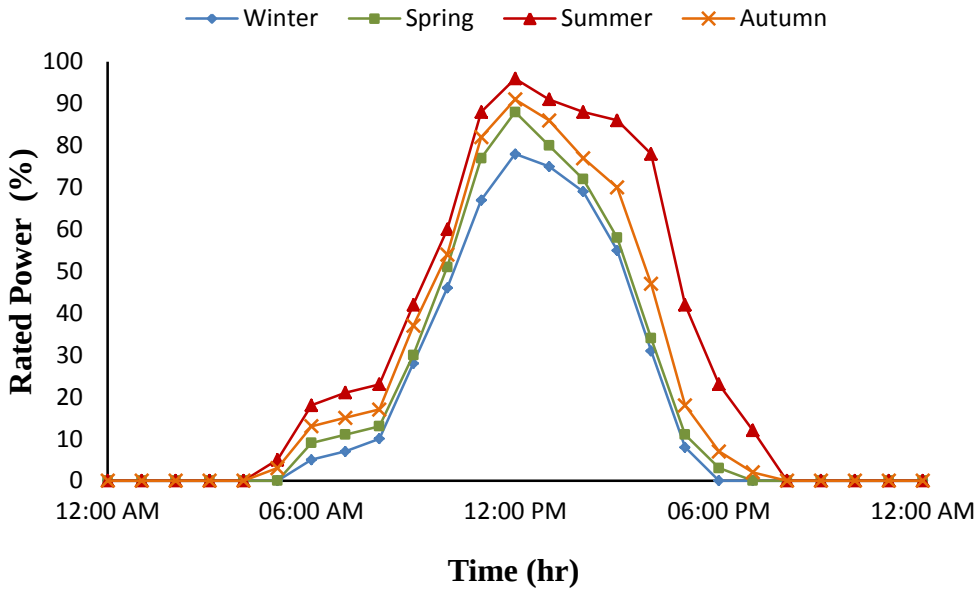

Figure 4.3: Average daily rated power profile of the PV panel for each season

Each PV panel has a maximum output power of 70 kW and can store up to 420 kWh of energy. Component's initial cost is amortized over their lifespan using 10 % discounting rate and zero salvage value. The main operational cost of the system is the cost of power purchased from the GCPV. According to the 2013 annual report issued by Gulf Regulation and Supervision Bureau (GRSB), the average cost of electricity supplied to bulk users is equivalent to 0.04076 $/kWh. Operating and maintenance cost for other system components are included.

b) Efficiency of system components

Values for the efficiencies of the different system components were sources from the technical literature. In 2013, solar modules available for consumers can have an efficiency of up to about 23 %, while commercially available panels can go as far as 27 % and are estimated using an industrial process analysis method, whereas those of the inverters ranges between 90 % and 95 % (see appendix B) and are calculated using the inter-industry method. The efficiency of the inverter drives the efficiency of a PV panel system because inverters convert direct-current (as produced by the PV panels) into alternating-current (as used by the electric grid) therefore the inverter's efficiency will affect strongly the overall efficiency of the GCPV system.

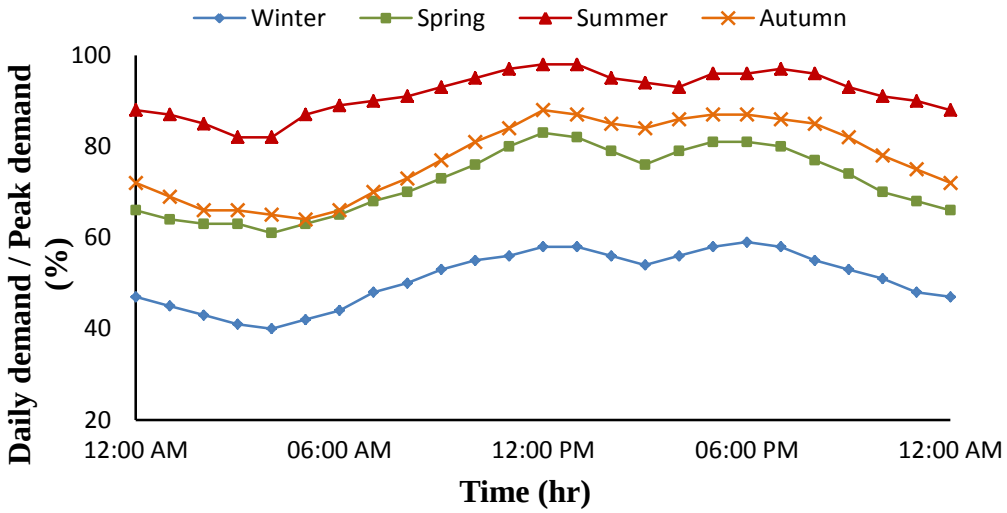

Figure 4.4: Average power demand of the system as percentage of peak demand

c) Useful life of system components

In most literature, the lifespan of a PV panel is taken as 25 years, and that is the value used in our case. Life span of the DC-AC inverter depends on operating conditions. Model parameters are summarized in Table 4.1.

4.4.3 Numerical Main Objective Function

The model parameters in the previous section with Table 4.1 will be substituted in the main objective function stated in eqn. 4.15 in order to convert it into an applicable numerical function ***K(z, a)*** and implement it in *BoWS*. The optimization problem will be performed with the Sequential Quadratic Programing (SQP). In this optimization problem, the design variables (*i.e.* rated capacities of GCPV) are typically of discrete nature, meaning that only certain values can be used for these variables. The rated capacity installed of each system component must be a multiple of the capacity of its individual units.

4.5 Results and Discussion

Table 4.2 depicts the results obtained upon applying optimization on the system under study to minimize the cost of PV system and to maximize the system efficiency, separately. When the system is operating in the grid-connected mode, the electrical grid and PV array are combined to fulfill the load demand. Due to the high capital and operating costs of system components the total cost of the GCPV system is almost tripled in compared to the initial cost of system which not exceed (as agreed with the sponsor) in the worst case somehow 300 m$. Initial cost and electricity cost is most sensitive to the cost of the PV module. On the other hand, when the design objective is

Table 4.1: Parameters of the Capacity Planning Problem that Implemented to set up the *BoWS* Method

Parameter	Value	Unit
Daily averaged SR	eqn. 2.15 for any n	W/m^2
SR at STC	1000	W/m^2
Temperature coefficient at MPP	0.52	% per °C
Effective PV module temperature at STC	25	°C
Average annual ambient temperature of PV cell at Kuwait area [8]	38.4	°C
Effective PV module temperature at site	eqn. 4.7	°C
Nominal PV module power at STC	250	W
Simulation sampling interval	1/60	hour
Sizing factor of ith inverter	Table 3.2	----
Feed in tariff (fixed	4.0	¢/kWh
Nominal annual discount rate	2.8	%
GCPV economical factor	eqn. 4.11	----
Energy conversion factor	98	%
Initial cost of SMC-PV module	4	$/W
ith inverter price	See Appendix B	$/W
PV module's installation cost	1500	$/module
Annual inflation rate (2013 - Kuwait)	2.1	%
Government subsidization rate	23.4	%
Ave. ann. maintenance cost of PV array	≈ 115	$/kW
Ave. ann. maintenance cost of ith inverter	≈ 21	$/kW
The ith inverter repair cost	≈ 350	$/kW
ith inverter model coefficients	{-0.2418, -1.127, 96.1}	----
Efficiency of SMC-PV module	23	%
Efficiency of the ith inverter	See Appendix B	%
Operating lifetime of PV panels	25	years
Useful life of DC-AC inverter	depends on the operating condition	years
Peak demand of the system	196.12	MW

to maximize system efficiency, the results are expected. As shown in Table 4.3, the electrical efficiency rises to a high value when energy was entirely supplied by the same

system components used to minimize system cost.

Table 4.2: Cost Minimization Results of the Capacity Planning Problem

Parameter	Value
PV capacity installed (MW)	97
Installation cost (bn$)	0.788
Operating cost (bn$)	0.035
System total cost (bn$)	0.895

Table 4.3: Efficiency Maximization Results of the Capacity Planning Problem

Connectivity to the grid	Value
PV capacity installed (MW)	97
PV annual energy produced (GWh)	9.723
PV panel output power (kW)	690
Inverter rated power per string (kW)	2500
System efficiency (%)	96.3

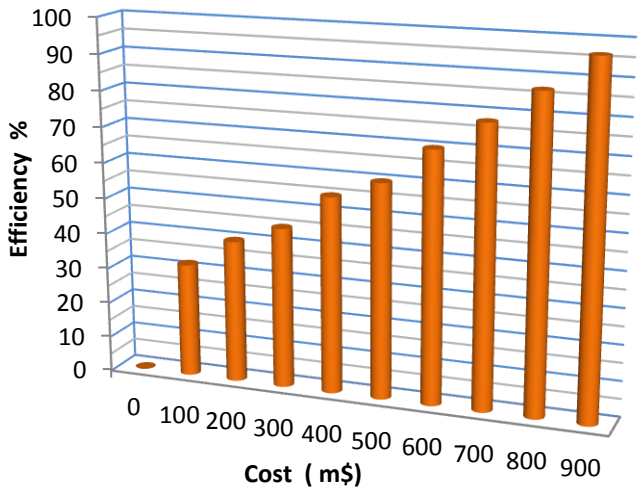

Figure 4.5: Cost vs efficiency of the optimized GCPV system

Fig. 4.5 will clarify the results in both tables. It is impossible to get the system configuration with the minimal cost and maximal efficiency simultaneously for the GCPV power system. The reason is that although increasing the size of the inverters can improve the system efficiency, the system cost grows greatly at the same time as shown in both tables. Selecting the middle point may be a trade-off between cost and efficiency for the PV system, but is neither the only nor the best method to reduce the system cost

and improve the system efficiency for its limited effect on them. Therefore it is not possible to achieve the two objectives simultaneously, but to find the best trade-offs between them, which can be graphically represented using the Pareto front concept. The Pareto front line of the main objective function specified in eqn. 4.15 is convex, but the curvature is not uniform. Fig. 4.6 shows the optimal solution obtained by the usual weighted-sum method. The number of solutions on the Pareto front is 30, but most of the solutions are concentrated in the middle region. Clearly, the solution obtained will depend on the values of the weights specified. By changing the weight of each objective function, multiple points in the Pareto front can be located and then the front can be constructed. Fig. 4.6 shows the wide range the designer can move within depending on the design criteria selected. The average slope of this curve can be interpreted as 'the cost of being green'. Steeper curve implies higher cost of increasing efficiency than a flatter one.

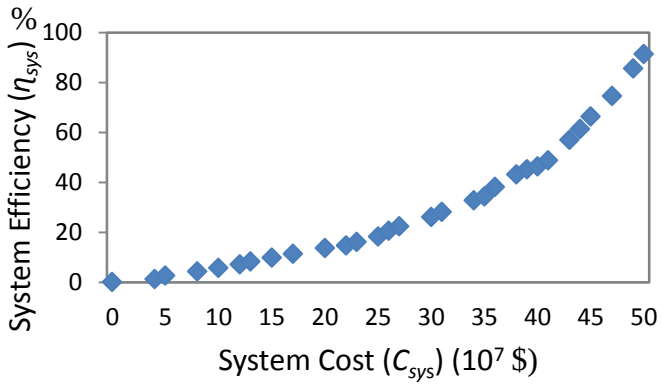

Figure 4.6: Pareto front and the solution space

Fig. 4.7 provides some insight on an application of the Pareto front for the design of the system. A line with a slope of energy price can be plotted on the Pareto plot. Moving the line to get into tangency with the curve will show the optimum solution directly. To explain that, let's examine the net effect of shifting from solutions *II* to solution *I*, both are shown in Fig. 4.7. The system cost will increase by the distance (*aO*), while the increasing in efficiency will generate energy credit that can be sold at a value equal to (*bO*), so there is a net gain of (*ab*) resulting from this shift. On the other hand, moving from solution *III* to solution *I* will reduce the system cost by the distance (*dO*), while the value of energy credit units that have to be purchased to offset the decrease in efficiency is (*cO*), so the net gain is the distance (*cd*). In both cases there was a gain for moving

towards solution *I*, the tangency point, so it is the most suitable solution if energy price is taken into consideration.

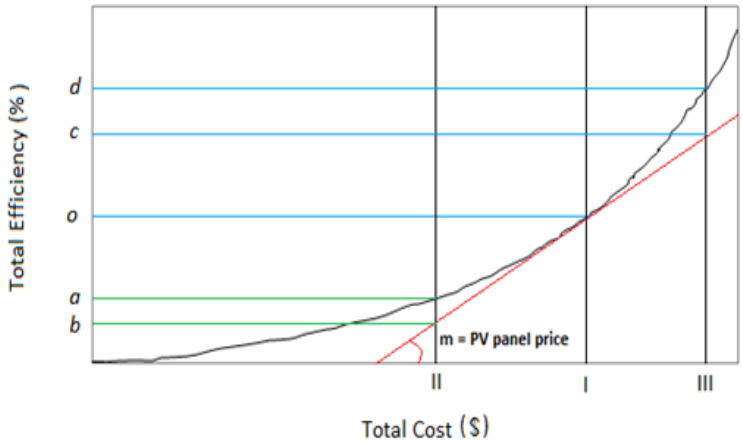

Figure 4.7: Determining the best trade-off based on PV panel price

The *BoWS* method converges in six iterations, obtaining fairly well distributed solutions as in Fig. 4.8. The offset distance selected on the Pareto front, λ_K, is 0.1; and the offset distances, λ_1 and λ_2, are calculated by eqn. 4.34. Table 4.3 provides a quantitative comparison of solutions in terms of computational cost (CPU time) and variance of segment lengths. The *BoWS* method is performed for the case of 30 discrete solutions on the Pareto front. In this well-conditioned bi-objective optimization problem with a convex Pareto front, it's clear that the proposed *BoWS* method is fast, its variance is very large and it has a better performance both in terms of CPU time and secant length variance. However, the uniformity of the solutions obtained by the proposed weighted sum method is satisfactory according to the maximum length criterion. On the other hand, the cost-efficiency main objective function made the *BoWS* to have relatively heavy computational cost due to additional calculations, such as obtaining the distances between adjacent solutions and selecting segments for further refinement.

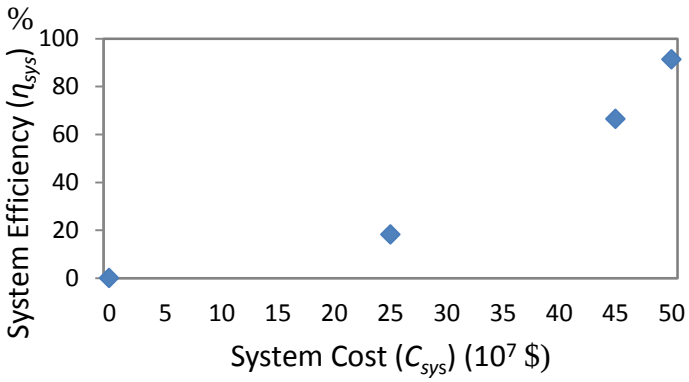

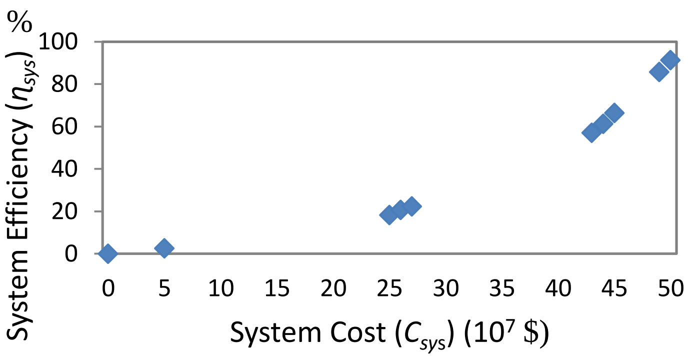

System Efficiency (n_{sys}) %
System Cost (C_{sys}) (10^7 \$)

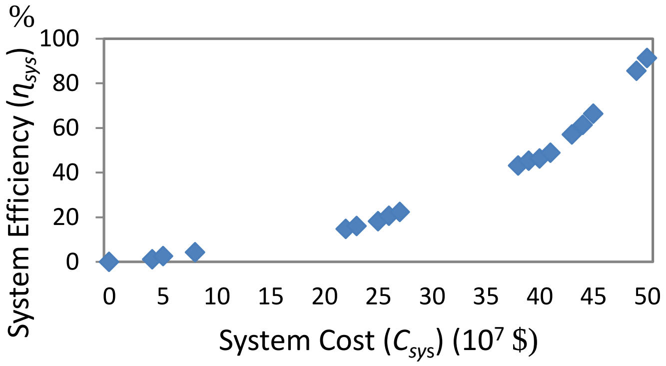

System Efficiency (n_{sys}) %
System Cost (C_{sys}) (10^7 \$)

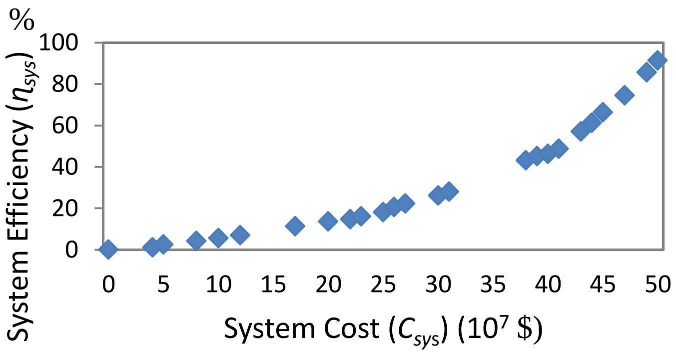

System Efficiency (n_{sys}) %
System Cost (C_{sys}) (10^7 \$)

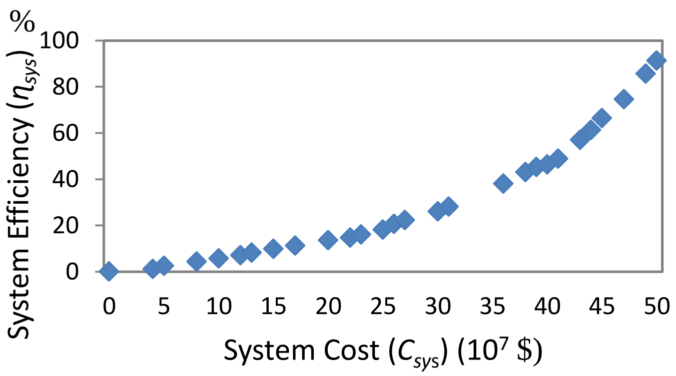

System Efficiency (n_{sys}) %
System Cost (C_{sys}) (10^7 \$)

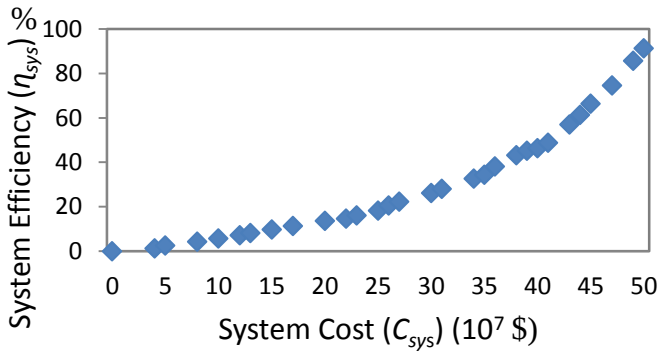

Figure 4.8: Results for cost-efficiency optimization with convex Pareto front

There are four important parameters that the user must set: the offset distance (λ_K); the Euclidean distance for determination of overlapping solutions (ε) used in Step 3 and Step 8; the constant for further refinement (c) used in Step 4; and the number of the Pareto front segments in the initial iteration ($d_{initial}$). The offset distance, λ_K, determines the final solution distribution density and can be chosen independently of other parameters. Values between 0.05 and 0.2 in the normalized objective space are recommended. The smaller λ_K is, the denser the final solution distribution becomes. The overlapping solution distance ε must be smaller than λ_K. In this method, ε is 50 % of the magnitude of λ_K, and well-distributed solutions are obtained. The multiplier c must be chosen carefully. If it is too small, no further refinement will be conducted in subsequent iterations, and the optimization will terminate prematurely. If it is excessively large, many overlapping solutions will be generated, and the computational cost will increase. By many trails, the optimization progresses well with reasonable computing time when c is between 1 and 2. The initial number of Pareto front divisions, $d_{initial}$, must be selected in the same way. A small initial will not lead the optimization to subsequent iterations of further refinement, but on the other hand, the computational cost will become too expensive with a large value of $d_{initial}$. In the same way of trials, a proper range is between 3 and 10. It is noted that the optimization behavior depends on the parameter selection to some extent. Currently the parameters can be chosen only heuristically, and more study is needed to investigate this issue. In particular, $d_{initial}$ and c should be selected in consideration of each other. For example, when a small $d_{initial}$ is used, a large c would help prevent premature convergence.

4.6 Conclusions

A strategy for GCPV system design using a *BoWS* (cost-efficiency) optimization model that aims in finding the optimal cost and gross capacity installed of GCPV panels under

some simplifying assumptions has been proposed in this thesis. The model can be used to get a quick, yet rough, estimation of the PV panel capacity needed and the economic and performance measures of a GCPV system, in order to help the planner narrow the options and assess the applicability of them. The proposed strategy of the *BoWS* method has been implemented using the SQP. The results show a clear trade-off between the two objectives sought: minimizing total cost and maximizing system efficiency, which was graphically represented through Pareto optimal front. It has been shown also that, even when optimally planned, the utilization of PV array powered electrical grid can be only justified when the main grid is not able to satisfy the load demand at the desired reliability level or when environmental criteria are considered. Among the possible PV panel combinations for this specific case study, GCPV system proved to be the best option in terms of cost and efficiency. The implementation of *BoWS* optimization model and its main objective (design) function highlights the impact of the simplifying assumptions embedded in the model.

The main contribution of this chapter is the development of novel cost-efficiency objective function implemented in a modified optimization model (*BoWS*) for the optimal design of GCPV system with PV array powered electrical grid via DC-AC inverters that overcome the deficiencies in previous studies. The model presented here is specifically useful for the design of extended GCPV system, similar to the power system of Alsybia power plant. The proposed cost-efficiency *BoWS* technique is generic and flexible, allowing different design criteria, power generation and conversion technologies, operational strategies and constraints, and system configurations to be incorporated comparatively not difficult.

The GCPV capacity planning technique proposed in this section has the advantage of being simple and quick. The case study presented has only 29 variables and constants and has 5 constraints, which is considered a linear programming problem. Another aspect of simplicity is that the model inputs are limited and easy to acquire. The model doesn’t require any knowledge about the network topology, the detailed variations of PV power supply and load demand, or the deep technical characteristics of the system components. This simplicity enables the system designer to get very quick estimates of the solution and test its feasibility before trying more constrained and complex problems. This model has been used to find the optimal configuration of the proposed GCPV system that can satisfy the demand at Alsybia power plant.

Chapter 5
Simulation of the Proposed GCPV System

5.1 GCPV Simulation Overview

Comprehensive monitoring of GCPV system requires adequate analysis of the calculated data. Research has deeply analysed and sized the proposed model for the components of a GCPV system, including equivalent circuit of the PV module or panel and configuration with dynamic response of the inverter. Other important aspects will be addressed later, related to the inclusion of the proposed PV system into a specific distribution network in Kuwait (mainly part of the power generation unit at Alsybia electrical network). Therefore, the key technology of a PV system includes PV cell modelling, maximum power point tracking (MPPT) algorithm, DC-DC converter and grid-connected DC-AC inverter.

When larger PV installations are designed, there is a need to understand their performance when integrated with the power system (a specific section of Alsabyia generation station part of Kuwait national grid). Therefore, simulations of large PV installations integrated within the electrical grid are necessary. Numerically the problem that needs to be solved is a combination of non-linear equations describing the PV generators, including the switching inverters, operational DC-DC converter and the PV generation with linear equations describing the rest of the power system. Many studies have discussed and proposed solutions to the numerical problems posed by GCPV power simulations [76, 77]. From a purely mathematical point of view, at each step of the simulation, the set composed of non-linear equations representing PV generators and linear equations describing the rest of the power system must be solved, using an iterative numerical algorithm [77]. Some power system simulation tools adopt this approach, such as PSIM and MATLAB/Simulink. This approach is accurate, but with the drawback of a heavy computational burden when simulating large distribution networks including PV systems [78]. In general, there are two main approaches that all PV simulation software used to treat these numerical problems.

5.1.1 Extended Linear System Technique

The first approach to overcome numerical problems, namely the Extended Linear System Technique (ELST) [77], is proposed in the following starting from the methods used to include rotating machines and switching devices in power system simulation.

The basic idea is to add a linear representation of the non-linear equation of the PV generator into the solution of the rest of the power system.

5.1.2 Separation of Nonlinear Equation Approach

To guarantee computational efficiency a different approach is used by separating the non-linear equations of the PV generators from the linear equations of the rest of the power system. This approach is referred to as Basic Linear System Technique (BLST) and is adopted by PSIM and MATLAB/Simulink and it is also used by ETAP (Electrical Transient Analyser Program) or EMTP (Electromagnetic Transient Program) [77, 78]. However, the non-linear equations introduce a dependency of the current injected by the PV generator on the terminal voltage, which in turns is related to the operating conditions of the whole power system. Such a dependency can cause numerical instability of the simulation [79].

5.2 GCPV System Simulation Setup

Simulation of a GCPV system using PSIM is the core of this chapter. The system discussed in this work consists of a PV module, a DC-DC boost converter, and a DC-AC inverter. The system described here uses a simplified PV cell model; however the model includes the effects of changing the SR. The maximum power of the PV module is tracked with the help of MPPT algorithm that is incorporated in the DC-DC converter. The inverter used to regulate the output-voltage of the converter is connected to the rest of the grid through a LC filter which ensures a clean current injection.

The detailed modelling and sizing of the proposed GCPV system have been discussed, performed and analysed in Chapter 3 and the output of the optimal cost-efficiency model of Chapter 4 have been used as inputs to the simulation process. A simulation model of the electric part of a grid-connected photovoltaic generator will be presented in this chapter. The model contains a detailed representation of the main components of the system that are the solar array, boost converter and the grid side inverter. PV array is connected to the utility grid by a boost converter to optimize the PV output and DC-AC inverter to convert the DC output voltage of the solar modules into the AC system. The grid interface inverter transfers the energy drawn from the PV module into the grid. The DC input of the inverter must be constant and it is controlled by the use of boost converter control circuit.

Fig. 5.1 shows the general topology of a PV generation system. The PV depicted below is a standard integrated PV system connected to a DC-DC converter and then pulse-

width modulation (PWM) DC-AC inverter. Since the output voltage of the PV module has a very wide variation voltage range, in general, the DC-DC converter is used to get constant high output DC voltage with MPPT to track the maximum power of the PV system. In order to use the DC output power for residence applications, it is required to convert the DC output power to AC power using a PWM inverter. The PV generation system either off grid which may be used isolated from the grid network or on grid that is connected to grid. An on grid PV system, feeds electricity directly into the grid, offsetting the amount of electricity supplied by the grid. If the amount of electricity produced by the system is greater than the amount being used by the residence, the excess is fed into the grid resulting in the account being credited by the amount fed in, causing the grid to act as a sort of electrical bank. An off grid system has no connection to the grid and must rely on a PV system for its electricity supply. Since there is no grid on at the night time or when the solar panels aren't producing sufficient power to supply the consumer's needs, a storage system as a battery bank is used to store excess power for later use when the supply from the solar panels is insufficient. This study is based on off grid PV generation system; however the storage system is not included in this section.

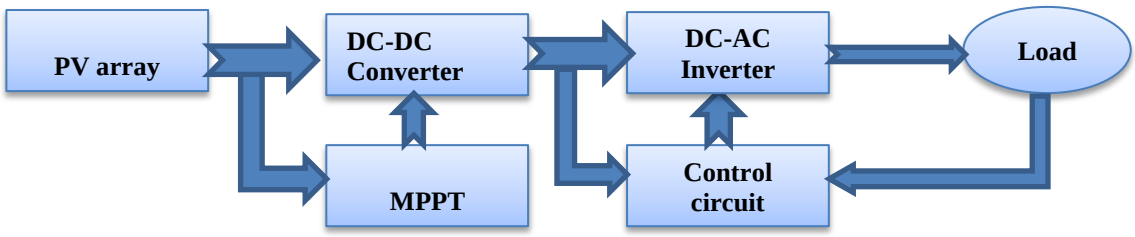

Figure 5.1: Schematic diagram of complete PV generation system

The simulation process is quite sophisticated. It uses a current-voltage (*I-V*) curve characterization of the SMC-PV module accounting for the instantaneous cell temperature (see Chapter 3). We chose to evaluate a 4384 m^2 off-grid PV array in Kuwait (see Table 3.2). Specifications (input variables for the simulation process) carried in the database and transferred to the PV simulation are:

- Total SR over Kuwait area.
- Actual capacity of the PV array.
- Length and width of the PV module.
- Open-circuit voltage.
- Short-circuit current.
- Voltage temperature coefficient.

- Current temperature coefficient.
- Number of modules in series.
- Number of modules in parallel.
- Panel configuration (Engineers can use Pareto front line output of Chapter 4 to take decisions about the optimal configuration of the PV panel according to their needs).
- Some important characteristics of the selected PV module such as efficiency, cell temperature, sizing factor and temperature coefficients.
- Some important characteristics of the selected inverter such as AC power, voltage, PV voltage range at maximum power, maximum efficiency and maximum input current.

The system characteristics are system voltage, current, panel capacity, mismatch and inverter power and efficiency at rated power. In the present program, which simulates GCPV system, the controller is assumed to achieve cell operation at the MPP. In the following sections of the chapter each of the important parts of the model will be introduced and explained. First the PV cell model is introduced. The model is simple, accurate, and takes SR into consideration. Then the MPPT control algorithm is discussed. The P&O method is then used in conjunction with the MPPT algorithm. In the results obtained from a PSIM simulation are also presented. Section 5.3.3 explains the reasons of using a boost converter for this application as a DC-DC converter, and it discusses the operating principle. Finally the last part of the system DC-AC inverter is discussed before the whole PV system is presented. The system simulation results are presented and discussed.

5.3 Individual Simulation Results

Simulation of the system is not an end in itself; it is to permit insight into the operation of the system in such a way that weaknesses can be identified [80]. The proposed model of the entire components and control system are all simulated in PSIM Software. The simulation results under PSIM show the control performance and dynamic behaviour of GCPV system.

5.3.1 Modelling and Simulation of SMC-PV Cell and Module

As mentioned in Chapter 3, the basic unit of a PV generator is the PV cell. An individual PV cell typically produces from 1 to 2 W. To increase the power, cells are electrically connected to form larger units, called PV modules. In practice, a PV module

consists of PV cells connected in series. Modules, in turns, can be connected in series and parallel to form larger units called PV panels. Panels connected in series constitute a PV array. Arrays connected in parallel constitute a PV generator. The single-diode equivalent circuit is the most commonly adopted model for PV cells, accounting for the photon-generated current and the physics of the *p-n* junction of a PV cell. The simulation structure of the PV model and the packaged model in PSIM has been shown in Fig. 5.2 and Fig. 5.3.

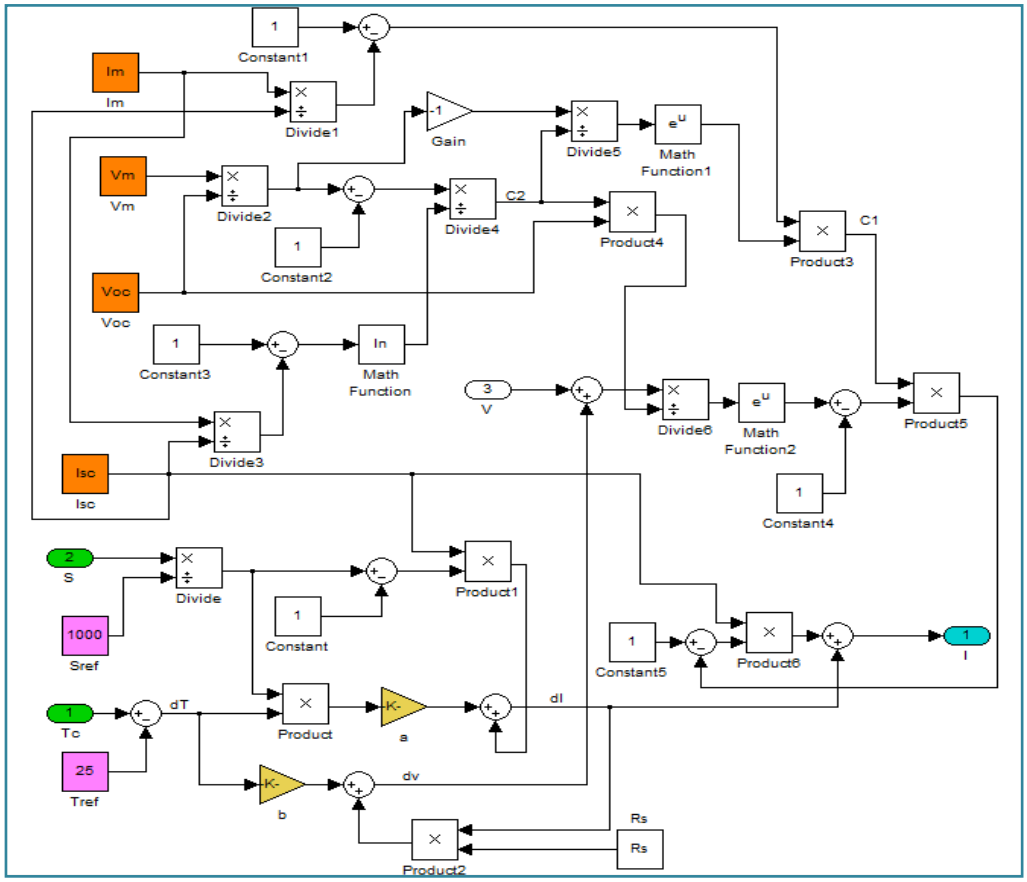

Figure 5.2: Simulation structure of PV model

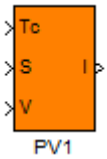

Figure 5.3: Packaged model of the PV cell

As mentioned earlier, the equivalent circuit of the PV cell, which can be expressed as a photodiode with a large *p-n* junction in parallel with an ideal current source can express PV modules, panel and array. Although an equivalent circuit of PV modules can express well the *I-V* characteristic, practical *I-V* characteristics of PV module are usually obtained by using polynomial approximate equations with coefficients obtained

experimentally [77]. This may result from the difficulty in estimating the correct model parameters. Recent progress in microprocessor performance has enabled us to calculate the parameters in real time. A PSIM program was used for to validate the developed solar module model. Fig. 5.4 shows the solar panel circuit model as it is implemented based on *SAIMA* results. The proposed simulation model of the PV module consists of a function supply, PV module equivalent circuit, current limiter to control the PV current in case of faults or shading, a DC chopper which changes operation points and a control circuit. The parameters used to define the PV cell are shown in Table 5.1.

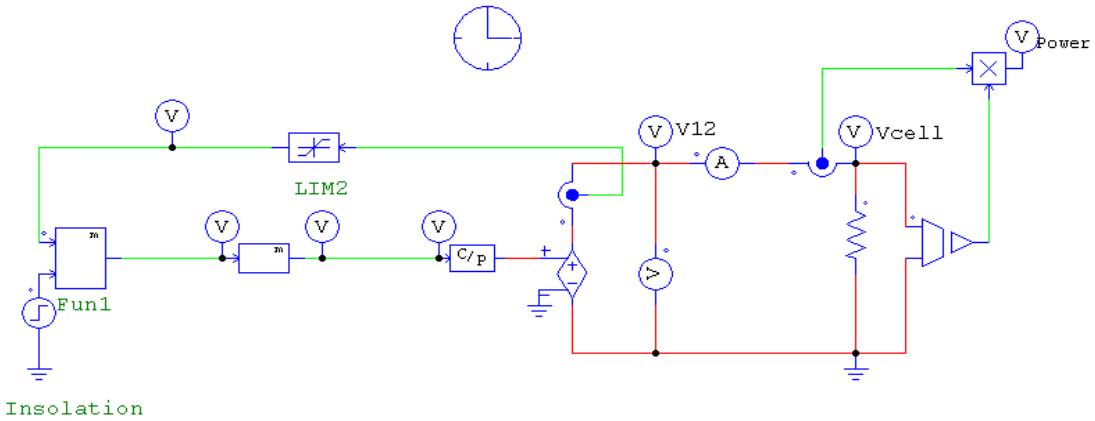

Figure 5.4: Proposed PV module circuit model

Table 5.1: Parameters of the PV Cell in PSIM Model

Parameter	Variable	Value
Current at Maximum Power	I_m	4.95 A
Voltage at Maximum Power	V_m	35.2 V
Open Circuit Voltage	V_{oc}	44.2 V
Short Circuit Current	I_{sc}	5.2 A
Temperature Coefficient of Short Circuit Current	a	0.015 A/°K
Temperature Coefficient of Open Circuit Voltage	b	0.7V/°K
Internal Series Resistance	R_s	0.217 Ω
Reference Solar Radiation	SR_{ref}	1000 W/m2
Reference Temperature	T_{ref}	25°C

The PV-side DC voltages, current and power are illustrated in Fig. 5.5 to Fig. 5.7. As expected the simulation results became consonant with *SAIMA* results which support the proposed model. The results obtained show that the PV module voltage, current and power settle to 52 V, 5.7 A and 293 W respectively after a brief transient due to the switching. These results gave us confidence in the PV module model. The output is a

voltage that drives an assumed resistive load, R_L. Note that the solar panel current can be varied by changing the load resistance and both voltage and current at the output of the solar panel can be tracked and measured.

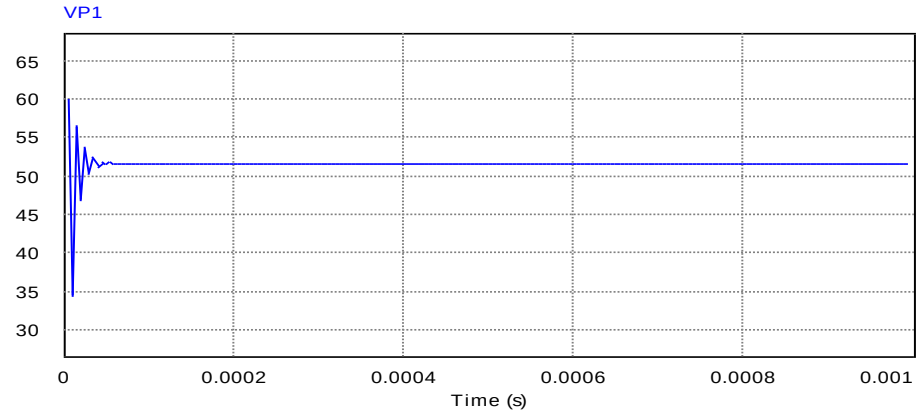

Figure 5.5: PV-side voltage waveform per module

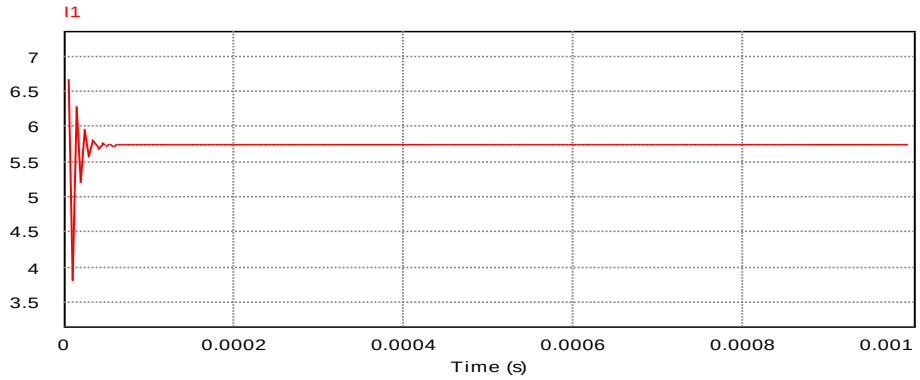

Figure 5.6: PV-side current waveform of per module

The output voltage, current and power of one panel of the proposed GCPV system are depicted in Fig. 5.8 and Fig. 5.9. It should be noted there is a very good agreement between expected (53 V, 5.8 A) and simulated signal (E_{PV}, I_{PV}).

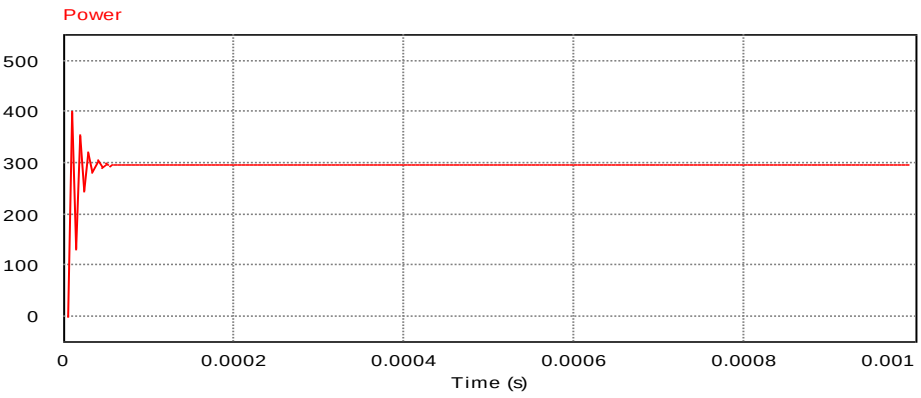

Figure 5.7: PV-side power waveform per module

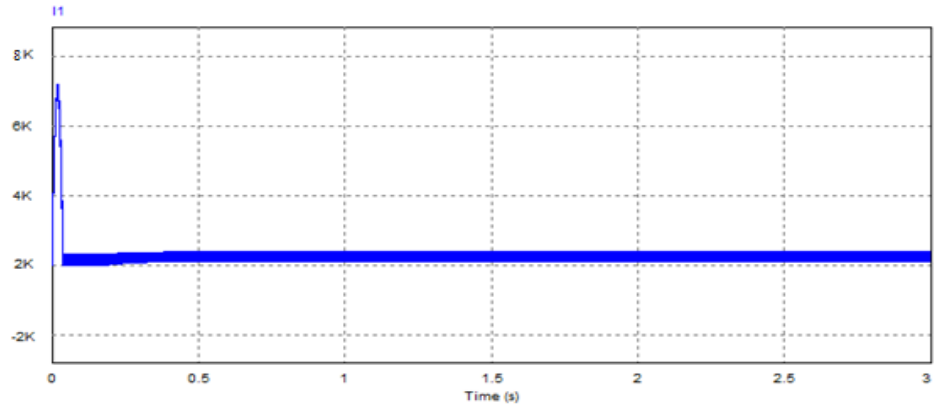

Figure 5.8: PV-side voltage waveform per panel

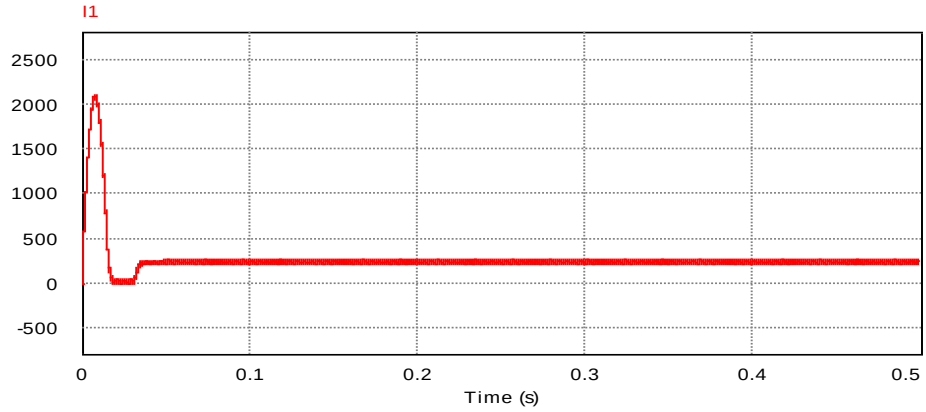

Figure 5.9: PV-side current waveform per panel

The simulation results for the *I-V* and *P-V* curves are shown in Fig. 5.10 and Fig. 5.11 (also see appendix C). Fig. 5.10 shows the *I-V* characteristic curve of one PV string whereas Fig. 5.11 shows the *P-V* characteristic curve. The model curves match with the *SAIMA* results at three remarkable points: short-circuit current, open-circuit voltage, and maximum power point. It can be noticed that the PV string behaves like a current source when the output voltage is less than a threshold value as the current changes very little with the change in output voltage. Whereas above the threshold voltage behaves more like a voltage source whit a sharp drop in current as the voltage is increased.

The span of the *I-V* curve of one PV string ranges from the short circuit current (I_{sc} = 275 A) at zero volts, to zero current at the open circuit voltage (V_{oc} = 3650 V). At the 'knee' of a normal *I-V* curve there is a point where the PV cell generates the maximum power and is called maximum power point, MPP, (I_{mp} = 250 A, V_{mp} = 3000 V). In an operating PV system, one of the jobs of the inverter is to constantly adjust the load, seeking out the particular point on the *I-V* curve at which the array as a whole yields the greatest DC power. At voltages well below V_{mp}, the flow of solar-generated electrical

charge to the external load is relatively independent of output voltage. Near the knee of the curve, this behaviour starts to change. As the voltage increases further, an increasing percentage of the charges recombine within the solar cells rather than flowing out through the load. At V_{oc}, all of the charges recombine internally. The maximum power point (MPP = $P_{max}(string)$ = 750 kW), located at the knee of the curve, is the (I, V) point at which the product of current and voltage reaches its maximum value.

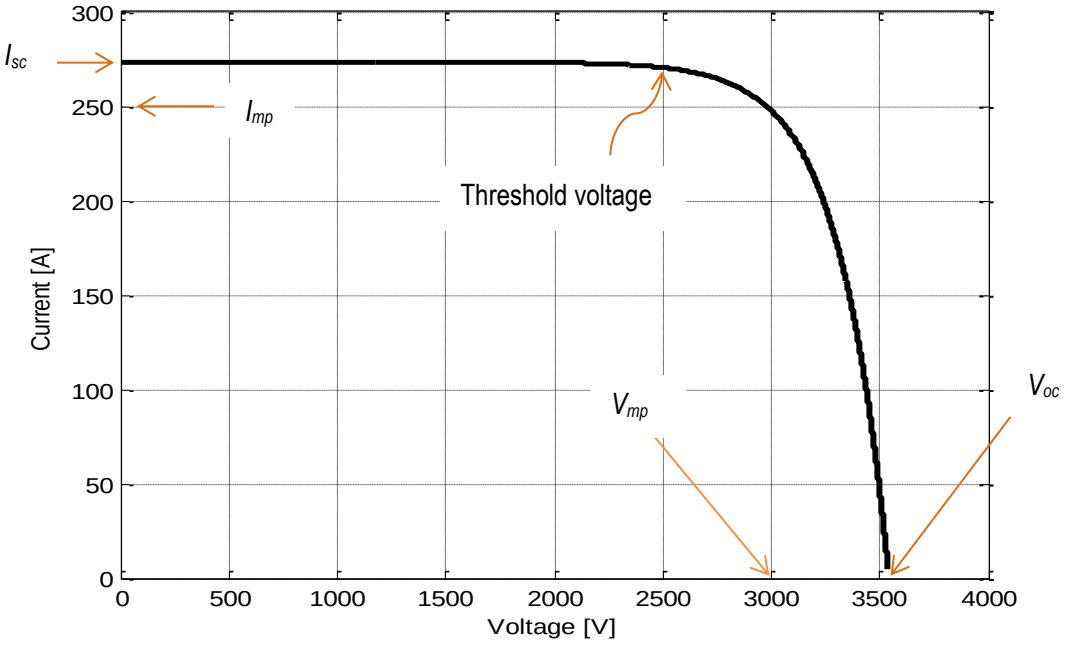

Figure 5.10: *I-V* characteristic of one SMC-PV string

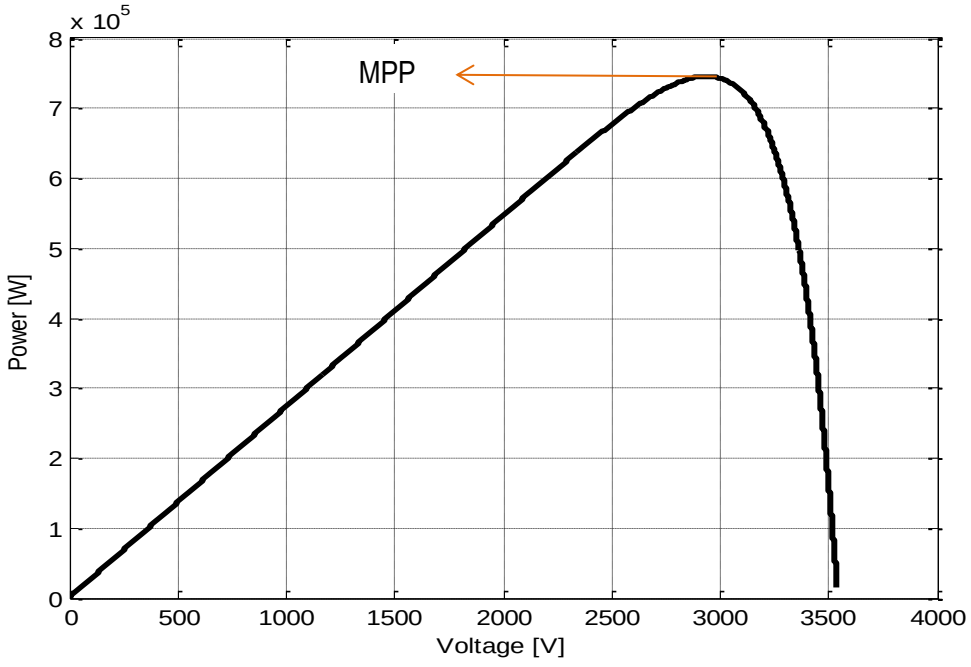

Figure 5.11: *P-V* characteristic of one SMC-PV string

5.3.2 Maximum Power Point Tracking (MPPT) Control Algorithm

A MPPT is used to extract the maximum power from the PV cell and transfer it to the load [81]. Since the output power of PV cell is related with many parameters such as SR, temperature and load, the output characteristic is nonlinear with respect to the output voltage. It is necessary for the PV system to work at the maximum power point under changing external environment to achieve best performance. Furthermore, this point depends on the SR and temperature of the panels and both conditions change during the day and are different depending on the season of the year. Moreover, SR can change rapidly due to changing atmospheric conditions such as clouds. It is very important to track the MPP accurately under all possible conditions so that the maximum available power is always obtained. Improving the tracking of the MPP with the developed control algorithms (see Fig. 5.13 and Fig. 5.14) is easier, not expensive and can be done even in plants which are already in use by updating their control algorithms, which would lead to an immediate increase in PV power generation and consequently a reduction in its price [82]. On the other hand trying to improve the efficiency of the PV panel and the inverter although important is not simple and could be very costly as it depends on many variables and manufacturing technologies available.

5.3.2.1 Comparison of Various MPPT Algorithm

Over the past decades various methods to find MPPT algorithm have been developed and published. These techniques differ in many aspects such as required sensors, complexity, cost, range of effectiveness, convergence speed, correct tracking when SR and/or temperature change. There are 19 different commonly used MPPT algorithms and among these techniques [82], the Perturb and Observe (P&O) and the Incremental Conductance (IC) algorithms are the most common. These techniques have the advantage of an easy implementation but they also have drawbacks, as will be shown later. Other techniques based on different principles are fuzzy logic control, neural network, fractional open circuit voltage or short circuit current, current sweep, etc. Most of these methods yield a local maximum and some, like the fractional open circuit voltage or short circuit current, give an approximated MPP, not the exact one. In normal conditions the *P-V* curve has only one maximum, so it is not a problem. However, if the PV array is partially shaded, there are multiple maxima in these curves. In order to relieve this problem, some algorithms have been implemented. In the next sections the most popular MPPT techniques are discussed.

5.3.2.1.1 Perturb and Observe (P&O) Method

The P&O method involves a perturbation in the operating voltage of the DC link between the PV array and the power converter. This method is easy to implement, because the sign of the last perturbation and the sign of the last increment in the power are used to decide what the next perturbation should be. If there is an increment in the power, the perturbation should be kept in the same direction and if the power decreases, then the next perturbation should be in the opposite direction. Based on these facts, the algorithm is implemented. The process is repeated until the MPP is reached. Then the operating point oscillates around the MPP.

5.3.2.1.2 Incremental Conductance (IC) Method

This method uses the fact that the slope of the *P-V* curve is positive on the left of MPP and negative on the right of MPP, it is an accurate and rapid method but it is complex and puts great requirements on the hardware

$\Delta P/\Delta V > 0$ *(*$\Delta P/\Delta I < 0$*)* on the left of MPP

$\Delta P/\Delta V < 0$ *(*$\Delta P/\Delta I > 0$*)* on the right of MPP

$\Delta P/\Delta V = 0$ *(*$\Delta P/\Delta I = 0$*)* at the MPP

By comparing the increment of the power vs. the increment of the voltage (current) between two consecutives samples, the change in the MPP voltage can be determined.

5.3.2.1.3 Fractional Open-Circuit Voltage Method and Fractional Short-Circuit Current Method

The former method uses the approximately linear relationship between the MPP voltage (V_{MPP}) and the open-circuit voltage (V_{oc}), which varies with the SR. A constant depending on the characteristics of the PV array has to be determined beforehand by determining the V_{MPP} and V_{oc} for different levels of SR. Once the constant is known, the MPP voltage V_{MPP} can be determined periodically by measuring V_{oc}. For the latter method, there is a relationship, under varying atmospheric conditions, between the short-circuit current, *Isc*, and the MPP current, I_{MPP}. Its implementation is just like in the fractional open-circuit voltage method.

5.3.2.2 Proposed MPPT Algorithm

MPPT algorithms are necessary in PV applications because the MPP of a PV panel varies with the SR, so the use of MPPT algorithms is required in order to obtain the

maximum power from a PV array. In this research, we choose the Perturb and Observe (P&O) method for its simplicity, relatively accuracy and rapid response [83, 84]. Fig. 5.12 shows the flowchart of P&O method. By comparing PV cell output power of each control cycle before and after the perturbation, the new perturbation direction can be determined. If the output power is increasing, the previous voltage perturbation direction will be followed in the new cycle. Otherwise, the voltage perturbation direction will change. By this algorithm, the operating point of PV cell can get closer to the maximum power point and finally reach a steady state.

5.3.2.3 MPPT Algorithm Simulation

One of the objectives of this study is to develop a model to test the dynamic performance of the MPPT algorithm shown in Fig. 5.12 independently of the converter used. A detailed model of a PV system, with the switching model of the power converter, is computationally very demanding while the time that can be simulated in a normal computer is only a few seconds. However, the simulation time required for testing the system with the SR profiles proposed in Chapter 2 can be up to several minutes, which can be difficult or impossible to achieve on conventional PC, if a complete model of the PV system would be used. The main limitation for such simulation is the limited amount of memory available on a conventional PC. For example, to increase the reference voltage and go back to compute the new output power the program has to check again all the power values with different average daily and monthly SR and this process takes several minutes. The model proposed here was developed in PSIM and consists of a PV array model, a DC-link capacitor and a controlled current source, which replaces the power converter. The MPPT control block generates the reference voltage using the algorithm under test. This model is depicted in Fig. 5.13. The reference voltage generated by the MPPT control block is converted to a current reference using the control scheme shown in Fig. 5.13. In this scheme, the error between the reference and the actual DC voltage (the output voltage of the PV array) is fed in a proportional gain, whose value depends on the DC link capacitance and the sampling period. The output of this gain is subtracted from the current of the PV module and the result is the reference current for the controlled current source.

As the model is more complex, the simulation time can be much longer, the time needed to simulate 130 seconds is only a few minutes, and the simulation time can be over 1000 seconds. However, if the model includes a detailed switching power converter model, for example a three phase inverter, the simulation time can be only a few seconds and the time needed for MPPT efficiency tests is much longer.

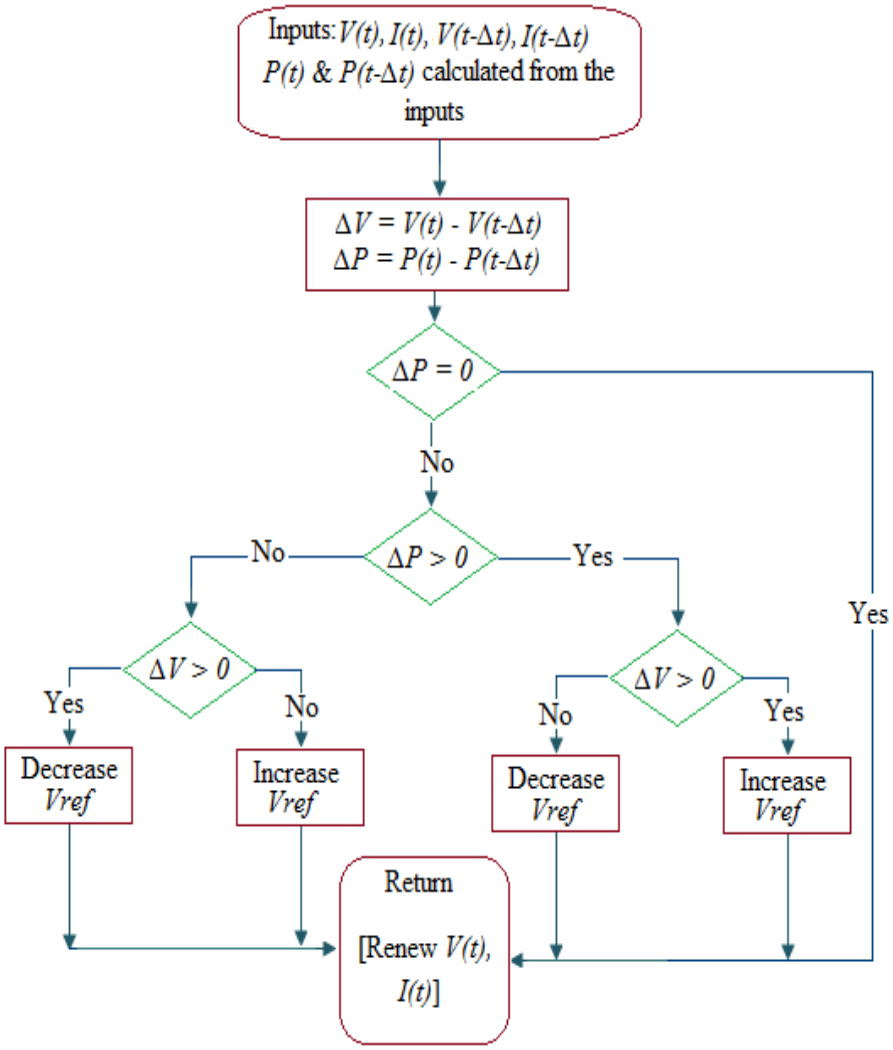

Figure 5.12: Flowchart of P&O method

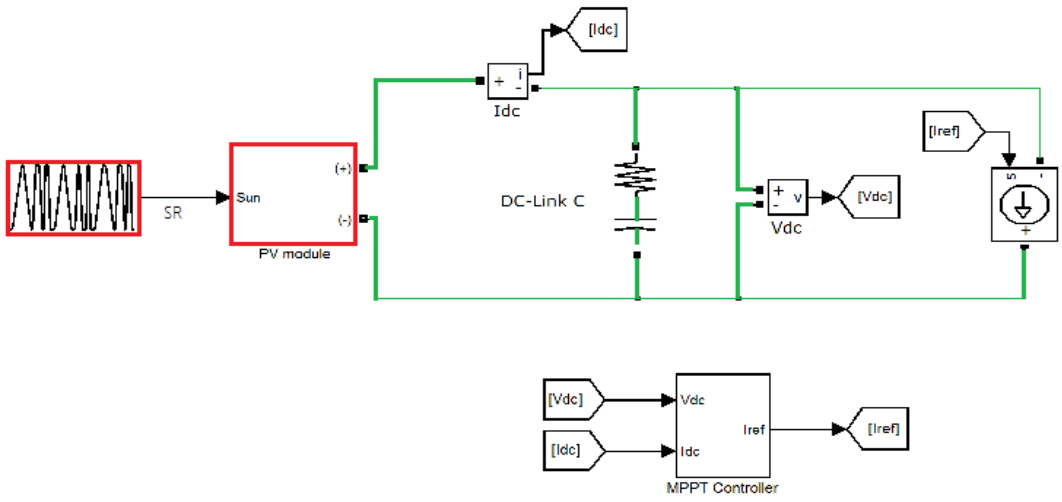

Figure 5.13: Control circuit used for simulation

The simulation model for the P&O MPPT algorithm is shown in Fig. 5.14. The new perturbation is decided based on previous and current output power as follows: if $\Delta P \times \Delta V > 0$, the operating voltage should increase; while if $\Delta P \times \Delta V < 0$, the operating

voltage should decrease. The operating voltage change is accomplished by adjusting the step size ΔD of the duty cycle D for the DC-DC converter. (The DC-DC converter will be introduced in the next section). This model has two parameters, the step size ΔD and the time between iterations. The smaller the P&O step size, the more accurate the result however, this will result in a longer simulation time.

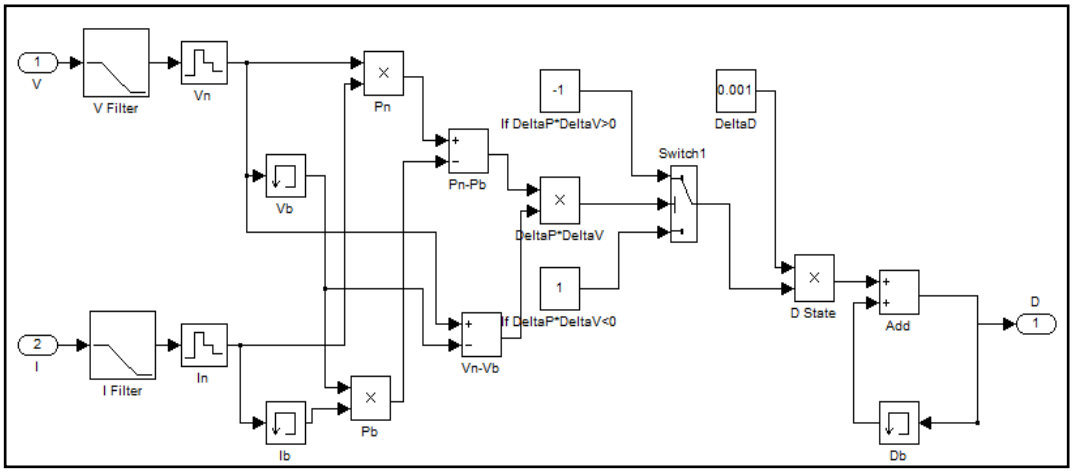

Figure 5.14: Simulation model for P&O MPPT algorithm

The parameters of the system study in this research are summarized in Table 5.2.

Table 5.2: System Parameters

Solar Panel Characteristics at STC	
Open-circuit voltage	900 V
Voltage at MPP	700.2 V
Short-circuit current	20 A
Current at MPP	17.6 A
DC-Link Capacitor	
Capacitance	700 µF
ESR	1 mΩ
Sampling frequency	
MPPT algorithm	25 Hz
V and *I* measurements	20 kHz

The characteristics of the solar array were chosen in order to fulfill the requirements of the inverter. The input voltage of the inverter (V_{MPP}) has to be greater than the peak line-to-line voltage of the output ($\sqrt{6} \times 230$ V ≈ 563 V). The current was selected so that the power level does not exceed 100 MW. The sample frequency of the MPPT algorithm should not be very high because the changes in the weather conditions are relatively slow compared to the dynamics of systems typically studied in control theory, whereas the sampling frequency of the voltage and current measurements was chosen according to the sampling time of a modern DSP.

5.3.3 DC-DC Converter with PV Module Simulation

The output voltage of a PV system is very low and fluctuates, as the SR and temperature change daily and seasonally. Therefore, a DC-DC converter is used to get constant high output DC voltage. Furthermore, a DC-DC converter serves the purpose of transferring maximum power from the solar PV cell to the load. The converter acts as an interface between the load and the PV cell. By changing the duty cycle *D*, the load impedance is varied and matched at the point of the peak power with the source, so as to transfer the maximum power [85]. There are four basic configurations and topologies of DC-DC converters as buck, boost, buck-boost and cuk. The boost type converter is considered the most advantageous to implement together with the MPPT algorithm for the following reasons:

a) The output voltage is always higher than the input PV cell voltage, which is useful as the PV cell needs to be connected to the grid eventually.
b) The topology of the boost converter is simple, easy to implement, low cost and has high efficiency.
c) The control of the boost converter is also relatively easy hence fluctuations can be minimized and also there is increase tracing accuracy.

5.3.3.1 Principle Operation of Boost Converter

The function of a boost converter is to regulate the output voltage from the PV array at different operating conditions. Fig. 5.15 shows the topology of a DC-DC boost converter, as a combination of power semiconductor switch operating at a switching frequency, a diode and an LC filter. For this converter, power flow is controlled by means of the on/off duty cycle of the switching transistor. When the switch is 'On' for t_{on} seconds, current flows through the inductor in clockwise, and energy $V_i\ I_1\ t_{on}$ is stored in the inductor. When the switch is 'Off' for t_{off} seconds, current will be reduced for increasing impedance. The only path of the inductor current is through diode D to the capacitor C and resistive load R. The polarity of the inductor will change. The energy accumulated in the inductor during the On-state will be released, $(V_c\text{-}V_i)\ I_1\ t_{off}$.

Hence,

$$V_i I_1 t_{on} = (V_c - V_i).I_1 t_{off} \tag{5.1}$$

we have

$$V_c = \left(\frac{t_{on} + t_{off}}{t_{off}}\right) \cdot V_i = \left(\frac{T}{t_{off}}\right) \cdot V_i = \left(\frac{1}{1+D}\right) \cdot V_i \tag{5.2}$$

where D is the duty cycle, which is the fraction of the commutation period T during which the switch is On. Since $\left(\frac{T}{t_{off}}\right) \geq 1$, the output voltage is always higher than the source voltage.

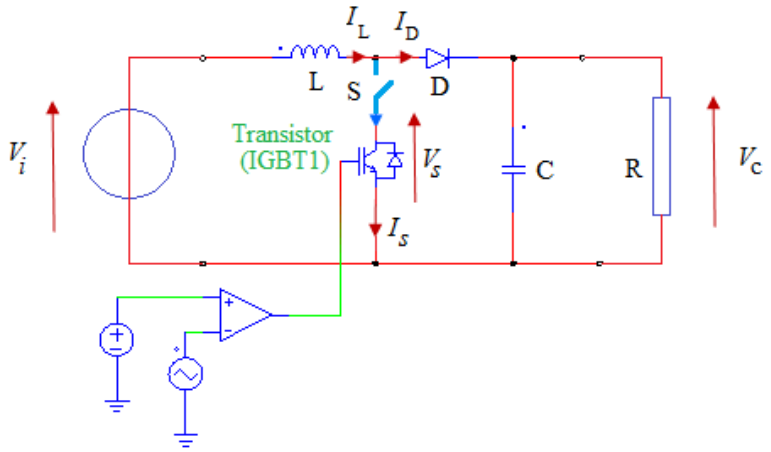

Figure 5.15: Topology of DC-DC boost converter

5.3.3.2 DC-DC Converter Simulation with MPPT Algorithm

The circuit model of the DC-side of the proposed GCPV system is shown in Fig. 5.16. It's composed of the developed circuit PV module model with DC-DC boost converter model. A PWM boost converter with the parameters shown in Table 5.3 are used for MPPT. The simulation model for DC-DC converter is shown in Fig. 5.17.

Table 5.3: Parameters of the DC-DC Converter PSIM

Parameter	Value
Inductor L	0.01 H
Capacitor C	2×10^{-3} F
Capacitor C_1	2×10^{-3} F
Resistor R	500 Ω

When temperature and SR are fixed, T = 25°C and SR = 1000 W/m^2, it can be seen from Fig. 5.18 that the system reaches the maximum power point at a time t = 0.2 s. The time t = 0 to t = 0.05 s is a period for the system to initiate its state, at time t = 0.05 s the PV cell has output voltage, but its current is zero therefore the output power is zero too. From time t = 0.05 s to t = 0.2 s, the simulated voltage output with the MPPT control based on P&O method overshoots and undershoots. However, after t =

0.2 s, the voltage value oscillates around 36 V in a very regular manner. This is due to the P&O method used here.

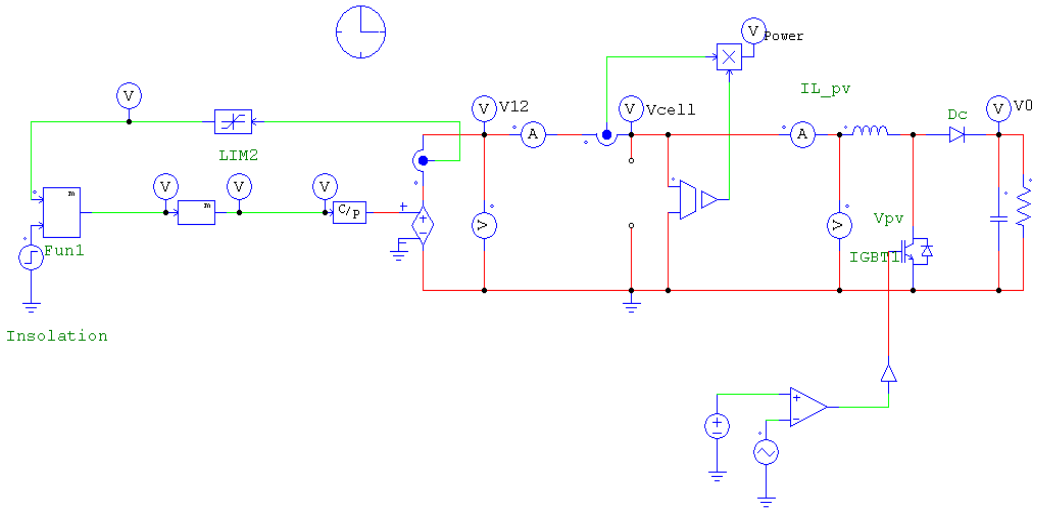

Figure 5.16: PV module with step up DC-DC converter circuit model

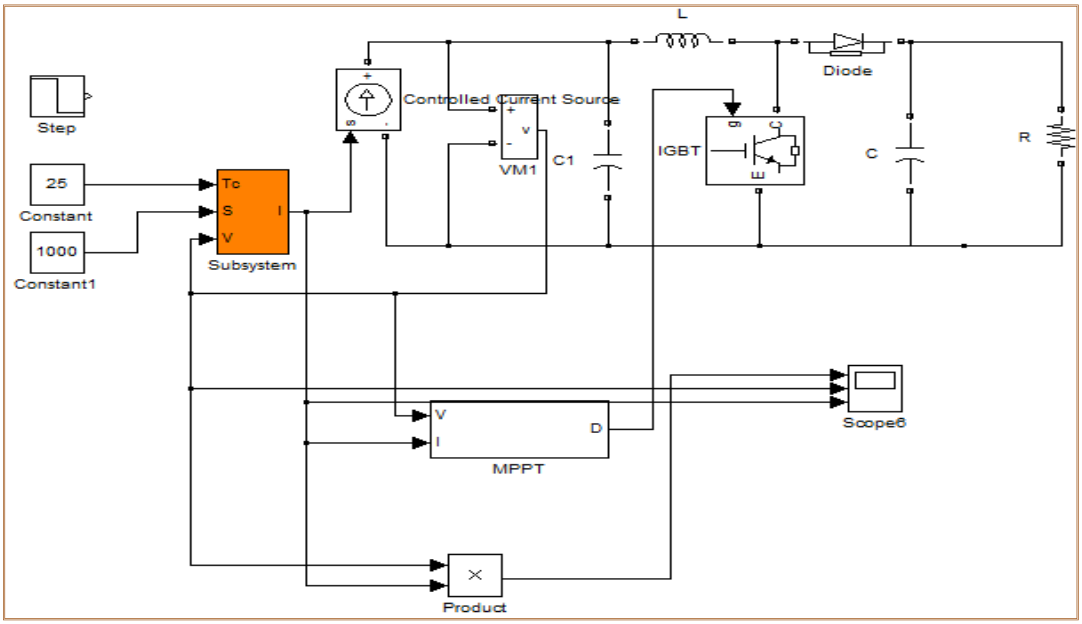

Figure 5.17: Converter simulation model

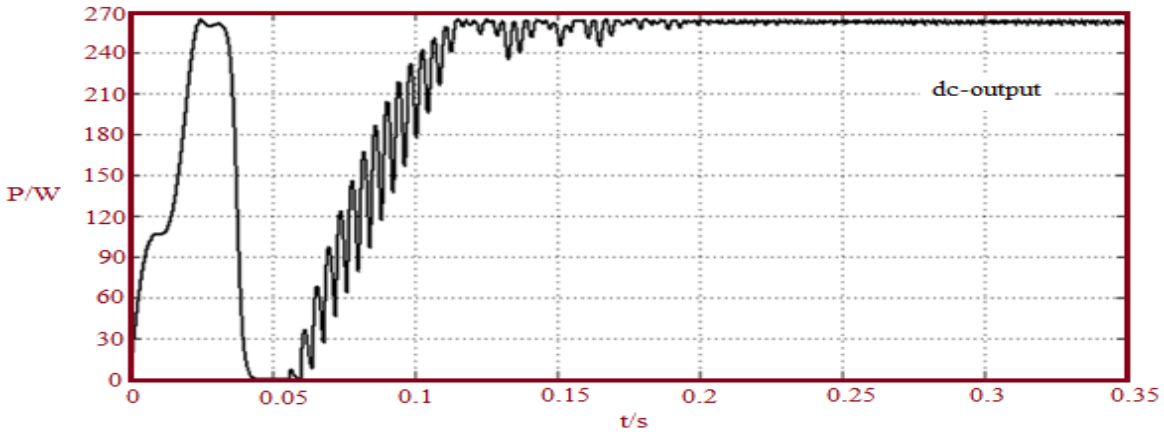

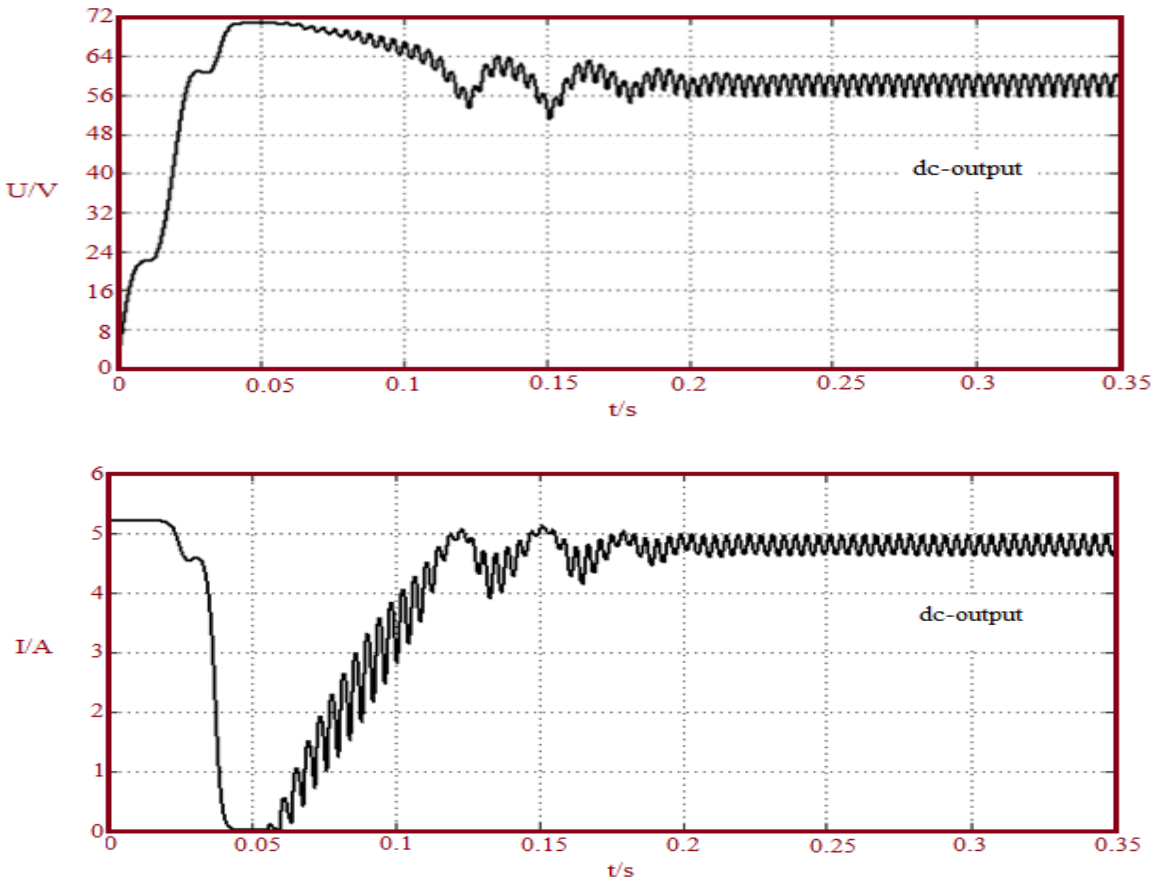

Figure 5.18: Simulation results for MPPT when temperature and SR keep unchanged, T = 25°C， SR = 1000 W/m^2

As shown in Fig. 5.19, the boost (step-up) converter has raised the output voltage of one PV string from 2.2 kV up to 15 kV. This voltage level can be now interfaced with a suitable DC-AC inverter. The output voltage is free from ripple and it is in the real time domain. The DC output current is shown in Fig. 5.20, ignoring the switching transient, its amplitude is almost 240 A.

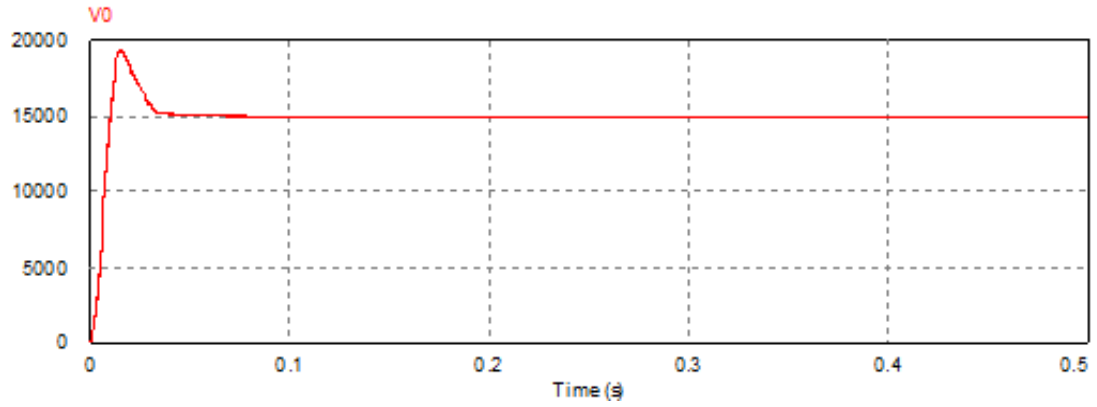

Figure 5.19: DC-DC boost converter output voltage of one PV string

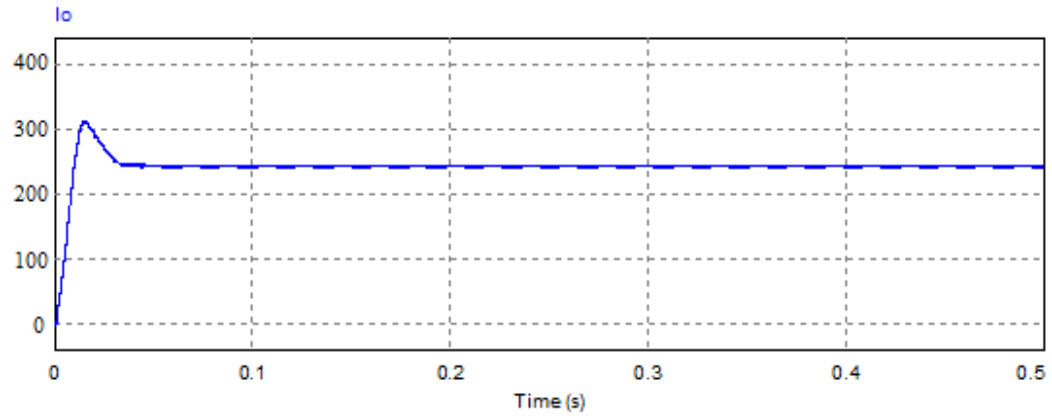

Figure 5.20: DC-DC boost converter output current of one PV string

In addition, the result of the DC output power of one PV panel is illustrated in Fig. 5.21. The output power of one panel is approximately 0.710 MW and it is 94.7% of its calculated value (0.75 MW) which is very satisfactory.

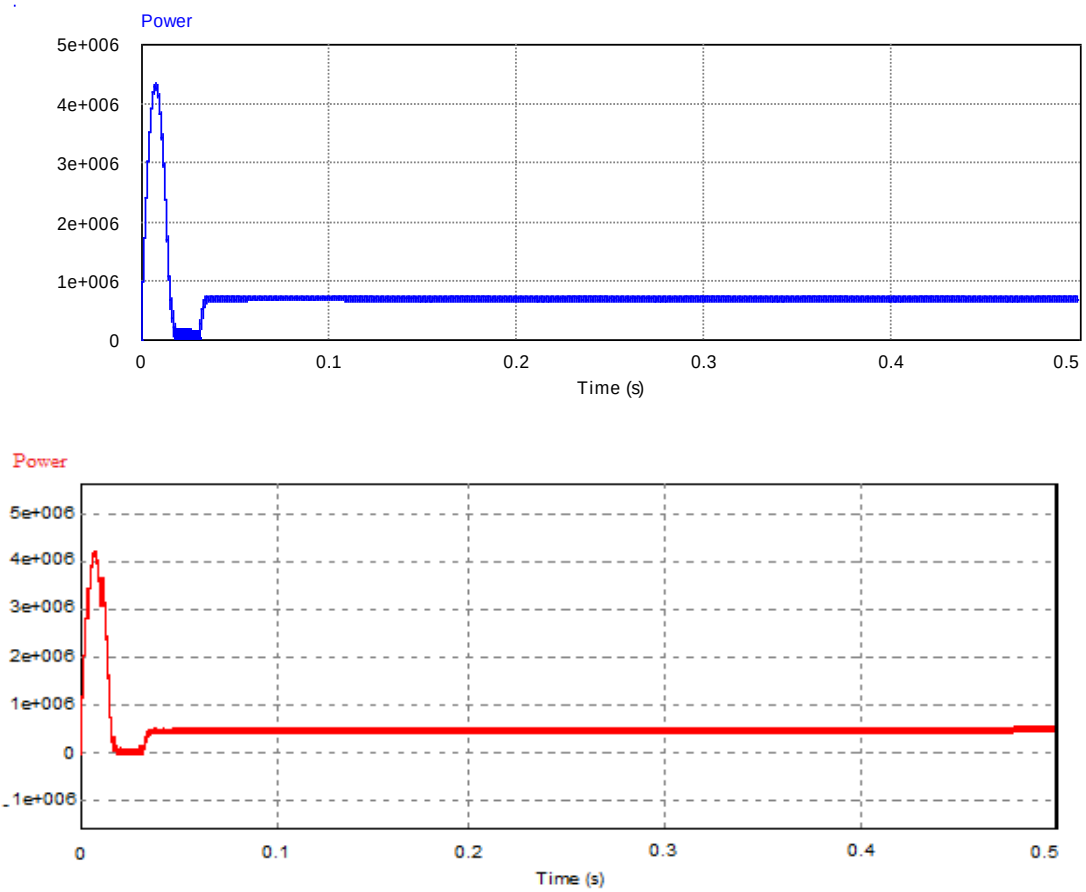

Figure 5.21: DC output power per panel with different LC filter & R

5.3.4 DC-AC Inverter Simulation Model

The DC voltage that a PV array produces has to be converted into an AC voltage so that it can be fed into Alsabyia grid. In this study a three-phase PWM inverter shown Fig. 5.22b with a low-pass filter shown in Fig. 5.22a was employed to perform this task. The

inverter is connecting the output DC bus voltage of the converter to the PV system providing the necessary conversion and regulation from the DC bus to the AC load. The output voltage is required to be sinusoidal and in phase with the grid voltage. The LC filter, which comprises an inductor and a capacitor driven by a voltage source, can generate good output voltage regulations at a particular frequency (50 Hz).

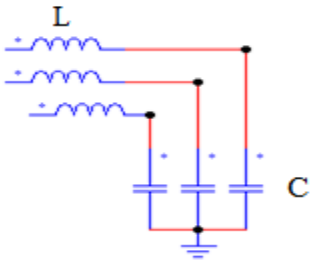

Figure 5.22a: Low-pass filter with LC components

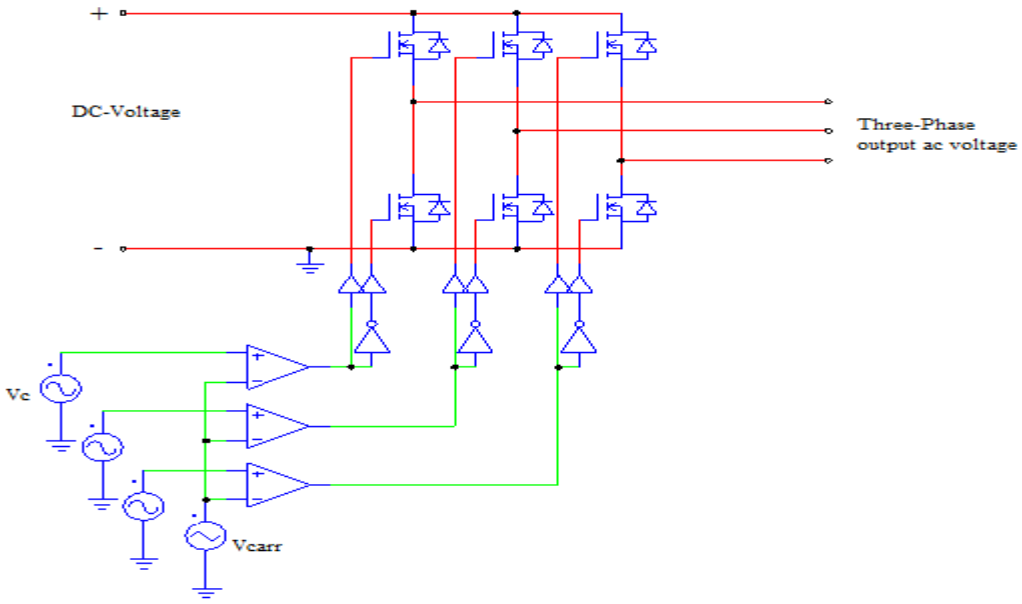

Figure 5.22b: Configuration of the proposed DC-AC PWM inverter circuit

Fig. 5.23 shows the simulation model of the whole GCPV system. The inverter is controlled using a current-mode control [85]. The reference current i^* is sent to compare with the DC-AC output current. The compared result is sent to a discrete PI controller to generate signals for a PWM generator (see Appendix G). The PWM signal can be used to control switches of the inverter. The frequency of the PWM waveform is set to 5 kHz, which can reduce the switching noise, simplify the system design and improve the dynamic performance [80]. Some important parameters related to the simulation process for the whole GCPV system have been shown in Table 5.4. PSIM has been implemented to simulate the proposed overall PV system.

Table 5.4: Parameters of the Full GCPV System Simulation Model

The AC voltage source (grid voltage)	PI controller	LC filter
Peak amplitude 155.5 V	Instantaneous time $T = 5 \times 10^{-7}$	L_1 = 10 mH
Phase = 0	Proportional gain $K_p = 6$	C = 2 µF
Frequency = 50 Hz	Integral gain $K_i = 256$	

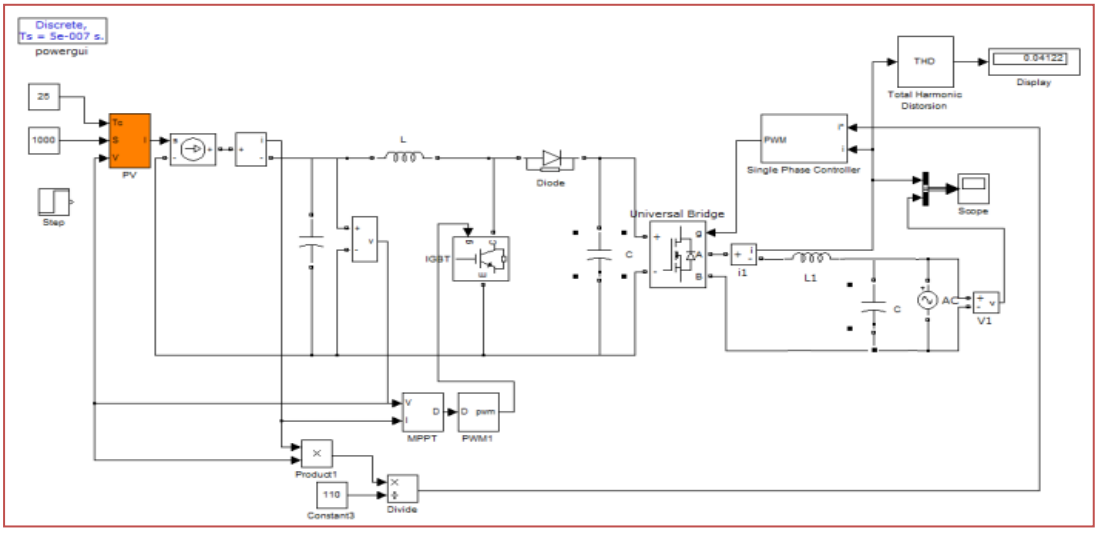

Figure 5.23: Simulation model for whole GCPV system

The simulation result shown in Fig. 5.24 is obtained when the temperature and SR are kept constant at T = 25°C, SR = 1000 W/m^2. After 0.05 s, the output current of the inverter is almost sinusoidal and in phase with the grid voltage. The total harmonic distortion (THD) % of the inverter's current is 4.122%, which satisfies UL1747 standard requirements for THD [85].

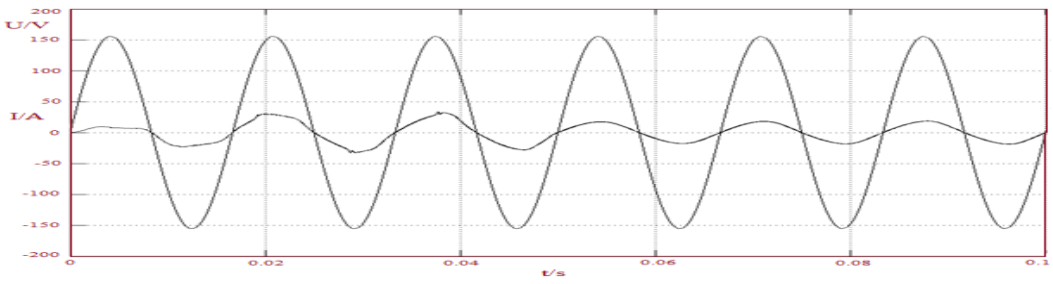

Figure 5.24: Simulation result when temperature and SR keep unchanged,
T = 25°C， SR = 1000 W/m^2

The overall simulation circuit model that proposed for the GCPV system is presented in Fig. 5.25 and is composed of the DC-side of the PV system and DC-AC PWM

inverter circuit adopted output LC filter. Basically, the circuit configuration has been considered according to its output results.

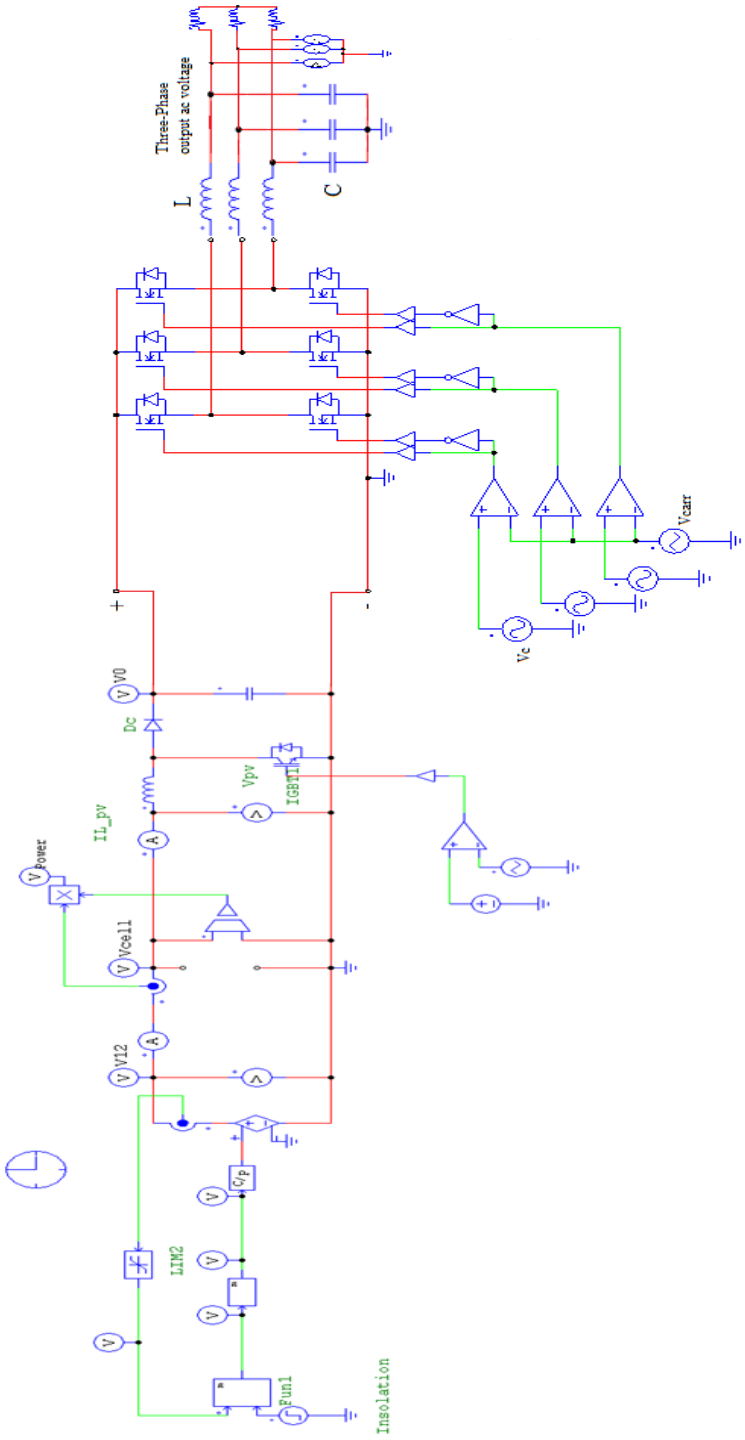

Figure 5.25: Overall simulation GCPV system circuit model

5.4 Overall Simulation Results

The overall system is simulated using PSIM software. The AC-side variables of the PWM inverter phase and line-line voltage square waveforms without output filter are

given in Fig. 5.26a and Fig. 5.26b, respectively. The corresponding three-phase load currents are depicted in Fig. 5.27a, Fig. 5.27b and Fig. 5.27c.

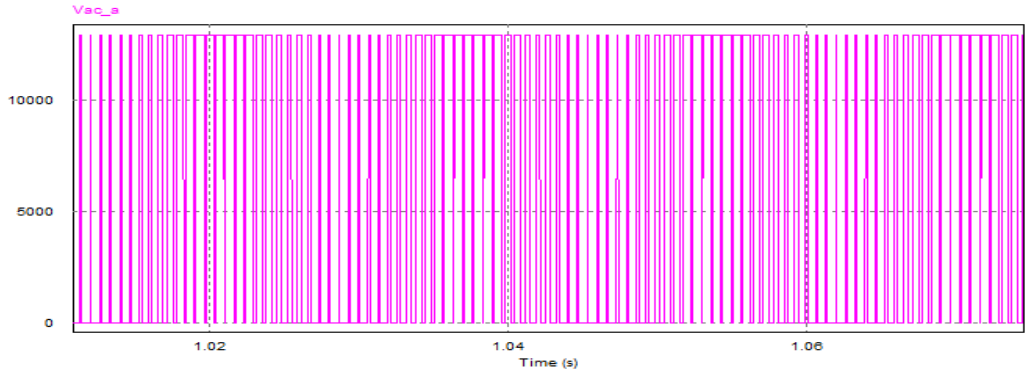

Figure 5.26a: PWM inverter phase voltage without output filter

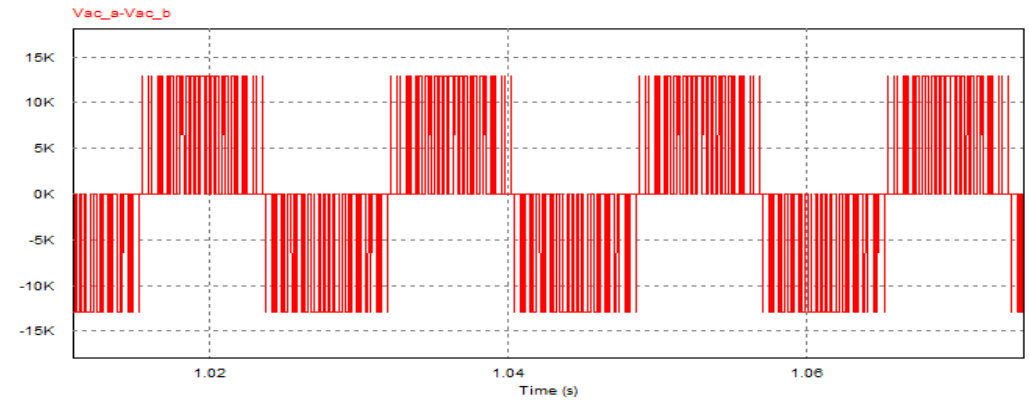

Figure 5.26b: PWM inverter line-line voltage without output filter

The PWM inverter converts the DC voltage to AC voltage with a good dynamic performance; but switching frequency is high and current ripple is large. The load voltage and current contain higher order harmonics that cause electromagnetic interference (EMI) problems and device heating. These high order harmonics are easily filtered out by using low-pass (LC) filter on the load side.

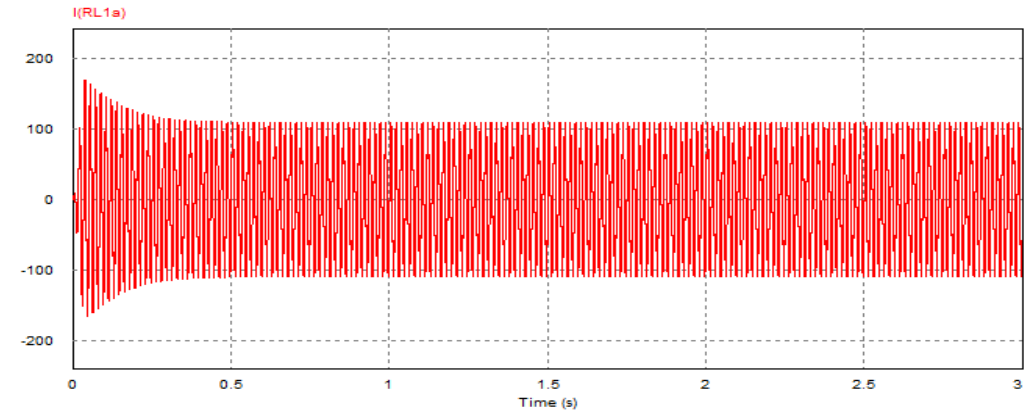

Figure 5.27a: Phase_a load current of PWM inverter

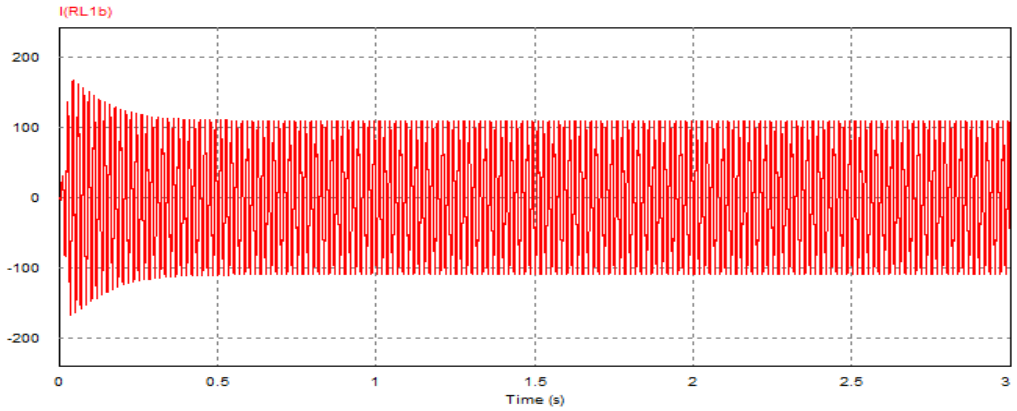

Figure 5.27b: Phase_b load current of PWM inverter

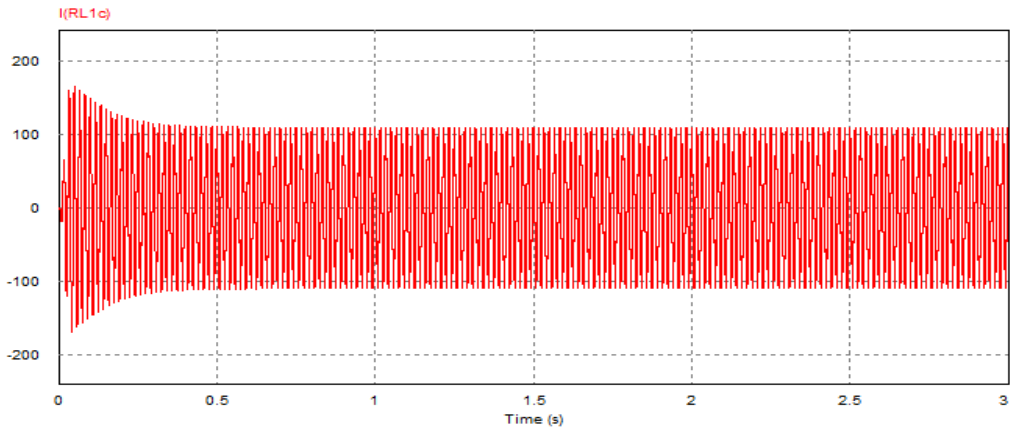

Figure 5.27c: Phase_c load current of PWM inverter

Thereafter, the zoom in output currents without LC filter is presented in Fig. 5.28.

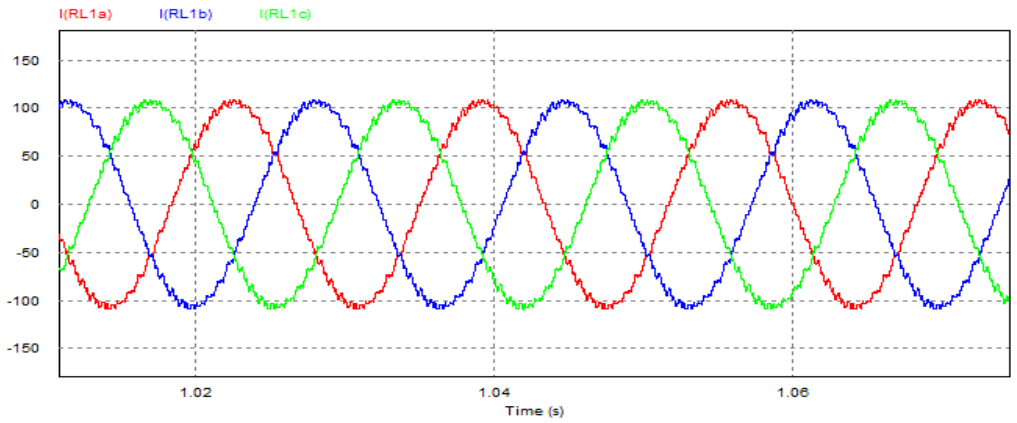

Figure 5.28: Zoom in output currents without filter

In contrast, the output voltage and current waveforms with LC output filter is shown in Fig. 5.29. A simple three-phase low-pass LC filter is connected to the three-phase terminals of the inverter to eliminate the high switching frequency harmonics and to satisfy the most demanding requirements at the load or grid side. After connecting the

filter, it can be easily noted that the three-phase load voltage became pure sinusoidal waveforms and the load current ripples are eliminated.

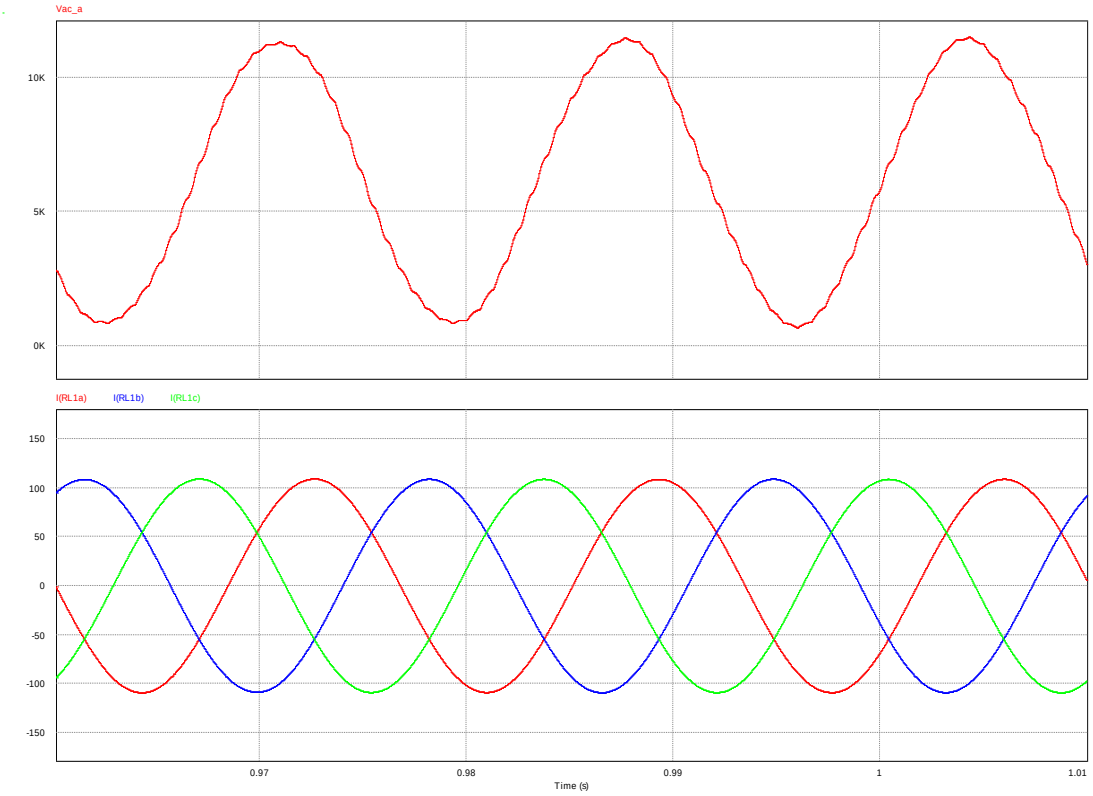

Figure 5.29: PWM inverter outputs waveforms with output filter

5.5 Conclusions

In this study a full GCPV model connected to a section of Alsabyia generation station part of Kuwait national grid has been developed, simulated and analysed. The PV module is modelled using an analytical description of PV cells. The maximum power of the PV module is tracked with an adjusted P&O MPPT algorithm based on boost DC-DC converter. A DC-AC inverter is employed to connect the PV module to Alsabyia grid and regulate the output voltage of the converter. The effects of unchanged temperature and SR have been simulated and analysed. The whole GCPV systems was built and simulated within the PSIM package and allows easy access to all its variables and system inputs. This model provides a very good tool to design size and analyse GCPV systems in a very reasonable time and with relative high accuracy. The overall simulation model is able to maintain constant voltage and good output voltage regulations especially with an LC filter. As a result, simulation times are significantly reduced, convergence problems avoided while results accuracy is saved: one can rapidly get reliable results conformed to own expectations and requirements.

Chapter 6
Integration of Proposed GCPV System to Kuwait Grid

6.1 Background

Kuwait's demand for electrical energy has risen by an average of 6% per year [8]. Unfortunately, Kuwait's generation capacity has not kept pace. In the summer of 2013, electrical demand rose to 13.8 GW, more than 90% of the country's capacity. Recently, Kuwait has planned to update its electrical grid to better meet future demand. In the past, Kuwait generated all of its electrical power from fossil fuels, mainly gas and steam turbines (see Chapter 1). Yet Kuwait also has an ambitious goal of supplying up to 15% of their electricity from renewable energy sources by 2030 [86].

GCPV systems are a relative new technology. The operational experience with PV systems itself is at an acceptable high level and today's installed PV systems are of a good quality and are able to operate without any problems for many years. The price level of the PV modules and the balance of system costs (inverter included) have decreased significantly [53]. The use to GCPV systems connected in parallel with the utility electric power network has become very favourable and is often supported by incentives from utilities and governmental bodies.

GCPV energy is the current subject of much commercial and academic interest. Recent work indicates that in the medium to longer term GCPV generation may become commercially so attractive that there will be large-scale implementation in many parts of the developed world such as Kuwait. The integration of a large-scale of GCPV system will have far reaching consequences not only on the distribution networks but also on the national transmission and generation system [87]. This PV generating unit may be liable to common mode failures that might cause the sudden or rapid disconnection of a large proportion of operating PV capacity. The effect of a large penetration of GCPV generation on the power system must therefore be considered carefully. In particular, the response of GCPV system to disturbances could aggravate these incidents.

Before connecting a PV system to the power network, the DC voltage of the PV modules must be converted into an AC voltage (see Chapter 5). Modelling, sizing and simulation of the PV system are required to prevent damages in the PV system caused by the utility network and vice versa as well as some protective devices. Other important aspects are the electrical installation procedures and electrical interference between

network and GCPV system. For some topics PV does put special constraints on the solution that are normally used by the utilities [88]. Hence, international work is required on utility aspects of GCPV systems.

The proposed GCPV system of up to approximately 100 MW rated power. And it is connected to the low-voltage generation grid of generation section I at Alsabiya Power Station within Kuwait electrical network to supply the maximum available power while voltage and frequency are determined by the mains. In order to find out the best way to integrate the proposed GCPV system with its extra capacity to the grid, it would be useful to conduct some power analysis. The analysis will consist of a load flow study to assess the condition of the network before the PV array is connected, and determine the best way to connect it. Also a fault analysis will be conducted to determine how the fault levels will change with the added capacity. This will allow us to investigate if any protection settings will need to be altered in order to identify conditions that will cause instability, and to create measures to avoid them. The integration process is conducted using electrical analyser programme called ERACS in order to carry out such analyses. Power flow studies allow engineers to analyse how power flows in an electrical network under various loading conditions. This allows the engineer to configure the system to efficiently deliver power. It can also be used to predict how the network would behave after future alterations. This is the main reason for conducting an analysis on the system in Kuwait.

Power analysis software works by treating every bus in the network as a node. Each node can have the following four variables: real power, reactive power, voltage, and phase angle. Different types of busses are classified depending on the variables that are known. A non-voltage controlled bus is a bus in which the real and reactive power is known, but the voltage is not. This is usually a bus without any generator source and is sometimes called a load bus. If the voltage and real power are known, it is referred to as a voltage controlled bus or a generator bus. This is often the case when a bus has generators connected to it. At least one bus in a study has to be designated as a slack bus. This bus has to have a power source connected to it, although only the voltage and phase angle are known. As the losses in the network are not going to be known until the final solution is computed, this bus is used to supply or absorb any complex power that is needed to account for these losses. For this reason the real and reactive power at this bus is unknown [89]. The unknown variables are then solved by first forming an admittance matrix. This represents the admittance of all of the components connected to

the busses. A network with *m* busses will have an *m* x *m* admittance matrix. Once the admittance matrix is constructed, nodal equations can be written as

$$\mathbf{Y \times V = I}$$

where

Y = the admittance matrix.

V = a column matrix of all of the bus voltages.

I = a column matrix of all of the respective currents.

The impedance matrix, **Z**, can be calculated by inverting the admittance matrix, leading to

$$\mathbf{Z \times I = V}$$

In either case, these equations can be solved by a number of iterative techniques such as Gauss-Seidel method and Newton-Raphson method.

6.2 Create Model Elements in ERACS

The first task was to collect information on the network In Kuwait. The data consisted of information on generators, transformers, and loads. Although ERACS has a library that contains model elements [90], none of them matched the data that was received from Kuwait. Therefore, the existing models had to be modified to suit the data from Kuwait network. This data was then used to model the network in ERACS. Where suitable information was unavailable, intelligent assumptions were made. Once the model was built and tested, four locations were chosen on the network to assess their suitability to have the PV array connected to it. Power flow studies were undertaken to gauge the condition of the network before and after the proposed PV array was connected. Also the power flow studies were analysed to calculate the amount of energy that was lost when transmitting power through the network. The network was then analysed to determine the increase in fault levels that occurred when the PV array was connected at each of the four locations.

6.2.1 Generator and Grid Models

The data that was received consisted of the MVA and voltage rating of the generators as shown in Table 6.1. The electricity of the Generation section I at Alsabiya Power Station within Kuwait electrical network is generated from fossil fuels, mainly steam and gas turbines. Since the largest generator was only 25 MVA it was assumed that all of the generators were modelled as gas turbines. Generally, steam turbines are larger. The

generators can either be modelled as a voltage behind impedance, or by using Parks Equations. Both models were tried, although no difference was observed in the solution. Both models converged on a result in the same number of iterations.

Table 6.1: Generators Data used to Create Model

Data Given			**Max. Power at 0.8 p.f**	
Generator ID	MVA	kV	MW	MVAR
G1	10.912	13.8	8.7296	6.5472
G2	10.912	13.8	8.7296	6.5472
G3	10.912	13.8	8.7296	6.5472
G4	10.912	13.8	8.7296	6.5472
G5	10.912	13.8	8.7296	6.5472
G6	20.606	13.8	16.4848	12.3636
G7	20.606	13.8	16.4848	12.3636
G8	20.606	13.8	16.4848	12.3636
G9	25.755	13.8	20.604	15.453
G10	25.755	13.8	20.604	15.453
G11	25.755	13.8	20.604	15.453
G12	25.755	13.8	20.604	15.453
G13	25.755	13.8	20.604	15.453
Total	**245.153**		**196.1224**	**147.0918**

Grid Feed

P = 538.56 MW

Q = 441.49 MVAR

I = 36.230 kA

Three phase fault infeed = 90 MVA x/r ratio = 14

Single phase fault infeed = 90 MVA x/r ratio = 14

There was a grid connection to the network (see Table 6.1). The data for this connection consisted of the single phase and three phase fault levels of 90 MVA, as well as the x/r ratios of 14. It was assumed that the grid would be connected to the network at a relatively high voltage to avoid power losses. Therefore it was connected to the 33 kV bus. The grid connection was left as a slack busbar, so this was automatically set to compensate for any energy losses in the network.

All of the generators were set up with a power factor of 0.8. Any differences between the generated and consumed reactive power would come from the grid connection. The total power output of the generators had to match the power consumed by the network. Since the daily load curve was known, the total power that the generators needed to generate at any time of the day was known. However, there were many different

generator configurations that could be used to supply the known power. An ideal generator configuration would be able to supply the loads with minimal power loss. Generators function most efficiently when they are operating close to full load. When generators run at a percentage of their full load (part load) they operate with less efficiency. The overall efficiency of a gas turbine depends on a number of factors, including the temperature and pressure of the gas fuel as well as characteristics unique to the generator [91]. As this information was unavailable, a different approach was used to determine the efficiency of the gas turbines at different load levels. Fig. 6.1 is a measure of the relative efficiency verses input power of a low performance and a high performance gas turbine. It was assumed that the gas turbines represented in the model would have operation characteristics somewhere between these two turbines.

A curve was drawn based on the average relative efficiency of the two turbines (Appendix F1). This curve was used to compute the relative input power for when a generator was operating at part load. The formula for this curve is:

$$0.94x^3 - 2.49x^2 + 2.53x + 0.02$$

Once a measure of the efficiency of each generator configuration was measured, the most efficient configuration could be found. The optimal generator configuration would also include enough spinning reserve to be able to maintain stability if one of the generators was disconnected [91]. The largest generators on the system were rated at 25.8 MVA. Therefore, the spinning reserve of this model had to be at least that large.

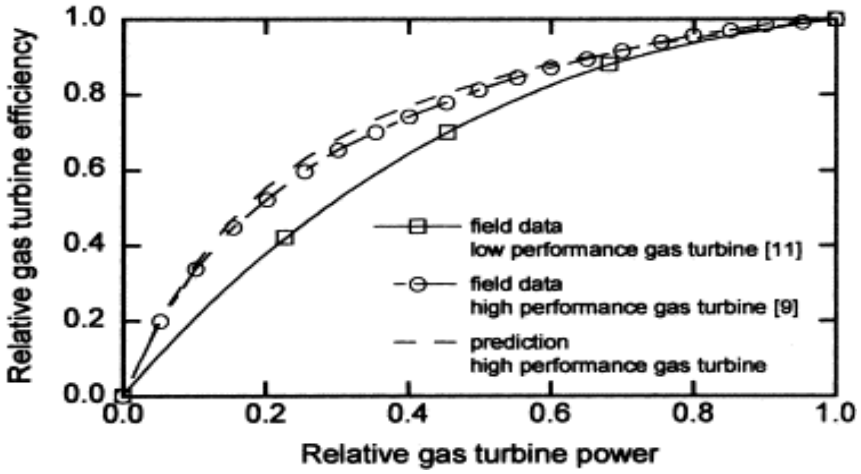

Figure 6.1: Part load efficiency data for two commercial gas turbines (source: [92])

At any time of the day, the generators needed to supply a minimal load of at least 136 MW. Because of this it was decided to have four of the biggest generators, configured to

output 95% of their rated power at all times. This left only 9 generators that had to be configured in an efficient way to supply the rest of the power.

A program was created that considered all of the possible generator configurations that would supply a given load, and selected the optimal configuration that best satisfied the above conditions. The program used the following procedure (See Appendix E for the full program code and the generator configurations):

1. Choose a given power output level.
2. Find all of the generator configurations that will produce the given power output.
3. Save the generator configuration that has a relative input power less than the relative input power from any other generator configurations, and has enough spinning reserve and has no generator that is loaded more than 95% of its rated capacity.

Although this may represent the ideal generator configuration based on the given constraints, it can be argued that this still isn't a realistic approach. The system operator wouldn't turn on a generator for an hour when the loads change slightly. Energy would be wasted turning on the generator and bringing it up to speed. Realistically, the process would be more dynamic, where each of the generator's power outputs is continuously being slightly altered as the loads continuously change throughout the day. Nevertheless, the system operator will still always be trying to run the system as stably and efficiently as possible, so it is assumed that the configuration that he will decide on will not be that different than the configurations used in the model.

6.2.2 Transformer Models

As shown in Table 6.2, the data on transformers consisted of the MVA rating, MW rating and the primary and secondary voltages. Although the library contained a large selection of transformer models, it contained no transformers at a voltage of 13.8 kV. Like the generators, existing models were modified to match the data. In order to keep the model impedances close to the real impedances of the transformers, models that had MVA ratings and voltages similar to the real transformers were used.

There was not any information available about the phase groups of the transformers. It was assumed that the 13.8 kV and 33 kV transmission network was a three wire system while the 415-V distribution network was connected as a four wire system. This

reasoning led to the decision to model all of the 13.8/0.415 kV transformers as Δ-Y. The 33/13.8 kV transformer was modelled as a Δ-Δ transformer. This arrangement leaves the 33 kV bus, as well as potentially all of the 13.8 kV busses without a voltage reference to earth. It is assumed that earthing transformers will be used where necessary.

Table 6.2: Rating of the Transformers used in the Model

Data Given				**Max. Power at 0.8 p.f**
Transformer ID	MVA	HV kV	LV kV	MW
T1	20.75	33	13.8	16.6
T2	15.5	13.8	0.415	12.4
T3	15.5	13.8	0.415	12.4
T4	15.5	13.8	0.415	12.4
T5	15.5	13.8	0.415	12.4
T6	15.5	13.8	0.415	12.4
T7	15.5	13.8	0.415	12.4
T8	15.5	13.8	0.415	12.4
T9	15.5	13.8	0.415	12.4
T10	15.5	13.8	0.415	12.4
T11	25.25	13.8	0.415	20.2
T12	25.25	13.8	0.415	20.2
T13	25.75	13.8	0.415	20.6
T14	25.75	13.8	0.415	20.6
T15	25.75	13.8	0.415	20.6
T16	25.75	13.8	0.415	20.6
T17	30.5	13.8	0.415	24.4
T18	30.5	13.8	0.415	24.4
T19	30.5	13.8	0.415	24.4
T20	30.5	13.8	0.415	24.4
T21	30.5	13.8	0.415	24.4
T22	30.5	13.8	0.415	24.4
T23	30.5	13.8	0.415	24.4
T24	30.5	13.8	0.415	24.4
T25	30.75	13.8	0.415	24.6
T26	30.75	13.8	0.415	24.6

6.2.3 Loads, Cables and Interconnectors Models

As shown in Table 6.3 and Table 6.4, the average monthly loads were obtained as well as the average daily loads for June. June had the highest average monthly load. Because of this, the loads for the month of June were used to simulate peak loads for the year. It was assumed that all of these loads were non-rotating, and therefore were modelled as shunt loads. These loads all had a power factor of 0.8 and were 415 volts.

Table 6.3: Average Monthly Loads of the Network

Month	Average load (MW)
January	92
February	105
March	116
April	128
May	148
June	159
July	154
August	155
September	147
October	131
November	122
December	103
Total	1560

Table 6.4: Average Daily Loads of the Network for June from 15/6/2012 to 30/6/2012

Hour	Average load (MW)	Hour	Average load (MW)	Hour	Average load (MW)
12-1 am	146	8-9	159	4-5	167
1-2	142	9-10	161	5-6	161
2-3	138	10-11	163	6-7	157
3-4	136	11-12	168	7-8	152
4-5	140	12-1 pm	170	8-9	150
5-6	146	1-2	170	9-10	150
6-7	152	2-3	170	10-11	147
7-8	156	3-4	170	11-12	147

There was not any available information concerning any cables or lines. The network that was being modelled was situated in an area of approximately 10 square miles. Based on this, the length of all of the interconnectors between busses was assumed to be 5 km. The 13.8 kV interconnectors were modelled as transmission lines, all of the transmission lines used identical model that shown in Table 6.5 as ERACS library suggested. The transformers were connected to the 13.8 kV busbars using 800 mm^2 copper cables. One cable was used for each of the transformers smaller than 30 MVA while two cables were used for the transformers greater than 30 MVA.

Table 6.5: Rating of the Transmission Lines used in the Network

Length	5 km
Current rating (summer)	0.525 kA
Resistance (per km)	0.1 Ω
Inductance (per km)	0.27 mH
Capacitance (per km)	0.6 μF

6.3 Proposed One-Line Diagram using ERACS

Once all of the elements were modeled, they had to be laid out in a one-line diagram as shown in Fig. 6.2. In this figure, the proposed locations for the GCPV system is marked A, B, C and D. There was no information available about the busbars on the network to show the layout of the generators, busses and loads. The voltages of the busses were determined by the data from the generators and transformers. Five 13.8 kV busses were used and connected to each other in a ring. There was also a 33 kV bus that was used for the grid connection. These generation busses supplied thirteen distribution busses that each supplied a shunt load. The loads were connected to their respective busses, depending on their sizes. Small loads were connected to buses supplied by transformers with small capacities and large loads were connected to buses supplied by transformers with large capacities. The transformers were connected to the generator busses in such a way that if one of the generator busses was de-energized, all of the distribution busses can still be energized. Also, any of the transformers that were connected in parallel were identical. This eliminated any uneven loading because of transformers with different impedances. Every distribution bus was supplied by two transformers, except Bus 7. This was supplied by only one 15.5 MVA transformer.

6.4 Connection of the PV System

A PV module performance is rated under standard test conditions (STC). This is a measure of how the module performs at 25℃ when it is exposed to light with an SR of 1kW m^{-2}. The actual output will depend on the SR that it is exposed to at the time. Using equations 3.15 to 3.18, we can calculate the actual output of the PV system. The PV system output is rated at 97.268 MW and is 94.45% efficient. The global SR horizontal model in Chapter 2 was used to obtain the average amount of solar irradiance that Kuwait received for each day in the year. This information was used to calculate the output of the PV array for an average day in June. A modelling software package called *HOMER* was used to obtain the SR calculations.

There was no way to directly model a PV system in ERACS. Instead, the PV array was represented as a synchronous generator for the power flow studies. ERACS represents a generator in the power flow studies as a voltage behind impedance.

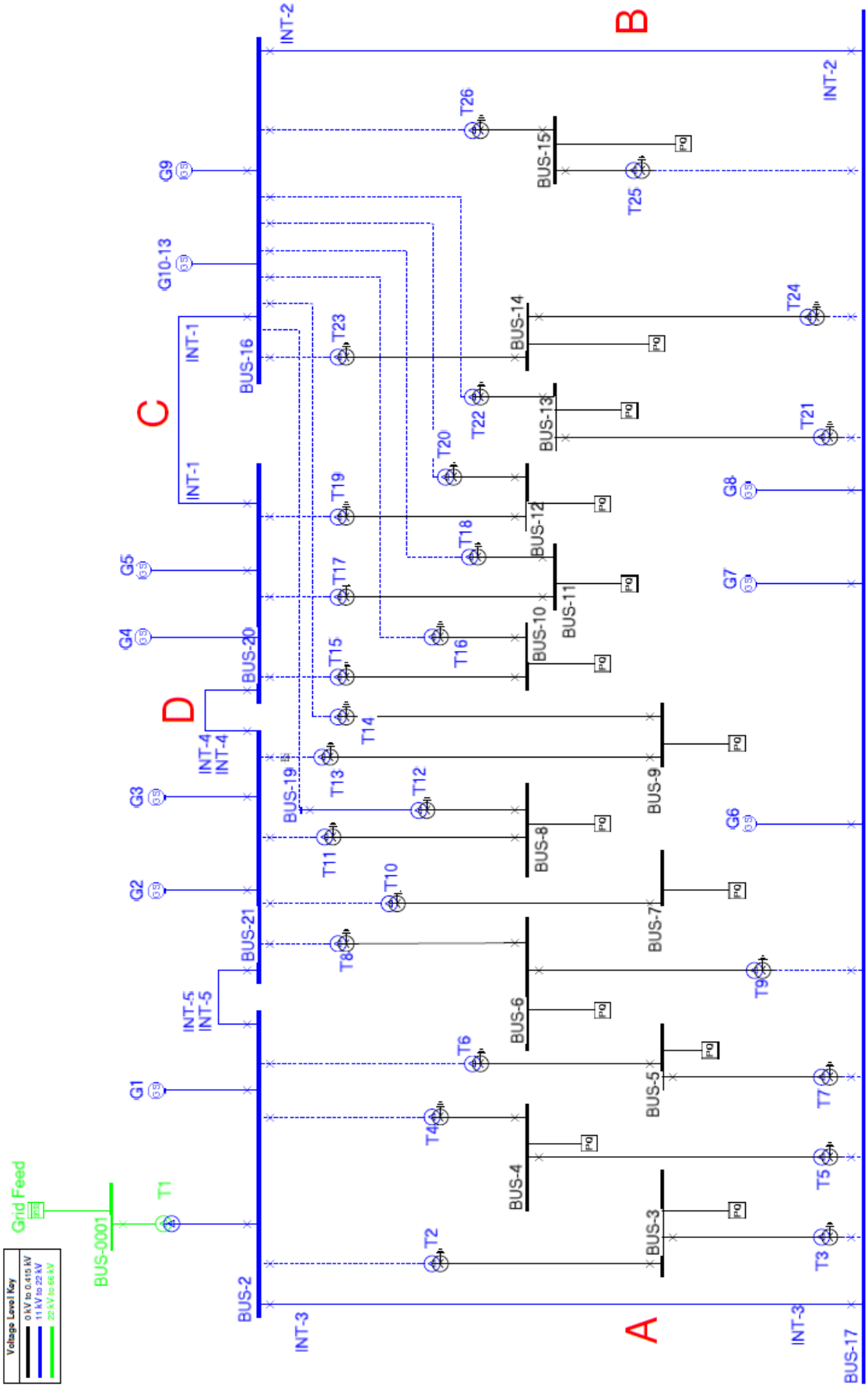

Figure 6.2: One-line diagram of the model network (ERACS Model)

Table 6.6: Power Output of the PV System for an Average Day in June

Time of day	Average SR for June (kw/m^2)	PV output power (MW)
04:00	0.000910	0.0840
05:00	0.090445	8.3090
06:00	0.150067	23.962
07:00	0.266280	39.620
08:00	0.427004	53.709
09:00	0.557581	67.440
10:00	0.622645	77.520
11:00	0.688820	81.520
12:00	0.700327	82.632
13:00	0.688568	81.170
14:00	0.624780	77.681
15:00	0.568003	67.693
16:00	0.455004	54.002
17:00	0.276702	39.811
18:00	0.150256	24.001
19:00	0.098122	8.8665

6.5 Power Flow Analysis

This study was focused on the effect of connecting a GCPV system to the network model. The only time that this would make a significant difference to the network was during the solar day, when the PV array was receiving enough SR to contribute power to the network. Therefore the power flow study mainly looked at how the network responded between 4:00 am to 7:00 pm. During the day the load varied by as much as 20% from the peak load of 170 MW. To capture this, a power flow analysis was conducted for every daylight hour.

When a component in an electrical network is disconnected, the power flow in the network changes. There are 35 different components on the network, which meant that there are 35 different configurations that the network could be in if only one component was de-energized. Each of these different power flows was analysed. Obviously, more than one component could be isolated at the same time, but this research only looked at situations of one component was isolated. As a consequence of this, each prospective

location needed to have a total of 510 power flow studies. A manual approach would have been too labour intensive. Therefore, a programme was created using *JitBit Macro Recorder* in order to conduct the power flow studies and record the results. The program used the following strategy:

1. Set up the network to correspond to the load conditions of a certain time of day. This involved specifying the power dissipated in the loads, as well as setting up the generators and the photovoltaic array to supply these loads. This also involved closing all of the switches in the network, ensuring that for the first load flow, all of the components were energised.
2. Run the initial load flow and save the results as a .csv file.
3. Isolate one of the components. Run another load flow and save the results.
4. Re-energise the isolated component, and de-energise another component. Conduct another load flow study and save the results as another .csv file.
5. Repeat step 4 until a load flow is carried out with each of the components isolated.
6. Set up the network for a different time of day and repeat the whole above procedure.

The data from the power flow studies then had to be analysed to determine the suitability of each location. The following criteria were used to assess each location:

a. The efficiency of the transmission system. The system must be able to deliver power to the loads with a minimal amount of energy loss. In order to calculate this for each configuration, the difference between the input power and the output power was calculated for each configuration. The difference between these numbers was the power loss at the time of the study. The power loss for each daylight hour was then added together to get the total energy lost in that configuration.
b. The flexibility of the system. The chosen system must be able to effectively transmit power to the loads even when a component is taken out of service for maintenance. In order to measure this, the current going through each component was analysed for each configuration. If a power flow study

found a component that was overloaded, in a certain configuration, the study was set aside for further analysis.

c. The amount of upgrading that needed to be done to the network. As we were increasing the generating capacity by as much as 50%, it would be reasonable to assume that some components would need to be upgraded to cope with the increased load flow. However, unnecessary upgrading would be a waste of money. A potential location for the PV system would not be deemed suitable if too many costly upgrades were needed.

As there was a large amount of data to analyse, a program was created using *Visual Basic for Applications* (*VBA*) to help organise the data. Once a component was selected to be analysed, the program accessed the .csv file from each of the load flow studies and obtained the current loading for that component. It then converted this data into a per unit amount and displayed it on a scatter diagram. This scatter diagram could then be used to determine which configurations caused the component to become overloaded. If several study configurations caused the component to be overloaded, the component was upgraded and the power flow studies were repeated. This processes continued until all of the components in the network were upgraded to handle the power from the GCPV system. The *VBA* program was also used to obtain the power that the generators and PV array produced and the power that was consumed in the loads.

There were some components that would have required a large upgrade to prevent them from getting overloaded in a few exceptional configurations. Suggesting an expensive upgrade would not have made economic sense. In this case, the configuration would be avoided by other means. Some possibilities would be configuring the power flow from the generators in a different way, or arranging a power outage to eliminate some of the excess load.

6.5.1 Power Flow Study without the PV System Connected

A Power flow study was first conducted on the original network without the photovoltaic array connected. In most configurations the interconnectors were not overloaded. However, when either Transformer 16 or Transformer 20 was isolated and there was minimal power generation from the generators connected to Bus 20, Interconnector 1 would become overloaded as shown in Fig. 6.3. This overload situation can be avoided by changing the generator to a different configuration if one of these transformers needed to be isolated. For instance, based on the network conditions at

6:00 am with Transformer 20 isolated, generating 8 MW from Generator 5 instead of from Generator 9 reduces the current through Interconnector 1 from 1.25 p.u. to 0.93 p.u. This also reduces the power loss in the network by 0.5 MW. However, this configuration increases the relative input power required by the generators from 80.3 MW to 82.7 MW.

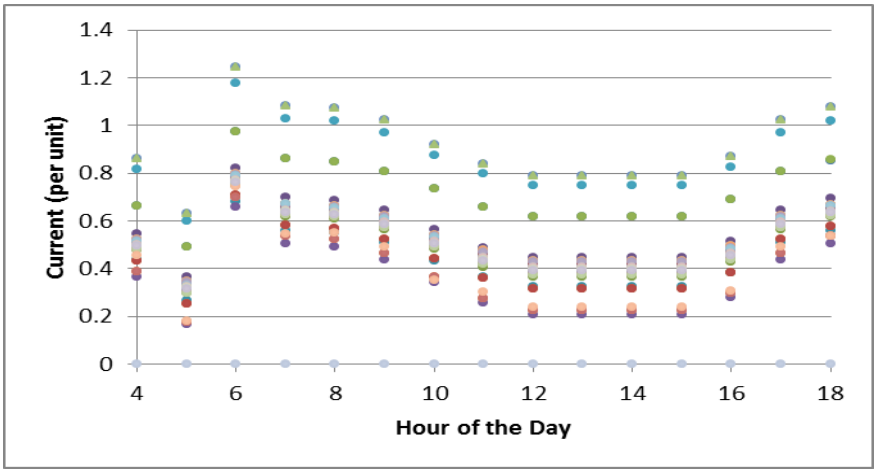

Figure 6.3: Current through interconnector 1 before the PV array is attached to the network

A similar situation occurs with Interconnector 2. At 2:00 am, there is only 11 MW being generated on Bus 17. This causes all of the loads that are supplied from Bus 17 to draw power through Interconnector 2, thus overloading it. A better solution would be to Generate 6 MW from Generator 7 instead of Generator 6. However, this increases the relative input power required by the generators from 65.8 MW to 71.0 MW. The Load peaks at 170 MW between 12:00 pm and 4:00 pm. If Transformer 14 is isolated during this time, Interconnector 4 will be slightly overloaded. As all of the generators are running near their full capacity, there is little choice in configuring the generation differently to avoid this. If Transformer 14 has to be isolated when the load is this high, it may be necessary to shed some of the load from Bus 9. Transformer 6 and Transformer 7 feed distribution Bus 5. When either of these transformers is isolated, the other transformer gets overloaded. This can only be alleviated by upgrading the transformers to a larger size. In order to avoid overloading one of these transformers, it will be necessary to shed some of the load from Bus 5 if one of these transformers is isolated.

The energy loss in a network depends on the configuration of the network at the time. For each location there were 35 different configurations. One way to compare the energy loss for each location is to take the average energy loss from all of the 35

configurations. However, some of these configurations would not occur on a regular basis while other configurations would be fairly common. An inefficient configuration will adversely affect the average energy loss, even if this configuration would hardly be used. Using the arithmetic mean to represent this data would not take this into account. Determining the likelihood of a network configuration is beyond the scope of this project. Instead the energy loss was based only on the configuration with no components isolated. The energy lost transmitting electricity to the loads for a day in June with no components isolated is 23.26 MWh.

6.5.2 Power Flow Study with the PV System Connected

As the PV system only contributes power to the network during daylight hours, the power flow would not change significantly during the night. Therefore the rest of the power flow study was restricted to the time between 4:00 am and 7:00 pm. Connecting the PV array to the network did not significantly affect the power flow through any of the distribution transformers. The observations that were made about the behaviour of the distribution system before the array was connected were still valid when the array was connected in each of the four locations. Therefore, the rest of the power flow analysis focused mainly on the 13.8 kV network.

The PV array was connected to the network at the four lettered locations shown in Fig. 6.2. In each of the four cases an initial power flow study was conducted to determine which components were overloaded. This information was used to determine which interconnectors needed to be upgraded. In the original configuration, each of the 13.8 interconnectors consisted of a single transmission line. If it was determined that an interconnector needed to be upgraded a number of transmission lines were put in parallel with the original line. The number of transmission lines that were used was determined by the current that was flowing through the interconnector. All of the transmission lines used in the network were modelled identically. In reality, it is not likely that several transmission lines of relatively small capacity would be built in parallel. Instead, a few lines with a higher capacity would be built. However this approach was chosen because it made it easier to compare different upgrades on different interconnectors.

6.5.2.1 PV Array Connected to Location A

In this scenario, the GCPV array was connected between Bus 2 and Bus 17. In order to accommodate the extra generation capacity, interconnectors were upgraded according to

Table 6.7. In this configuration, Interconnector 9 was still operating at close to its maximum capacity at 12:00 pm, when the PV array was generating at its maximum power. Because of this, this interconnector may still need to be upgraded further. The energy lost transmitting the power between 4:00 am and 7:00pm, with no components isolated is 44.27 MWh.

Table 6.7: Interconnectors upgrade when the PV array was connected to Location A

Interconnector Location	Original Configuration		Upgraded configuration	
	Interconnector ID	Number of Transmission Lines in Parallel	Interconnector ID	Number of Transmission Lines in Parallel
Between busbars 16 and 20	1	1	1a	1
			1b	1
Between busbars 16 and 17	2	1	2	1
Between busbars 17 and 18	3	1	not applicable	
Between busbar 17 and PV array	not applicable		3a	3
			3b	3
Between busbars 20 and 21	4	1	4	1
Between busbars 2 and 21	5	1	5a	3
			5b	3
Between busbar 2 and PV array	not applicable		9a	2
			9b	2

6.5.2.2 PV Array Connected to Location B

Location B involved connecting the PV array between Busses 16 and 17. Table 6.8 summarises the upgrades that were required for this configuration. As shown in Fig. 6.4, Interconnector 3 is overloaded at various times of the day in four different configurations. It is also operating close to its maximum capacity in a few other configurations. Based on this, this interconnector may still need to be upgraded further.

When Transformer 14 is isolated, Interconnector 4 gets overloaded. This is a consequence of having the majority of the power coming from only one source, the PGCV array. One way of avoiding the situation is to generate 12 MW from the generators on Bus 21. However, this means that the amount of power that can be generated from the proposed PV array in this configuration will be restricted. The energy lost transmitting the power between 4:00 am and 7:00 pm, with no components isolated is 47.14 MWh.

Table 6.8: Interconnectors upgrade when the proposed PV array was connected to Location B

Interconnector Location	Original Configuration		Upgraded configuration	
	Interconnector ID	Number of Transmission Lines in Parallel	Interconnector ID	Number of Transmission Lines in Parallel
Between busbars 16 and 20	1	1	1a	2
			1b	2
Between busbars 16 and 17	2	1	not applicable	
Between busbar 16 and PV array	not applicable		2a	2
			2b	2
Between busbars 2 and 17	3	1	3	1
Between busbars 20 and 21	4	1	4	1
Between busbars 2 and 21	5	1	5a	1
			5b	1
Between busbar 17 and PV array	not applicable		9a	3
			9b	3

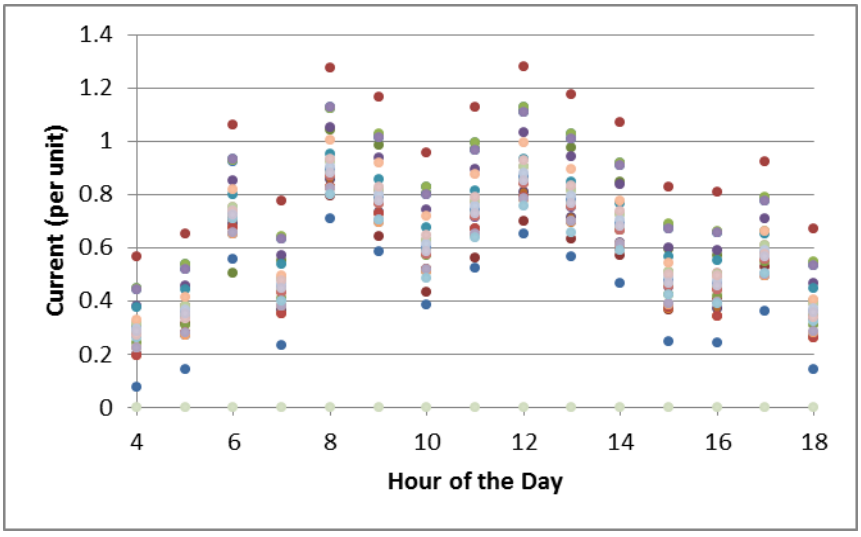

Figure 6.4: Current through interconnector 3 after the proposed PV array is connected with location B

6.5.2.3 PV Array Connected to Location C

At location C, the PV array is connected between Bus 16 and 20. Table 6.9 summarises the upgrades that were done for this location. There were no significant issues with this configuration. The energy lost transmitting the power between 4:00 am and 7:00pm, with no components isolated is 44.46 MWh.

Table 6.9: Interconnectors upgrade when the PV array was connected to Location C

Interconnector Location	Original Configuration		Upgraded configuration	
	Interconnector ID	Number of Transmission Lines in Parallel	Interconnector ID	Number of Transmission Lines in Parallel
Between busbars 16 and 20	1	1	not applicable	
Between busbar 16 and PV array	not applicable		1a	2
			1b	2
Between busbars 16 and 17	2	1	2a	3
			2b	3
Between busbars 2 and 17	3	1	3	1
Between busbars 20 and 21	4	1	4a	2
			4b	3
Between busbars 2 and 21	5	1	5	1
Between busbar 20 and PV array	not applicable		9a	3
			9b	3

6.5.2.4 PV Array Connected to Location D

At Location D, the proposed PV array is connected between Bus 20 and 21. Table 6.10 summarises the upgrades that were done for this location. Interconnector 2 can become overloaded for a few hours around 11:00 am as clearly obvious in Fig. 6.5. This will occur when Transformer 23 or Transformer 26 is isolated. This is because the power will be forced through Transformer 24 and Transformer 25 in order to feed the loads. As a consequence of this, the power will flow through the interconnector instead. As this only occurs for a small time period it can be avoided fairly easily by not isolating one of these transformers at this time. If one of these transformers has to be isolated at this time, a different generator configuration will have to be used.

Interconnector 2 can also become overloaded if Interconnector 2a or 2b is taken out for maintenance. The energy lost transmitting the power between 4:00 am and 7:00 pm, with no components isolated is 41.27 MWh

Table 6.10: Interconnectors upgrade when the PV array was connected to Location D

Interconnector Location	Original Configuration		Upgraded configuration	
	Interconnector ID	Number of Transmission Lines in Parallel	Interconnector ID	Number of Transmission Lines in Parallel
Between busbars 16 and 20	1	1	1	1
Between busbars 16 and 17	2	1	2a	1
			2b	1
Between busbars 2 and 17	3	1	3	1
Between busbars 20 and 21	4	1	not applicable	
Between busbar 20 and PV array	not applicable		4a	2
			4b	2
Between busbars 2 and 21	5	1	5a	1
			5b	2
Between busbar 21 and PV array	not applicable		9a	3
			9b	3

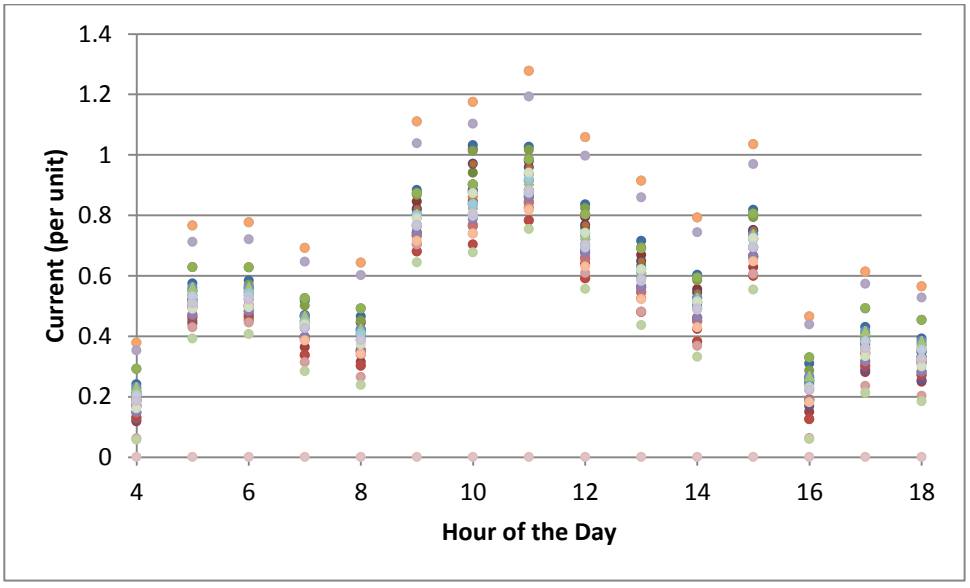

Figure 6.5: Current through interconnector 2 after the proposed PV array is connected with location D

6.5.2.5 Loads through the Interconnectors that are Connected Directly to the Proposed PV Array

The PV array generates power near its maximum capacity around midday. When this happens, the interconnectors that connect the PV array to the rest of the network are almost fully loaded. If one of these interconnectors is isolated at this time, it will overload at least one of the remaining interconnectors. This can be seen clearly in Fig. 6.6. In this case, the PV array is connected in position C. It can be seen that in most configurations, Interconnector 9b operates below its rated capacity for the whole day. However, if Interconnector 9a is isolated, interconnector 9b is overloaded from 8:00 am to 3:00 pm by almost 60%. Similar results are obtained when any interconnector that is connected to the GCPV system in any of the four positions is isolated.

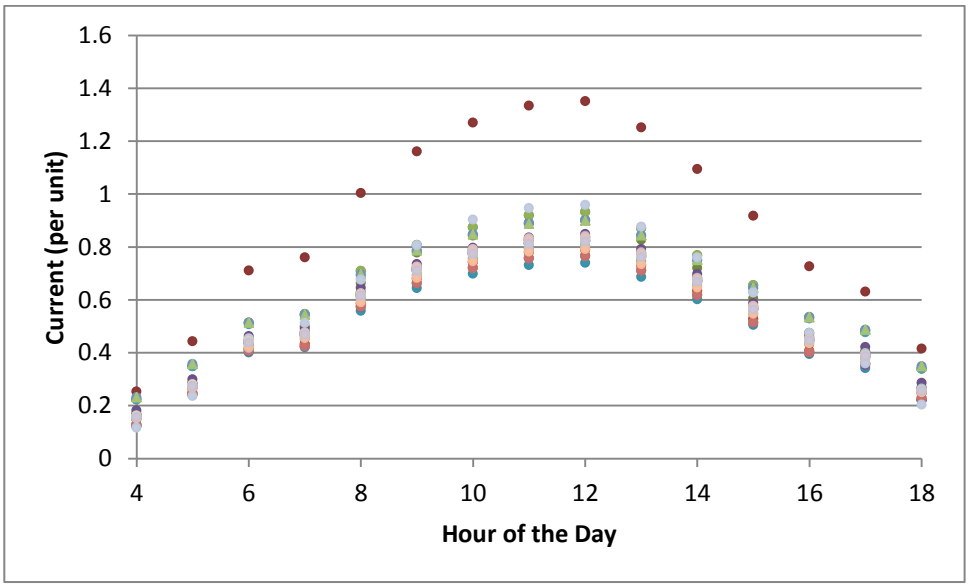

Figure 6.6: Current through interconnector 9a when proposed PV array connected to position C

Although these situations can be avoided by simply upgrading the interconnector, it can be argued that it will be uneconomical to increase its capacity by 60% for one potentially rare configuration. Instead, the approach taken in this report was to decrease the power that the PV array can generate when this configuration occurs. The extra power would have to come from the generators or grid feed. Table 6.11 is the recommended PV levels that can be generated if one of the interconnectors is isolated.

Table 6.11: Maximum Allowable Output Power of the Proposed PV Array when one of the Array Interconnectors is Isolated

PV Location	Interconnector Configuration	Original PV Array Output		Capped PV Array Output	
		Peak Interconnector Load (per unit)	PV Array Output (MW)	Peak Interconnector Load (per unit)	PV Array Output (MW)
A	3b energised, 3a isolated	1.43	81.5	0.987	67
	9b energised, 9a isolated	1.41	82.6	0.996	57
B	2b energised, 2a isolated	1.21	82.6	0.999	83
	9b energised, 9a isolated	1.54	81.5	0.994	70
C	1b energised, 1a isolated	1.17	82.6	0.999	83
	9b energised, 9a isolated	1.35	82.6	0.995	70
D	4b energised, 4a isolated	1.32	82.6	0.997	74
	9b energised, 9a isolated	1.52	82.6	0.986	60

6.6 Fault Analysis

The fault level in a network is a function of the impedance at the time of the fault as well as a function of the energy that is available to feed into the fault [93]. Connecting the PV system to the network will increase the amount of energy that is available to feed into a fault. Upgrading the interconnectors will lower the impedance. Therefore it is reasonable to assume that when the proposed PV array is connected to the network, the fault levels will increase. The ratings of circuit breakers are based on the symmetrical current that they can interrupt [93]. Hence, knowledge of the maximum fault currents that the breakers will be required to interrupt is essential to avoid damage to equipment.

This research will look at all four prospective locations and determine the maximum fault levels that the network will experience. These fault levels will be compared to the fault levels of the network before the array was connected. Finally, measures will be introduced in order to restrict any large fault currents to acceptable levels. The acceptable fault level of a network would depend on the rating of all of the components in that network that will experience the fault current. Unfortunately, this information was unavailable. In order to determine an appropriate fault level, fault studies were conducted on each bus on the original network before the PV array was connected. This information was compared to the fault levels of HV switchgear that is commercially

available. From this, the acceptable fault levels for each busbar in the model were chosen.

When the network was modelled for the power flow studies, the GCPV system was represented as a synchronous generator. The output power was set to match the output power of the GCPV system at the time. This was appropriate for the power flow study, as ERACS modelled the generators as a voltage behind an impedance. However this is not the case with fault studies. For fault calculations, ERACS takes into account factors such as the inertia of the generators [90]. This would make using a synchronous machine as a model for a PV system inaccurate. A better model was needed.

Fig. 6.7 is a representation of a typical large-scale PV array. One approach to model such a system in ERACS would be to model each part of the system individually [94]. If information was available about all of the components in this system, this would result in an accurate model. However, this level of accuracy was not needed for this case study. Instead, a grid connection was used to model the PV array. In order for the grid connection to be a good representation of the PV array, the maximum short circuit current had to be calculated for the array. ERACS uses this information to determine the impedance of the connection to the network and to calculate the contribution that the PV array will make to a fault [90].

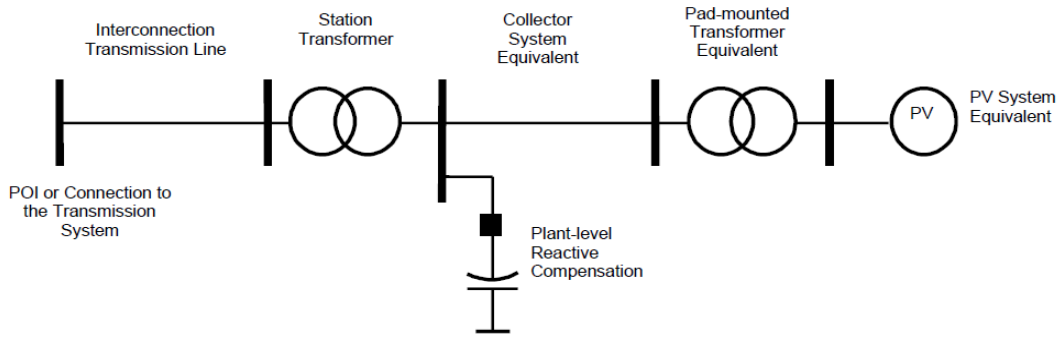

Figure 6.7: Single-machine equivalent load flow representation

If a PV module is shorted, it is output current will be 1.25 times its usual current. This is because there are certain circumstances in which the module may be exposed to conditions that are better than the rated STC [95]. Therefore, the fault current was taken as 125% of the full load current at the time of the study. The x/r ratio was set to 10.

This fault study's objective was to determine the maximum fault levels for the network. One way of obtaining this data would be to proceed in a similar fashion as was done for the power flow study. A fault analysis could be done for every network configuration at

various times of the day. This information could then be analysed to determine the maximum fault levels for different parts of the network. However, the maximum fault levels would occur when the network has the ability to feed the most energy into the fault. For instance, at 1:00 am, there are only six generators supplying power to the network, while the PV system is not supplying any power. It would be reasonable to assume that the fault levels at this time would be relatively low when they are compared to a time when more generators are connected to the network. Based on this, it was decided to determine when the network will have the most available fault energy and concentrate the fault analysis to that particular time of the day.

As the fault levels are also related to the impedance of the network, it was assumed that the fault levels would be highest when the overall impedance of the network was at its lowest. This condition occurred when none of the components in the network were isolated. Therefore, the fault studies were also confined to these situations. In order to record the maximum fault levels, a three phase fault was simulated on each of the five 13.8 kV busbars. These results were analysed to find the maximum fault level for each busbar. If it was determined that this fault level was higher than the proposed short circuit rating of the busbar, measures were taken to reduce these fault levels.

6.6.1 Choosing Component Ratings

A fault study was first conducted on the original network before the PV array was connected. These results were used as a benchmark to determine acceptable fault levels that the components could withstand. The maximum fault levels of all of the generation busbars are shown in Fig. 6.8. With the exception of Bus 16, all of the busses have a maximum fault level below 40 kA before any GCPV system was connected.

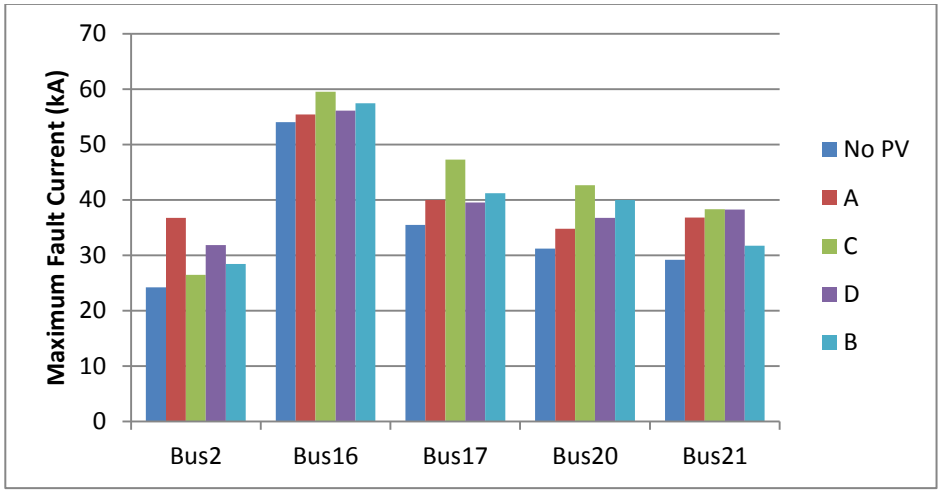

Figure 6.8: Maximum fault levels for the 13.8 kV busbars

Table 6.12 is a summary of some of the ratings of commercially available switchgear. The three seconds withstand current for these models are either 16, 25, 31.5, or 40 kA. Based on this information, it will be assumed that the switchgear in the model has a three second withstand rating of 40 kA. Therefore, any upgrades to the network should keep fault currents below this level. The fault levels on Bus 16 are 54 kA. This fault current is higher than the withstand rating of any switchgear that was researched for this study. This suggests that this part of the model is inaccurate.

Table 6.12: Ratings of Various Commercially Available Switchgear

Manufacture	Model	Rated voltage (kV)	Short time withstand current (kA/3s)	Circuit breaker breaking capacity
Schneider Electric	Mcset	17.5	25	25
	[16]		31.5	31.5
			40	40
			50 for 1 second	50 for 1 second
Schneider Electric	PIX	17.5	25	25
	[16]		31.5	31.5
			40	40
			50	50
ABB	VD4	17.5	16	
	[17]		31.5	
			40	
			50	
Schneider Electric	WS	17.5	16	16
	[18]		20	20
			25	25
			31.5	31.5

Fig. 6.9 shows the fault levels of all of the 13.8 kV interconnectors. In the original configuration, before any PV array was connected, all of the interconnectors are represented using the same model, as a 5 km long identical transmission line. Therefore, all of the transmission lines will have the same fault withstand level. The maximum fault level occurred on Interconnector 5 as 6.95 kA. For that reason it will be assumed that the transmission line model can withstand 7 kA.

6.6.2 Fault Study Results

Excluding Bus 16, there are three instances that have a fault current above the 40 kA threshold. One way of limiting the fault current that flows into a busbar is to limit the fault current flowing through the interconnectors that are connected to the busbar. This

can be accomplished by placing reactors in series with the interconnectors. These have a high reactance while having a negligible resistance. This means that they will raise the impedance of the interconnector, but will cause minimum energy loss. However, because the reactors have large impedance, they will have a voltage drop across them. This should be minimal during normal operation but will rise significantly when fault current flows through them.

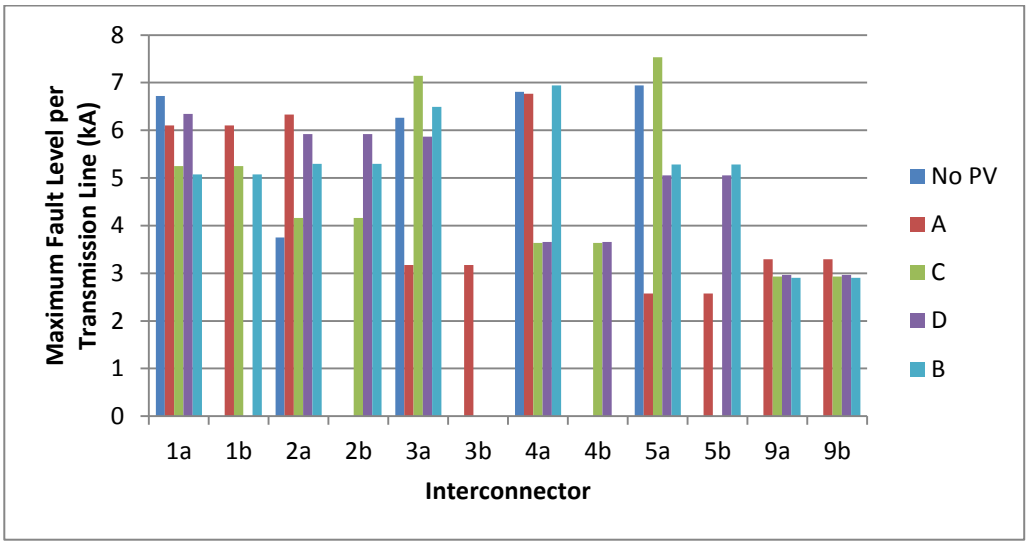

Figure 6.9: Maximum fault levels for the 13.8 kV interconnectors

The reactance of the reactor has to be chosen so that it limits the fault current in the circuit to acceptable levels. In this case this requires reducing the fault current in the busbar to below 40 kA. In order to find the amount of reactance that is needed, fault studies were conducted using reactors with various reactance ratings. (All of the reactor models had a resistance of zero.) For each circumstance, the fault current in the reactor and busbar were recorded. Also, the voltage drop across the reactor during normal load conditions was also noted. These results were charted to find the minimum reactance that would be needed to limit the fault current to below 40 kA.

This can be seen clearly in Fig. 6.10 and Fig. 6.11 with reference to Bus 17. Bus 17 was overloaded when the PV array was connected in Location C. Identical reactors were placed on the Interconnectors 2a and 2b. It can be seen from these results that in order to limit the reactance to below 40 kA, 0.42 ohms has to be added to each interconnector. The voltage drop during normal load conditions is negligible. Since the model that was used contained no resistance, there was no power loss from the reactor. In reality, a reactor will have a small resistance, but the power energy loss from it during normal conditions would be minimal.

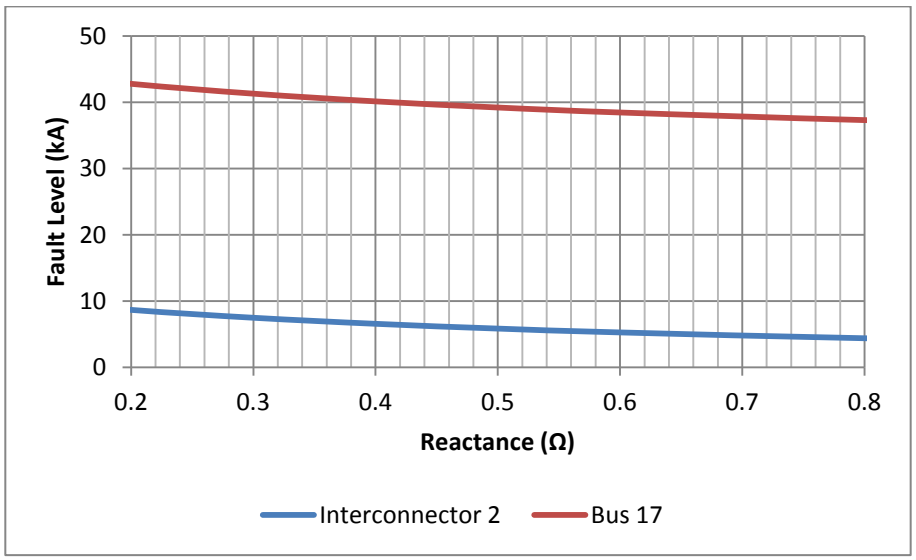

Figure 6.10: The effect on the fault levels of changing the reactance of Interconnector 2 with the GCPV array connected at Location C

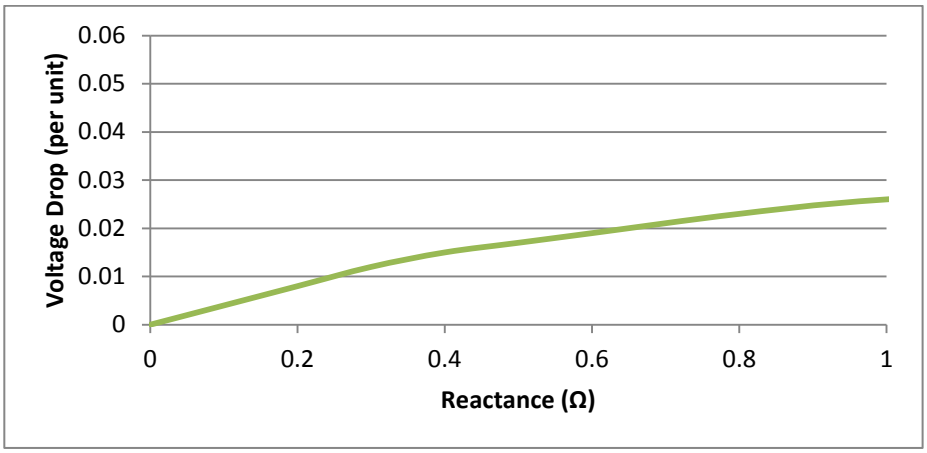

Figure 6.11: The effect on the voltage drop across the reactor when changing its reactance

Table 6.13 shows the minimal reactances that are needed to limit the fault currents in the three configurations in question to safe levels.

Table 6.13: The Minimum Reactance Required to Limit the Fault Currents in the 13.8 kV Busbars to Acceptable Levels

PV array location	Reactor locations		Minimal reactance required per unit reactance (Ω)
B	L9a	L9b	0.2
C	L2a	L2b	0.5
	L9a	L9b	0.4

Fig. 6.9 shows the maximum fault levels of all of the 13.8 kV interconnectors with the proposed PV array connected in all four prospective locations. There are two lines that have a fault level higher than the maximum withstand level of 7 kA. The fault currents in these interconnectors can similarly be reduced by using reactors. However, in this case the fault currents in the interconnectors can also be made safe by upgrading the interconnectors. This option was used. Another transmission line was added in parallel to the overloaded lines. Although this achieved the objective, as the fault current was split between more transmission lines, it also reduced the impedance of the fault path. This in turn increased the overall fault current, which threatened to overload the busbar that the interconnectors are connected to. Fig. 6.12 shows how the fault current in the 13.8 busbars change when the transmission lines and reactors are added to the network based on Location C. Although the fault levels raise slightly with the addition of the transmission lines, the reactors in the network are still adequate to limit the fault current levels to below 40 kA.

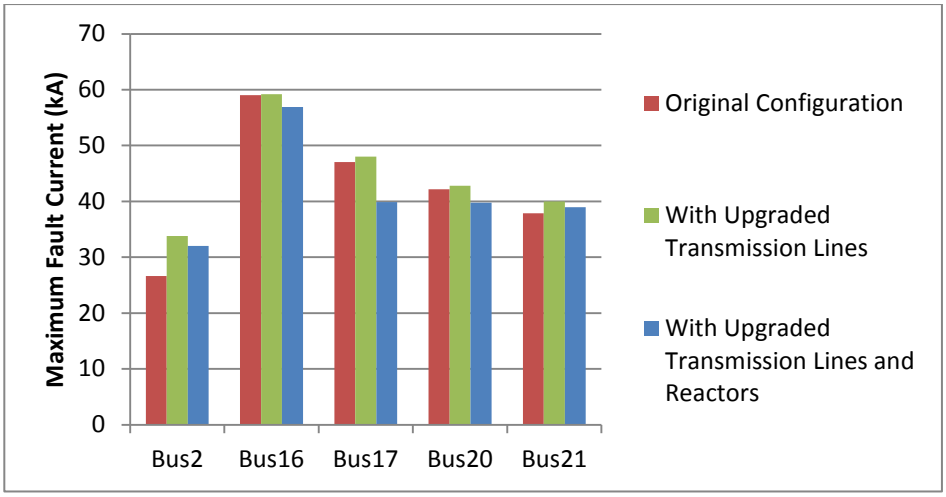

Figure 6.12: Comparison of fault currents in the busbars when the network is upgraded (Location C)

Fig. 6.13 shows how the fault current changes in the interconnectors when the transmission lines and reactors are added to the network (Location C). The reactors drastically reduce the fault currents in the interconnectors in which they are connected. It is worth noting that the addition of the reactors also raises the maximum fault levels in Interconnectors 1 and 5. In this case though, all of the fault currents are still below 7 kA.

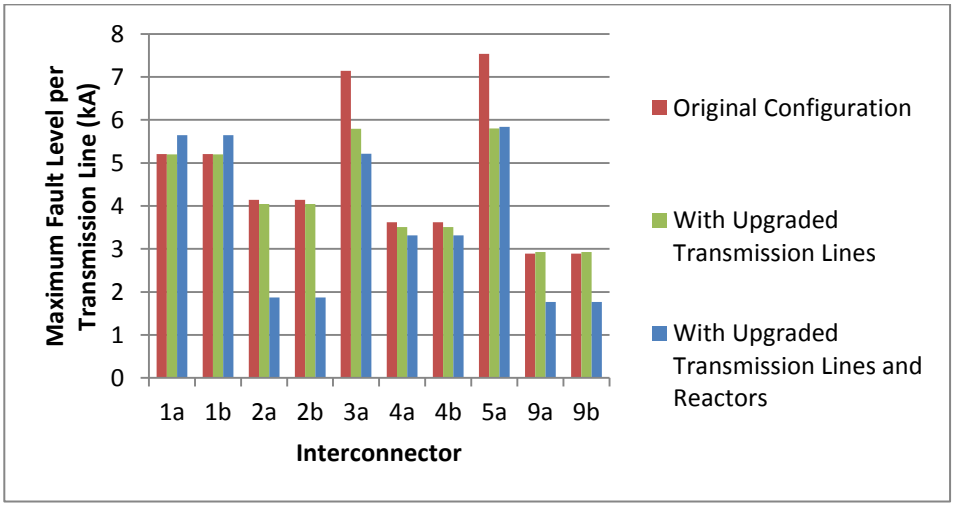

Figure 6.13: Comparison of fault currents in the interconnectors when the network is upgraded (Location C)

6.7 Conclusion and Future Work

The goal of this project was to use ERACS to analyse the effect of connecting the proposed GCPV system to the model network. Power flow studies were used to determine the components that would become overloaded during normal operation and to suggest any upgrades that were needed. Fault studies were used to measure how the fault level changed when the suggested upgrades were implemented. When the fault levels were too high, measures were taken to reduce them. Table 6.14 is a summary of the results.

Table 6.14: Summary of the Results from the Power Flow and Fault Studies

PV location	Transmission lines added		Reactors added	Energy loss between 4:00 am and 7:00 pm (MWh)
	From power flow study	From fault study		
A	15	0	0	44.27
B	13	0	2	47.14
C	18	2	4	44.46
D	12	0	0	41.27

The least energy is lost when the GCPV array is connected to Location D. This is also the location that required the least amount of upgrades. Only 12 transmission lines were added, and no devices were needed to limit fault levels. In comparison, when the PV system was connected to Location C, 20 transmission lines and 4 reactors had to be added. Based on this information, this suggests that connecting the PV system to Location C would require greater infrastructure upgrades. It is interesting to note that

upgrading the network does not necessarily improve the efficiency. Location C suffers from the second worst energy loss. Furthermore, it was notable what the effect of altering one component had on the overall performance of the network. For instance, reactors were placed into the network to reduce the fault current in certain areas. The impedance that the reactors added to the network resulted in electricity flowing in different transmission lines that had lower impedance. This in turn ran the risk of overloading these transmission lines.

This case study used the average loads that the system will experience in June. June is when the peak load would be experienced for the year. It was assumed that if the system is adequate to supply these loads in June, it would also work in other months, when the load is less. The case study does not take into account that the loads will fluctuate. There will be times where the loads will be higher than the average load. In addition, Kuwait's demand for electrical energy has risen by an average of 6% per year. The project does not account for the rise in demand either. Instead, this study attempted to work out the minimal level of upgrades that were needed to connect the GCPV array to the network. In reality, any upgrades to the network would have to take into account the future requirements. Fig. 6.14 is the fault levels of all four of the transmission busbars before any PVs are connected. These levels appear to be abnormally high. In comparison, the maximum short circuit levels experienced in the UK at 11 kV are 250 MVA [92].

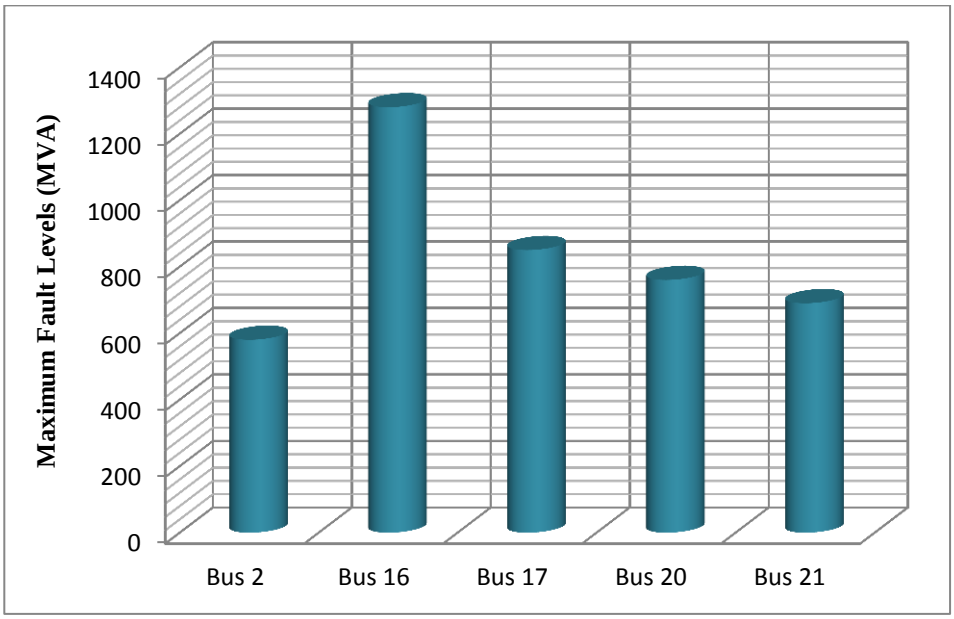

Figure 6.14: Maximum fault levels of the original network model

There was limited information available about the actual layout of the network. It is possible that the original network contains reactors that would limit the fault levels. It is

also possible that there may be more than 5 generator busbars, and the generators may be connected to the network in a different configuration. This would change the impedance of the network which would also affect the fault levels. Also, the generator busses in the model are connected in a closed ring. It is possible that there is a normally open point in this ring, which would also limit fault currents. Ultimately, in order to get a better idea of the fault levels, a more detailed model needs to be created. This would involve accessing more information about the network that was not available at the time. The original approach to the study was very linear. First of all, a model of the network was to be built. Then power flow studies were going to be conducted on the model. Finally the fault levels in the network were going to be studied. In reality, information obtained from the power flow and fault studies were used to change the original model. Changing the network configuration to reduce fault levels effects how the network responds during normal load conditions. A better approach would be to study the power flow and fault currents simultaneously.

The fault analysis was carried out by simulating three phase symmetrical faults on all of the 13.8 kV busbars. The effect of asymmetrical fault current was not studied. The asymmetrical current may substantially increase the overall fault current, depending on when the fault occurs relative to the AC voltage waveform. This may increase the fault currents to dangerous levels that were not predicted in this study. Future fault studies should investigate asymmetrical faults. All of the loads were represented as non-rotating shunts. In reality, a proportion of these loads would be rotating. Rotating loads would respond differently in fault conditions. Also, induction motors would contribute to voltage collapse. In order to get an idea of the stability of the network, future studies would have to consider the effect of rotating loads.

Chapter 7
Conclusions and Future Work

7.1 Conclusions

Motivated by insufficient power supply capabilities and high peak loadings in Kuwait, solar energy availability in Kuwait area as a potential renewable energy resource has been investigated and estimated. In this research, the objectives of the original plan (formulated in Section 1.3) have already been accomplished. The visibility and potential of SR over Kuwait area has been investigated taking into consideration the geographical and temporal variability of PV energy sources inside Kuwait (first objective). A trigonometric SR model that is applicable for Kuwait taking into consideration the metrological data for Kuwait area has been developed. The hourly, daily, and monthly SR on the horizontal surfaces over Kuwait area has been estimated giving a clear indication of the visibility and potential of solar energy in Kuwait. Moreover, the SR data for Kuwait area is used as an input to a selected PV module with a specific electrical data. Thereafter, simplifying mathematical modelling for different PV configuration of modules and panels has been presented by developing an analytical PV model based on extracted physical parameters (second objective). Modelling of the selected topology of the PV generation system has been performed (fourth objective). The wiring and modelling of the PV cells or modules is presented showing the *I-V* characteristic curves of the proposed PV module at different SR intensities, and we clarified that the data for these curves is important in determining the module or array peak power rating by plotting the *P-V* curves at different SR intensities. In addition, deriving a mathematical model and designing equations to obtain theoretical predictions have been met (third objective).

An optimal GCPV system has been modelled using iterative manual algorithm approach (*SAIMA*) to figure out the size of the array configuration (fifth objective). The *SAIMA*-based sizing algorithm had been used to successfully select a PV module and inverter such that the PV array size with required output power and its relative energy were achieved. However, the main drawback of the proposed GCPV system is its high price. Hence, the optimal inverter sizing and then system efficiency for predetermined PV array size (see Chapter 3 and use *SAIMA*) are much necessary to make the GCPV system as profitable as possible. Therefore, a novel design method in order to optimize the GCPV cost-efficiency Pareto front curve has been conducted using *BoWS* with one main objective function (sixth objective). This novel method which is based on the

approximation of Pareto frontier using *BoWS* has been explored to determine the optimal cost-efficiency configuration (including inverter sizing) for proposed GCPV system with predetermined array. This work is done by defining a bi-objective system cost and efficiency as the main objective function and the modified electrical limitations as the constraints of *BoWS*. The SQP method is used to identify the optimal Pareto front line. The *BoWS* is modified so that the presented method can be applied to all inverters with different sizes and topologies, and as a result to all GCPV system sizes. Since an accurate efficiency model for inverter and proposed model for PV module are used, the annual produced energy of GCPV system and as a result its numerical objective function is calculated with high accuracy. Through running the proposed method, the optimal economic design and appropriate configuration are determined and Pareto line is performed after specific iterations. On the other hand, the proposed model has several limitations. First, the variable and stochastic natures of supply and demand are not taken into account. This might lead to a significant error, given the large variance in PV supply and system load demand. In addition to the consideration outlined above, in the grid-connected mode, the model assumes continuous grid connection without interruptions, whereas in reality, the connectivity with the grid is not perfect. Realistically, in the absence of a GCPV system that can satisfy the load demand independently, the supply reliability within the micro-grid cannot exceed the reliability of the connection with the grid.

Furthermore, a computer simulation for the developed model of GCPV system has been undertaken using PSIM software to integrate the proposed GCPV system to Kuwait national grid by using boost converter, PWM inverter and low-pass LC filter (seventh objective). The best array configuration with highest sizing factor and economical components has been selected as an input data to build a comprehensive simulation model which is implemented in PSIM software. A higher efficiency by maximum power point tracking (MPPT) control algorithm has been introduced using P&O method (eighth objective). The simulated GCPV model has elucidated to what extent that the proposed model can interface with Kuwait electrical network.

The proposed GCPV array with its optimal configuration is penetrated into Kuwait national grid (ninth objective). The GCPV generation model that has been built was incorporated within low-voltage generation grid of generation section I at Alsabiya Power Station within Kuwait electrical network to analyse the impact on the power

system of incorporating a significant amount of PV generation. It is obvious that this issue need more investigation in future study.

7.2 Future Work

This work has shown the optimal proposed GCPV model was built based on the incident SR on horizontal surfaces over Kuwait area. This suggests the need for further studies of inclined surfaces over areas, with same proposed trigonometric model to be more realistic and accurate. As the *BoWS* method with the explored design procedure was not taking into account the variable and stochastic natures of supply and demand, even more, the proposed grid-connected mode assumes continuous connections without interruptions, a study may be made on a way to specify deep electrical parameters of the supply and demand to reach the optimum operating point. In addition to the consideration outlined above, a possible control and protection electrical circuits connected with the inverters in order to not loss electricity in case of grid turbulences.

One can improve the proposed strategy of the GCPV cost-efficiency Pareto curve to effectively solve bi-objective optimization problem whose Pareto front has non-convex regions with uniform curvature at which most of the solutions obtained are concentrated in these regions. In the future we intend to investigate specializations and adaptations of our general methodology to more complicated GCPV cost functions. For example, in convex nonlinear complicated cost problem curvature the Pareto front will not reside on the surface of the feasible set and its approximation may not benefit from convexity. Our conclusion is that the results are promising and this fact encourages us to continue working in this address, considering additional hard multi-objective problems with three objective functions such as PV array size, cost and efficiency.

The PV generating unit may be liable to common mode failures that might cause the sudden or rapid disconnection of a large proportion of operating PV capacity. This suggests a dynamic stability study during the penetration process of the GCPV system must therefore be considered carefully.

References

1. A. Al-Hasan, "*Electricity Generation Cost Between Proposed Photovoltaic Station and Conventional Units in Kuwait*", Renew Energy, Vol. 12, No. 3, pp 291-301, 1997

2. R. J. Overstraeten and R. P. Mertens, " *Physics, Technology and Use of Photovoltaics*", Adam Hilger Ltd, 1986

3. "*A Progress Report on Electricity Supply First Quarter 2014*", UAE Power Authority (UAEPA), 2014

4. "*World's largest photovoltaic power plants*", PV resources, 2014. [Online] Available: http://www.pvresources.com/en/top50pv.php

5. Ministry of Electricity and Water, Kuwait, "*Statistical Year Book*", 2009

6. A. Ghoneim, A. Al-Hasan, A. Abdullah, "*Economic Analysis of Photovoltaic Powered Solar Domestic Hot Water Systems at Kuwait*", Renew Energy, Vol. 25, pp 81-100, 2002

7. Kuwait Society of Engineers, *The International Engineering Congress on Alternative Energy Application: "Option or Necessity"* Kuwait, November 3-5, 2009

8. Ministry of Electricity and Water, Kuwait, "*Statistical Year Book*", 2013

9. Z. Yuwen, "*Survey on the Development of Solar Energy Application and Future Trend*", Electric Power, Vol. 36, pp. 63-69, Sep. 2003

10. M. Iqbal, "*An Introduction to Solar Radiation*", Academic Press, ISBN:0-12-373752-4, Canada, 1983

11. M. Chegaar and A. Chibani, "*A Simple Method for Computing Global Solar Radiation*", Review Renewable Energy, Chemss, pp. 111-115, 2000

12. K. Bakirci, "*Correlations for Estimation of Daily Global Solar Radiation with Hours of Bright Sunshine in Turkey*", Energy, Vol. 34, pp. 485-501, 2009

13. T. Muneer, S. Younes, and S. Munawwar, "*Discourses on Solar Radiation Modelling*", Renewable and Sustainable Energy Reviews, Vol. 11, pp. 551-602, 2007

14. C. Helen, "*Power Estimating Clear-Sky Beam Irradiance from Sunshine Duration*", Solar Energy, Vol. 71, pp. 217-224, 2001

15. J. Remund, M. Levevre, T. Ranchin, and L. Wald, "*Constructing Maps of the Link Turbidity Factor of Solar Energy*", Internal Document, SoDa Project D5-2-1, consult http://www.soda-is.com. , Bern, 2003

16. H. Suehrcke, "*On the Relationship Between Duration of Sunshine and Solar Radiation on Earth's Surface; Angstrom's Equation Revisited*", IEEE Trans. on SR., Vol. 12, pp. 417-425, 2000

17. R. Jordan, and J. Threlkeld, "*Handbook of Fundamentals*", ASHRAE, American Society of Heating, Refrigeration and Air Conditioning Engineers, Vol. 64, P. 45, Atlanta, 1958

18. B. Liu, and R. Jordan, "*Daily Insolation on Surfaces Tilted Toward the Equator*", Trans. ASHREA, Vol. 67, pp. 526-541, 1961

19. T. Muneer, "*Solar Radiation Modelling for the United Kingdom*", PhD thesis, CNAA, London, 1987

20. F.J. Olmo, J. Vida, I. Foyo, Y. Castro-Diez and L. Alados-Arboledas, *"Prediction of global irradiance on inclined surfaces from horizontal global irradiance"*, Elsevier Trans. on Energy System, Vol. 24, pp. 689–704, 1999

21. NASA website, *"Kuwait area over 22 years"*

22. T. Markvart, and L. Castaner, "*Practical Handbook of Photovoltaics Fundamentals and Applications*", 1st Edition, Alsevier, 2003

23. R. Gottschalg, "*The Solar Resource for Renewable Energy Systems and the Fundamentals of Solar Radiation*", 2nd Edition, Sci-Notes Ltd, 2001

24. P. Anigstein, and R. Sanchez Pena, "*Analysis of Solar Panel Orientation in Low Altitude Satellites*", IEEE Trans. on Aerospace and Electronic Systems, Vol. 34, No. 2, pp. 569-578, 1998

25. J. Duffie, and W. Beckman, "*Solar Engineering of Thermal Processes*", 3rd Edition, Jone Wiley & Sons Inc., New York, 2006

26. NASA Surface Meteorology and Solar Energy-Location. Atmospheric Science Data Centre. Twenty Two Years Average Data of NASA SSE Model (1983-2005) http://www.eosweb.laec.nasa.gov

27. Solar Energy Research Institute, SERI, "*Photovoltaics Technical Information Guide*", SERI/SP – 271-2452, U.S. Department of Energy, Washington, D.C.,2005

28. D. S. Shugar, "*Photovoltaics in the Utility Distribution System: the evaluation of the system and distributed benefits*", IEEE Photovoltaic Specialists Conference, Orlando, May 1990

29. "*Photovoltaic Systems for Electric Utility Investments*", Executive Conference, AboDabi, UAE, 4-7 October 2009

30. Energy 4 Next Generations Conference, "*Photovoltaics Activities in Singapore and South-East Asia*", Amsterdam, Netherlands, 4-5 November 2010

31. Y. X. Lee, and S. Dubey, "*Numerical Simulation of a Photovoltaic Thermal System for Student Hostel in Singapore*", Applied Energy Trans. Vol. 84, pp. 986-996, 2010

32. H. S. Rauschenbach, "*Solar Cell Array Design Handbook*", 1st Edition, Van Nostrand Reinhold Company, New York, 1980

33. R. H. Bube, "*Photovoltaic Materials*", Imperial College Press, London, 1998

34. International Energy Agency, IEA, "*Photovoltaic Systems for Electric Utility Applications*", Opportunities Critical Issues and Development perspectives, Taormina, Italy, 1990

35. Centre for Renewable Energy and Sustainable Technology, CREST, "*Renewable Energy Policy Project*", Washington D.C., http://www.solstice.crest.org

36. P. Maycock, "*The State of the PV Market* ", Solar Today (Academic Press), London, Jan/Feb pp32-35, 2004

37. T. H. Kuehn, J. W. Ramsey, and J. L. Threlkeld, "*Thermal Environmental Engineering*", 3rd Edition, Prentice-Hall, Englewood Cliffs, NJ., 1998

38. K. Rosen, and A. Meier, "*Energy Use of U.S. Consumer Electronics At the End of the 20th Century*", Lawrence Berkeley National Laboratory, LBNL-46212, 2000

39. Real Goods Trading Corporation, "*Solar Living Source Book*", Ukiah, CA, USA, 2002

40. J. Wiles, "*Photovoltaic Power Systems and the National Electric Code: Suggested Practices*", Sandia National Laboratories, SAND-0674, Albuquerque, NM., 2001
41. Roadmap, "*PV Industry Technology Roadmapping Workshop*", Chicago, June 23-25, 1999

42. National Centre for Photovoltaics, NCPV, "*Best Laboratories PV Cell Efficiencies for Various Technologies*", USA, 2010, www.nrel.gov/ncpv

43. M. Green, "*Crystalline-and-Polycrystalline Solar Cells: Renewable Energy Sources for Fuels and Electricity*", 2nd Edition, Island Press, Washington D.C., 2006

44. M. P. Peloso, P. Chaturvedi, P. Wurfel, B. Hoex, and A. G. Alberle, "*Observations on the Spectral Characteristics of Silicon Wafer Solar Cells*", Proceedings of 35th IEEE Photovoltaic Specialists Conference, Honolulu, USA, 2010

45. M. Amin, "*Energy Infrastructure Defence Systems* ", IEEE, Vol. 93, No. 5, pp. 861-875, 2005

46. Y. Liao, W. Chang Li, P. Li, and A. Wu Ruan, "*Novel Test Approach for Interconnect Resources in Field Programmable Gate Arrays*", Journal of Electronic Science and Technology, JEST, Vol. 9, pp. 85-89, March 2011

47. H. Qian, J. Zhang, J. Sheng-Lai, and W. Yu, "*A High-Efficiency Grid-Tie Battery Energy Storage System*", IEEE Transactions on Power Electronics, pp. 886-896, 2011

48. D. Yang, and H. Yin, "*Energy Conversion Efficiency of a Novel Hybrid Solar System for Photovoltaic, Thermoelectric and Heat Utilization*", IEEE Transactions on Energy Conversion, pp. 662-670, 2011

49. C. Lashway, "*Photovoltaic System Testing Techniques and Results* ", IEEE Transactions on Energy Conversion, Vol. 3, No. 3, pp. 503-506, 1988

50. B. Kroposki, and R. DeBlasio, "*Technologies for the new millennium: Photovoltaics as a distributed resource*", in Proc. IEEE Power and Engineering Society Summer Meeting, Vol. 3, pp. 1798-1801, July 2000

51. K. Stokes and J. Bigger, "*Reliability, cost, and performance of PV-powered water pumping systems: a survey for electric utilities*" , IEEE Transactions on Energy Conversion, Vol. 8, Issue 3, pp. 506 – 512, Sept. 1993

52. "*Creating Energy Independence Florida Solar Energy Centre (FSEC)*", a research institute of the University of Central Florida, 2007

53. G. Nofuentes, J. Aguilera, and F.J. Munoz, "*Tools for the profitability analysis of grid-connected photovoltaics*", Progress in Photovoltaics: Research and Applications, Wiley, Vol. 10, pp. 555–570, December 2002

54. S. I. Sulaiman, T. K. A. Rahman, and I. Musirin, "*Novel intelligent sizing algorithm for grid connected photovoltaic system design*", International Review on Modelling and Simulations, Vol. 3, No. 4, pp. 639-652, August 2010

55. S. I. Sulaiman, T. K. A. Rahman, and I. Musirin, "*Sizing Grid-Connected Photovoltaic System*", Symposium on Industrial Electronics and Applications (ISIEA2011), Sept. 2011, Langkawi, Malaysia

56. A. M. Omar and S. Shaari, "*Sizing verification of photovoltaic array and grid-connected inverter ratio for the Malaysian building integrated photovoltaic project*", International Journal of Low-Carbon Technologies, Vol. 4, No. 4, pp. 254-257, October 2009

57. S. B. Kjaer, J. K. Pedersen, and F. Blaabjerg, "*A review of single-phase grid-connected inverters for photovoltaic modules*", IEEE Transactions on Industry Applications, Vol. 41, No. 5, pp. 1292- 1306, Sept-Oct 2005

58. A. Alarcon-Rodriguez, E. Haesen, G. Ault, J. Driesen and R. Belmans, *"Multi-objective planning framework for stochastic and controllable distributed energy resources"*, Renewable Power Generation, IET, Vol. 3, Issue 2, pp. 227 –238, June 2009

59. M. Badejani, M. Masoum and M. Kalantar, *"Optimal design and modeling of grid-connected PV-wind systems"*, In Power Engineering Conference, AUPEC Australasian Universities, pp. 1 –6, Dec. 2007

60. G. Carpinelli, G. Celli, F. Pilo, and A. Russo, *"Distributed generation siting and sizing under uncertainty"*, In Power Tech Proceedings, IEEE Porto, Vol. 4, pp. 7-12, 2001

61. G. Celli, E. Ghiani, S. Mocci and F. Pilo, *"A multi-objective evolutionary algorithm for the sizing and siting of distributed generation"*, Power Systems, IEEE Transactions, Vol. 20, Issue 2, pp. 750 – 757, May 2005

62. R. Dufo-Lpez and L. Bernal-Agustn, *"Multi-objective design of PV-diesel systems"*, Renewable Energy, Vol. 33, Issue 12, pp. 2559 – 2572, 2008

63. R. Chedid, H. Akiki and S. Rahman, "*A decision support technique for the design of hybrid solar-wind power systems*", Energy Conversion, IEEE Transactions, Vol. 13, Issue 1, pp. 76 – 83, March 1998

64. A. Keane and M. O'Malley, *"Optimal allocation of embedded generation on distribution networks"*, Power Systems, IEEE Transactions, Vol. 20, Issue 3, pp. 1640 – 1646, Aug. 2005

65. W. Kellogg, M. Nehrir, G. Venkataramanan and V. Gerez, *"Generation unit sizing and cost analysis for grid-connected photovoltaic and hybrid wind/PV systems"*, Energy Conversion, IEEE Transactions, Vol. 13, Issue 1, pp. 70 – 75, March 1998

66. E. Koutroulis, D. Kolokotsa, A. Potirakis and K. Kalaitzakis, *"Methodology for optimal sizing of stand-alone photovoltaic generator systems using genetic algorithms"*, Solar Energy, Vol. 80, Issue 9, pp. 1072 – 1088, 2006

67. W. Lingfeng and C. Singh, *"Compromise between cost and reliability in optimum design of an autonomous photovoltaic power system using mixed-integer PSO algorithm"*, In Clean Electrical Power, ICCEP International Conference, pp. 682 – 689, 2012

68. M. Muselli, G. Notton and A. Louche, *"Design of photovoltaic power generator with optimization of energy management"*, Solar Energy, Vol. 65, Issue 3, pp. 143 – 157, 2012

69. A. Saif, H. Zeineldin, S. Kennedy and J. Kirtley, *"Multi-objective capacity planning of a PV-battery hybrid power system"*, In Proceeding of IEEE Int. Energy Conf. (ENERGYCON2010), pp. 1 –6, Dec. 2010

70. D. Singh and K. Verma, *"Multi-objective optimization for photovoltaic system planning with load models"*, Power Systems, IEEE Transactions, Vol. 24, Issue 1, pp. 427 – 436, Feb. 2009

71. I. Das and J. Dennis, *"Normal-Boundary Intersection: A New Method for Generating Pareto Optimal Points in Multi-criteria Optimization Problems"*, SIAM J Optimization, Vol. 8, pp. 631 – 657, 1998

72. A. Messac and C. Mattson, *"Generating Well-Distributed Sets of Pareto Points for Engineering Design using Physical Programming"*, Optimization Engineering, Issue 3, pp. 431 – 450, 2002

73. I. Das and J. Dennis, *"A closer look at drawbacks of minimizing weighted sums of objectives for Pareto set generation in multi-criteria optimization problems"*, Structural Optimization, Vol. 14, pp. 63-69, 1997

74. Y. Kim and de Weck, *"A weighted-sum method for multi-objective optimization: Pareto front generation"*, Structural and Multidisciplinary Optimization, in press, 2004

75. S. Shan and G. Wang, *"An efficient Pareto set identification approach for multiobjective optimization on black-box functions"*, Journal of Mechanical Design, Issue 127, Vol. 5, pp. 866 – 871, Jan. 2005

76. M. H. Kim, M. G. Simoes, and B. K. Bose, "*Neural network based estimation of power electronic waveforms*", IEEE Transaction on power electronics, Vol. 11, No. 2, pp. 383-389, March 1996

77. A. Kalirasu and S. S. Dash, "*Modelling and Simulation of Closed Loop Controlled Buck Converter for Solar Installation*", International Journal of Computer and Electrical Engineering, Vol. 3, No. 2, pp. 1793-8163, April 2011

78. J. Jervase, H. Bourdoucen, and A. Al-Lawati, " *Solar Cell Parameter Extraction using Genetic Algorithms*", Meas. Sci. Technol., 12, pp. 1922-1925, 2001

79. S. Jianhui, Y. Shijie, Z. Wei, W. Minda, S. Yuliang, and H. Huiruo, *"Investigation on Engineering Analytical Model of Silicon Solar Cells"*, [J]. Acta Energiae Solaris Sinica, 2001, 6(22): 439-412

80. D. JC. MacKay, *"Sustainable Energy - Without the Hot Air"*, UIT Cambridge, 2009.[Online]Available:http://www.inference.phy.cam.ac.uk/sustainable/book/tex/cft.pdf, [Accessed 21/10/2012]

81. M. Ahmad and S. Mekhilef, *"Design and Implementation of a Multi-Level Three-Phase Inverter with Less Switches and Low Output Voltage Distortation"*, Journal of Power Electronics, vol. 9, pp. 594-604, 2009

82. S. Chin, J. Gadson, and K. Nordstrom, *"Maximum Power Point Tracker"*, Tufts University Department of Electrical Engineering and Computer Science, 2003, pp. 1-66

83. J. J. Nedumgatt, K. B. Jayakrishnan, S. Umashankar, D. Vijayakumar, and D. P. Kothari, *"Perturb and Observe MPPT Algorithm for Solar PV Systems-modelling and Simulation"*, in annual IEEE India Conference (INDICON), Dec. 2011, pp. 1–6

84. L. Chun-xia and L. Li-qun, *"An Improved Perturbation and Observation MPPT Method of Photovoltaic Generate System"*, in 4th IEEE Conference on Industrial Electronics and Applications, ICIEA 2009, May. 2009, pp. 2966–2970

85. UL1741, *" Inverter, Converter, and Controllers for Use in Independent Power System"*

86. *"Amir reaffirms Kuwait moving to cut emissions – UN chief urges action at Qatar climate talks"*, Kuwait Times, 5 December 2012

87. P. Denholm and R. Margolis, *"Very Large-Scale Deployment of Grid-Connected Solar Photovoltaics in the United States: Challenges and Opportunities"*, NREL/CP-620-39683, July 8-13, 2006, Denver, Colorado

88. B. Stuart, *"The US Utility-Scale Photovoltaic Solar Landscape"*, PV magazine of photovoltaic markets & Technology, November 10, 2011, U.S. solar

89. J. Arrillaga and C. P. Arnold, *"Computer Modelling of Electrical Power Systems"*, New York, John wiley & Sons Ltd., p. 64, 1983

90. *"ERACS Technical Manual"*, ERA Technology Limited, Surrey, UK, 2004

91. Energy and Environmental Analysis, *"Technology Characterization: Gas Turbines"*, Environmental Protection Agency, Washington DC, 2008

92. B. M. Weedy, *"Electric Power Systems"*, UK: John Wiley & Sons Ltd., 1992

93. J. D. Glover, M. S. Sarma and T. J. Overbye, *"Power System Analysis and Design"*, Connecticut: Cengage Learing, 2008

94. A. Ellis, M. Behnke, C. Barker and S. N. Labs, *"PV system modelling for grid planning studies"*, in Photovoltaic Specialists Conference (PVSC), New Mexico, 2011

95. J. Wiles, *"Photovoltaic Power Systems and the National Electrical Code: Suggested Practices"*, New Mexico State University, New Mexico, 2001

Appendix A

1) Matlab code for Computing Solar Radiation on Horizontal Surfaces over Kuwait Area

```
%Matlab code for computing solar radiation on horizontal surfaces over
%Kuwait area

clear
L=29.33*pi/180;     %Latitude angle of Kuwait area in radian
i=0;
for n=1:365         %Day number
    i=i+1;

delta=23.45*sin(360*(n+284)/365*pi/180);  %Declination angle of the sun
delta=delta*pi/180;                        %in radian
H_SR=acos(-tan(L)*tan(delta));             %Sunrise or sunset hour angle
sin(peta)=cos(L)*cos(delta)*sin(H_SR)+(H_SR)*sin(L)*sin(delta);
                                %Solar altitude angle as a function of H_SR
S_ET(i)=(33048/pi)*(1+0.034*cos(360*n/365*pi/180))*sin(peta);
%Average daily extra-terrestrial solar insolation on horizontal
surfaces %in Wh/m^2
K_t(i)=-3.8071e-6*n^2+0.001124*n+0.6139;     %Clearness index
S_H(i)=K_t(i)* S_ET(i);    %Daily SR on horizontal surfaces over Kuwait area

end

 %title('Daily Horizontal Solar Radiation in Kuwait')
    n=1:365;
    plot(n,S_H,'LineWidth',2)
    v=[0 400 0 9000];
    axis(v);
    xlabel('Day Number')
    ylabel('Solar Radiation [Wh/seqm]')

grid
pause

     I_month(1)=mean(S_H(1:31));
     I_month(2)=mean(S_H(32:59));
     I_month(3)=mean(S_H(60:90));
     I_month(4)=mean(S_H(91:120));
     I_month(5)=mean(S_H(121:151));
     I_month(6)=mean(S_H(152:181));
     I_month(7)=mean(S_H(182:212));
     I_month(8)=mean(S_H(213:243));
     I_month(9)=mean(S_H(244:273));
     I_month(10)=mean(S_H(274:304));
     I_month(11)=mean(S_H(305:334));
     I_month(12)=mean(S_H(335:365));

%title('Monthly Average Horizontal Solar Radiation in Kuwait')
    nn=1:12;
    bar(nn,I_month,.6)
    v=[0 12 0 9000];
    axis(v);
    xlabel('Month')
    ylabel('Average Solar Radiation [Wh/seqm]')
grid
```

```
clear
    L=29.33*pi/180;
    i=0;
for n=1:365
    i=i+1;
    k=0
delta=23.45*sin(360*(n+284)/365*pi/180);
delta=delta*pi/180;
H_SR=acos(-tan(L)*tan(delta));

for t=6:18;
    k=k+1;
H=15*(t-12)*pi/180;   %Hour angle in radian as a function of solar time
sin(peta)=cos(L)*cos(delta)*cos(H)+sin(L)*sin(delta);
                      %Solar altitude angle as a function of H
S_ET(i,k)=(33048/pi)*(1+0.034*cos(360*n/365*pi/180))*sin(peta);
K_t(i)=-3.8071e-6*n^2+0.001124*n+0.6139;
S_H(i,k)=K_t(i)* S_ET(i); %Hourly SR on horizontal surfaces over Kuwait
                      %area
end

 %title('Hourly Horizontal Solar Radiation in Kuwait')

    n=1:365;
    plot(i,S_H)
    v=[0 365 0 1000];
    %axis(v);
    xlabel('Day Number')
    ylabel('Solar Radiation [Wh/seqm]')

grid
    S_H(1)=mean(S_H(1:31))
    S_H(2)=mean(S_H(32:59))

pause

%Computing daily and hourly SR for selected days of the year (to check)

clear
    L=29.33*pi/180;
    i=0;

    n=30; %Day Number
    k=0
delta=23.45*sin(360*(n+284)/365*pi/180);
delta=delta*pi/180;
H_SR=acos(-tan(L)*tan(delta));

for t=6:18;   %Solar time
    k=k+1;
H=15*(t-12)*pi/180;
sin(peta)=cos(L)*cos(delta)*cos(H)+sin(L)*sin(delta);
S_ET(i,k)=(33048/pi)*(1+0.034*cos(360*n/365*pi/180))*sin(peta);
K_t(i)=-3.8071e-6*n^2+0.001124*n+0.6139;
S_H(i,k)=K_t(i)* S_ET(k);

   end
   S_H11=S_H;

    n=185; %Day Number
    k=0
delta=23.45*sin(360*(n+284)/365*pi/180);
delta=delta*pi/180;
H_SR=acos(-tan(L)*tan(delta));
```

```
for t=6:18;    %Solar time
    k=k+1;
H=15*(t-12)*pi/180;
sin(peta)=cos(L)*cos(delta)*cos(H)+sin(L)*sin(delta);
S_ET(i,k)=(33048/pi)*(1+0.034*cos(360*n/365*pi/180))*sin(peta);
K_t(i)=-3.8071e-6*n^2+0.001124*n+0.6139;
S_H(i,k)=K_t(i)* S_ET(k);

   end
   S_H61=S_H;

    n=337; %Day Number
    k=0
delta=23.45*sin(360*(n+284)/365*pi/180);
delta=delta*pi/180;
H_SR=acos(-tan(L)*tan(delta));

for t=6:18;    %Solar time
    k=k+1;
H=15*(t-12)*pi/180;
sin(peta)=cos(L)*cos(delta)*cos(H)+sin(L)*sin(delta);
S_ET(i,k)=(33048/pi)*(1+0.034*cos(360*n/365*pi/180))*sin(peta);
K_t(i)=-3.8071e-6*n^2+0.001124*n+0.6139;
S_H(i,k)=K_t(i)* S_ET(k);

   end
   S_H111=S_H;

end

  t=6:18;
      plot(t,S_H11,'k','LineWidth',2)
      plot(t,S_H61,'r.-','LineWidth',2)
      plot(t,S_H111,'b--','LineWidth',2)
  xlabel('Day Hour')
  ylabel('Solar Radiation [Wh/seqm]')
  %title('Hourly Solar Radiation on June 15')
grid
  legend('January 30', 'June 30', 'November 30')
  v=[6 18 0 8000];
  axis(v)
pause

hold
```

2) SIMULINK code for Calculating and Plotting the *I-V* and *P-V* Characteristics of the Selected PV Module According to the Kuwait SR.

```
%Matlab code for Calculating and Plotting the I-V and V-P
%Characteristics of the Selected PV Module According to the Kuwait SR

clear
    pp=1;
    i=0;
    P1max=0.0;           %Initial conditions for the selected PV module
    P2max=0.0;
    P3max=0.0;
    P4max=0.0;
    P5max=0.0;

for v=0:0.001:0.833;     %Open-circuit voltage ranges for the PV cell
```

```
    i=i+1;
    I1(i)=-0.424e-6*exp(18.527*v)+2.17*pp;     %PV module photogenerated
                                               %current
    V1(i)=v;
if  I1(i) > 2.17;
       V1(i)=0;
       I1(i)=0;
    end

    P1(i)=V1(i)*I1(i);                    %Output power for the PV module
if  P1(i) >= P1max;
       P1max=P1(i);
       V1max=V1(i);
       I1max=I1(i);
    end

end

plot(V1,I1,'k','LineWidth',2.5), grid
hold
ylabel('Current [A]')
xlabel('Voltage [V]')

clear
    pp=0.75;
    i=0;
for v=0:0.001:0.833;
    i=i+1;
    I2(i)=-0.424e-6*exp(18.527*v)+2.17*pp;
    V2(i)=v;
if  I2(i) > 2.17;
       V2(i)=0;
       I2(i)=0;
    end

    P2(i)=V2(i)*I2(i);
if  P2(i) >= P2max;
       P2max=P2(i);
       V2max=V2(i);
       I2max=I2(i);
    end

end

plot(V2,I2,'r','LineWidth',2.5), grid
hold
ylabel('Current [A]')
xlabel('Voltage [V]')

clear
    pp=0.5;
    i=0;
for v=0:0.001:0.833;
    i=i+1;
    I3(i)=-0.424e-6*exp(18.527*v)+2.17*pp;
    V3(i)=v;
if  I3(i) > 2.17;
       V3(i)=0;
       I3(i)=0;
    end

    P3(i)=V3(i)*I3(i);
if  P3(i) >= P3max;
       P3max=P3(i);
       V3max=V3(i);
```

```
        I3max=I3(i);
    end

end

plot(V3,I3,'b','LineWidth',2.5), grid
hold
ylabel('Current [A]')
xlabel('Voltage [V]')

clear
    pp=0.25;
    i=0;
for v=0:0.001:0.833;
    i=i+1;
    I4(i)=-0.424e-6*exp(18.527*v)+2.17*pp;
    V4(i)=v;
if  I4(i) > 2.17;
        V4(i)=0;
        I4(i)=0;
    end

    P4(i)=V4(i)*I4(i);
if  P4(i) >= P4max;
        P4max=P4(i);
        V4max=V4(i);
        I4max=I4(i);
    end

end

plot(V4,I4,'b','LineWidth',2.5), grid
hold
ylabel('Current [A]')
xlabel('Voltage [V]')

clear
    pp=0.1;
    i=0;
for v=0:0.001:0.833;
    i=i+1;
    I5(i)=-0.424e-6*exp(18.527*v)+2.17*pp;
    V5(i)=v;
if  I5(i) > 2.17;
        V5(i)=0;
        I5(i)=0;
    end

    P5(i)=V5(i)*I5(i);
if  P5(i) >= P5max;
        P5max=P5(i);
        V5max=V5(i);
        I5max=I5(i);
    end

end

plot(V5,I5,'b','LineWidth',2.5), grid
hold
ylabel('Current [A]')
xlabel('Voltage [V]')

plot(V1max, I1max,'k*','LineWidth',3.5)
plot(V2max, I2max,'r*','LineWidth',3.5)
plot(V3max, I3max,'b*','LineWidth',3.5)
```

```
plot(V4max, I4max,'g*','LineWidth',3.5)
plot(V5max, I5max,'m*','LineWidth',3.5)

text(12,3.351,'pp=1.0')          %Outputs of the PV module according to
                                 %Kuwait SR
text(12,2.667,'pp=0.75')
text(12,1.752,'pp=0.5')
text(12,0.925,'pp=0.25')
text(12,0.433,'pp=0.1')
x=[0 1 0 3];
axis(x)

hold

pause
plot(V1,P1,'k','LineWidth',2.5), grid
hold

plot(V2,P2,'r','LineWidth',2.5)
plot(V3,P3,'b','LineWidth',2.5)
plot(V4,P4,'b','LineWidth',2.5)
plot(V5,P5,'m','LineWidth',2.5)
plot(V1max, P1max,'k*','LineWidth',3.5)
plot(V2max, P2max,'r*','LineWidth',3.5)
plot(V3max, P3max,'b*','LineWidth',3.5)
plot(V4max, P4max,'g*','LineWidth',3.5)
plot(V5max, P5max,'m*','LineWidth',3.5)

text(16,53,'pp=1.0')
text(16,39,'pp=0.75')
text(16,25,'pp=0.5')
text(16,12,'pp=0.25')
text(16,4,'pp=0.1')

ylabel('Power [W]')
xlabel('Voltage [V]')
x=[0 1 0 2];
axis(x)

pause

hold
```

Appendix B

Table B1: Important Characteristics of Several High-Power PV Modules [Source: http://www.greenpeace.org/international/en/Guide-to-Greener-Electronics/18th-Edition/]

Module	Shell SP150	Kyocera KC158G	Sharp SKK-300	Sharp NE-K125U2	Uni-Solar SSR256
Material	Mono-crystal	Multi-crystal	Mono-crystal	Poly-crystal	Triple junction a-Si
Rated power P_{dc}, STC (W)	150	158	300	125	256
Voltage at max. power (V)	34	23.2	50.6	26.0	66.0
Current at max. power (A)	4.40	6.82	5.9	4.80	3.9
Open-circuit voltage, E_{oc} (V)	43.4	28.9	63.2	32.3	95.2
Short-circuit current, I_{sc} (A)	4.8	7.58	6.5	5.46	4.8
Length (m)	1.619	1.290	1.892	1.190	11.124
Width (m)	0.814	0.990	1.283	0.792	0.420
Efficiency (%)	11.4	12.4	16.8	13.3	5.5

Table B2: Inverters Bank Characteristics for Grid-Connected Systems [Source: http://www.greenpeace.org/international/en/Guide-to-Greener-Electronics/18th-Edition/]

Manufacturer	Xantrex	Sunny Boy	Xantrex	Xantrex	Sunny Boy
Model	PV 10	SB20000	STXR-25000	STXR-15000	SB25000
AC power (W)	10000	20000	25000	15000	25000
AC voltage (V)	2080, 3φ	1980-2510	2110-2640	2110-2640	1900-2800
PV voltage range at max. power (V)	3300-6000	1250-2550	440-850	440-850	2500-3000
Max. input voltage (V)	6000	2550	1200	1200	3000
Max. input current (A)	319	150	-	-	250
Maximum efficiency (%)	95	96	94	92	94
Inverter price ($/W)	2.3	2.1	2.5	2	3.5

Appendix C

Matlabe/Simulink code for Calculating and Plotting the *I-V* and *P-V* characteristics of one proposed PV string.

```
clear
pp=1;
i=0;
P1max=0.0;
P2max=0.0;
P3max=0.0;
P4max=0.0;
P5max=0.0;
ns_m=72;  % No of series cells per module
np_m=3;

ns_p=43  % No of series modules per panel;
np_p=42 % No of parallel modules per panel;


for v=0:.01:0.833*ns_m;
    i=i+1;
    I1(i)=-0.424e-6*np_m*exp(18.527*v/ns_m)+2.17*pp*np_m;
    V1(i)=v;
    if I1(i) > 2.17*np_m;
       V1(i)=0;
       I1(i)=0;
    end

    P1(i)=V1(i)*I1(i);
    if P1(i) >= P1max;
       P1max=P1(i);
       V1max=V1(i);
       I1max=I1(i);
    end

end

V1=V1*ns_p;
I1=I1*np_p;
P1=P1*ns_p*np_p;
P1max=P1max*ns_p*np_p;
V1max=V1max*ns_p;
I1max=I1max*np_p;

plot(V1,I1,'k','LineWidth',2.5), grid
hold
ylabel('Current [A]')
xlabel('Voltage [V]')
pause

plot(V1,P1,'k','LineWidth',2.5), grid
ylabel('Power [W]')
xlabel('Voltage [V]')
```

Appendix D

Summary of Matlab code of *SAIMA*

```
%Summary of Matlab code of SAIMA for sizing the proposed GCPV system

clear
P_PV=energy*S_S/(365*S_H*EFF_conv); % DC output power of the proposed PV array
energy=200e+9;
S_S=1000;
S_H=j;
EFF_conv=0.97;
k=0;
i=k+1;
m=k+1;
    for X(i,k) from X(1,k) to X(5,k)

end_for

    for X1=150,34,4.40,43.4,4.8,1.619,0.814,11.40, %PV module (1)
  PV1 := X1;
 end
    for X2=158,23.2,6.82,28.9,7.58,1.290,0.990,12.4, %PV module (2)
   PV2 := X2;
 end
    for X3=300,50.6,5.9,63.2,6.5,1.892,1.283,16.8, %PV module (3)
   PV3 := X3;
 end
    for X4=125,26.0,4.80,32.3,5.46,1.190,0.792,13.3, %PV module (4)
   PV4 := X4;
 end
    for X5=256,66.0,3.9,95.2,4.8,11.124,0.420,5.5, %PV module (5)
   PV5 := X5;
 end

     prompt = ' What is the selected PV module type? ';
     result = input(prompt);
find(X,i,k,first)

    for [X(i,k),Y(m,k)] from [X(1,k),Y(1,k)] to [X(5,k),Y(5,k)]

end_for

    for Y1=10000,2080,3300,6000,319,95, %Inverter(1)
   inv1 := Y1;
 end
    for Y2=20000,2510,1250,2550,150,96, %Inverter(2)
   inv2 := Y2;
 end
    for Y3=25000,2640,440,1200,200,94, %Inverter(3)
   inv3 := Y3;
 end
    for Y4=15000,2640,440,1200,200,92, %Inverter(4)
   inv4 := Y4;
 end
    for Y5=25000,2800,2500,3000,250,94, %Inverter(5)
   inv5 := Y5;
 end

     prompt = ' What is the selected inverter type? ';
     result = input(prompt);
find(Y,m,k,first)
disp(type,((i,k),(m,k))
fprintf('%i\n',(X(i,k),Y(m,k))
```

```
clear
f_o=0.2;
q=(i,m);                    % Type of PV module and inverter combination
E_sys=200e+9;
P_PVE=100e+6;             % Estimated output power of the proposed PV array
E_PV(max)(q)=E_stc(max)(q)*[1-(T_Emax(q)*(t_cmin(q)-t_STC))];% Maximum voltage at
                                                  % maximum power of the PV module
E_PV(min)(q)=E_stc(max)(q)*[1-(T_Emax(q)*(t_cmax(q)-t_STC))];% Minimum voltage at
                                                  % maximum power of the PV module
E_PV(min)_f(q)=0.925*E_PV(min)(q); % Final minimum voltage at maximum power
                                   % of the PV module
E_inv(max)_ad(q)  =EFF_inv(q)*E_inv(max)(q);      % Maximum input voltage of the
                                                   % inverter
E_inv(min)_ad(q)  =(EFF_inv(q)+EFF_Edrop)*E_inv(min)(q);    % Minimum input voltage
                                                    % of the inverter
        if (E_PV(max)(q)>E_inv(min)_ad(q))
        elseif (E_PV(max)(q)<E_inv(max)_ad(q))
goto(9,10)
return
     else
         n_p(i)=I_inv(q)/[(1+f_o)*I_SC(q)];      % Maximum number of parallel
                                                  % strings
         n_s(mp)(q)=E_inv(max)_ad(q)/E_PV(max)(q);
         n_s(oc)(q)=E_inv(max)_ad(q)/E_OC(max)(q);
         n_s(min)(q)=E_inv(min)_ad(q)/E_PV(min)_f(q);   % Minimum number of PV
                                                        % modules per string
         Z(q)=round(n_s(mp)(q),0) ;
         Z1(q)=round(n_s(oc)(q),0) ;
         P(q)=round(n_s(min)(q),0) ;

     end
end

       if (Z(q)<Z1(q))
          n_s(max)(q)=Z(q);     % Maximum number of PV modules per string
       else if (Z(q)>Z1(q))
          n_s(max)(q)=Z1(q);
     end

end

for n_t(cal)(q)= n_p(q)*n_s(q);      % Calculated total number of PV modules
    n_t(exp)=P_PVE/P_PV ;              % Expected total number of PV modules
    I_cal(q)=n_p(q)*I_sc(q);         % Maximum calculated current of the array
    E_cal(q)=n_s(q)*E_oc(max)(q);   % Maximum calculated voltage of the array

      if (n_t(cal)(q)<n_t(exp))
goto(9,10)
return
      else
          I_cal(q)=n_p(q)*I_sc(q);
          E_cal(q)=n_s(q)*E_oc(max)(q);
      end

      if (E_cal(q)>E_sys)
        elseif (I_cal(q)>I_inv(q))
goto(9,10)
return
       else
           P_PVact=n_t(cal)*P_PVmaxp ;                    % for one panel
           Sf=P_PVact/P_inv ;
           Panels=P_PV/P_PVact;        % Total number of panels in the array
           Per_inv(q)=Sf*Ym ;
```

```
            A_panel=n_t(cal)*A_m(q);
        end

    end

for j=3.19:4.39:5.77:6.81:7.68:7.94:7.58:7.11:6.09:4.84:3.46:2.82,
                                                              %Total SR
    j
  S_H:=j;
        for j from 3.19 to 2.82
 end_for
            energy_exp=P_PVact*EFF_conv*365*j/S_S ;              % for one panel
end

disp(n_s(min)(q),n_p(q),Array,(P_PVact*Panels),(Sf*Panels),(energy_exp*Panels)
, A_panel)

    v=[0 100 0 100];
    axis(v);
    plot(Per_inv(q),Sf,'LineWidth',20) ;
    xlabel('Percentage of inverter rated power%') ;
    ylabel('Sizing factor %') ;

grid
  legend('Type (q) combination )
  v=[0 100 0 100];
  axis(v);

pause

hold
```

Appendix E

1) Program Code (C Program) used for Optimal Generator Configuration

This program was used to calculate the optimal generator configuration for the power flow and fault studies.

```
#include<stdio.h>

#include <stdlib.h>


main()

{

int         i,j,k=0;                        /*counters*/

int         pwrcnt;                         /*counter for different output powers*/

int         gnumber=9;                      /*number of generators*/

float       pwrout=0;                       /*total power output of generators per iteration*/

float       pwrin=0;                        /*total power input of generators per iteration*/

float   effpin;       /*total input power for the most efficient configuration of a given output power*/

float rating[9]={8.7296, 8.7296, 8.7296, 8.7296, 8.7296, 16.4848, 16.4848, 16.4848, 20.604};
                                            /*generator  power ratings*/

float       in[9]={0};                      /*generator input powers*/

float       out[9]={0};                     /*power output of each individual generator*/

float       relout[9];                      /*relative power output of each individual generator*/

float results[9];                           /*individual generator input power for the most efficient
                                            configuration of a given output power*/

float       reserve[9];

float       spinr=0;


for (pwrcnt=170; pwrcnt<171; pwrcnt++)

{

            effpin=512;                     /*sets the efficiency at an arbitrary high value to start*/

            while(1)            /*loop to run through all of the possible power outputs*/

            {
```

```
                for (i=0; i<=rating[k]; i++)
                {
                        for (j=0; j<gnumber; j++)
pwrout=pwrout+out[j];   /*adds output of each generator and saves sum as pwrout*/


if (pwrcnt==pwrout)     /*if the output power matches the power level for this iteration*/
                        {
                                for (j=0; j<gnumber; j++) /* computes the relative power*/
                                {
                                        relout[j] = out[j]/rating[j];
                                        printf("  %.f  ", out[j]);
                                }
                                for (j=0; j<gnumber; j++) /* computes the relative input power*/
                                {
        in[j] = out[j]/(0.94*(relout[j]*relout[j]*relout[j])-
       2.49*(relout[j]*relout[j])+2.53*relout[j]+0.02);
pwrin=pwrin+in[j];      /*adds input of each generator and saves sum as pwrin*/
                                }
                                printf (" ++%.f++ \n", pwrin);


if (pwrin < effpin)     /*if this iteration is more efficient than the previous (most efficient) iterations
(effpin)...*/
                                {
for (j=0; j<gnumber; j++)  /*save the generator configuration as results*/
                                {
                                        if (out[j]==0)
                                                reserve[j]=0;
                                                else reserve[j]= rating[j] - out[j];
                                        spinr= spinr+reserve[j];
                                }
                                if (spinr>=20.604)
                                {
```

```
for (j=0; j<gnumber; j++)              /*save the generator configuration as results*/
                                                    results[j] = out[j];
                                              effpin = pwrin;     /*save the total output power as effpin*/
                                        }
                              }
                    }
                    spinr=0;
                    pwrout=0;
                    pwrin=0;
                    out[k]++;

                    if (out[0] > rating[0]*.9)     /*moves count on to next significant digit*/
                    {
                              out[0]=0;
                              out[1]++;
                              for (j=1; j<gnumber; j++)
                              {
                                        if (out[j] > rating[j]*.9)
                                        {
                                                  out[j]=0;
                                                  out[j+1]++;
                                        }
                              }
                    }
          }
          if (out[0]==0 && out[1]==0 && out[2]==0 && out[3]==0 && out[4]==0 && out[5]==0 &&
          out[6]==0 && out[7]==0 && out[8]==0) /*stops the loop when all of the possible power levels
          have been tested*/
                    break;
}
for (j=0; j<gnumber; j++)          /*prints the most efficient power configuration and total relative input
                                                    power for this power level*/
{
```

```
            printf("%.f   ", results[j] );
}
             printf("  --pwrin for %i = %f--\n",pwrcnt, effpin);
}
}
```

2) Program Code (*Visual Basic for Applications* (VBA) Program) used for Extracting Specific Data

This program was used to extract specific data from all of the power flow studies. It would take a value from a specific cell in each of the study results files and save it to a different spreadsheet. The program was slightly altered depending on the data that needed to be extracted.

```
Sub GetRecords()

ans = MsgBox("Update Records?  This may take several minutes", vbQuestion + vbYesNo,
"Record Refresh")                                    'message box to confirm if user wants to start update

If ans = vbNo Then GoTo mend                         'exit if answer is no


Dim Path As String          'file name of results file

Dim Col As Integer          'column that selected record will be copied to

Dim Ro As Integer           'row that selected record will be copied to


Sheets("Sheet3").Select

   Col = 2

   Ro = 2


tPath = Workbooks(ThisWorkbook.Name).Worksheets("Sheet2").Range("G6")

pos = InStrRev(tPath, "\", -1)

cPath = Left(tPath, pos)

Path$ = cPath

Select Case Right$(Path$, 1)

    Case "\":   filename1$ = Dir(Path$)

    Case Else:  filename1$ = Dir(Path$ & "\")

 End Select
```

```
' Loop through the specified directory and
' copy data  from .csv files to this workbook

    Do While Len(filename1$) > 0
    If InStr(1, filename1$, ".csv", 1) > 0 And filename1$ <> (ThisWorkbook.Name) Then

    Workbooks.Open (Path$ & filename1$)
    Range("I33:I33").Select
    Selection.Copy
    ThisWorkbook.Activate
    Cells(Ro, Col).Activate
    ThisWorkbook.ActiveSheet.Paste
    Workbooks(filename1$).Close

    If (Col > 34) Then
       Ro = Ro + 1
       Col = 2
    Else: Col = Col + 1
    End If
    End If
    filename1$ = Dir()
    Loop
mend:
End Sub
```

Appendix F

1) Generator Efficiency Curve

Generator efficiency curve adapted from Fig. 5.1 and used to calculate the gas turbine relative input power (source: T.S. Kim [5]).

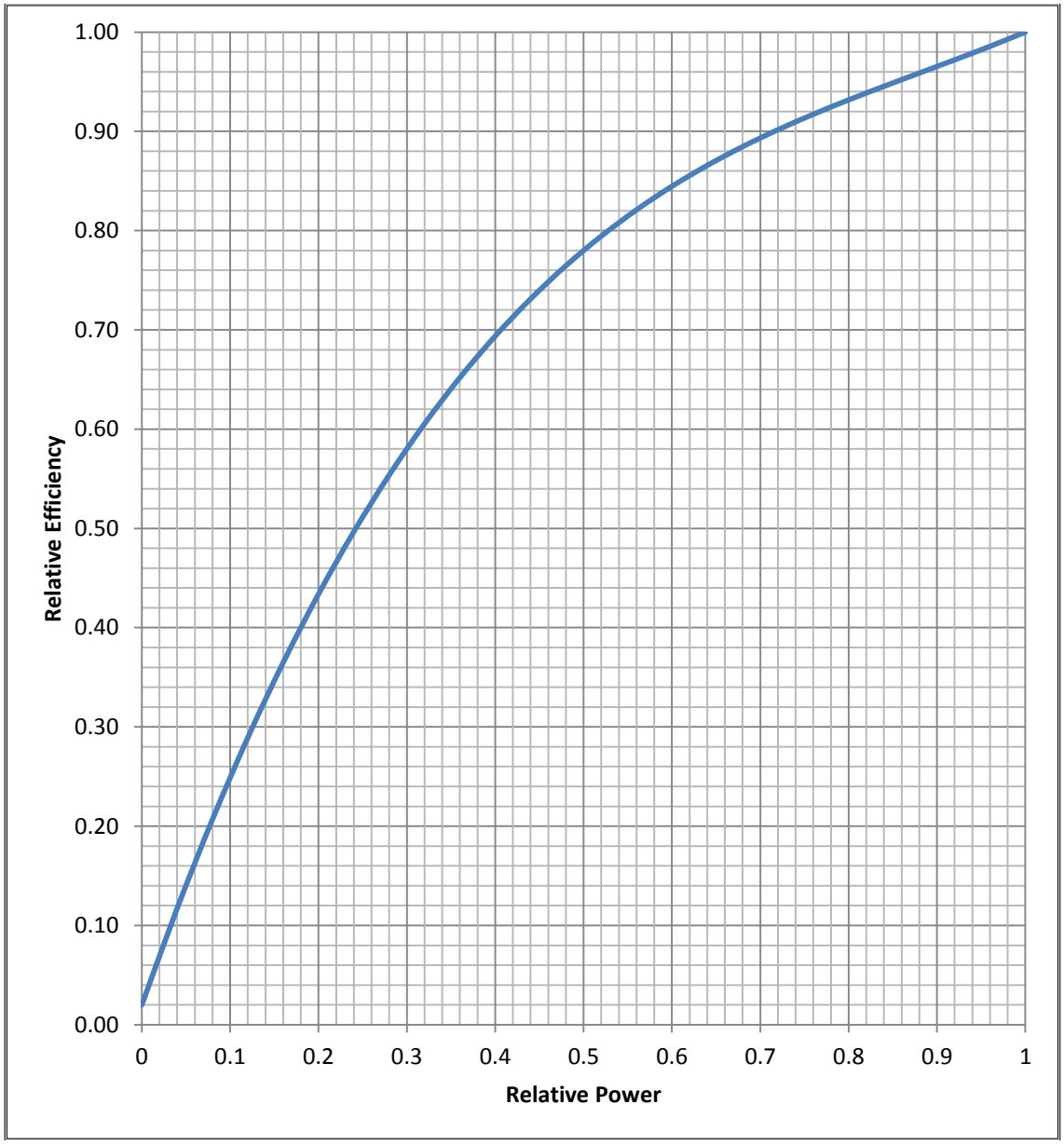

2) Power Outputs used in Studies

a. Without PV Connected

Hour	Generator (MW)												
	1	2	3	4	5	6	7	8	9	10	11	12	13
0	8	6	6	8	6	12	11	11	0	19.6	19.6	19.6	19.6
1	6	6	0	0	0	11	11	11	19	19.6	19.6	19.6	19.6
2	6	6	6	6	6	11	0	0	19	19.6	19.6	19.6	19.6
3	6	0	0	0	0	11	11	11	19	19.6	19.6	19.6	19.6
4	8	8	6	6	0	12	11	11	0	19.6	19.6	19.6	19.6
5	8	6	6	8	6	12	11	11	0	19.6	19.6	19.6	19.6
6	8	8	6	0	0	11	11	11	19	19.6	19.6	19.6	19.6
7	8	6	6	6	0	11	11	11	19	19.6	19.6	19.6	19.6
8	8	8	6	6	0	12	11	11	19	19.6	19.6	19.6	19.6
9	8	8	6	8	0	12	11	11	19	19.6	19.6	19.6	19.6
10	8	6	6	6	6	12	11	11	19	19.6	19.6	19.6	19.6
11	8	8	8	8	6	11	11	11	19	19.6	19.6	19.6	19.6
12	8	8	8	8	8	11	11	11	19	19.6	19.6	19.6	19.6
13	8	8	8	8	8	11	11	11	19	19.6	19.6	19.6	19.6
14	8	8	8	8	8	11	11	11	19	19.6	19.6	19.6	19.6
15	8	8	8	8	8	11	11	11	19	19.6	19.6	19.6	19.6
16	8	8	6	8	6	12	11	11	19	19.6	19.6	19.6	19.6
17	8	8	6	8	0	12	11	11	19	19.6	19.6	19.6	19.6
18	8	6	6	6	0	12	11	11	19	19.6	19.6	19.6	19.6
19	8	8	6	0	0	11	11	11	19	19.6	19.6	19.6	19.6
20	8	8	8	8	6	12	11	11	0	19.6	19.6	19.6	19.6
21	8	8	8	8	6	12	11	11	0	19.6	19.6	19.6	19.6
22	8	8	8	6	6	11	11	11	0	19.6	19.6	19.6	19.6
23	8	8	8	6	6	11	11	11	0	19.6	19.6	19.6	19.6

b. With PV Connected

Hour	Generator (MW)													PV System (MW)
	1	2	3	4	5	6	7	8	9	10	11	12	13	
0	8	6	6	8	6	12	11	11	0	19.6	19.6	19.6	19.6	0.0
1	6	6	0	0	0	11	11	11	19	19.6	19.6	19.6	19.6	0.0
2	6	6	6	6	6	11	0	0	19	19.6	19.6	19.6	19.6	0.0
3	6	0	0	0	0	11	11	11	19	19.6	19.6	19.6	19.6	0.0
4	8	8	6	6	0	12	11	11	0	19.6	19.6	19.6	19.6	0.1
5	6	6	6	0	0	11	11	0	19	19.6	19.6	19.6	19.6	8.3
6	8	6	0	0	0	11	11	0	14	19.6	19.6	19.6	19.6	24.0
7	6	6	6	0	0	10	10	0	0	19.6	19.6	19.6	19.6	39.6
8	0	0	0	0	0	9	9	9	0	19.6	19.6	19.6	19.6	53.7
9	0	0	0	0	0	7	0	0	8	19.6	19.6	19.6	19.6	67.4
10	6	0	0	0	0	0	0	0	1	19.6	19.6	19.6	19.6	77.5
11	2	0	0	0	0	0	0	0	6	19.6	19.6	19.6	19.6	81.5
12	0	0	0	0	0	8	1	0	0	19.6	19.6	19.6	19.6	82.6
13	4	0	0	0	0	7	7	0	0	19.6	19.6	19.6	19.6	74.1
14	5	5	0	0	0	10	9	0	0	19.6	19.6	19.6	19.6	63.1
15	6	6	6	0	0	11	0	0	13	19.6	19.6	19.6	19.6	50.1
16	8	8	6	0	0	11	11	11	0	19.6	19.6	19.6	19.6	33.9
17	6	6	0	0	0	12	11	11	19	19.6	19.6	19.6	19.6	17.7
18	8	8	6	0	0	12	11	11	19	19.6	19.6	19.6	19.6	3.5
19	8	8	6	0	0	11	11	11	19	19.6	19.6	19.6	19.6	0.0
20	8	8	8	8	6	12	11	11	0	19.6	19.6	19.6	19.6	0.0
21	8	8	8	8	6	12	11	11	0	19.6	19.6	19.6	19.6	0.0
22	8	8	8	6	6	11	11	11	0	19.6	19.6	19.6	19.6	0.0
23	8	8	8	6	6	11	11	11	0	19.6	19.6	19.6	19.6	0.0

3) Load Flow Data

Each data point on the scatter diagrams represents the condition of the component in question at a specific time when the network is in a specific configuration.

a. No PV System Connected

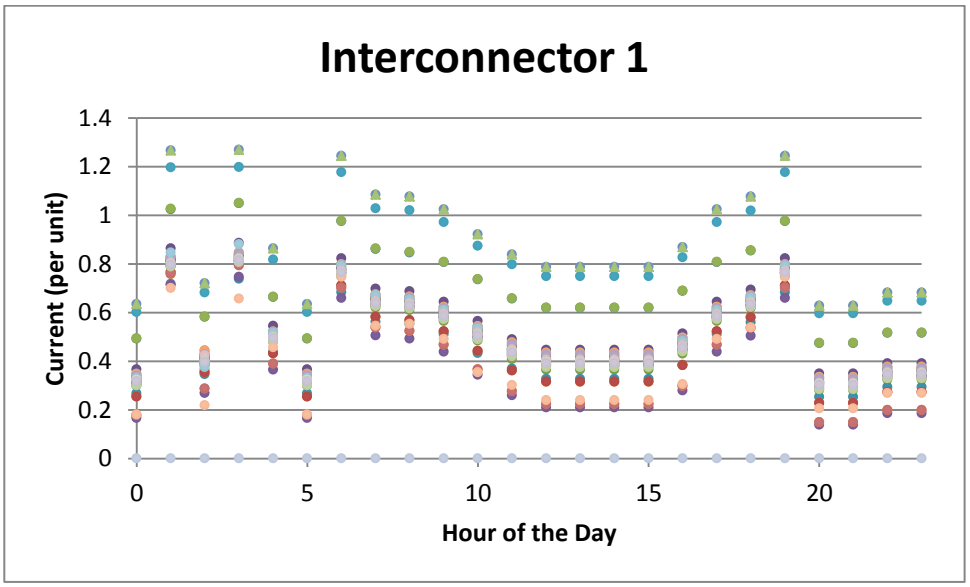

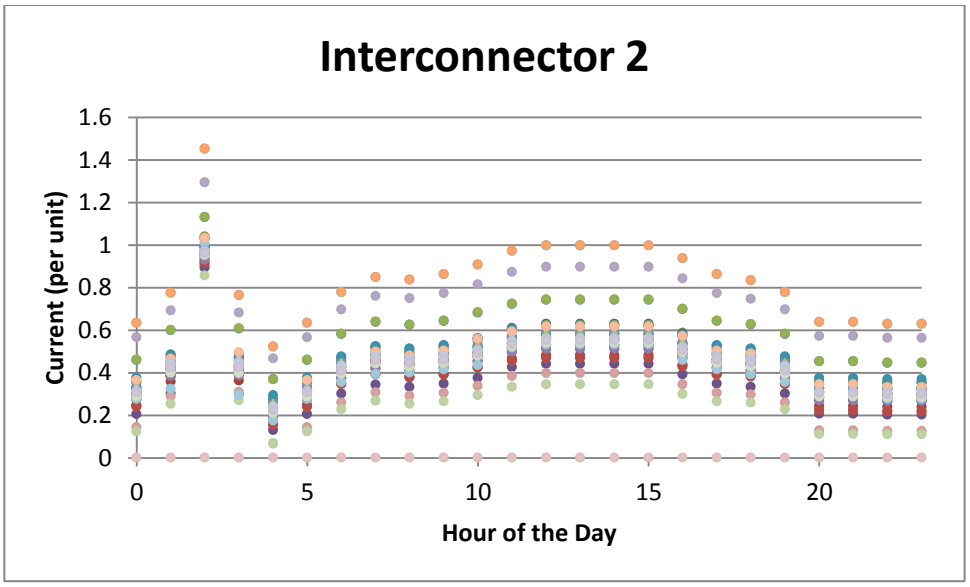

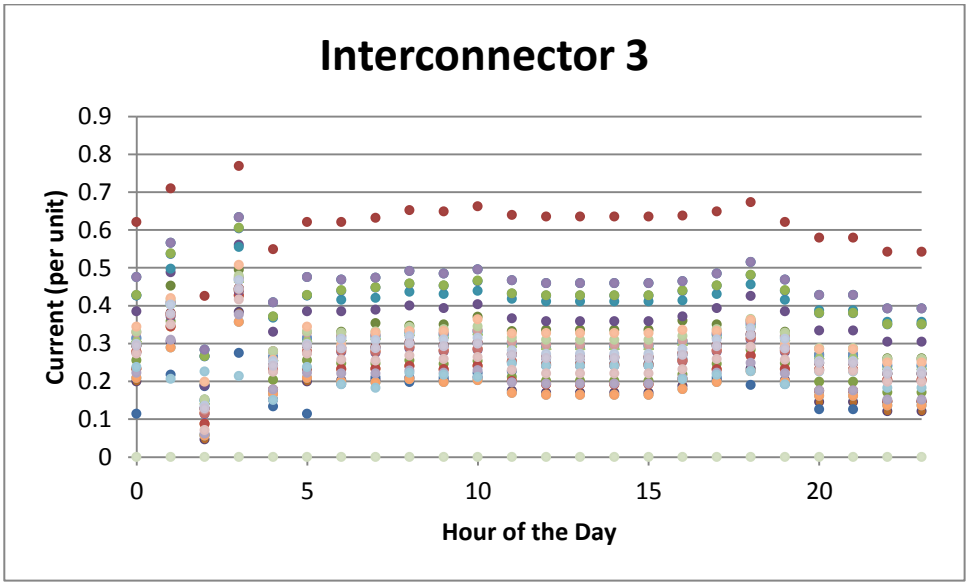
Interconnector 3
Current (per unit)
0.9
0.8
0.7
0.6
0.5
0.4
0.3
0.2
0.1
0
0
5
10
15
20
Hour of the Day

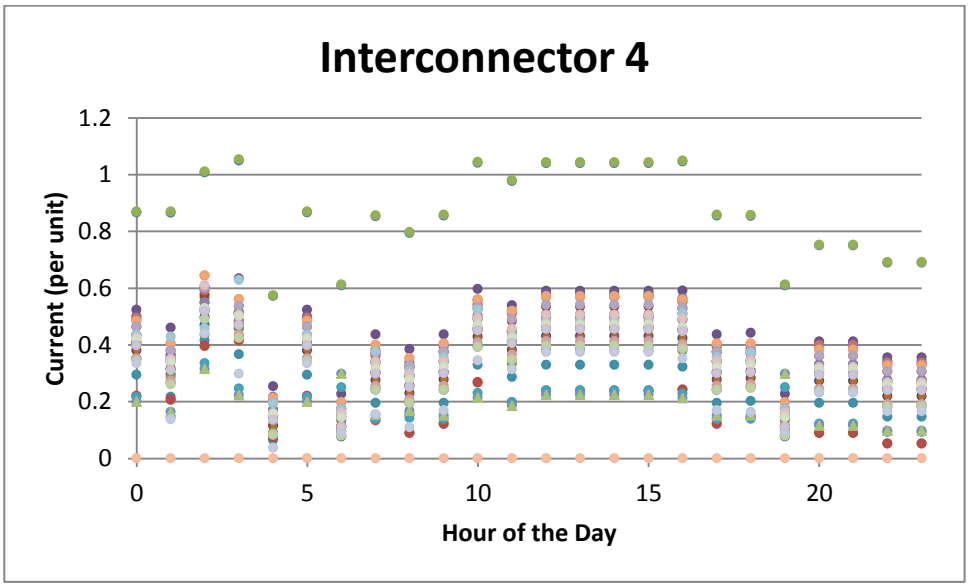
Interconnector 4
Current (per unit)
1.2
1
0.8
0.6
0.4
0.2
0
0
5
10
15
20
Hour of the Day

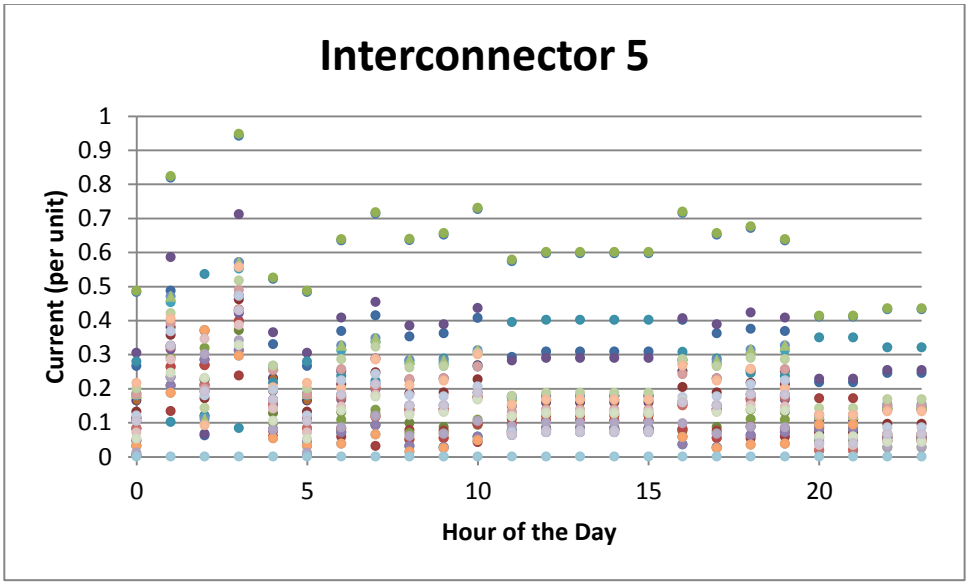
Interconnector 5
Current (per unit)
1
0.9
0.8
0.7
0.6
0.5
0.4
0.3
0.2
0.1
0
0
5
10
15
20
Hour of the Day

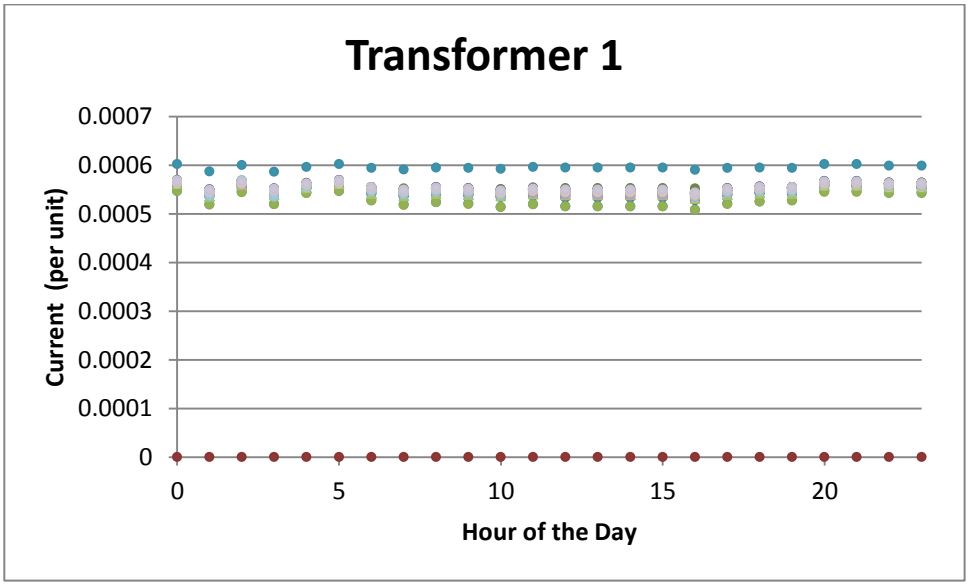
Transformer 1
Current (per unit)
0.0007
0.0006
0.0005
0.0004
0.0003
0.0002
0.0001
0
0
5
10
15
20
Hour of the Day

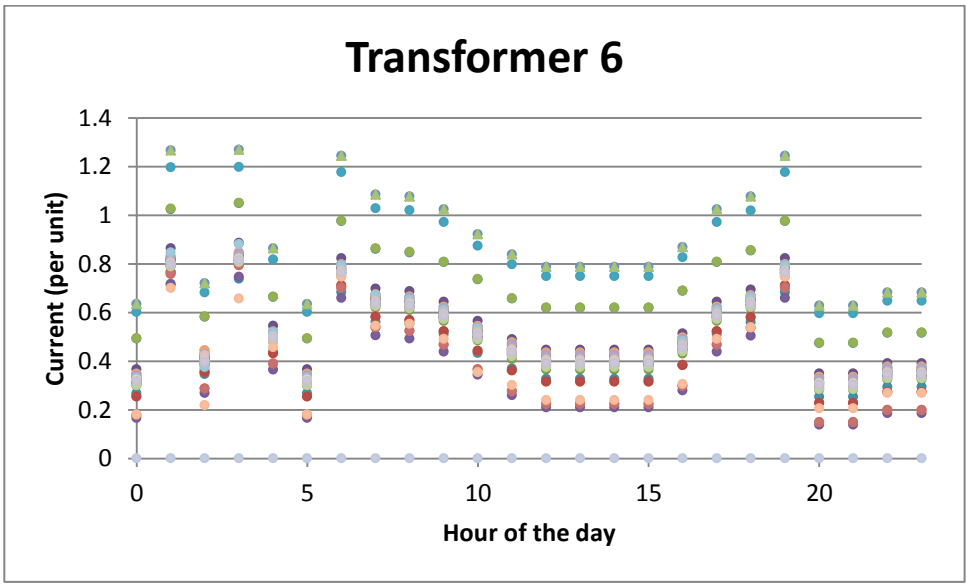
Transformer 6
Current (per unit)
1.4
1.2
1
0.8
0.6
0.4
0.2
0
0
5
10
15
20
Hour of the day

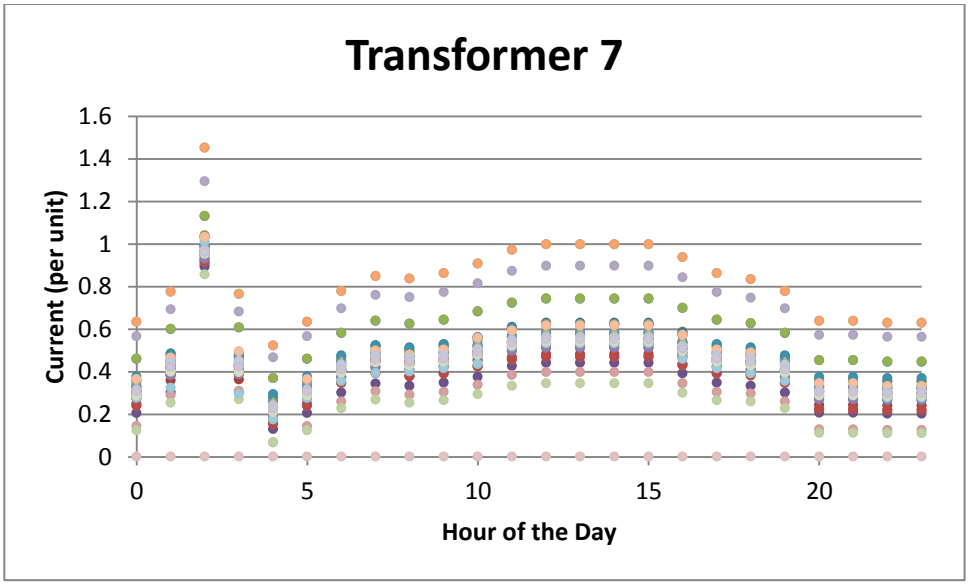
Transformer 7
Current (per unit)
1.6
1.4
1.2
1
0.8
0.6
0.4
0.2
0
0
5
10
15
20
Hour of the Day

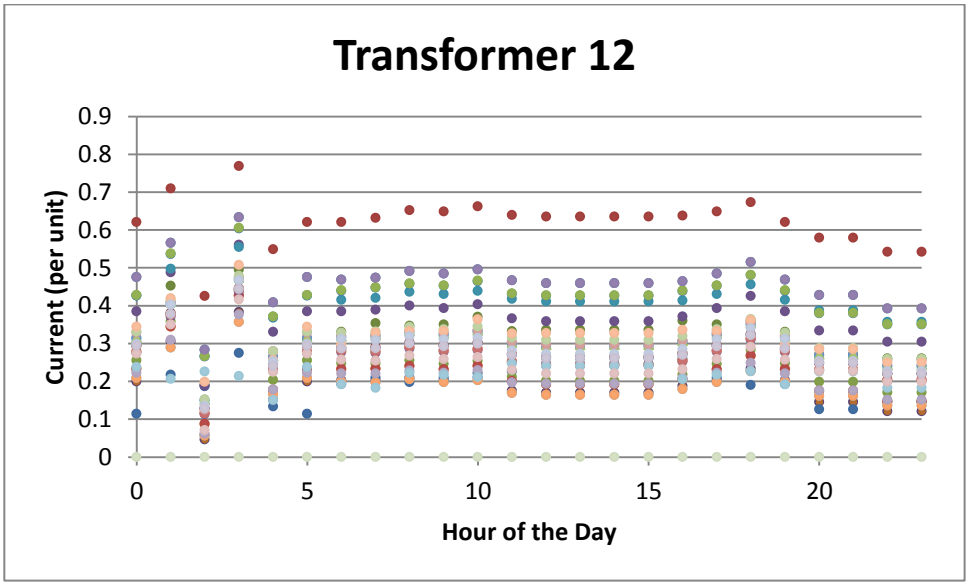
Transformer 12
Current (per unit)
0.9
0.8
0.7
0.6
0.5
0.4
0.3
0.2
0.1
0
0
5
10
15
20
Hour of the Day

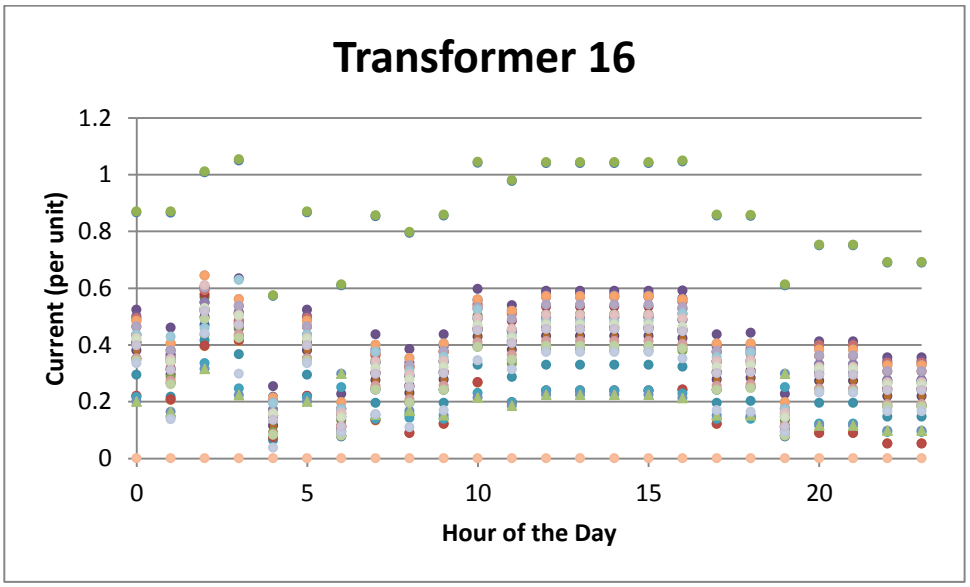
Transformer 16
Current (per unit)
1.2
1
0.8
0.6
0.4
0.2
0
0
5
10
15
20
Hour of the Day

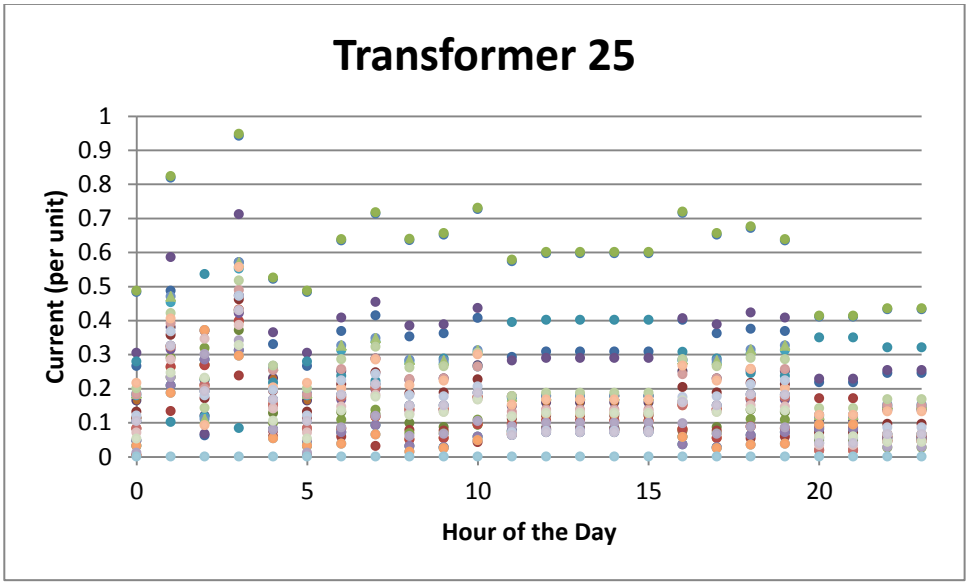
Transformer 25
Current (per unit)
1
0.9
0.8
0.7
0.6
0.5
0.4
0.3
0.2
0.1
0
0
5
10
15
20
Hour of the Day

b. PV System Connected at Location A

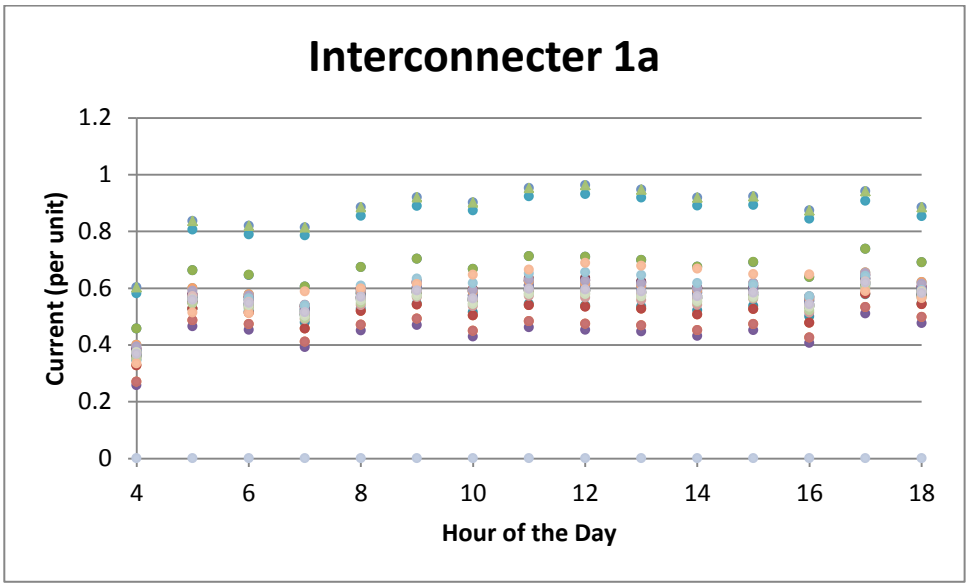

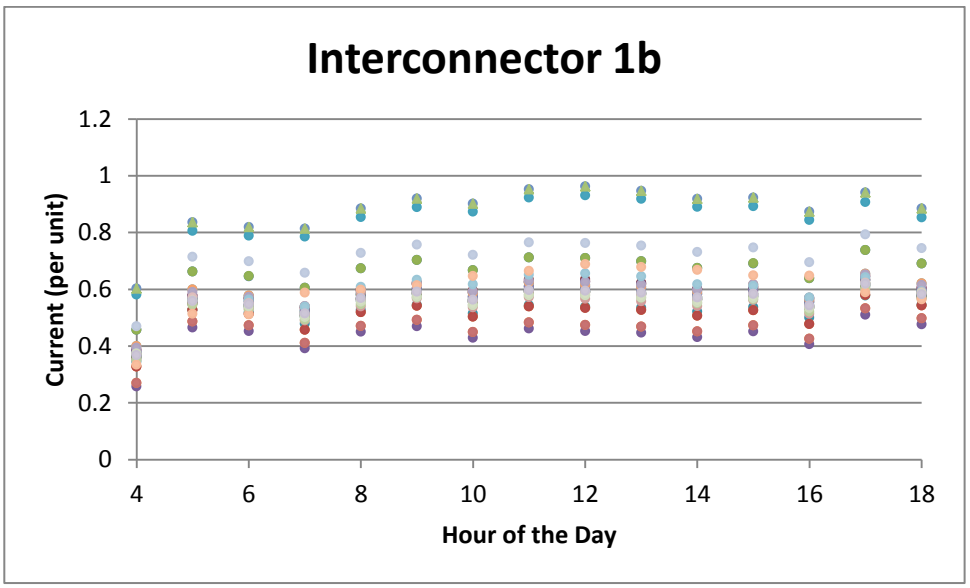

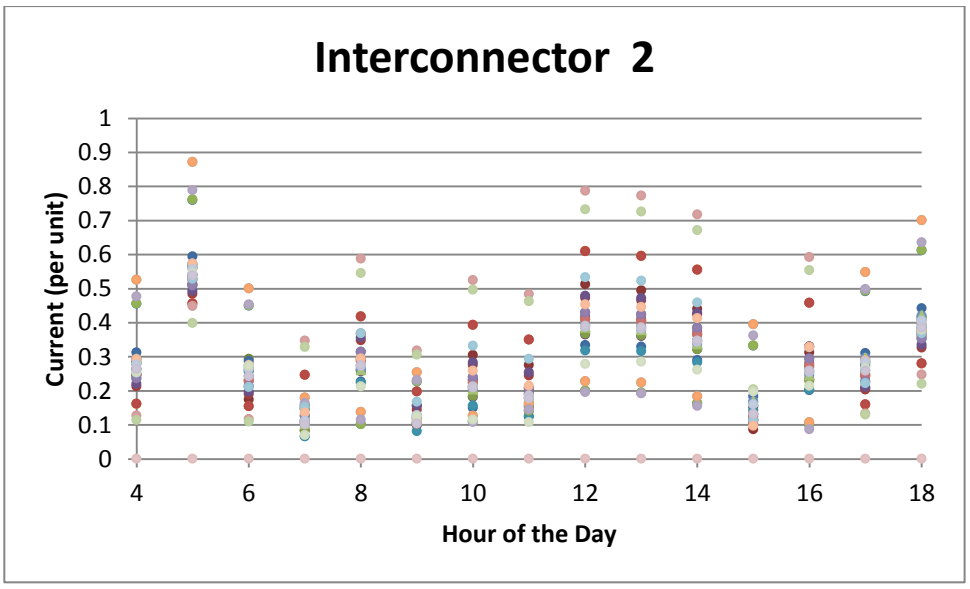

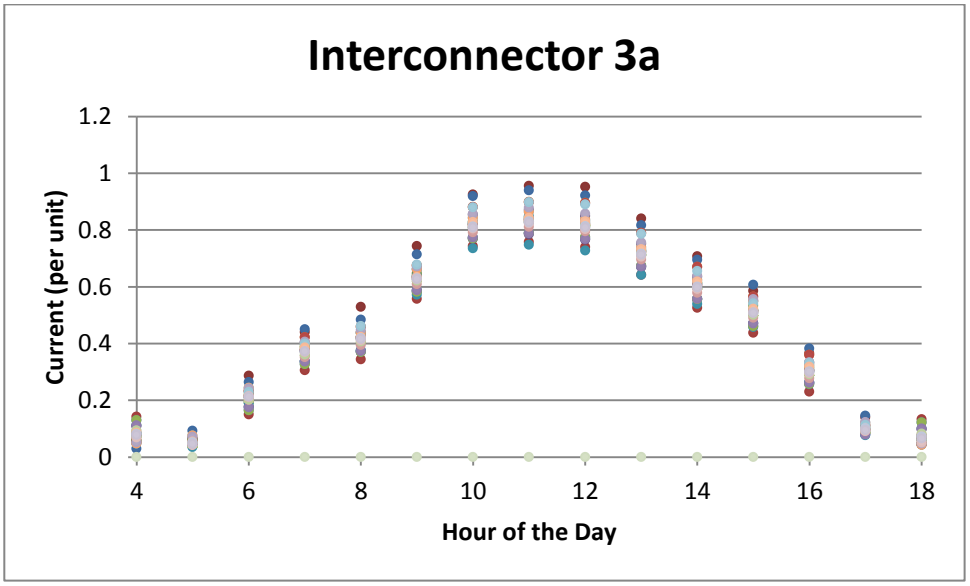
Interconnector 3a
Current (per unit)
1.2
1
0.8
0.6
0.4
0.2
0
4
6
8
10
12
14
16
18
Hour of the Day

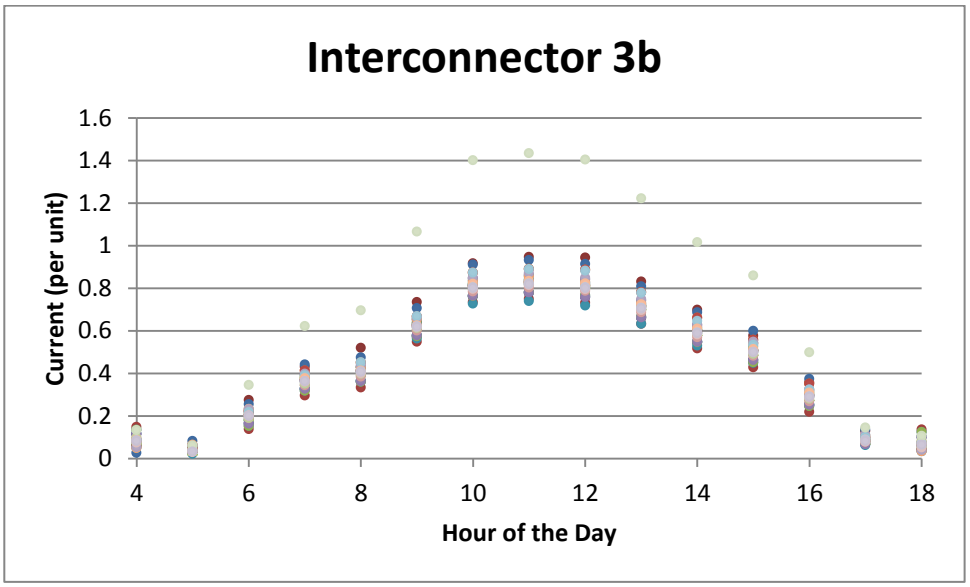
Interconnector 3b
Current (per unit)
1.6
1.4
1.2
1
0.8
0.6
0.4
0.2
0
4
6
8
10
12
14
16
18
Hour of the Day

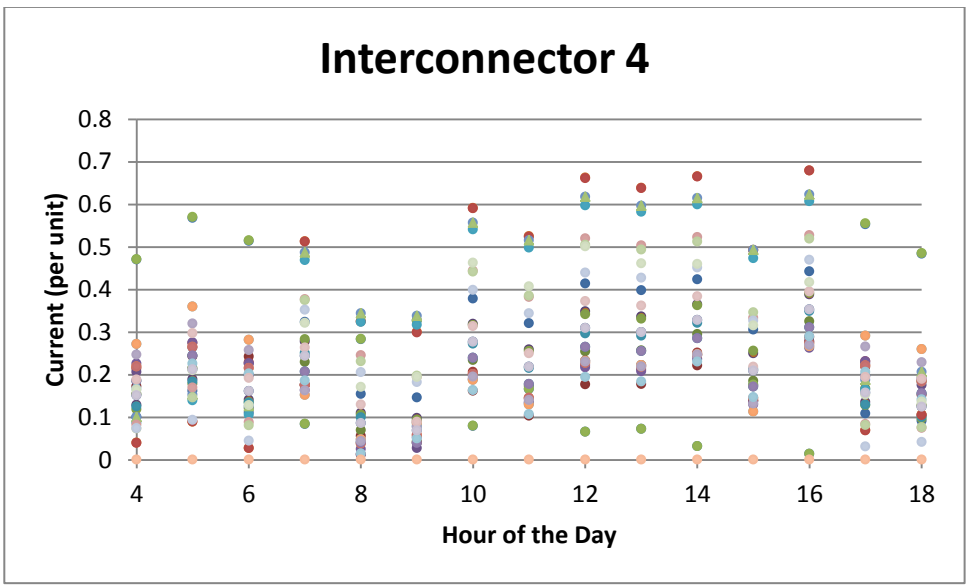
Interconnector 4
Current (per unit)
0.8
0.7
0.6
0.5
0.4
0.3
0.2
0.1
0
4
6
8
10
12
14
16
18
Hour of the Day

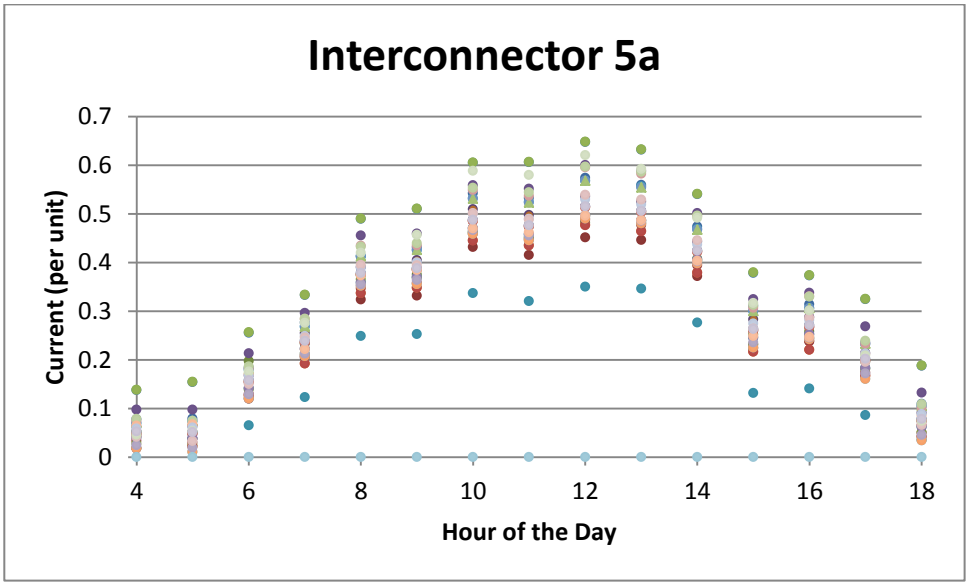
Interconnector 5a
Current (per unit)
0.7
0.6
0.5
0.4
0.3
0.2
0.1
0
4
6
8
10
12
14
16
18
Hour of the Day

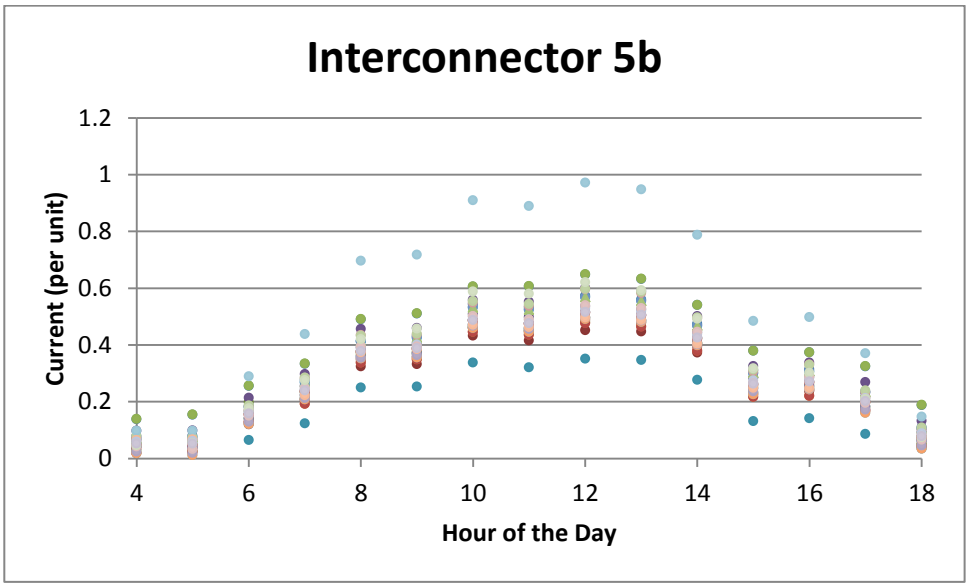
Interconnector 5b
Current (per unit)
1.2
1
0.8
0.6
0.4
0.2
0
4
6
8
10
12
14
16
18
Hour of the Day

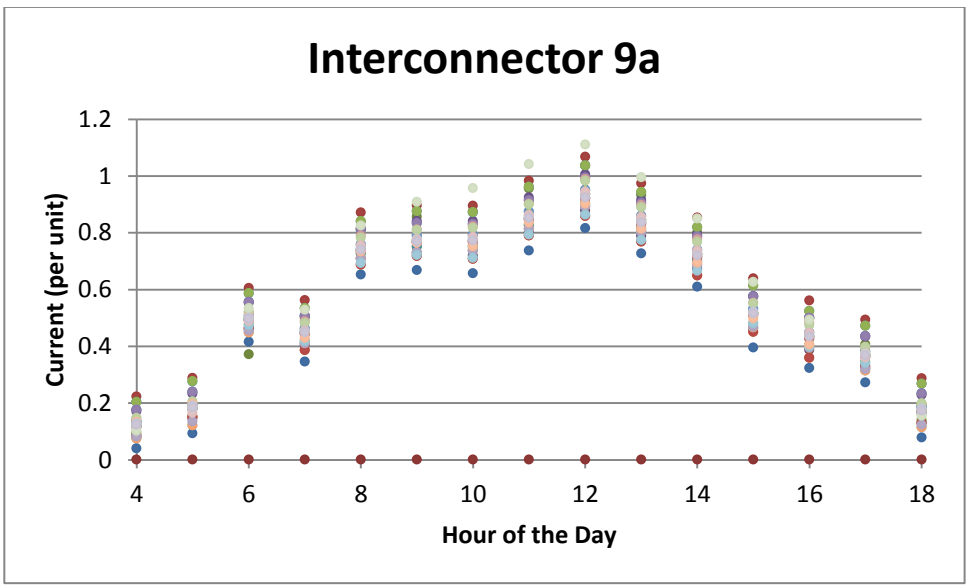
Interconnector 9a
Current (per unit)
1.2
1
0.8
0.6
0.4
0.2
0
4
6
8
10
12
14
16
18
Hour of the Day

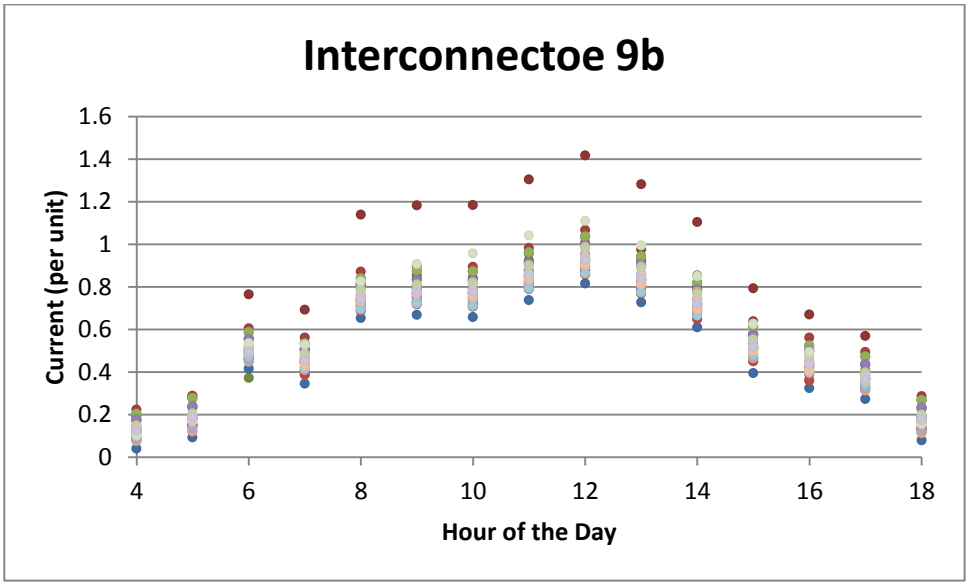

c. PV System Connected at Location B

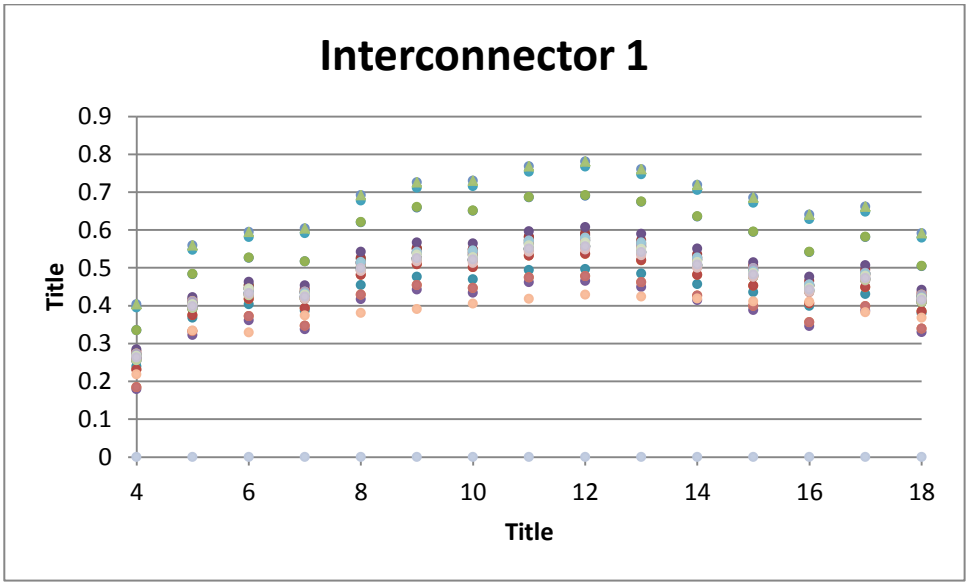

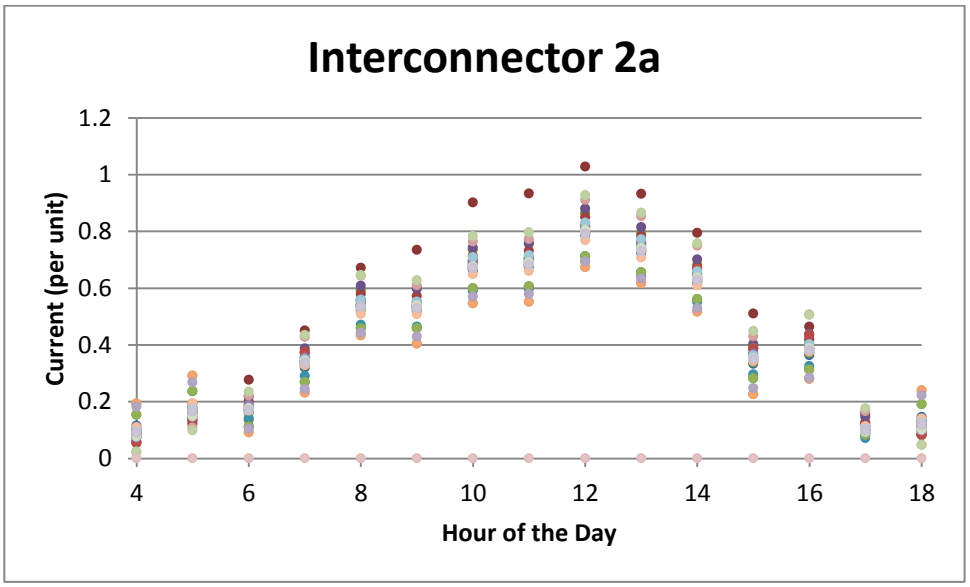

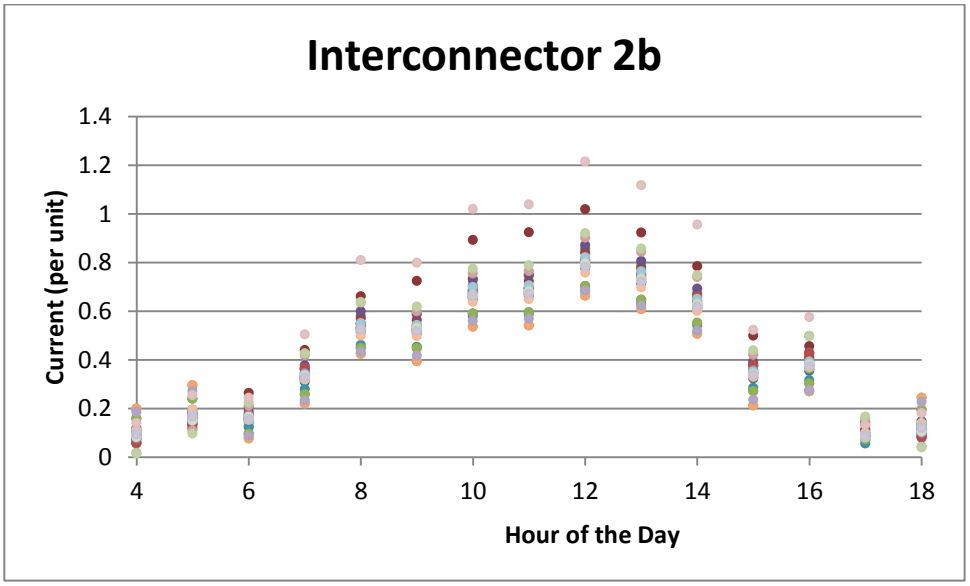
Interconnector 2b
Current (per unit)
1.4
1.2
1
0.8
0.6
0.4
0.2
0
4
6
8
10
12
14
16
18
Hour of the Day

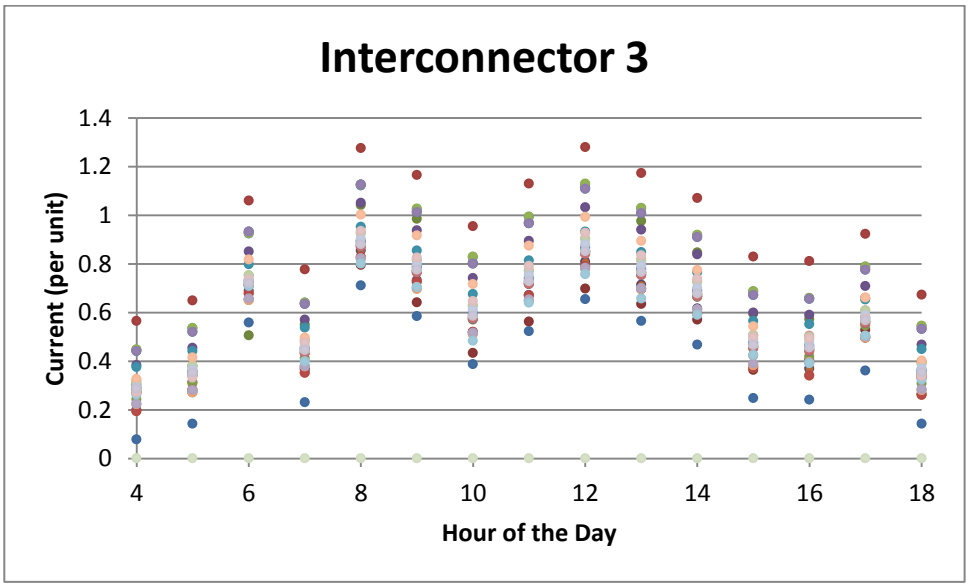
Interconnector 3
Current (per unit)
1.4
1.2
1
0.8
0.6
0.4
0.2
0
4
6
8
10
12
14
16
18
Hour of the Day

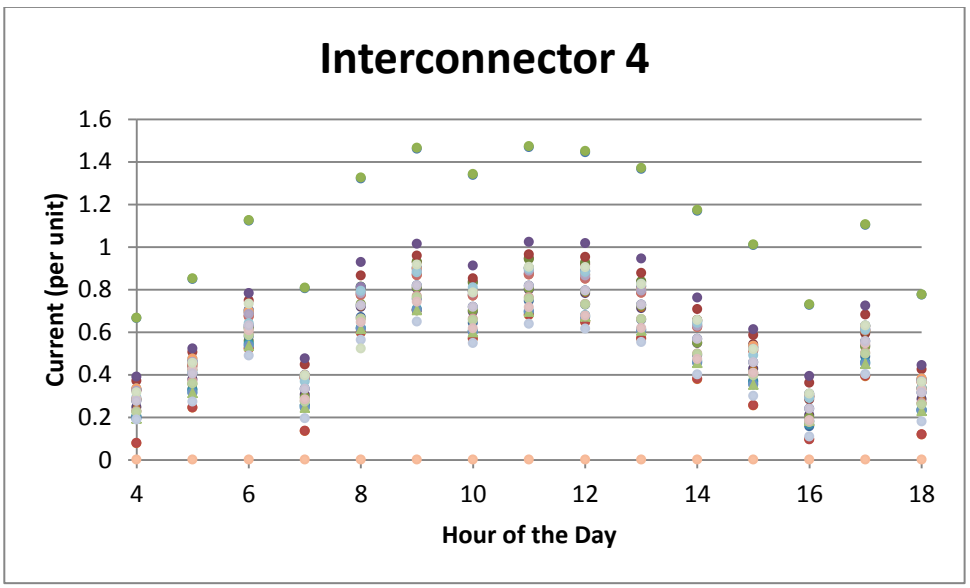
Interconnector 4
Current (per unit)
1.6
1.4
1.2
1
0.8
0.6
0.4
0.2
0
4
6
8
10
12
14
16
18
Hour of the Day

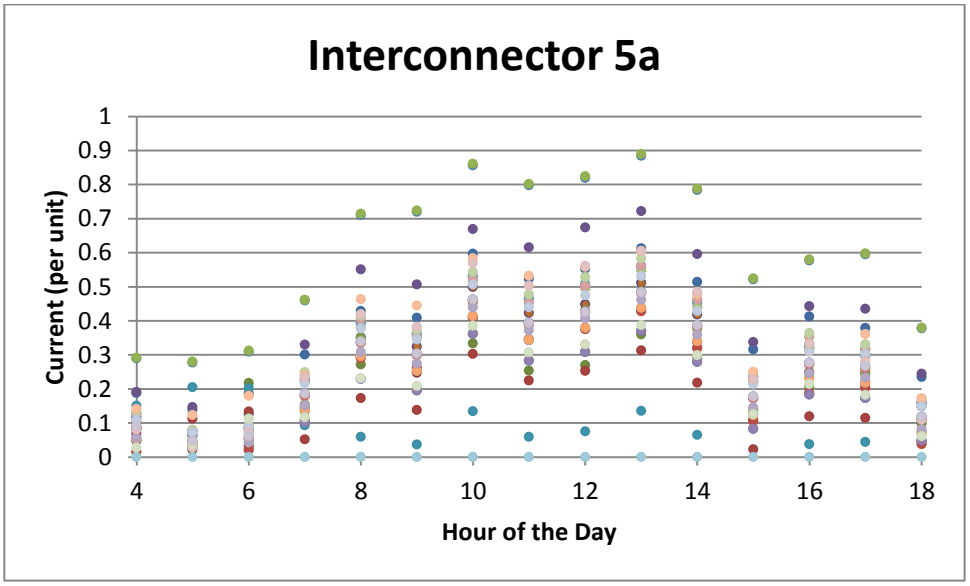
Interconnector 5a
Current (per unit)
1
0.9
0.8
0.7
0.6
0.5
0.4
0.3
0.2
0.1
0
4
6
8
10
12
14
16
18
Hour of the Day

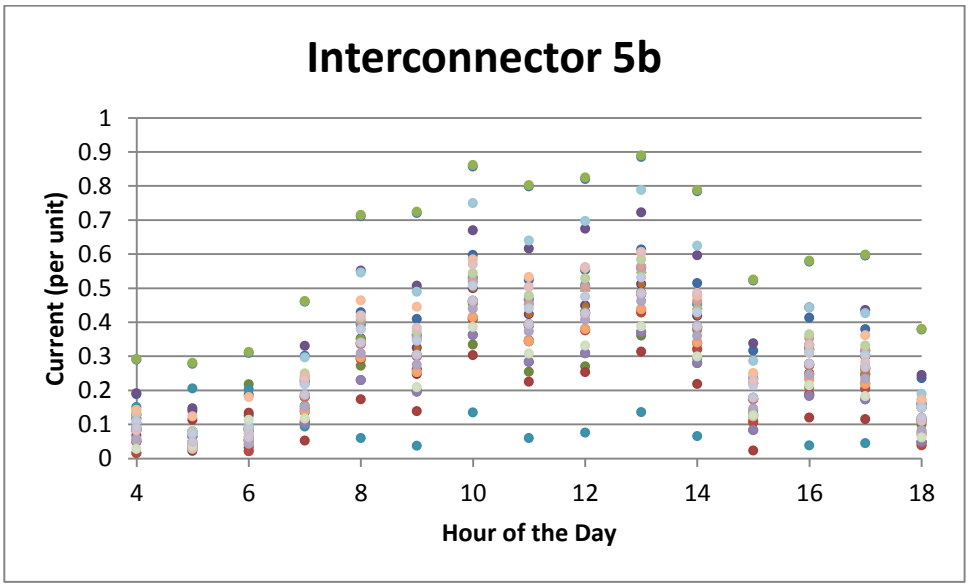
Interconnector 5b
Current (per unit)
1
0.9
0.8
0.7
0.6
0.5
0.4
0.3
0.2
0.1
0
4
6
8
10
12
14
16
18
Hour of the Day

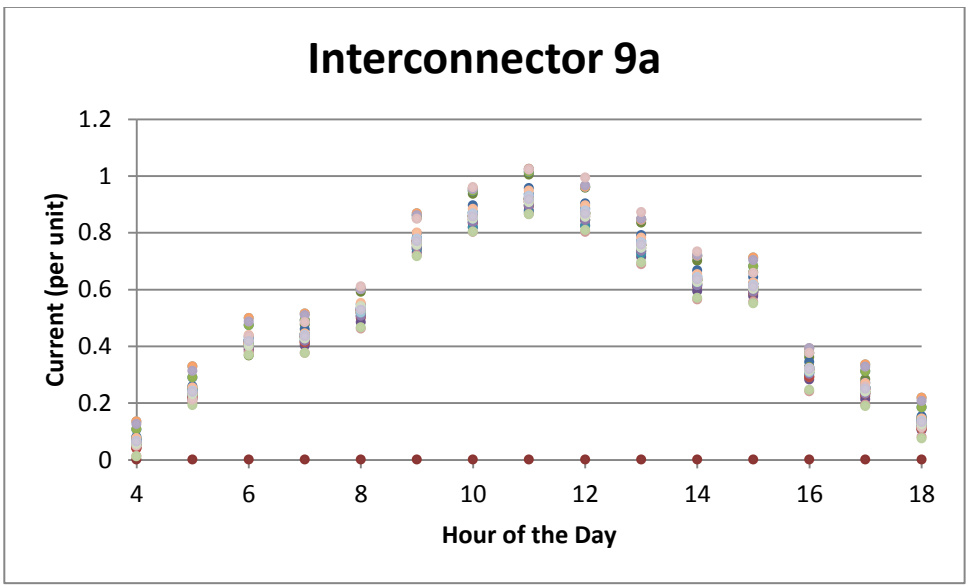
Interconnector 9a
Current (per unit)
1.2
1
0.8
0.6
0.4
0.2
0
4
6
8
10
12
14
16
18
Hour of the Day

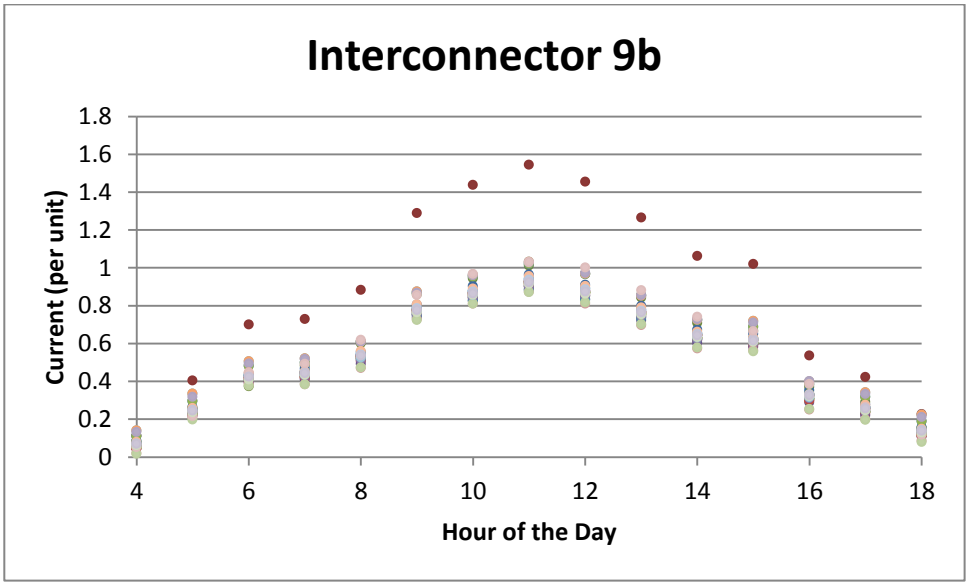

d. PV System Connected at Location C

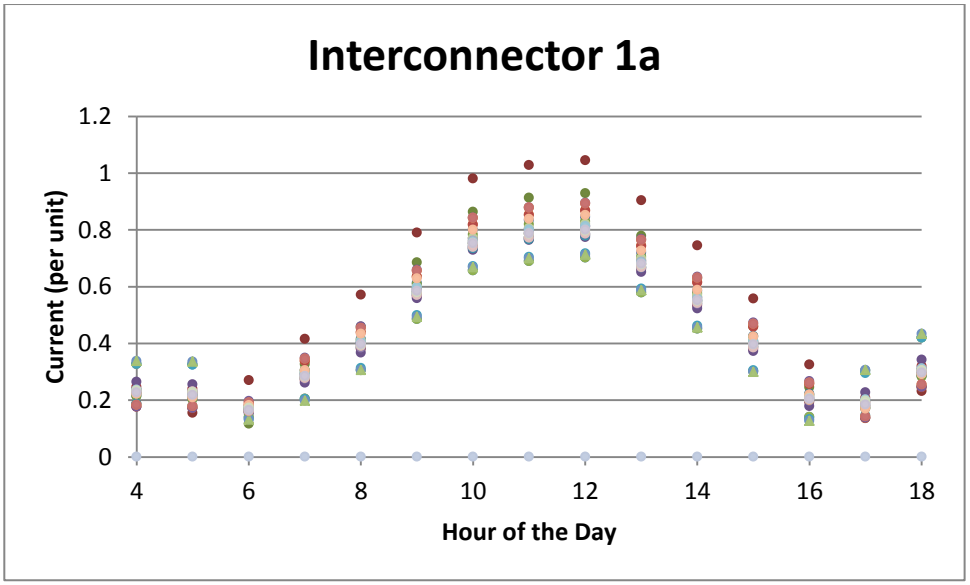

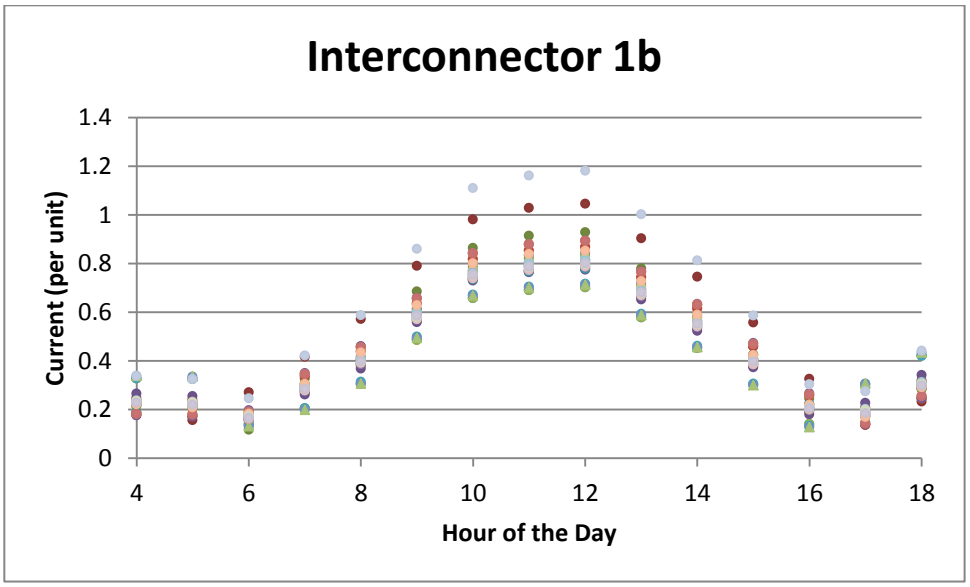

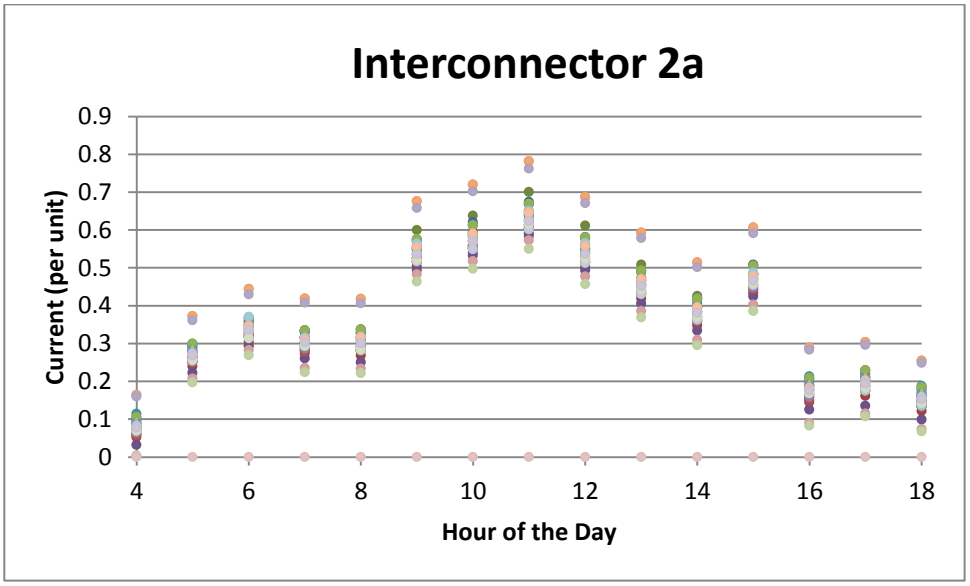
Interconnector 2a
Current (per unit)
0.9
0.8
0.7
0.6
0.5
0.4
0.3
0.2
0.1
0
4
6
8
10
12
14
16
18
Hour of the Day

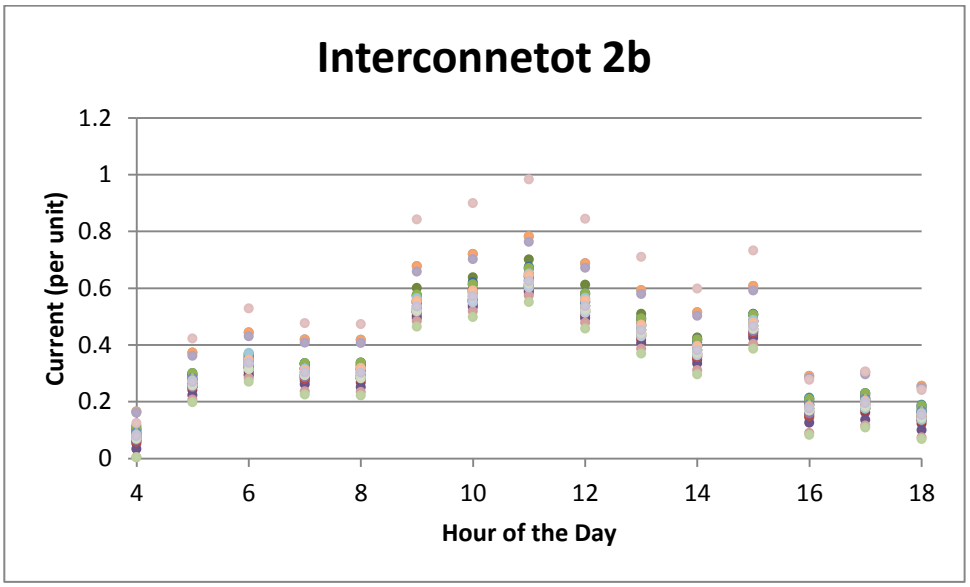
Interconnetot 2b
Current (per unit)
1.2
1
0.8
0.6
0.4
0.2
0
4
6
8
10
12
14
16
18
Hour of the Day

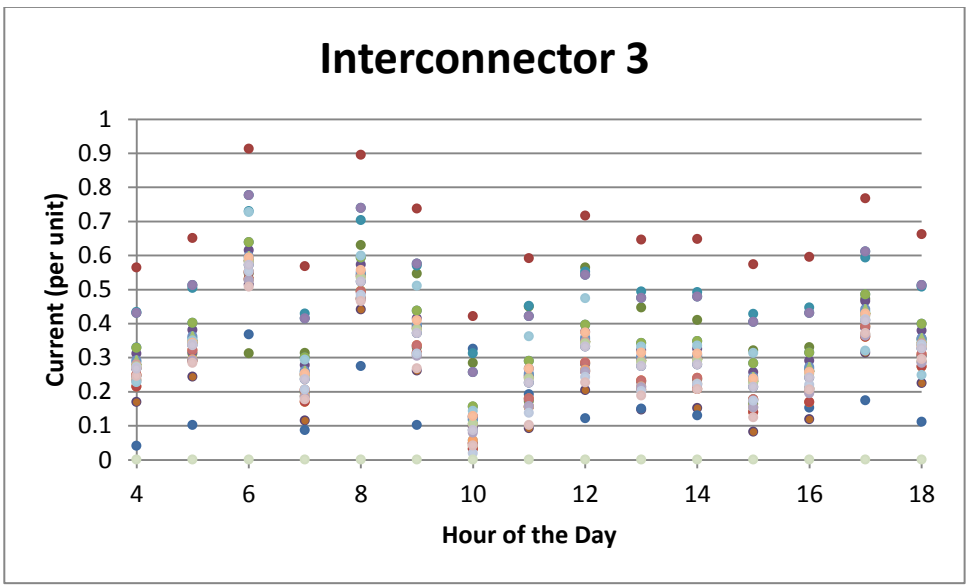
Interconnector 3
Current (per unit)
1
0.9
0.8
0.7
0.6
0.5
0.4
0.3
0.2
0.1
0
4
6
8
10
12
14
16
18
Hour of the Day

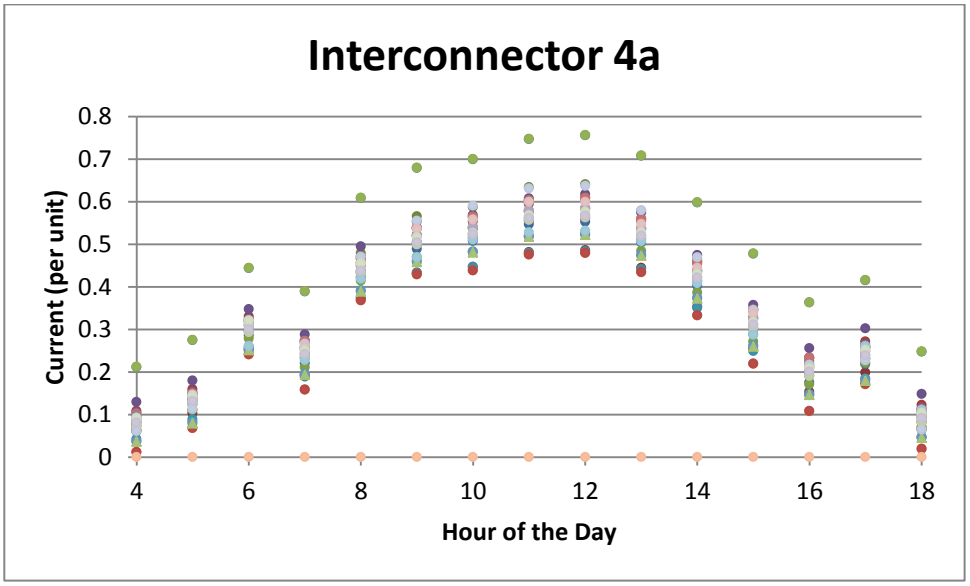
Interconnector 4a
Current (per unit)
0.8
0.7
0.6
0.5
0.4
0.3
0.2
0.1
0
4
6
8
10
12
14
16
18
Hour of the Day

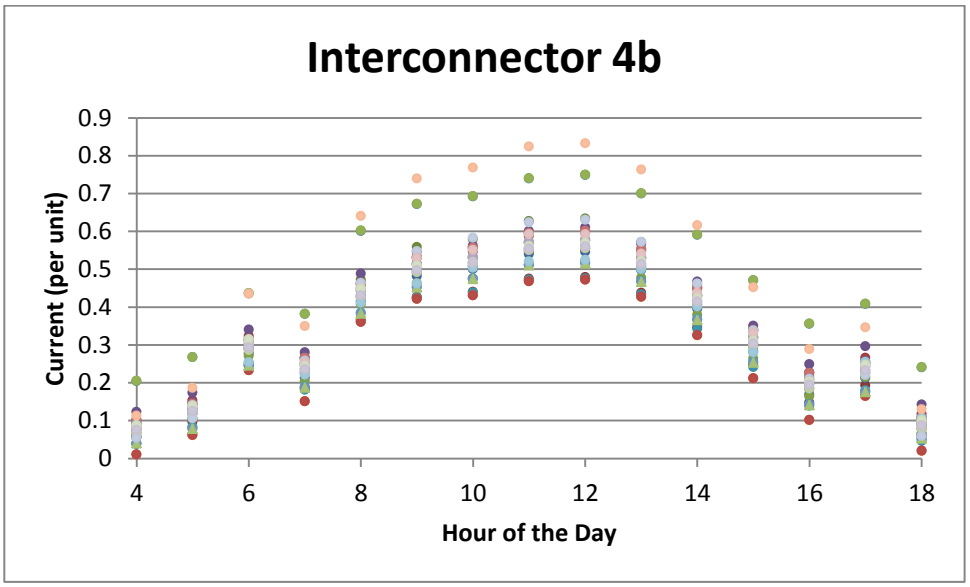
Interconnector 4b
Current (per unit)
0.9
0.8
0.7
0.6
0.5
0.4
0.3
0.2
0.1
0
4
6
8
10
12
14
16
18
Hour of the Day

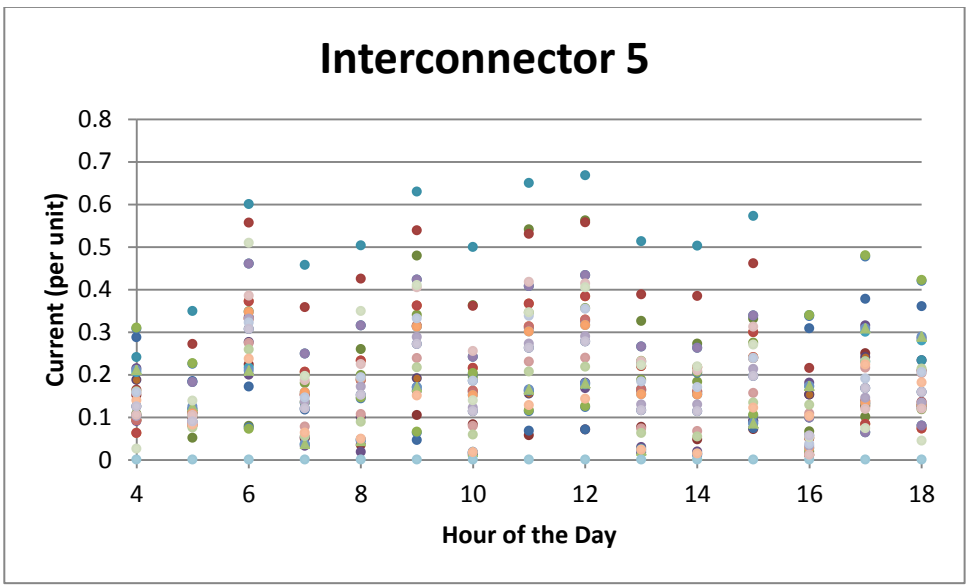
Interconnector 5
Current (per unit)
0.8
0.7
0.6
0.5
0.4
0.3
0.2
0.1
0
4
6
8
10
12
14
16
18
Hour of the Day

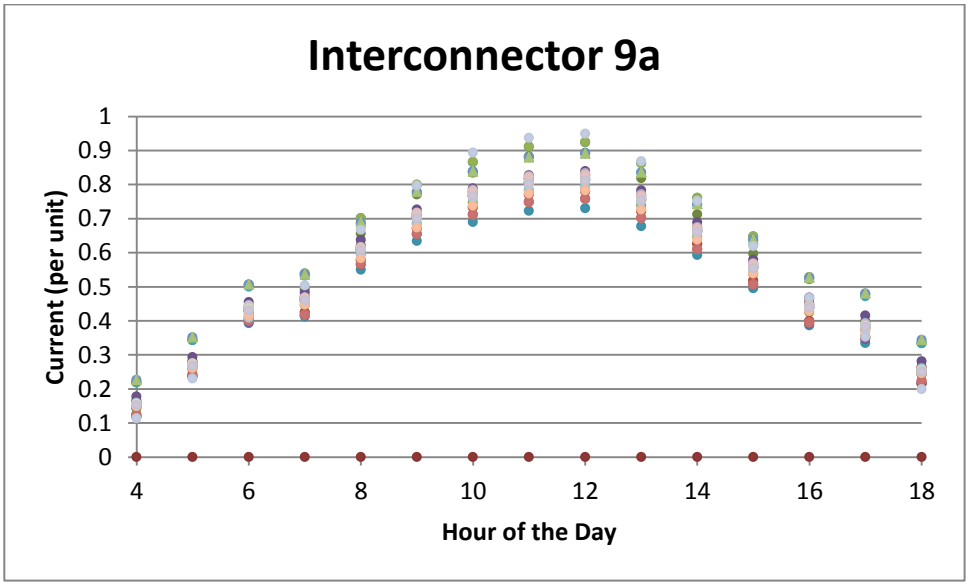

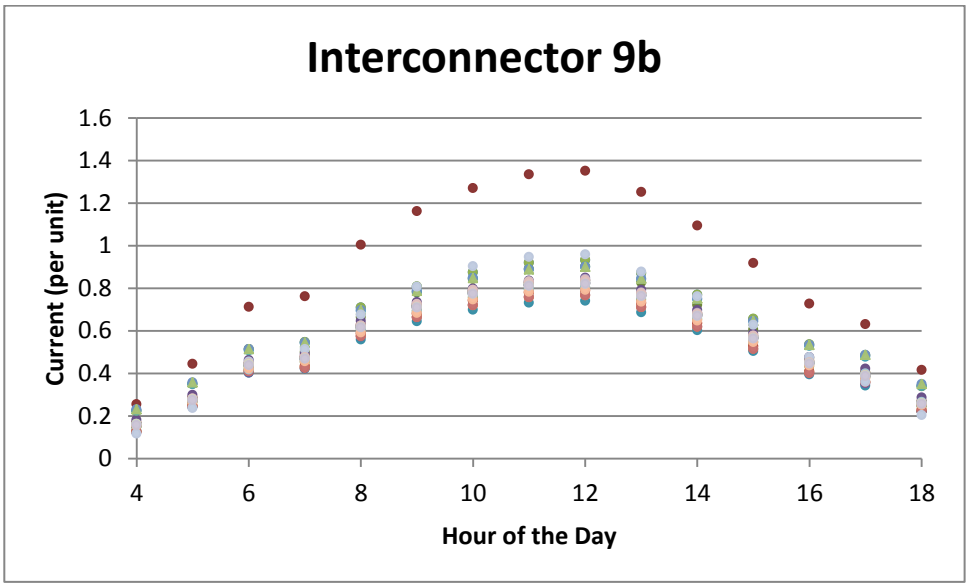

e. PV System Connected at Location D

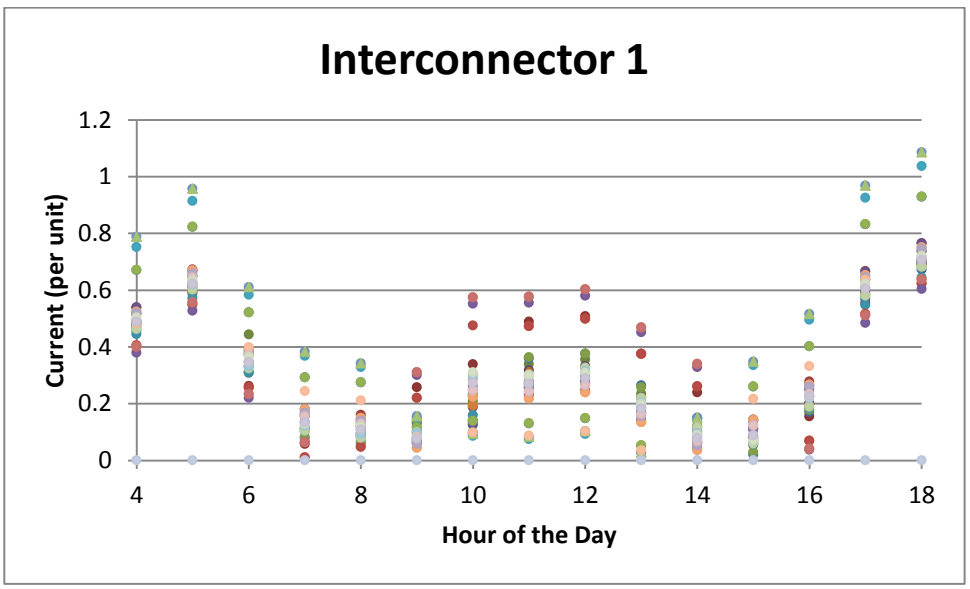

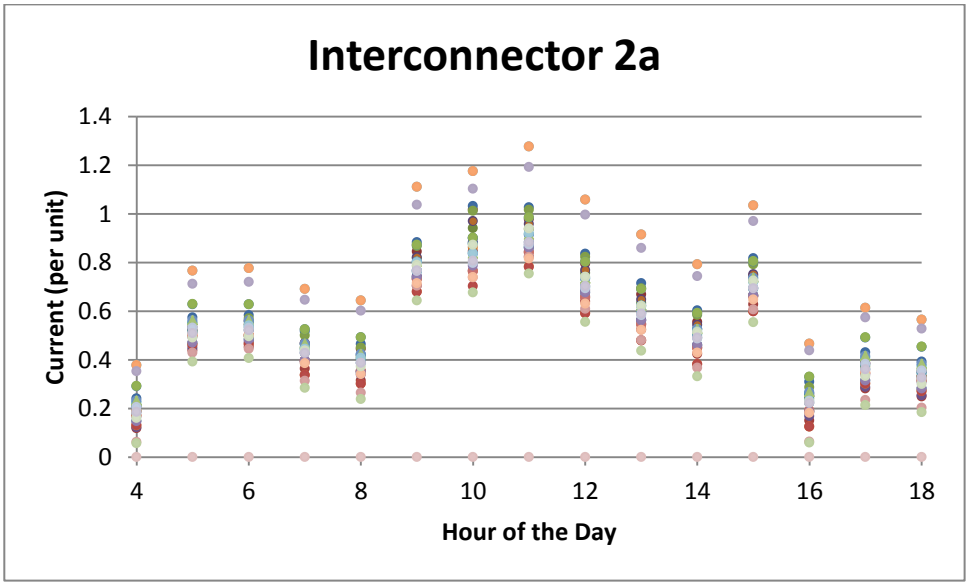
Interconnector 2a
Current (per unit)
1.4
1.2
1
0.8
0.6
0.4
0.2
0
4
6
8
10
12
14
16
18
Hour of the Day

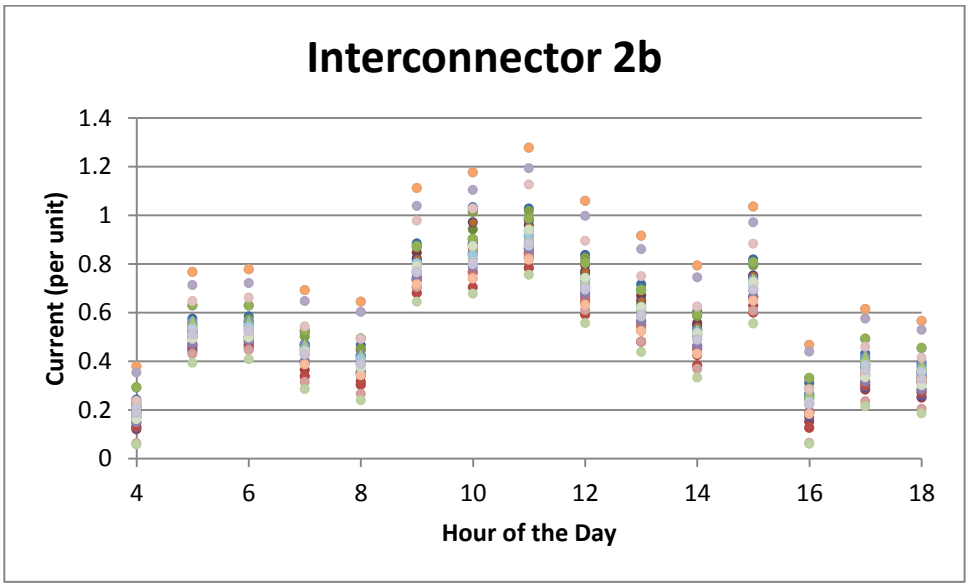
Interconnector 2b
Current (per unit)
1.4
1.2
1
0.8
0.6
0.4
0.2
0
4
6
8
10
12
14
16
18
Hour of the Day

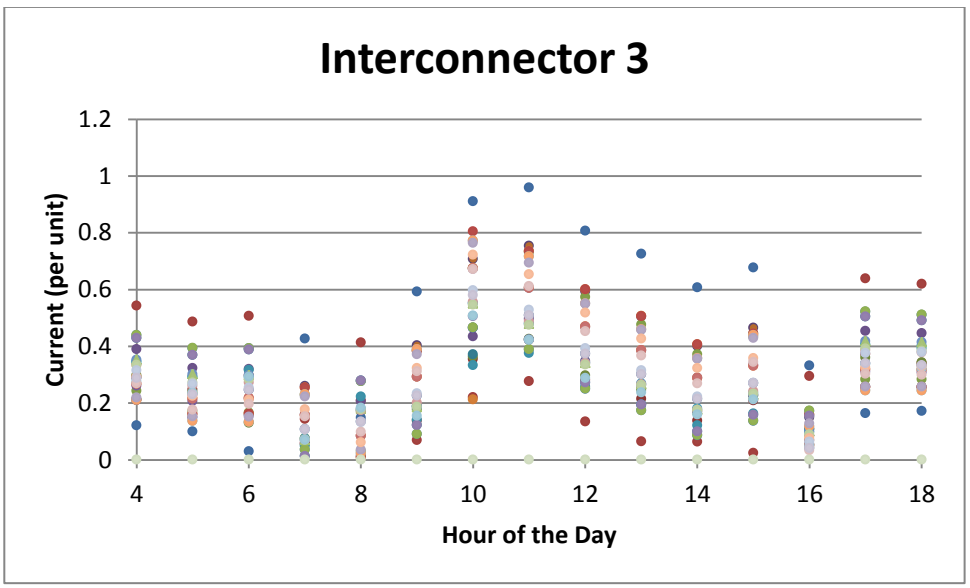
Interconnector 3
Current (per unit)
1.2
1
0.8
0.6
0.4
0.2
0
4
6
8
10
12
14
16
18
Hour of the Day

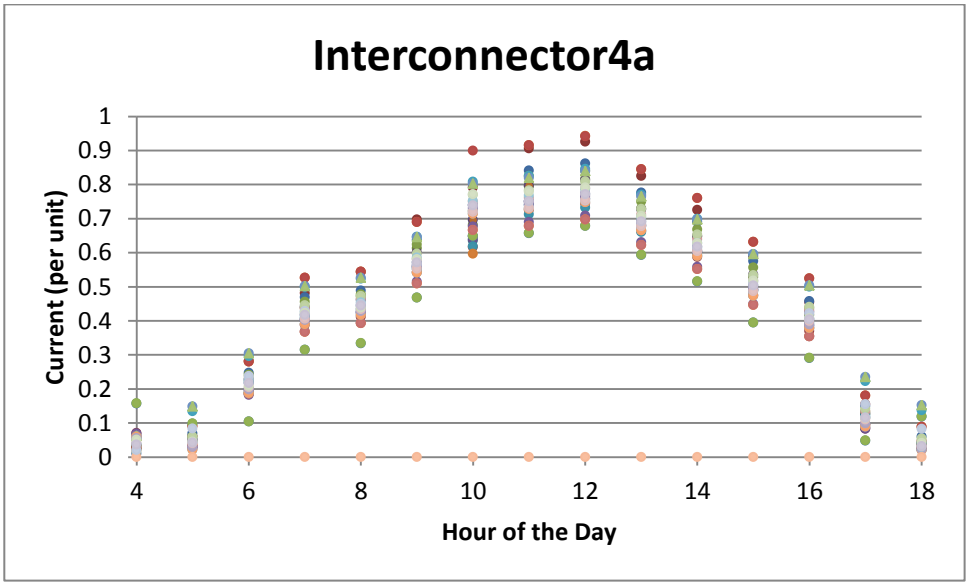
Interconnector4a
Current (per unit)
1
0.9
0.8
0.7
0.6
0.5
0.4
0.3
0.2
0.1
0
4
6
8
10
12
14
16
18
Hour of the Day

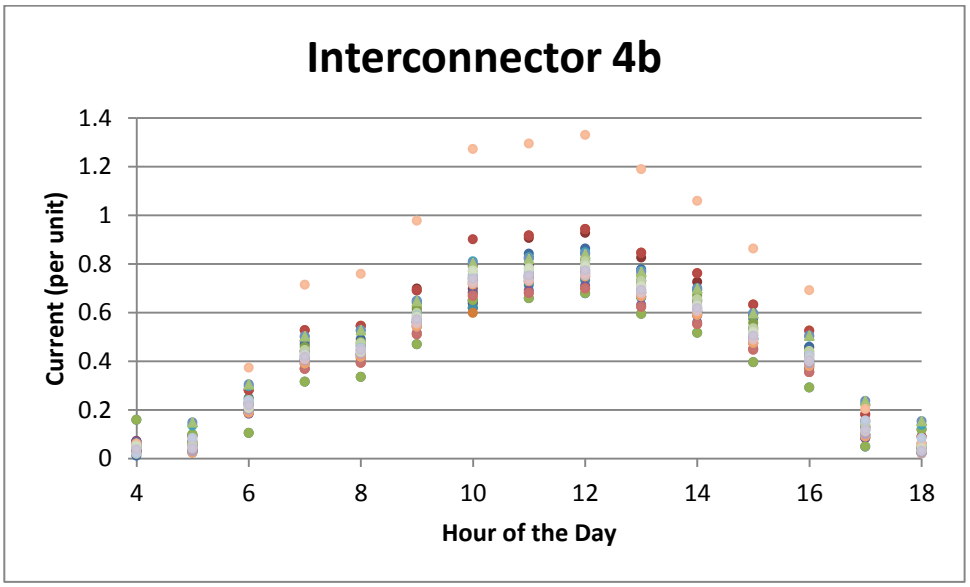
Interconnector 4b
Current (per unit)
1.4
1.2
1
0.8
0.6
0.4
0.2
0
4
6
8
10
12
14
16
18
Hour of the Day

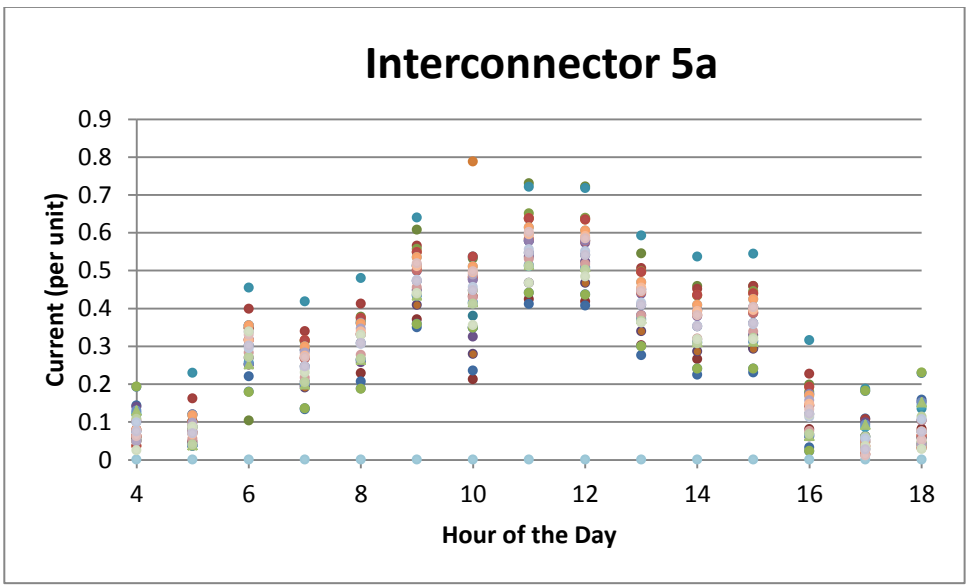
Interconnector 5a
Current (per unit)
0.9
0.8
0.7
0.6
0.5
0.4
0.3
0.2
0.1
0
4
6
8
10
12
14
16
18
Hour of the Day

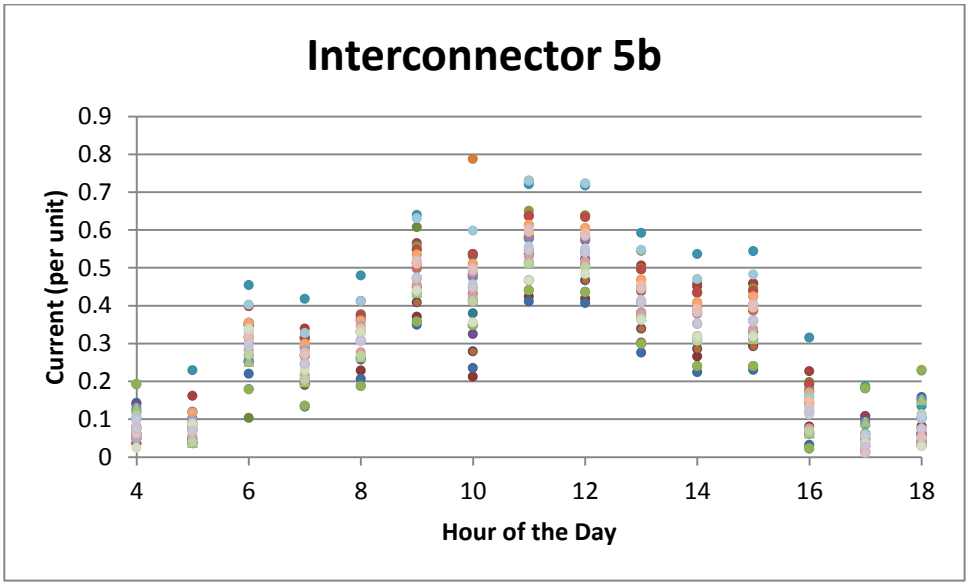
Interconnector 5b
Current (per unit)
0.9
0.8
0.7
0.6
0.5
0.4
0.3
0.2
0.1
0
4
6
8
10
12
14
16
18
Hour of the Day

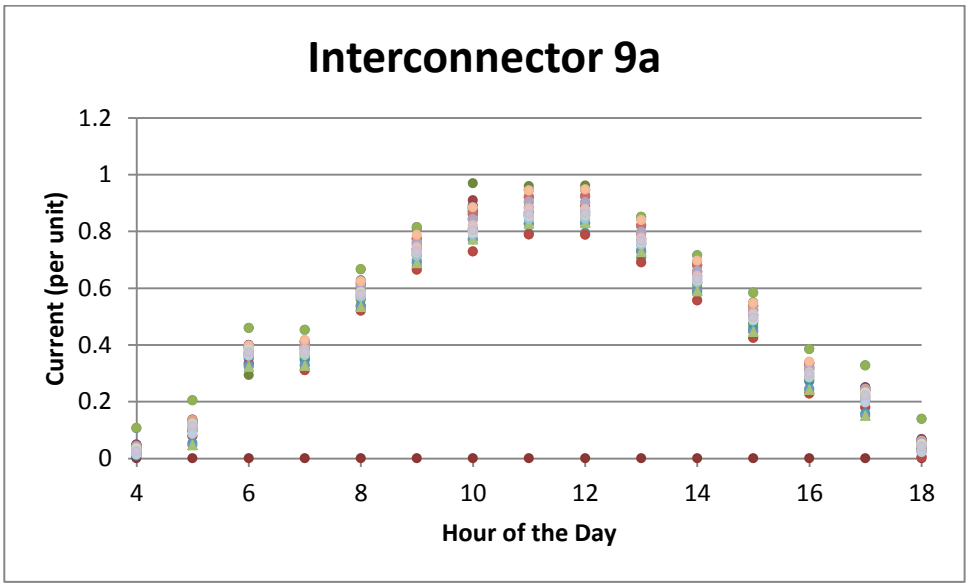
Interconnector 9a
Current (per unit)
1.2
1
0.8
0.6
0.4
0.2
0
4
6
8
10
12
14
16
18
Hour of the Day

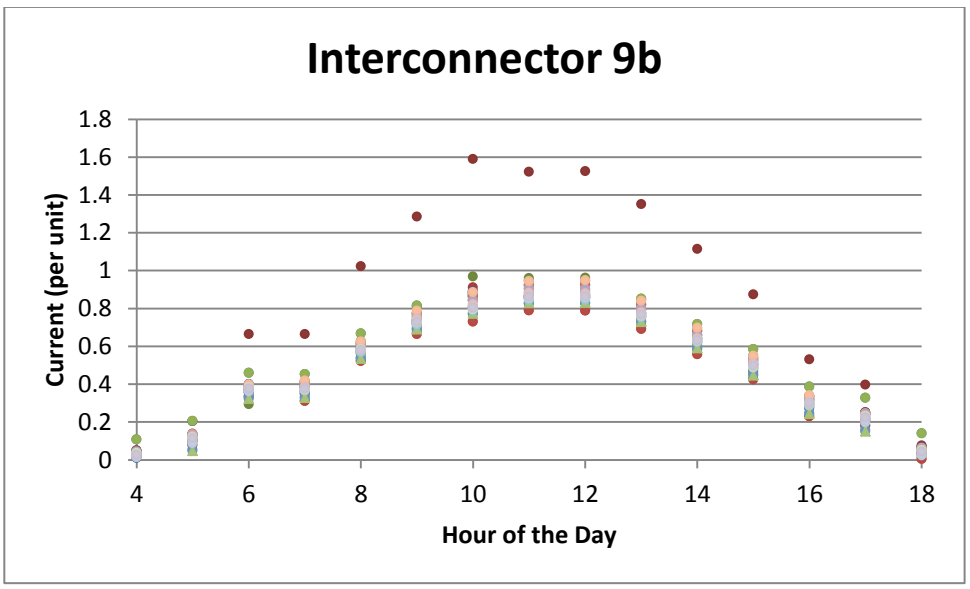
Interconnector 9b
Current (per unit)
1.8
1.6
1.4
1.2
1
0.8
0.6
0.4
0.2
0
4
6
8
10
12
14
16
18
Hour of the Day

Appendix G

Structure of single-phase (1-φ) controller [85]